Development of a novel 3D *in vitro* model to measure cellular response to antioxidant doped highly cross-linked ultra high molecular weight polyethylene wear debris

Lauren Elizabeth Yarrow-Wright

Submitted in accordance with the requirements for the degree of
Doctor of Philosophy

The University of Leeds

School of Mechanical Engineering

September, 2018

The candidate confirms that the work submitted is her own and that appropriate credit has been given where reference has been made to the work of others.

Acknowledgements

I should like to begin by thanking my team of supervisors, Professor Joanne Tipper, Professor Sophie Williams and Dr Eric Hewitt, for their guidance and support throughout my project. As my primary supervisor, Professor Joanne Tipper, has put in a great deal of time and effort to support my project and myself as a student. Professor Sophie Williams provided much needed engineering guidance and Dr Eric Hewitt provided biology support and a steady supply of RAW 264.7 murine macrophages when needed. I am very grateful indeed for all the feedback and support from you all.

I would also like to extend my thanks to everyone past and present in the Eileen Ingham lab in the Faculty of Biological Sciences that has helped me with my work or simply been a friend. In particular, Dan, our lab manager, has provided me individually with much guidance but, also as part of our wider lab group, has looked after the needs of us all. Our lab has boasted some excellent technicians, past and present, who are the backbone of the lab and have helped me immensely; in particular Sha Zhang, Lisa Allinson, Emily Caseley, Nicola Conway and Fiona Walker. I would like to thank the past and present PhDs and postgrads of the Tipper and Ingham groups for all your assistance and friendship during my project; in particular Saurabh Lal, Imran Asif, Katie Timms, Trang Nguyen, Nic Gowland, Aiqin Liu, Helen Lee, Jeni Smith and Ruth Craven for all their project specific help.

On a similar note, I would like to extend my thanks to the Institute of Medical and Biological Engineering for providing the equipment and lab space necessary to create wear debris during my project. I should like to thank the lab manager, Phil Wood, and the fantastic technicians: Irvin Homan, Jane Cardie, Keith Dyer and Camille Hammersley. Additionally I would like to thank Ksenija Vasiljeva for training me on the six station wear rig and Raelene Cowie for all your support with the wear rigs over the years. I would also like to thank our admin staff - namely Cheryl Harris and Debra Baldwin – who have sorted out our PhD lives most of the time and are the unsung heroes behind the scenes.

I would like to thank my incredible group of friends who have been in my life for the last 19 years. Amy Hill, Rachael Birch, Helen Holbrey and Lindsey Parker – you are my extended family and, although we may not see each other as much as we used to in our school and college days, it is always the same when we meet up. You have all seen me through the last six years. I

would like to thank Lindsey in particular who suggested the PhD programme in the first place and helped me with my application all those years ago. I maintain I would not have received my place on the programme without your help. Not only that but I had the pleasure of working next door to you for several years which I miss dearly.

I would like to thank my amazing family – nothing I say here will ever convey just how much I owe you all or how much I appreciate your love and support. I love you all to the moon and back. My parents – Dawn and Nigel Yarrow – have been my number one supporters throughout the peaks and troughs of the last few years and I will be forever grateful for your unceasing love and support . My sister – Emily – thanks for providing me with an ear to listen, although I'm dreadful at communication, I appreciate it more than you realise. Owen and Jack – my wonderful nephews - and Hallie – my beautiful new niece, you are the little loves of my life. You all make me extremely happy and proud constantly – I don't know what I have done to deserve to be the aunty to two such amazing boys and one tiny princess.

And finally, the large love of my life, my wonderful husband, Sam. I told you on our wedding day just how much I loved you then and it has multiplied exponentially since. Some say it was mad to get married whilst doing a PhD but I'm so glad we did – I can't imagine not being married to you. You have loved me at my best and worst and stuck with me through thick and thin – you were taking your vows seriously it seems even before we made them. You are my best friend in the whole world and, without you, there is no way I would have ever got this far with my PhD. I cannot articulate how much you have done for me through this process and I will be forever grateful. It is to you, my soul mate, that I dedicate my PhD because I quite simply could not have done it without your love and kindness.

This thesis is also dedicated to my special boy and beloved Springer spaniel, Robbie, who died just before I handed this in.

I am certain I have missed a few names along the way so if I have then please consider yourself thanked sincerely and completely for your help – just because I haven't managed to remember your name here does not mean your input was any less valuable or appreciated.

Abstract

Osteolysis, and subsequent aseptic loosening, is the leading cause of revision in total hip replacements. The biological response to ultra-high molecular weight polyethylene (UHMWPE) wear debris is known to trigger the release of several inflammatory mediators such as tumour necrosis factor-alpha (TNF-α), interleukin-1β (IL-1β), interleukin-6 (IL-6), interleukin-8 (IL-8), leukotriene B4 (LTB_4) and prostaglandin E2 (PGE_2); all of which are involved in the signalling cascade that triggers the differentiation of osteoclasts and begins osteolysis. UHMWPE has undergone modifications such as cross-linking (to reduce the volume of wear debris produced) and antioxidant doping (to neutralise free radicals produced by irradiative crosslinking and prevent oxidative embrittlement). Previous studies at the University of Leeds, using peripheral blood mononuclear cells (PBMNCs) cultured on wear particle containing agarose gel, have shown that antioxidant doped, highly cross-linked UHMWPE may reduce the production of osteolytic cytokines in comparison to highly cross-linked UHMWPE. This model has limitations; namely donor heterogeneity associated with the use of PBMNC's in addition to the use of a 2D model for what is a 3D *in vivo* environment. The aims of this study were to develop a novel 3D model in which mononuclear phagocytes and wear particles were encapsulated within a gel and to use the model to compare the cellular production of osteolytic cytokines when treated with highly cross-linked UHMWPE and antioxidant doped, highly cross-linked UHMWPE wear debris.

Three different cell types (PBMNC's, U937 human histiocytes and RAW 264.7 murine macrophages) and two gel types (agarose and type I rat tail collagen) were investigated during the development of the 3D model. It was found that the use of RAW 264.7 murine macrophages and UHMWPE wear debris simultaneously trapped inside a collagen gel matrix was the most promising model. A large volume of sterile highly cross-linked UHMWPE wear debris (with and without antioxidant doping) was generated using pin-on-plate (POP) multidirectional wear simulator rigs for use in the 3D model. RAW 264.7 murine macrophages were cultured with both unfractionated UHMWPE wear debris, or a filtered, critical size range (0.1 – 1 μm) of UHMWPE wear debris. RAW 264.7 murine macrophages cultured in the 3D model with unfractionated UHMWPE wear debris showed no difference in oxidative stress levels or TNF-α, IL-1β, IL-6, KC (CXCL-1 – a murine

homologue of IL-8), LTB_4 and PGE_2 levels produced in response to highly cross-linked UHMWPE wear debris with and without antioxidant doping compared to the cells only controls. Similarly, RAW 264.7 murine macrophages cultured in the 3D model with a critical size range (0.1 – 1 μm) of UHMWPE wear debris showed no difference in oxidative stress levels or TNF-α, IL-1β, IL-6, KC, LTB_4 and PGE_2 levels when treated with highly cross-linked UHMWPE wear debris with and without antioxidant doping compared to the cells only controls. RAW 264.7 murine macrophages were also stimulated with LPS in the 3D model and then treated with Protein Kinase C (PKC) inhibitors (Calphostin C and Bisindolylmaleimide I), 5-lipoxygenase (5-LO) inhibitors (MK 886 and REV 5901), Cycloxygenase (COX) inhibitor (Indomethacin) and antioxidants (α –tocopherol and pentaerythritol tetrakis(3,5-di-*tert*-butyl-4-hydroxyhydrocinnamate)) after three hours. RAW 264.7 murine macrophages treated with both PKC inhibitors and both antioxidants showed reduced levels of TNF-α and IL-6 when compared to the LPS only control. All inhibitors and antioxidants reduced the production of IL-1β when compared to the LPS only control. Cells treated with Calphostin C exhibited a reduced production of LTB_4 and PGE_2 when compared to the LPS only control.

Microscopy images of RAW 264.7 murine macrophages cultured in the novel 3D model incubated with 0.1 – 1 μm antioxidant doped, highly cross-linked UHMWPE wear debris and FluoSpheres® showed that the RAW 264.7 murine macrophages sequestered the UHMWPE wear debris in the perinuclear lysosomes, indicating attempted phagocytosis, which is consistent with the previous studies.

Overall, the RAW 264.7 murine macrophages cultured in the novel 3D model largely failed to produce inflammatory and osteolytic cytokines, chemokines and mediators in response to the UHMWPE wear debris generated in this study. However the novel model showed some promise by demonstrating the link between vitamin E and PKC in reducing the production of inflammatory and osteolytic mediators as shown in previous studies. The novel culture model requires further work to produce a more accurate *in vitro* representation of the 3D periprosthetic environment for use in future studies.

Table of Contents

List of Tables

List of Figures

List of Abbreviations

Abbreviation	Full description
%	Percentage
°C	Degrees Celsius
1X	One times
2D	Two dimensional
3D	Three dimensional
5-LO	5-lipooxygenase
10X	Ten times
25X	Twenty five times
µg	Micrograms
µl	Microlitres
µm	Micrometres
µmol	Micromoles
AMP	Adenosine monophosphate
ANOVA	Analysis of variance
ASR	Articular surface replacement
ASTM	American Society for Testing and Materials
ATP	Adenosine triphosphate
AOX	Antioxidant
BMI	Body mass index
BSA	Bovine serum albumin
CD	Cluster of differentiation
CL	Confidence limits
cm	centimetres
Co	Cobalt

CO_2	Carbon dioxide
COC	Ceramic on ceramic
COM	Ceramic on metal
COP	Ceramic on polyethylene
COX	Cycloxygenase
Cr	Chromium
dH_2O	Distilled water
DMEM	Dulbecco's modified eagles medium
DMSO	Dimethyl sulfoxide
DPBS	Dulbecco's phosphate buffered saline solution
DSC	Differential scanning calorimetry
E.coli	Escherichia coli
EDTA	Ethylenediaminetetraacetic acid
ELISA	Enzyme-linked immunosorbent assay
EU	Endotoxin units
FBS	Foetal bovine serum
FDA	Food and drug administration
FEGSEM	Field emission gun scanning electron microscopy
FITC	Fluoroscein isothiocyanate
FTIR	Fourier transform infrared spectroscopy
G	Gauge
g	G force
g	Grams
GM-CSF	Granulocyte-Macrophage Colony-Stimulating Factor
GPa	Giga pascal

GUR	Granular UHMWPE Ruhrchemie
H^+	Hydrogen ion
H_2	Hydrogen
H_2O_2	Hydrogen peroxide
H_2SO_4	Sulfuric acid
HALS	Hindered amine light stabilisers
HBA	Heated blood agar
HDPE	High density polyethylene
HEPES	4-(2-hydroxyethyl)-1-piperazineethanesulfonic acid
HRP	Horse radish peroxidase
HSC	Haematopoietic stem cell
IL-1	Interleukin one
IL-1β	Interleukin one beta
IL-6	Interleukin six
IL-8	Interleukin eight
Inc	Incorporated
KC	Keratinocyte-derived chemokine
kGy	Kilogray
KOH	Potassium hydroxide
L	Litres
LAL	Limulus amebocyte lysate
LC	Lethal concentration
LDPE	Low density polyethylene
LLDPE	Linear low density polyethylene
LFA-1	Lymphocyte function-associated antigen-1
LPS	Lipopolysaccharide
LTB_4	Leukotriene beta four
Ltd	Limited

M	Moles
m	Metre
MCL	Mammalian cell lysis solution
MCSF	Macrophage colony stimulating factor
MEM	Minimum essential medium
Mg	Magnesium
mg	Milligrams
MHC	Major histocompatibility complex
MITF	Microphthalmia-associated transcription factor
ml	Millilitres
mm	Millimetres
mM	Millimolar
Mmol	Millimoles
MOM	Metal on metal
MOP	Metal on polyethylene
MPa	Mega pascal
MRad	Mega rad
MTT	3-(4,5-dimethylthiazol-2-yl)-2-5-diphenyltetrazolium bromide
N	Newton
NA	Nutrient agar
NaOH	Sodium hydroxide
ng	Nanograms
NHS	National Health Service
Ni	Nickel
NJR	National Joint Registry
nm	Nanometres

NSAID	Non-steroidal anti-inflammatory drugs
O_2	Oxygen
OH	Hydroxide
OPG	Osteoprotegerin
Pa	Pascal
PBMNC	Peripheral blood mononuclear cells
PBS	Phosphate buffered saline solution
pg	Picograms
PGE_2	Prostaglandin E2
PKC	Protein kinase C
PLC	Public Limited Company
PMA	Phorbol-12-myristate-13-acetate
PMMA	Polymethylmethacrylate
POP	Pin-on-plate
Ppi	Pyrophosphate
ppm	Parts per million
psi	Pounds per square inch
PVC	Polyvinyl chloride
R_a	Surface roughness
RANK	Receptor Activator of Nuclear factor Kappa-B
RANKL	Receptor Activator of Nuclear factor Kappa-B Ligand
rcf	Relative centrifugal force
RGD	Arginylglycylaspartic acid
ROS	Reactive oxygen species
rpm	Revolutions per minute
RPMI	Roswell Park Memorial Institute Medium

SAB	Sabouraud dextrose agar
SEM	Standard error of the mean
SUFE	Slipped upper femoral epiphysis
TBHP	Tert-butyl hydroperoxide
TEMPO	2,2,6,6-Tetramethylpiperidin-1-yl)oxyl or (2,2,6,6-tetramethylpiperidin-1-yl)oxidanyl
TEMPOL	4-hydroxy-2,2,6,6-tetramethylpiperidin-1-oxyl
Tf	Flow transition temperature
Tg	Glass transition temperature
THR	Total hip replacement
TKR	Total knee replacement
Tm	Melting temperature
TMB	3,3’,5,5’-Tetramethylbenzidine
TMHQ	Trimethylhydroquinone
TNF-α	Tumour necrosis factor alpha
TRAP	Tartrate-resistant acid phosphotase
TWEEN-20	Polysorbate 20
U	Unit
UHMWPE	Ultra-high molecular weight polyethylene
UK	United Kingdom
USA	United States of America
UV	Ultra-violet
v/v	Volume per volume
VE	Vitamin E
w/v	Weight per volume
XL	Cross-linked

Chapter 1
Introduction

1.1 Biomaterials

Williams (1999) defines a biomaterial as a “nonviable material used in a medical device, intended to interact with biological systems” (Williams, 1999). Biomaterials, such as metals, ceramics or polymers, range extensively in their use and their exposure to the body, from hours to decades. It is important that a biomaterial should be biocompatible. Williams (1999) defines biocompatibility as “the ability of a material to perform with an appropriate host response in a specific application” (Williams, 1999). The biocompatibility of individual biomaterials varies according to their application but general qualities include: resistance to thrombogenicity, resistance to infection, lack of immunogenicity and lack of toxicity. The biological reactivity of the biomaterial varies depending on the application; for example, a hydroxyapatite coated femoral stem would be expected to interact with the surrounding femoral bone to encourage bone growth in order to fix the stem in place whereas a pacemaker would be expected to remain inert and have no chemical or biological reactivity. A lack of adverse biological reactivity is the general expectation of all biomaterials. Examples of the applications of biomaterials include: stents, dental implants, vascular grafts, breast implants and joint replacement prostheses.

1.2 Joint replacements

Synovial joints, such as the hip and knee, may become damaged, e.g. the development of osteophytes, micro-fractures and loss of cartilage (Man and Mologhianu, 2014), and lose function with age or disease. The pain from such damage can be managed with analgesics and physiotherapy however, ultimately, in order to restore function to a joint damaged beyond repair; the joint must be replaced with a biomaterial implant. Joint replacement surgery removes the damaged joint and replaces it with a synthetic biomaterial implant made from either metal, polymer or ceramic materials or a combination of these. The purpose of a joint replacement is to replace the damaged or missing bone and cartilage tissue with synthetic biomaterial alternatives and thus restore function to the joint. A joint implant must have the following qualities: biocompatibility (as defined above, Section 1.1), full joint functionality and no rapid degradation (low friction, low wear). In terms of biological reactivity, joint replacements must remain inert whilst in place unless using hydroxyapatite coated stems, which are used to encourage bone growth onto the

stem in place of cementation. According to the National Joint Registry (NJR), a total of 232,241 joint replacement surgeries were carried out both privately and on the National Health Service (NHS) during 2017 (Table 1.1) (National Joint Registry, 2017). There are a number of different types of total joint replacements which include: hip, knee, ankle, elbow and shoulder. The most common types of total joint replacements are the hip and knee with 107,506 and 125,188 surgeries completed respectively in 2017 (Table 1.1) (National Joint Registry, 2017).

Table 1.1 The number of joint replacement surgeries performed both privately and on the NHS in 2017; according to the NJR (National Joint Registry, 2017).

Joint	NHS	Independent
Hip	68,162	39,344
Knee	70,690	44,498
Ankle	743	171
Elbow	805	44
Shoulder	6187	1597
Total	**146,587**	**85,654**

1.3 Hip replacements

1.3.1 Hip anatomy

The hip is a ball and socket synovial joint, which connects the lower limbs to the torso, supports the weight of the upper body whilst moving or stationary, has a role in posture and allows several types of movement: flexion, extension, adduction, abduction, internal and external rotation (Traina, De Fine and Affatato, 2012). The hip joint (Figure 1.1A) is composed of a rounded femoral head at the femoral epiphysis (Figure 1.1B) which sits in the acetabular cup, a socket formed by the convergence of the ilium, ischium and pubis bones of the pelvis (Figure 1.1C). The femoral head is covered in hyaline cartilage except for the fovea and the acetabular cup is lined with a rim of fibrocartilage known as the labrum. Cartilage, connective tissue consisting of chondrocytes which secrete extracellular matrix components such as collagen and proteoglycans, undergoes compression upon loading (Anderson and Johnstone, 2017) and prevents bone interfaces meeting directly thereby reducing friction. The proteoglycans contained within the cartilage can attract and bind water molecules which confers compressibility on the cartilage tissue. Additionally, the interface between the femoral head and the acetabular cup contains the synovial bursae, the

synovial membrane filled with synovial fluid, which lubricates the joint; allowing movement and preventing friction (Molini *et al.*, 2011). The whole hip joint is itself surrounded by a fibrous membrane, the capsule, which protects the joint. The intracapsular ligaments, which reinforce the hip joint, are attached to and form part of this protective capsule: these consist of the iliofemoral, ischiofemoral and pubofemoral ligaments (Molini *et al.*, 2011). Additionally, the ligamentum teres physically joins the femoral head and acetabular cup together (Navarro-Zarza *et al.*, 2012).

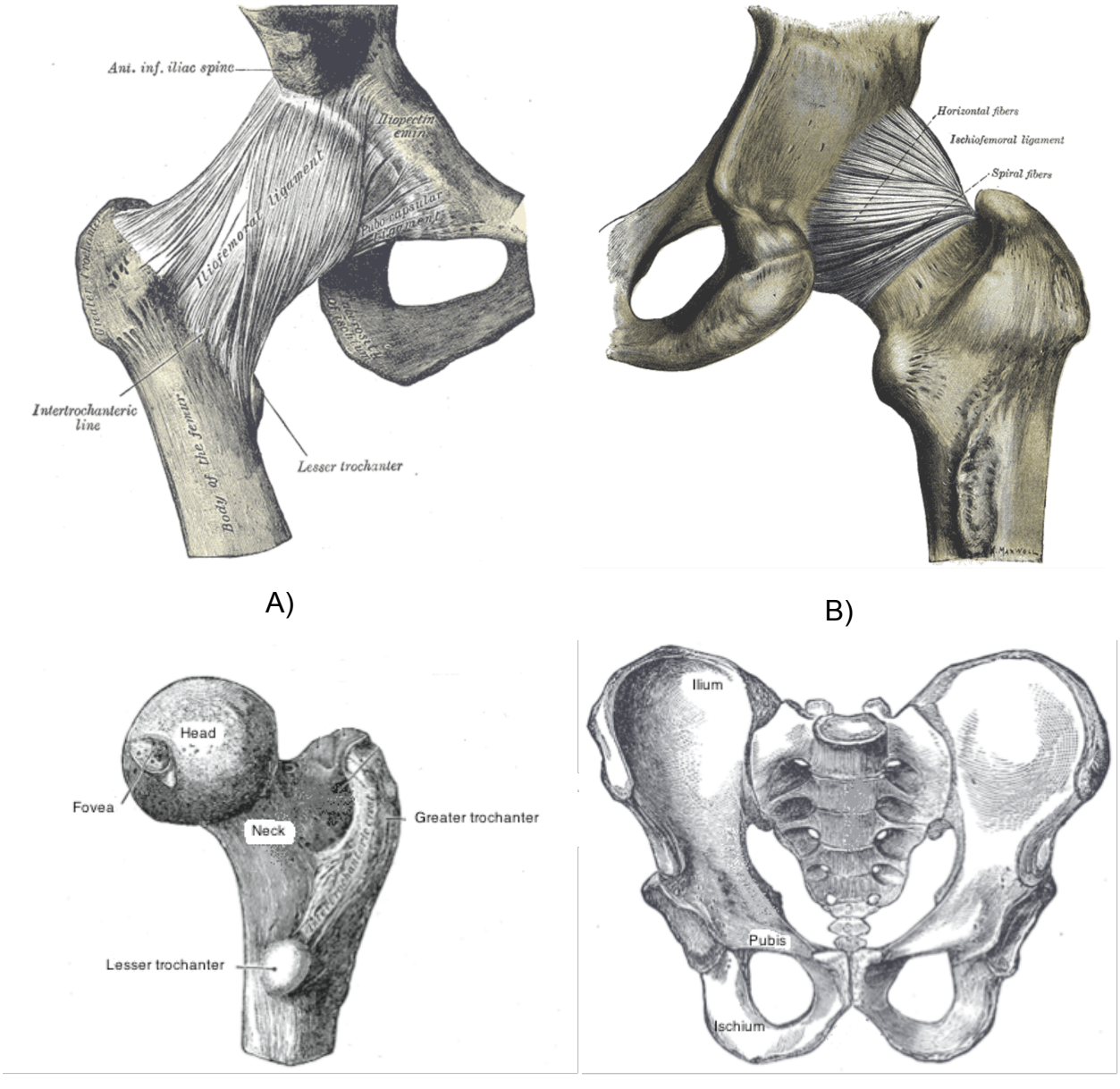

Figure 1.1 Anatomical diagrams of the hip joint adapted from Grays Anatomy: A) depicts the hip joint as found *in vivo* with the femoral head encased in the acetabular cup and capsule (composed of the iliofemoral and pubocapsular ligament) anterior view, B) depicts the hip joint as found *in vivo* with the femoral

head encased in the acetabular cup and capsule (composed of the ischiofemoral ligament) posterior view, C) depicts the femoral epiphysis and D) depicts the pelvis showing the convergence of the ilium, ischium and pubis bones to form the acetabulum (Gray, 2019a, 2019b, 2014a, 2014b).

1.3.2 Diseases and injuries of the hip

There are a multitude of conditions (Table 1.2) that can lead to the need to replace the hip joint with an artificial implant. Many are the result of age and deterioration over time. It should be noted that 88% of all hip replacements performed in 2016 were as a result of osteoarthritis (National Joint Registry, 2017). However, there are also some conditions that can affect patients of any age. Severe damage of the hip is debilitating and extremely painful for patients of any age. Initially, conditions may be managed with a variety of analgesics, such as paracetamol, and non-steroidal anti-inflammatory drugs (NSAIDs), such as ibuprofen and naproxen, alongside physiotherapy (Zhang *et al.*, 2016). Additionally, corticosteroids, such as hydrocortisone, may be injected into the joint to reduce inflammation and relieve pain (Zhang *et al.*, 2016). However, once these treatments begin to fail and pain levels increase, mobility decreases and the condition begins to severely impact upon the patient's quality of life, the patient may undergo hip replacement surgery, whereupon the affected joint is replaced with a synthetic biomaterial implant that mimics the mechanical activity and natural morphology of the joint.

Table 1.2 NJR data for 2016 indicating the reasons for hip replacement surgery and the percentage of patients associated with each (National Joint Registry, 2017).

Reason for surgery	% of total patients
Osteoarthritis	88
Femoral neck fracture	8
Avascular necrosis	2
Hip dysplasia/congenital dislocation	1
Inflammatory arthropathy	1
Chronic trauma	1
Metastatic cancer/malignancy	1
Previous surgery (non-trauma)	<1
Perthes disease	<1
Slipped Upper Femoral Epiphysis (SUFE)	<1

Failed hemiarthroplasty	<1
Skeletal dysplasia	<1
Previous infection	<1
Previous arthrodesis	<1
Other	1
Total (%)	100

1.3.3 Types of hip replacement

There are three types of hip replacement surgery that may be performed: hip resurfacing, hemi-arthroplasty and total hip replacement (THR). THR replaces both bearing surfaces with biomaterial implants, i.e. both the femoral head and the acetabular cup, whereas the hemi-arthroplasty only replaces one bearing surface and a hip resurfacing replaces the acetabular cup and caps the femoral head rather than replacing it fully.

THR is carried out by first dislocating the hip in order to remove the femoral head and neck. The acetabulum is then reamed to remove any osteophytes present, and (if using a cemented cup) the subchondral plate. The acetabulum is then lined with a synthetic biomaterial cup, often an insert within a cup, which may or may not be cemented into place. The medullary canal of the femur is opened up and a synthetic biomaterial femoral stem is implanted down the centre; either cemented or fixed biologically. The synthetic biomaterial femoral head is then attached to the stem (Petis *et al.*, 2015).

For a THR, there are four different types of fixation: cemented, uncemented, hybrid and reverse hybrid. A cemented THR consists of both a cup and stem cemented in place using polymethylmethacrylate (PMMA) whereas in an uncemented THR neither the cup or stem is cemented in place. Instead, they are either roughened, porous or coated with hydroxyapatite to promote bone growth up to and onto the implanted components to achieve biological integration (Tonino, Thèrin and Doyle, 1999). A hybrid THR consists of a cemented femoral stem coupled with an uncemented acetabular cup whereas a reverse hybrid THR consists of an uncemented femoral stem coupled with a cemented acetabular cup.

A hip resurfacing consists of a large cap, which covers the surface of the femoral head and is fixed in place with cement, and a matching material cup which lines the acetabulum. Until recently, hip resurfacing devices were only available with metal on metal (MOM) bearings; typically comprised of cobalt chromium alloy. However, recently, ceramic on ceramic (COC) hip resurfacings have been developed and are

beginning to become available clinically (Khan *et al.*, 2018). The hip resurfacing surgical procedure preserves bone stock, as it removes less femur to accommodate the cap, and was thought to be useful for patients under 60 years of age with healthy bone as it allowed for further revision surgeries later on. Additionally, the large femoral cap of the hip resurfacing reduces the likelihood of dislocation (Mont *et al.*, 2006). DePuy issued a recall of their MOM resurfacings, articular surface replacement (ASR), in 2010 due to early failure rates and very few MOM hip resurfacings are currently performed (Silverman, Ashley and Sheth, 2016).

1.3.4 Materials used in hip replacements

A THR can consist of five possible material combinations: ceramic on ceramic (COC), ceramic on metal (COM), ceramic on polyethylene (COP), metal on metal (MOM) and metal on polyethylene (MOP) (National Joint Registry, 2017). The femoral stem is made from metal with a metal or ceramic head whereas the acetabular cup can be made from metal, ceramic or polymer. MOP is the most common combination of materials used and therefore the present day gold standard; representing 87.1% of all cemented primary THRs and 30.4% of all primary THRs (National Joint Registry, 2017).

1.3.4.1 Metals

Metal alloys, a mixture of two or more elements of which one is a metal, are typically used in an orthopaedic context as pure metals are usually too soft, too brittle and too reactive, i.e. susceptible to corrosion. Creating metallic alloys allows the desirable characteristics of several metals or other elements to be combined into one optimal material. Initially, stainless steel was used, as in the original Charnley implant (Charnley, 1961), however, at present, cobalt chromium is the most common metal alloy used in hip implants; in particular femoral stems. Other metals, such as titanium, aluminium and vanadium, can be also found in metal femoral stems; these metals are too soft for use as a bearing surface (Moretti *et al.*, 2012). There is some debate as to whether wrought or cast metal alloys are better. Studies show that wrought alloys have increased tensile and fatigue strength, corrosion resistance and are lower wearing than cast alloys (Devine and Wulff, 1975; Medley *et al.*, 1996). The carbon content of metal alloys used in orthopaedics can also be varied; high (>0.2%) or low (<0.07%). Higher carbon content increases the hardness but reduces the ductility and increases the brittleness of the metal (Milosev *et al.*, 2009). As a result, metal-on-metal THA's have a very low wear rate; typically around 0.01 mm per year (Milosev *et al.*, 2009).

1.3.4.2 Ceramics

Ceramics are crystalline, inorganic materials. Ceramics are typically hard and strong

materials however their brittleness and inability to deform leads to an increased risk of fracture; particularly if there are any imperfections present on the ceramic surface or within the bulk structure (Traina *et al.*, 2013). Ceramics are the material closest to native bone in terms of their structure, high compression strength and inability to bend (Hannouche *et al.*, 2005). Ceramics produce very low volumes of wear debris; for example, a 12 year study by Jazrawi et al. (1999) found that ceramic on ceramic THA's had an average wear rate of 0.016 mm per year. There are two types of ceramic orthopaedic materials: alumina and zirconia. Zirconia is no longer currently used by itself however it is mixed with alumina to form a composite material, zirconia toughened alumina (ZTA) (Willmann, 1998).

1.3.4.3 Polymers

Polymers are the least hard material used in orthopaedic implants; they are less resistant to deformation than metals or ceramics. However, polymers exhibit a high level of toughness; they are able to absorb energy and exhibit plastic deformation before fracture occurs because they are viscoelastic and therefore ductile, which means they have the propensity to creep, i.e. deform over time due to mechanical stress (Bracco *et al.*, 2017). Polymers used in an orthopaedic context are typically chemically inert, i.e. they do not react directly with any chemical species in the body. The most common type of polymer used in orthopaedic implants is ultra-high molecular weight polyethylene (UHMWPE) which is commonly used in the acetabular cup component of THR's (Charnley, 1961; Ingham and Fisher, 2005). Metal-on-polyethylene THA's have a higher wear rate than MOM or COC; typically around 0.02 mm per year (Milosev *et al.*, 2009).

1.3.5 Failure and revision of hip replacements

There are a number of reasons why a hip replacement may fail (Table 1.4) and it is often a combination of these that leads to eventual revision surgery. The revision rates for all types of hip replacement gradually increases over time post-implantation (Table 1.3).

Table 1.3 Revision rates of primary hip replacements up to 13 years post-implantation (National Joint Registry, 2017).

Year(s) post-implantation of primary	Revision rate (%)
1	0.78
3	1.56
5	2.41
7	3.47

10	5.21
11	5.47
13	6.83

In the UK, there were 97, 341 revision surgeries performed between 2003 and 2016 (National Joint Registry, 2017). The most common reason for revision surgery was aseptic loosening which accounted for 50.1% of all revision surgeries between 2003 and 2016 (Table 1.4) (National Joint Registry, 2017). Dislocation/subluxation and pain tended to be the causes for early revisions whereas aseptic loosening tended to be responsible for revisions performed later (National Joint Registry, 2017). The risk of further revision surgeries once a revision has been performed is increased compared to revision rates for primary replacements (Table 1.5) (National Joint Registry, 2017).

Table 1.4 Reasons for primary hip revisions between 2003 and 2016 according to the National Joint Registry 14th Annual Report. Note that the percentages do not add up to 100% as revisions are often multifactorial and the reasons for them not mutually exclusive (National Joint Registry, 2017).

Reason for revision	Percentage of revisions (%)
Aseptic loosening	50.1
Pain	20.5
Lysis	15.4
Dislocation/subluxation	15.2
Implant wear	14.1
Periprosthetic fracture	10.1
Other indication	7.6
Malalignment	5.6
Implant fracture	3.6
Infection	3.5
Head-socket (size) mismatch	0.8
Adverse reaction to particulate debris	11.0

Table 1.5 Post-implantation re-revision rates following first revision hip replacement (National Joint Registry, 2017).

Year(s) post-implantation of revision	Re-revision rate (%)
1	4.95
3	8.98
5	11.74

1.4 Inflammation, osteolysis and aseptic loosening

Any biomaterial, such as a THR, is perceived by the body as a threat and elicits a foreign body response whereupon the immune system attempts to eject or neutralise the foreign matter. This process can cause problems for the biocompatibility of joint replacements and can lead to their failure.

The body can respond to a foreign body in two ways: the innate and adaptive immune responses. The innate immune response is non-specific but is able to respond immediately whereas the adaptive response is specific to the foreign body encountered but occurs after several days. A foreign body is defined as any material, biological or synthetic, that is non-self; for example, bacteria, viruses and fungi as well as medical implants and scaffolds. The response to the joint replacement is also size dependent: the response to the bulk implant and large wear debris (>10 μm) differs from the response to smaller wear debris (0.1 – 10 μm) and ions.

1.4.1 Innate immune response: inflammation

The innate immune system responds to a THR by initiating inflammation which proceeds in four stages: initial events, cellular invasion, tissue remodelling and resolution.

Initial events

When the THR is implanted, the surgery breaches the skin and mucosal epithelia and triggers inflammation. Initially platelets and the complement system are activated which initiated vasodilation. The products of the complement system (complement proteins such as C5a) attract neutrophils and mononuclear phagocytes to the implant site. The mononuclear phagocytes secrete pro-inflammatory cytokines, such Tumour Necrosis Factor – Alpha (TNF-α), Interleukin-1β (IL-1β) and Interleukin-6 (IL-6), and chemokines, such as Interleukin-8 (IL-8) (Nich, Goodman and Hospital, 2014). Chemokines attract more leukocytes to the implant site whereas cytokines stimulate vasodilation during cellular invasion and activate leukocytes (Janeway *et al.*, 2001).

Cellular invasion

The permeability of the local blood vessel walls increases, which allows the extravasation of leukocytes, such as monocytes and neutrophils, and plasma, containing complement proteins, from the blood to the periprosthetic tissue. A decreased blood flow rate and the upregulation of adhesion molecules, such as Lymphocyte Function-associated Antigen 1 (LFA-1), allows the transient adhesion of leukocytes to the blood vessel walls. Extravasation and diapedesis then occur – this is where the leukocytes move from the blood vessels into the affected tissue. Complement proteins, proteins complementary to phagocytes that are carried in the plasma, coat the foreign material in a process called opsonisation and mark it for destruction by phagocytosis (Janeway *et al.*, 2001). Phagocytes recognise the opsonised foreign material as non-self and attempt to phagocytose it. Additionally, in order to aid the destruction of the foreign body, neutrophils undergo a process called oxidative burst; the release of highly reactive oxygen species to aid chemical destruction.

However, THR's are non-biodegradable and cannot be destroyed by phagocytosis. This results in the continuous activation of macrophages as they continue to release cytokines to recruit further leukocytes to the implant site. The macrophages become frustrated as they are unable to phagocytose the implant and fuse together to form foreign body giant cells; multi-nucleated cells with large vacuoles. The foreign body giant cells coalesce together to form granulomatous tissue which encapsulates the THR from the rest of the body (Anderson, Rodriguez and Chang, 2008). Necrosis of the local tissue may occur when macrophages adhere to the implant and destroy the tissue surrounding it. Additionally, necrobiosis can occur if macrophages become epitheloids which secrete enzymes to destroy the surrounding extracellular matrix (Craig *et al.*, 2017).

Tissue remodelling

The body attempts to heal the implant site by remodelling the tissue. Cytokines produced by macrophages attract mesenchymal and endothelial cells to the implant site. Endothelial cells revascularise the implant site which allows the infiltration of other cell types to the affected area. The extracellular matrix is reformed by collagen and proteoglycans produced by the mesenchymal cells. Granulation tissue, i.e. fibrous connective tissue, then forms to encapsulate the implant which is later replaced by scar tissue during fibroplasia (Anderson, Rodriguez and Chang, 2008). The scar tissue exhibits abnormal biomechanical and biological properties (i.e. it is stiffer and less elastic) and possesses a disordered matrix.

Resolution

Finally, the body attempts to extrude, resorb, integrate or encapsulate the material to return to its normal state. Extrusion and resorption are not possible for a THR as implantation is too deep and the implant is not biodegradable respectively. Some integration is possible with hydroxyapatite coated titanium alloy femoral stems (Tonino, Thèrin and Doyle, 1999) which allows bone to grow up to and onto the implant to biologically fix it in place. Encapsulation is the usual resolution for THR's. The body compromises and tolerates the presence of the implant by "walling" the implant off from the rest of the body with fibrotic scar tissue which increases in thickness over time (Ingham and Fisher, 2000).

1.4.2 Adaptive immune response

The adaptive immune system requires several days in order to respond specifically to the foreign body. For pathogens, once the macrophage has phagocytosed the pathogen, it presents the foreign antigens on its surface and migrates to the lymph node. Here, the now antigen-presenting cell attaches the foreign antigen to the major histocompatibility complex (MHC) II and presents them to the T-cell receptors (Janeway *et al.*, 2001). This presentation stimulates the clonal expansion of T-helper cells with foreign antigen specific receptors and T-helper cells release cytokines, which stimulate the production of antibodies against the foreign antigen by B cells (Janeway *et al.*, 2001). Antibodies allow the specific targeting of the foreign material by their specific antigens and label them for destruction by phagocytosis. A small number of memory B cells remain that are primed to produce the necessary antibody to the foreign antigen, allowing a more rapid and effective response upon reinfection (Janeway *et al.*, 2001). As an implant expresses no antigens, it is unaffected by the adaptive immune response except in cases where metal THR's induce an allergic response.

1.4.3 Allergic Response

Nickel (Ni) and chromium (Cr) ions from metal THR components may induce a type IV hypersensitivity reaction (Granchi *et al.*, 2012) through interaction with peptides in the body to form antigens. These antigens form a complex with MHC II and the adaptive immune response proceeds, producing antibodies against the metal ions. Targeted cells are destroyed by CD4+ T cells and continued macrophage activation forms foreign body giant cells and granulomatous tissue which can result in the formation of pseudotumours (Bergschmidt, Bader and Mittelmeier, 2012).

1.4.4 Biological response to wear particles and ions

In addition to the body responding to the bulk implant, the body will also produce an immune response to the wear particles shed by the implant. The biological response

to wear debris varies based on the type of material the wear debris is composed of and the size of the wear particles.

1.4.4.1 Metals

Metal THR's generate wear debris but are also susceptible to galvanic corrosion (Tipper *et al.*, 2005). Different metals establish an electrochemical potential difference; rapidly corroding the more reactive metal, which sheds metal ions into the surrounding tissue. Wear debris may be generated when a metal-on-metal contact point occurs, which results in rapid wear if there is a size mismatch between components or the angle between components is sub-optimal. Metal wear particles can also release further metal ions into the surrounding tissue (Brown, Fisher and Ingham, 2006). Metal wear particles are typically below 100 nm and so do not typically induce inflammation or osteolysis, both of which are size-dependent, but their size allows them to be taken up passively by surrounding cells via endocytosis and pinocytosis (Brown, Fisher and Ingham, 2006). Cobalt chromium alloys are the most common metal used in THR's and release both cobalt (Co) and chromium (Cr) ions. Although necessary for cellular function, cobalt ions at high concentrations (328.5 parts per billion in patient blood levels) become cytotoxic; they cause swelling and oxidative stress in the mitochondria and abnormal changes in the nuclear envelope (Goode *et al.*, 2012). Additionally, at high concentrations, both cobalt and chromium (136 parts per billion in patient blood levels) ions are genotoxic and can cause DNA damage (Brown, Fisher and Ingham, 2006). DNA damage can generate mutagenic cells and may lead to cancer if the mutagenic cells are not apoptosed; mitochondrial oxidative stress impacts apoptosis. Metal wear particles may also lead to the formation of pseudotumours; an inflamed tissue mass, consisting of local soft tissue necrosis, granulomatous tissue and the presence of macrophages and lymphocytes, surrounding the implant (Pandit *et al.*, 2008a). There is significant patient variation in the pseudotumour symptoms experienced; some may go unnoticed and be detected only through routine imaging or some may cause high levels of damage and pain, resulting in a revision of the THR (Pandit *et al*, 2008b). Pseudotumour formation may be related to metal hypersensitivity (Granchi *et al.*, 2006).

1.4.4.2 Ceramics

Ceramic THR's have lower wear rates and produce lower volumes of wear debris than metal or polymer THR's (Dorlot, Christel and Meunier, 1989). Ceramic wear debris appears to be well tolerated by the body (Niche *et al.*, 2003). Ceramic wear debris has been shown to be less cytotoxic (Germain *et al.*, 2003), is less likely to stimulate the production of osteolytic cytokines (Catelas *et al.*, 1999) and induce less inflammation in the periprosthetic tissue (Nizard *et al.*, 1992).

1.4.4.3 Polymers

UHMWPE wear particles vary greatly in size; from several millimetres to nanometres. Large particles, >10 μm, are walled off by foreign body giant cells and granulomatous tissue (Ingham and Fisher, 2000). The majority of UHMWPE wear debris was previously found to be between 0.1 – 10 μm, which is within the phagocytosable size range, and able to be engulfed by the local macrophages (Green *et al.*, 1998; Matthews *et al.*, 2001). However, a more recent study by Richards *et al.* (2008), analysing tissue samples from seven failed Charnley hip prostheses, have found the majority of UHMWPE wear debris to be between 0.1 – 0.99 μm. As UHMWPE is chemically inert, the macrophages are unable to digest the wear particles and inflammation persists. Particles between 0.1 – 1 μm activate macrophages which then participate in the downstream signalling cascade that results in osteolysis and aseptic loosening. A review by Dumbleton *et al.* (2002) analysed several publications regarding the link between UHMWPE wear rates and osteolysis and found the threshold necessary for osteolysis to occur is a wear rate of more than 0.1 mm per year. The activated macrophages continuously attempt to phagocytose the material and continue to produce pro-inflammatory cytokines and chemokines which result in an influx of further macrophages. The continued release of pro-inflammatory and osteolytic cytokines, such as TNF-α, IL-1β and IL-6, and other inflammatory mediators, such as prostaglandin E2 (PGE_2), results in the activation of osteoclasts and stimulates osteoclasts to resorb the bone surrounding the implant, i.e. osteolysis (Ingham and Fisher, 2005). Osteolysis loosens the fixation between the prosthesis and the surrounding bone , i.e. aseptic loosening, which leads to implant failure and revision surgery.

Tipper *et al.* (2000) carried out a retrieval study on 18 failed acetabular cups; failure was caused by osteolysis and aseptic loosening. This study showed that the majority of UHMWPE wear debris retrieved was between 0.1 – 0.5 μm and that large particles (>10 μm) made up the minority of the particle numbers despite representing a large volume of the total particles (Tipper *et al.*, 2000). Green *et al.* (1998) found that Ceridust® particles between 0.3 and 10 μm were the most biologically active and stimulated the production of inflammatory cytokines, TNF-α, IL-1β and IL-6, in murine peritoneal macrophages. Similarly, Matthews *et al.* (2001) found that Ceridust® particles between 0.1 – 1 μm stimulated the highest production of inflammatory cytokines; TNF-α, IL-1β, IL-6, Granulocyte-Macrophage Colony-Stimulating Factor (GM-CSF) and Prostaglandin E2 (PGE_2) in human peripheral blood mononuclear cells (Matthews, Green, *et al.*, 2000). Additionally, higher volumes of particles to cell numbers (100:1 and 10:1) produced more inflammatory cytokines in PBMNC's than 1:1 and 0.1:1 particle volumes to cell numbers ratios (Green *et al.*, 1998; Matthews *et*

al., 2000b). However, Liu *et al.* (2015) found that nanometre sized UHMWPE particles, unlike micrometre sized UHMWPE particles, did not induce significantly elevated inflammatory and osteolytic cytokines and chemokines (TNF-α, IL-1β, IL-6 and IL-8) in PBMNC's after 12 and 24 hours.

Bone remodelling

Bone remodelling is a normal process in the body; occurring constantly. Bone remodelling is a two stage process: firstly, old bone is resorbed by osteoclasts and secondly, new bone is formed by osteoblasts. This process is mediated by osteocytes which release hormones into the bone microenvironment and detect strain. Bone remodelling also controls the calcium serum levels in the body. Bone remodelling can be affected by how the skeleton is loaded; increased loading leads to increased bone formation and decreased loading leads to increased bone resorption (Proff and Römer, 2009). Additionally, factors such as age, gender and disease can affect the balance of bone formation versus resorption. A common example of this is osteoporosis as described in Section 1.3.2.1.

Osteoclastogenesis

Osteoclasts are derived from myelopoietic progenitor cells, which are originally derived from haematopoietic stem cells (HSC's), through a four stage process; commitment, differentiation, multinucleation and activation (Yavropoulou and Yovos, 2008). The myelopoietic progenitor cell initially forms a granulocyte-macrophage colony forming unit (GM-CFU) (Menaa, Kurihara and Roodman, 2000). The first stage, commitment, begins with the promotion of an osteoclastic lineage via various transcription factors within the GM-CFU; such as PU.1 (Laslo *et al.*, 2006), Microphthalmia-associated transcription factor (MITF) and c-FOS (Miyamoto *et al.*, 2001). The surrounding microenvironment, consisting of osteoblasts and stromal cells, plays a vital role in osteoclastogenesis also. Cell-to-cell contact between the pre-osteoclast cells and surrounding microenvironment is essential for the various signalling pathways involved during osteoclastogenesis. Local macrophages initially produce macrophage colony stimulating factor (M-CSF) which allows the preosteoclast cells to enter the cell cycle so they may proliferate – the production of M-CSF is upregulated by TNF-α and IL-1 during inflammation (Weir *et al.*, 1996). The second stage, differentiation, is triggered by the production of Receptor Activator of Nuclear factor Kappa-B Ligand (RANKL) by bone cells, osteoblasts, osteoclasts and osteocytes, which is also upregulated by TNF-α and IL-1 (Wei *et al.*, 2005), which binds to the Receptor Activator of Nuclear factor Kappa-B (RANK) receptor expressed on the surface of the pre-osteoclast. This triggers an intracellular signalling cascade which results in the expression of osteoclastic genes such as Cathepsin K (Matsumoto *et al.*, 2004) and Tartrate-Resistant Acid Phosphotase (TRAP) (Kim *et al.*,

2005). This process is regulated by osteoprotegerin (OPG) which binds to RANKL and inhibits the differentiation of osteoclast precursor cells (Yavropoulou and Yovos, 2008). The third stage, multinucleation, is triggered by the binding of RANKL to the RANK receptor on a preosteoclast. Two RANK positive (RANK+) mononuclear cells fuse and the RANKL signal is transferred; propagating the signal. The now binucleated cell becomes the master fuser cell and fuses with another RANK+ cell; continuing the multinucleation process (Kim, Day and Morrison, 2005; Vignery, 2005; Kim and Kim, 2006). The final stage, activation, is established through the creation of two polarised structure within the cell membrane; the ruffled membrane and the sealing zone; an actin ring-like structure which isolates the bone resorption environment from the general extracellular space. Cell-extracellular matrix adhesion is facilitated by integrins, αvβ3 and RGD, which are also expressed and bind to osteopontin and bone sialoprotein (Teitelbaum, 2006).

Osteolysis and aseptic loosening

Chemokines attract the newly-formed osteoclasts which migrate to the site of bone resorption (Han *et al.*, 2014). The osteoclasts then bind to the bone; the osteoclastic cell membrane contains integrins, αvβ3 and RGD, which can bind to osteopontin and sialoprotein expressed on the surface of bone. Once the bone resorption pit has been separated from the surrounding environment, H^+ ions (Holliday *et al.*, 2005) and various digestive enzymes are secreted by osteoclasts, such as Cathepsin K (a collagenase I enzyme) (Costa *et al.*, 2011) and matrix metalloproteinases (Inada *et al.,* 2003). The combined effect of acidifying the bone resorption pit (via H^+ ions) and digesting the bone matrix enzymatically results in the dissolution of bone in the resorption pit. This process occurring around a prosthesis results in the loosening of the fixation of the prosthesis, i.e. aseptic loosening, and will ultimately result in the revision of the implant.

1.5 Ultra-high molecular weight polyethylene

UHMWPE was developed as a bearing material with a metal femoral head by Charnley in 1962. Metal on polyethylene THR's are the present day gold standard.

1.5.1 Chemical, mechanical and physical properties of UHMWPE

Ultra-high molecular weight polyethylene (UHMWPE) is linear homopolymer of ethylene, i.e. it contains only one type of monomer repeated in a linear chain (Figure 1.2 A and B). There are four types of polyethylene: low density polyethylene (LDPE), linear low density polyethylene (LLDPE), high density polyethylene (HDPE) and UHMWPE. UHMWPE differs from other types of polyethylene by its molecular weight; LDPE and LLDPE are typically <50,000 $g.mol^{-1}$ and HDPE is typically around 200,000

g.mol^{-1} whereas UHMWPE ranges between 2 and 6 million g.mol^{-1}; for example, GUR 1020 UHMWPE has a molecular weight of around 2 million g.mol^{-1} and GUR 1050 UHMWPE has a molecular weight of around 5 million g.mol^{-1} (Kurtz, 2004a). The hydrocarbon polymer chain is capable of rotating around the carbon-carbon bonds to form ordered crystalline sheets known as lamellae and disordered amorphous regions; both of which are linked by tie molecules (Figure 1.2C). The lamellae are typically between 10 and 50 nm thick and between 10 and 50 µm long (Kurtz *et al.,* 1999) with spaces of approximately 50 nm between (Bellare, Schnablegger and Cohen, 1995). The higher the degree of crystallinity, the greater its mechanical properties, i.e. creep resistance, high elasticity, higher yield strength and higher fatigue strength (Brach Del Prever *et al.*, 2009).

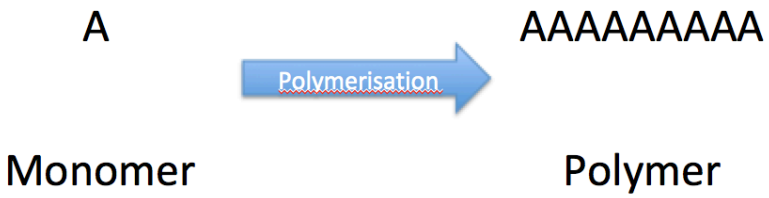

A)

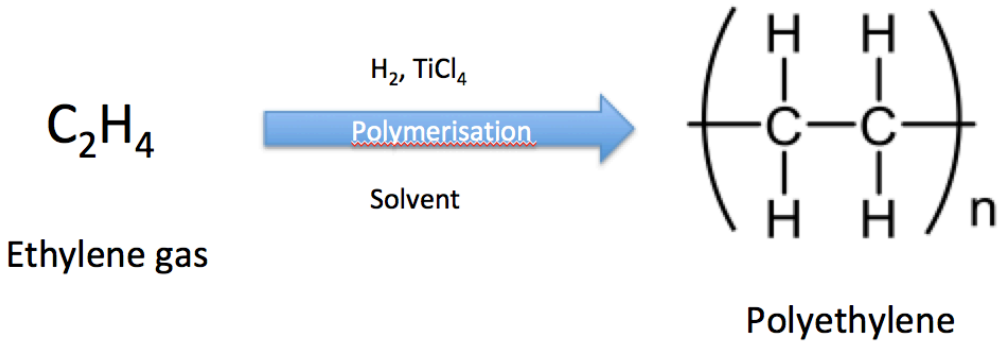

B)

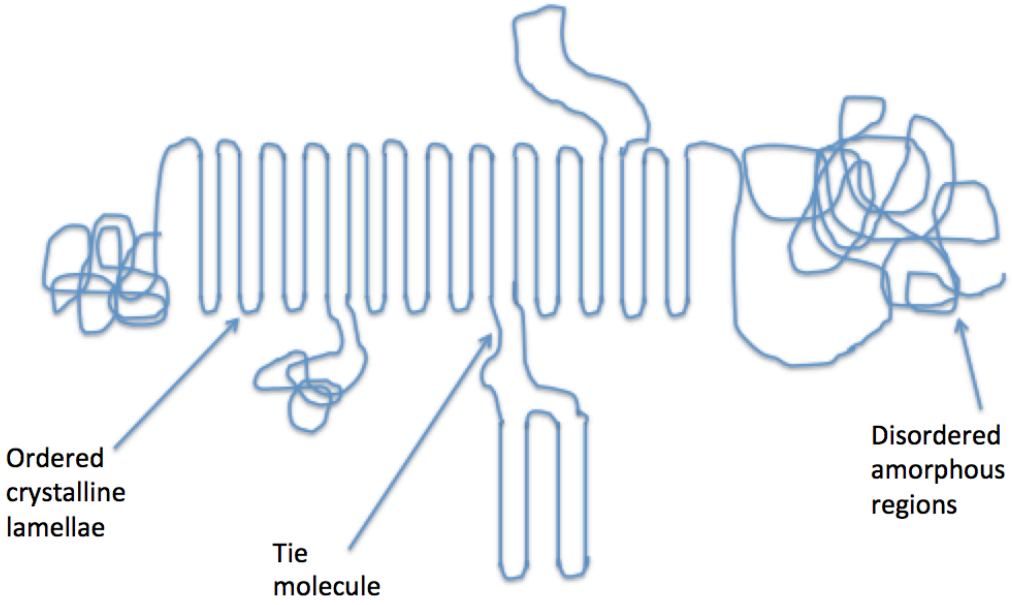

C)

Figure 1.2 Polymerisation of UHMWPE:A) polymerisation of monomer to form linear homopolymer, B) polymerisation of ethylene to form UHMWPE and C) Physical structure of UHMWPE showing ordered crystalline lamellae, disordered amorphous regions and tie molecules.

Polymers, such as UHMWPE, behave in a temperature dependent manner and as such are defined by their glass transition temperature (T_g), melting temperature (T_m) and flow transition temperature (T_f) measured using differential scanning calorimetry (DSC) (Table 1.6). T_g is defined as the temperature at which the polymer become brittle, T_m is defined as the temperature at which most crystalline regions of the polymer have melted and T_f is defined as the temperature at which the polymer becomes liquid and flows. Because UHMWPE has a molecular weight of over 500,000 $g.mol^{-1}$, the chain entanglement prevents this and UHMWPE exhibits no flow transition temperature (Kurtz, 2004a). Additionally, the increased molecular weight affects the mechanical properties of UHMWPE. UHMWPE demonstrates increased abrasive wear resistance and impact strength (Table 1.6) (Kurtz, 2004a).

Table 1.6 Table of the mechanical and chemical properties of UHMWPE (Edidin and Kurtz, 2000; Kurtz, 2004a)

Mechanical and chemical properties	UHMWPE
Mw ($g.mol^{-1}$)	2 -6 million
T_g (°C)	-160
T_m (°C)	125 - 138
Poissons ratio	0.46

Specific gravity	0.932 – 0.945
Tensile modulus of elasticity (GPa)	0.8 – 1.6
Tensile yield strength (MPa)	21 - 28
Tensile ultimate strength (MPa)	39 – 48
Tensile ultimate elongation (%)	350 - 525
Impact strength (Izod)	>1070 – no break
Degree of crystallinity (%)	39 - 75

1.5.2 Manufacturing of UHMWPE

UHMWPE is synthesised and manufacturing in a three stage process: polymerisation, consolidation and machining with specific details of each process being proprietary to each company (Kurtz, 2004b). In the first stage, ethylene gas is passed over a titanium tetrachloride catalyst in the presence of hydrogen gas in a reaction known as the Ziegler process (Birnkraut, 1991). This process was first developed at the Max-Planck Institute and commercialised by Ruhrchemie (changed to Hoechst and now known as Ticona) in the 1950's. The types of UHMWPE resin produced this way are designated type 1 (GUR 1020), type 2 (GUR 1050) and type 3 (1900H). Each resin differs by the size and morphology of its particles (Kurtz, 2004b). Each resin also differs, according to the standards ASTM F648 and ISO5834-1, by the mass of trace impurities present (types 1 and 2 contain less than type 3). Type 3 1900H UHMWPE is no longer produced, although stockpiling means Biomet are still machining implants from this resin. This material was not used in this study and will not be elaborated on further. Labelling type 1 and 2 resins follows a particular format. For example, GUR 1020 is broken down as follows: G (granular) U (UHMWPE) R (Ruhrchemie) 1 (weight of resin) 0 (presence or *absence* of calcium stearate) 2 (Mw average) 0 (Hoechst internal code designation). Calcium stearate was an additive until the late 1990's to act as a residual catalyst scavenger. (Kurtz, 2004b)

The UHMWPE resin produced is then consolidated by one of four methods: compression moulding, ram extrusion, hot isostatic pressing and direct compression moulding. Because UHMWPE does not flow, standard thermoplastic processing methods, i.e. melting, are unable to be used. Consolidation works by thermally activating polymer chains (high temperature) and increasing the proximity of the polymer resin particles (high pressure) over time to allow neighbouring polymer chains to entangle (self diffusion). Compression moulding uses a press to create sheets, although these are then often turned into rods and other shapes, whereas ram extrusion feeds powder into a heated mantle and is then extruded by a hydraulic ram

to create rods. GUR 1020 is typically compression moulded whereas GUR 1050 is typically ram extruded although this is not always the case. Hot isostatic pressing of ArCom™ UHMWPE involves creating a cylinder of UHMWPE using cold isostatic pressing following by sintering in a furnace whilst in a sealed argon pouch. Direct compression moulding, rather than pressing into a sheet, pressed the resin into its final shape, e.g. an acetabular cup, so no machining step is needed. Each consolidation method produces slight differences in morphology, mechanical and material properties but there is no consensus at present as to which method is superior (Kurtz, 2004b).

The UHMWPE material is then machined, e.g. into an acetabular cup (Kurtz, 2004b). The material is milled and turned followed by roughing and finishing. Occasionally, the material is preshaped or preformed to save time on this step (Kurtz et al., 1999). Machining may leave macroscopic asperities on the surface of UHMWPE which contribute to the initial difference in surface roughness between a UHMWPE acetabular cup and a metal femoral head. Initial wear rates in MOP THR's remove the macroscopic asperities on the UHMWPE surface whereas long term wear is controlled by the microscopic asperities on the metal surface (Cooper, Dowson and Fisher, 1993).

1.5.3 Sterilisation and long term storage of UHMWPE

Once the UHMWPE orthopaedic components have been manufactured and machined, they are then packaged and sterilised. Sterilisation is carried out in order to eliminate any biological contamination that could lead to infection or early implant failure. Initially, UHMWPE components were gamma irradiated (25 – 40 kGy) in air in gas permeable packaging (Isaac, Dowson and Wroblewski, 1996). This method was discontinued due to the oxidation degradation of the polymer during long term storage, caused by persistent free radicals, which result in the loss of mechanical properties of the polymer (Jahan *et al.*, 1991; Premnath *et al.*, 1996). Gamma irradiation of UHMWPE is now carried out in barrier packaging to block gas diffusion. The packaging is first evacuated of existing air and then be backfilled with an inert gas such as argon or nitrogen or simply placed under vacuum (with or without an oxygen scavenger). This minimises oxidative degradation whilst in long term storage. Some crosslinking of UHMWPE occurs when irradiated which may result in lower wear rates of components sterilised this way when compared to other methods (McKellop *et al.*, 1999). UHMWPE components may also be sterilised with ethylene oxide or gas plasma in gas permeable packaging to allow the sterilising medium contact with the polymer. Ethylene oxide is highly toxic and therefore effective at eliminating bacterial, fungal and viral contamination. Similarly, gas plasma, either peracetic acid or hydrogen peroxide eliminates biological contamination (Feldman and Hui, 1997). Both

methods work by diffusing into the surface layers of the polymer and then diffuse out again. Neither method binds the molecules to the surface of the polymer and so do not change the properties of the polymer nor have a negative effect *in vivo*. As with manufacturing methods, there is a lack of consensus as to which sterilisation method is superior.

UHMWPE orthopaedic components are then stored in their packaging until implanted. In Europe, this shelf life has been standardised to no more than 5 years whereas in the USA there is no standard for the maximum shelf life (Kurtz, 2004c).

1.5.4 Assessing the mechanical performance of UHMWPE

1.5.4.1 Generation of wear debris

In order to assess the mechanical performance of different UHMWPE materials, UHMWPE wear debris can be artificially generated using hip simulators or wear simulator rigs. A hip simulator is a rig that uses implant components, both the femoral stem head and acetabular cup, and carries out cycles of movement, based on typical walking gait and the kinetics and kinematics experienced within the hip joint, accelerated over a shorter period of time. Several years of use of an implant can be simulated in a matter of weeks; one million cycles is typically equivalent to one year of activity. This method produces clinically relevant wear debris due to anatomically accurate mechanics and the use of implant components (Barbour, 1999; Tipper et al., 2006). Simpler wear simulator rigs, such as pin on plate (Lancaster *et al.*, 1997; Galvin *et al.*, 2006), pin on disc, ring on flat or crossed cylinders (Affatato *et al.*, 2008), use a simplified, but still multidirectional, set up under kinematic conditions based on those experienced within the hip joint to produce clinically relevant wear debris. It is possible to use either a smooth or rough plate in the rig – a smooth plate is representative of the clinical *in vivo* situation as it mimics the surface roughness of the implant whereas a rough plate is artificially scratched in order to increase friction and therefore the amount of wear debris produced. The wear debris produced is clinically relevant in both cases however the amount of biologically active wear debris produced i.e. between 0.1 – 10 μm in size is increased when a rough counterface is used (Endo *et al*, 2001; Ingram *et al.*, 2004). Additionally, the pin and plate are submerged in lubricant. This can be a number of different things such as water or cell culture medium (typically RPMI 1640 cell culture medium), which can contain 25% (v/v) FBS and/or sodium azide. The lubricant is designed to mimic the natural synovial fluid present in the joint and therefore provide as close to natural a lubrication regime as possible. The use of cell culture medium supplemented with FBS is considered the most accurate as it mimics the protein corona found on wear debris retrieved from periprosthetic tissue. The body naturally coats the UHMWPE wear debris in a layer of proteins from the extracellular tissue fluid and this affects how the body interacts with

and responds to the particles (Scholes and Unsworth, 2006). Sodium azide is used in mechanical studies to prevent infection in the lubricant however it is highly toxic to cells so debris created in this way cannot be cultured with cells.

1.5.4.2 Wear debris isolation

Once UHMWPE wear debris is generated, it must then be isolated from the lubricant in which it has been produced (or from cadaveric periprosthetic tissue or synovial fluid) (Wolfarth *et al.*, 1997) (ASTM F561) in order to characterise it in terms of size and volume distribution using field emission gun scanning electron microscopy (FEGSEM). The presence of lipids, proteins and salts in the lubricant or natural tissue/fluid would make characterisation incredibly difficult and therefore the particles must be isolated. The tissue or lubricant/synovial fluid must first be digested either chemically using acidic (hydrochloric (Margevicius *et al.*, 1994) or nitric acid) or basic conditions (sodium or potassium hydroxide) (Baxter *et al.*, 2009) or enzymatically (using Proteinase K) (Baxter *et al.*, 2009), papain, protease or collagenase (Campbell *et al.*, 1996) in order to remove any proteins present. It is useful to be able to digest periprosthetic tissue and synovial fluid because clinically relevant material is directly yielded from a patient or animal model however the volume of particles recovered is poor which is a severe limitation. There is significant variation in the effectiveness of the different digestion methods available. Enzymatic methods are typically less efficient than chemical methods as they do not digest and remove all the tissue present, and by extension; all the lipids, proteins and salts, in the sample. Of the chemical methods, sodium or potassium hydroxide and nitric acid appear to be the most effective (Baxter *et al.*, 2009) however care must be taken with the concentrations used in order to preserve the surface morphology of the particles and not destroy the polycarbonate filters used for filtration. Both chemical and enzymatic methods of isolation are time consuming as the chemicals can require several days to work effectively. Tipper *et al.* (2000) selected potassium hydroxide as the most efficient chemical digestion step and developed the remainder of the isolation method used in this study (Tipper *et al.*, 2000). Upon completion of protein digestion with potassium hydroxide, Tipper *et al.* (2000) used a mixture of chloroform and methanol to extract any lipids present via chemical separation. Tipper *et al.* (2000) then used ice-cold ethanol to precipitate any remaining proteins before diluting with ultrapure water, centrifuging and filtering the supernatant into the requisite sizes prior to imaging using FEGSEM and analysis using Image proPlus. This method has been in continuous use at the Institute of Medical and Biological Engineering at the University of Leeds (Howling *et al.*, 2001; Richards *et al.*, 2008).

1.5.5 Clinical, wear and biological performance of virgin UHMWPE in hips

UHMWPE produces the greatest volume of wear debris in comparison to metal and

ceramic materials as it is typically articulated against metal or ceramic components; both of which are considerably harder than a comparatively soft polymer therefore the increased friction leads to the production of wear debris. Typical *in vitro* wear rates for virgin (i.e. non-cross-linked) UHMWPE are around 50 mm^3 per million cycles (Endo *et al.*, 2002). *In vivo* wear rates vary greatly; between 2 to 226 $mm^3.year^{-1}$ (Martell, Berkson and Jacobs, 2000). It is widely believed that UHMWPE wear debris is responsible for osteolysis, and in turn aseptic loosening, which is the cause of 50% of all revision surgeries (National Joint Registry, 2017).

Friction based wear between articulating joint prostheses components is influenced by factors such as angle of implantation, femoral head size vs. acetabular cup size (size mismatching the components) (Brown, Fisher and Ingham, 2006), surface roughness (rougher surfaces create more wear debris) (Kurtz *et al.*, 1999) and differences in materials used, i.e. metal vs. polyethylene (difference in toughness and difference in surface roughness). Studies on wear debris production in MOP hip implants have shown that wear debris produced in the short term is caused by macroscopic asperities (imperfections) on the UHMWPE component surface and wear debris produced in the long term is caused by microscopic asperities on the metal component surface (Cooper, Dowson and Fisher, 1993). A retrieval study of UHMWPE wear debris from Charnley prostheses showed that virgin UHMWPE wear debris ranged in size between 0.1 μm and >1000 μm and particles over 10 μm formed the largest volume of particles however most particles were within the range of 0.1 – 0.5 μm (Tipper *et al.*, 2000). Tipper *et al.* (2000) found that the retrieved particles displayed a range of morphologies including platelet-like, fibril-like, small granules and aggregated particles. Other studies have confirmed that virgin UHMWPE wear particles are typically between 0.1 and 1.0 μm in size (Wu, Peng and Tipper, 2013).

1.6 Modifications and optimisations of UHMWPE material

There are a number of modifications to UHMWPE that can improve their functionality and longevity in a joint replacement. The most common modifications include cross-linking and antioxidant doping.

1.6.1 Cross-linking

In order to reduce the volume of wear particles produced by UHMWPE *in vivo*, UHMWPE can be cross-linked using gamma irradiation in an inert atmosphere (such as nitrogen or argon). This radiolytically breaks the carbon and hydrogen bonds; creating alkyl free radicals which recombine and crosslink the polymer chains to one another (via covalent bonds) creating a network (Figure 1.3). Cross-linking improves the material's resistance to wear thus generating lower volumes of wear particles

compared to non cross-linked material. The level of radiation can be varied to acquire different levels of cross-linking; common doses include 10 MRad, 8 MRad, 5 MRad and 2.5 MRad although this varies between companies and is often proprietary (Galvin *et al.*, 2006). UHMWPE is described as moderately cross-linked at 2.5 MRad whereas UHMWPE is described as highly cross-linked with a radiation dose of between 5 and 10 MRad.

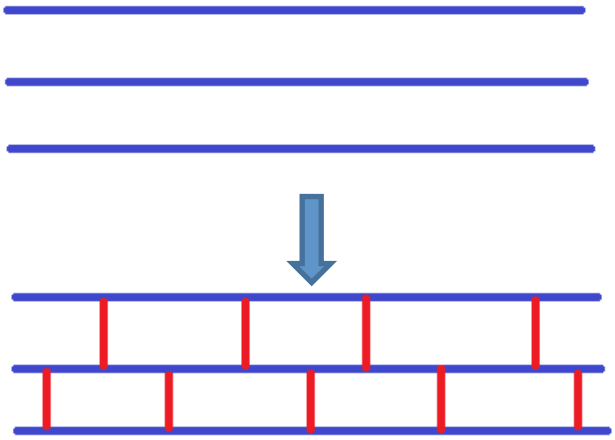

Figure 1.3 Covalently linked UHMWPE polymer chains to form a network; UHMWPE chains shown in blue and covalent bonds shown in red.

Cross-linked UHMWPE produces a smaller volume of wear debris, typically an 80% reduction, than virgin UHMWPE i.e. UHMWPE that has not been cross-linked or modified in any way (Popoola *et al.*, 2010). The wear particles themselves are also smaller, which are more biologically active compared to the larger particles produced by virgin UHMWPE (Endo *et al.*, 2001). The volume of cross-linked UHMWPE wear debris is significantly decreased compared to virgin UHMWPE (35 mm^3 per million cycles and 50 mm^3 per million cycles) (Endo et al., 2002). A study by Galvin *et al.* (2006) shows that as the level of crosslinking increases (0 MRad, 5 MRad and 10 MRad), the wear factor (against smooth plates) decreases (the wear factors are 2.2 $mm^3.Nm^{-1}$, 1.8 $mm^3.Nm^{-1}$ and 0.6 $mm^3.Nm^{-1}$ respectively); As crosslinking, decreases the wear rate of UHMWPE, it follows that the osteolytic potential of the wear debris may also be decreased, as it takes longer to reach a sufficient threshold volume in the periprosthetic tissue although it must be noted than the threshold volume for cross-linked UHMWPE is not yet known. Despite this difference in size, there is currently no consensus on the difference in biological activity of wear debris from virgin UHMWPE and cross-linked UHMWPE (Bracco and Oral, 2011). The alkyl free radicals produced by cross-linking can cause oxidative damage to the polymer structure and the material can continue to degrade whilst in storage and when implanted. The alkyl free radicals react with oxygen from the air and begin a cascade of oxidation reactions; producing

highly reactive species such as peroxyradicals (Table 1.7) which form carbonyl species such as ketones, esters and carboxylic acids. These can cause chain scission, which degrades the polymer's mechanical integrity. The polymer becomes brittle, oxidative embrittlement, and the fatigue strength is reduced through loss of crystallinity (Sutula *et al.*, 1995; Collier *et al.*, 1996; Oral *et al.*, 2006; Costa and Bracco, 2009). One solution to neutralise any residual free radicals in the cross-linked polymer is post irradiation melting. The polymer is heated to above its melting point to release free radicals which may then recombine. However, post-irradiation melting negatively affects the mechanical properties of UHMWPE by causing a loss in crystallinity and reducing fatigue strength. Another method of free radical neutralisation is annealing where the polymer is heated below its melting point. However, this too, has significant issues associated with it; such as an increased weakness of the polymer to oxidation when in air and failure to remove the free radicals so oxidation still occurs (Wang *et al.,* 2006).

Table 1.7 Common reactive oxygen species and their chemical structures; all of which are possible to produce when alkyl free radicals react with oxygen from the air.

Reactive oxygen species	Chemical structure
Oxygen	$\bullet O_2$
Superoxide anion	$\bullet O_2^-$
Peroxide	$\bullet O_2^{2-}$
Hydrogen peroxide	H_2O_2
Hydroxyl radical	$\bullet OH$
Hydroxyl anion	OH^-

1.6.2 Antioxidants

As an alternative to remelting or annealing, which result in a loss of crystallinity and fatigue strength, it is possible to dope the polymer with antioxidant compounds, such as vitamin E, to dispel free radicals from cross-linked UHMWPE (Bracco and Oral, 2011). As cross-linking increases the potential life of a THR by reducing the volume of wear debris produced so does antioxidant doping by reducing the amount of free radical present in the polymer structure and minimising aging and oxidative embrittlement during storage and implantation.

An antioxidant prevents oxidation by itself being oxidised and neutralising oxidising agents, as they are reducing agents, and free radicals. Antioxidants neutralise free radicals, reactive species with an unpaired electron, and terminate further chain reactions, i.e. preventing propagation.

There are currently only two types of antioxidant doped, cross-linked UHMWPE clinically available – vitamin E and hindered phenol cross-linked UHMWPE. However there are a number of alternative antioxidants currently at various stages of research such as polyphenols, nitroxides, hindered amines, lanthanide compounds and anthocyanins.

Vitamin E

Vitamin E is a natural antioxidant and prevents against free radical induced oxidative damage in the cell membrane. Vitamin E is an essential vitamin in the human body; deficiency results in serious neurological and neuromuscular symptoms such as nerve and muscle lesions and retinal abnormalities (Sokol, 1993). Vitamin E is known to prevent oxidant-induced inflammation (Conner and Grisham, 1996) and has a beneficial effect on cardiovascular diseases such as atherosclerosis (Singh, Devaraj and Jialal, 2005). There are eight different types of vitamin E – tocopherols (α, β, γ and δ) and tocotrienols (α, β, γ and δ). α –tocopherol is the most common in nature and is the type used as an orthopaedic UHMWPE stabiliser (Brigelius-Flohé and Traber, 1999). An α-tocopherol molecule consists of two parts (Figure 1.4A): the chroman head, the fused ring structures with the functional phenol group, and the phytyl tail, the long saturated or unsaturated aliphatic linear structures (Burton, 1990). Synthetic vitamin E, rather than natural, is used to dope orthopaedic UHMWPE and both naturally occurring and synthetic vitamin E are safe for human consumption. (Bracco and Oral, 2011). Vitamin E is synthesised industrially from the intermediates trimethylhydroquinone (TMHQ) and isophytol (Figure 1.4B) (Mercier and Chabardes, 1994). Synthetic vitamin E was first used as a stabiliser for polyolefins (i.e. alkenes) in the 1980's (Adamirova, 1982). The use of synthetic vitamin E in UHMWPE acetabular cups for orthopaedic use was first approved by the FDA in 2007; followed by tibial trays for use in knees in 2008 (Oral and Muratoglu, 2009). The American Society for Testing and Materials also produced a standard for vitamin E doped UHMWPE for orthopaedic use in 2007 (ASTM F2695-12). There are now a number of vitamin E, cross-linked UHMWPE orthopaedic products clinically available; such as Vivacit-E® produced by Zimmer Biomet.

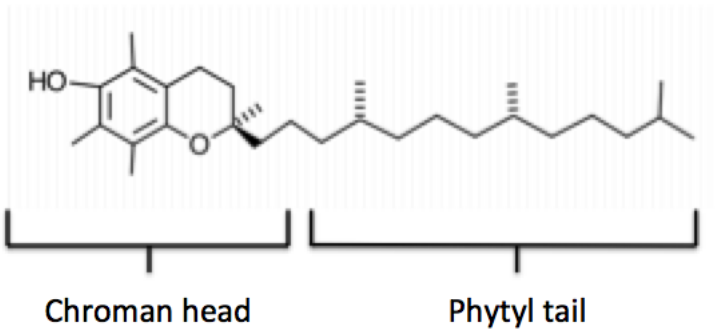

A)

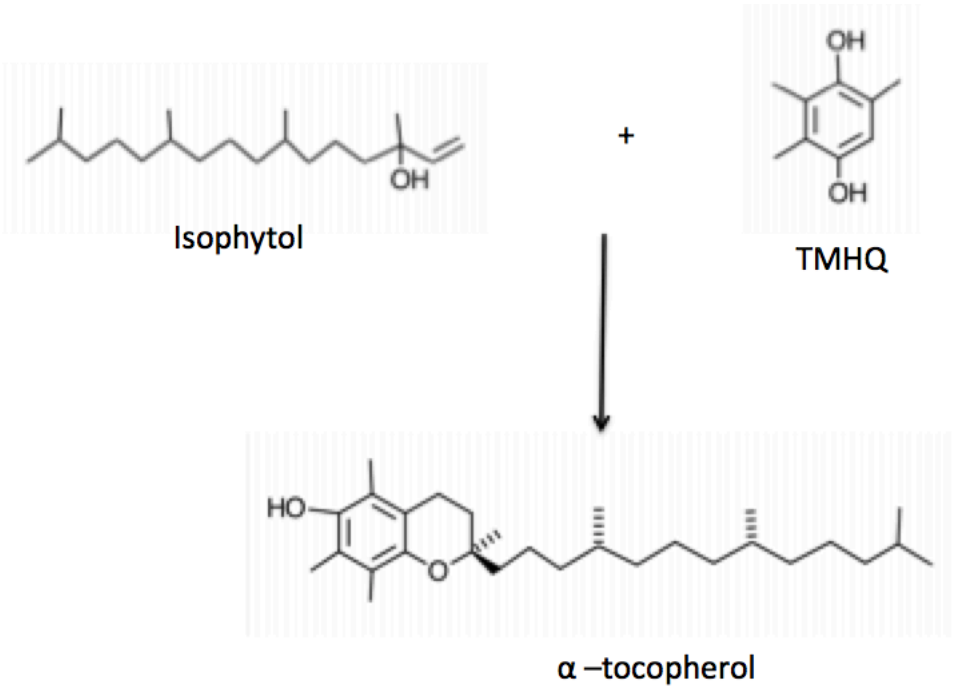

B)

Figure 1.4 Vitamin E (α-tocopherol) molecular structure (A) and industrial synthesis (B) (adapted from Sheppard *et al.*, 1993).

Vitamin E is used in medical grade UHMWPE (at a clinical dose of 1000 ppm (Bladen *et al.*, 2013a)) as a stabiliser because its antioxidant activity prevents oxidative degradation of the polymer caused by residual free radicals that are trapped within the structure from the sterilisation (gamma irradiation) and crosslinking (ionising radiation) processes. The role of vitamin E in UHMWPE is twofold: it confers oxidative resistance onto the material (i.e. it prevents oxidative damage by itself being oxidised) and it also preserves or improves the mechanical properties of the material such as fatigue strength; maintaining wear resistance through prevention of oxidative embrittlement. Vitamin E achieves its anti-oxidant activity by itself being oxidised. It can react with peroxy and alkyl macroradicals in a cyclic manner which results in the

regeneration of the tocopherol radical. The tocopherol radical can then go on to react over and over again thus only a small amount of vitamin E is required for doping UHMWPE to achieve an antioxidant effect (Bracco and Oral, 2011).

Vitamin E can be added to UHMWPE in two different ways: blending and diffusion. Blending involves adding vitamin E to the UHMWPE powdered resin, which is then consolidated and irradiated in order to sterilise and crosslink the polymer. Since vitamin E is present during the crosslinking process, it can also react with the alkyl free radicals generated and reduce the crosslinking efficiency (Oral *et al.*, 2005). Diffusion involves adding vitamin E to the polymer at a later stage. The UHMWPE is first consolidated and then irradiated (to sterilise and crosslink). After these processes are complete, the material is then soaked in a solution of vitamin E at a high temperature. It is then homogenised, by heating the polymer below its melting point in an inert gas, to ensure that the vitamin E is distributed beyond the surface and throughout the material. However it is not clear whether the distribution of vitamin E is even throughout the material or how far vitamin E has diffused into the polymer. Since vitamin E is not present during the crosslinking process, the crosslinking efficiency is not reduced however the polymer is not protected from free radical damage during sterilisation and crosslinking. Diffusion results in higher concentrations of vitamin E present in the polymer, as it is not lost through reaction with free radicals, which affords the polymer greater oxidative protection in the long term (Oral *et al.*, 2007).

There are concerns that the vitamin E added to the polymer, whether blended or diffused, may leach out *in vivo* and, if so, the effects of free vitamin E in the joint is unknown. There are two possibilities of how this may occur: vitamin E may leach from either the bulk material or the wear particles. Studies have shown that, under manufacturing conditions, no vitamin E leaches from the material; suggesting vitamin E is not leaching during the manufacturing process. However studies show that vitamin E does leach out of the material in water at physiological temperatures (Oral *et al.*, 2008; Costa and Bracco, 2009) so it is plausible that some vitamin E may leach from the implant material when in the body. Although the studies show that even when implants are treated harshly (boiled in hexane) to remove as much vitamin E as possible, they still exhibit improved oxidative resistance (compared to unstabilised UHMWPE) and low wear volumes. This suggests some vitamin E is retained in the material even under extreme circumstances and is able to act sufficiently as an antioxidant. This is supported by the tocopherol radicals ability to regenerate itself with every oxidation reaction cycle, therefore only a small of vitamin E is required to confer oxidative resistance onto the material (Bracco and Oral, 2011). Studies have not yet taken place to evaluate whether vitamin E leaches from wear particles and, if so, therefore there is a need to carry out such studies as wear particles could be a

significant source of free vitamin E in the body. It would also be useful to compare the quantity of vitamin E that leaches from the bulk material to that leached from wear particles to establish which (if any) is the primary source of free vitamin E in the body.

Studies at the University of Leeds have shown that the presence of vitamin E does not significantly affect the wear rate and wear particle size of virgin UHMWPE. It does however affect the inflammatory potential of wear particles; significantly lower levels of TNF-α are released (Bladen *et al.*, 2013a). There is speculation that the immunogenicity and inflammatory potential of vitamin E wear particles may be different in comparison to virgin UHMWPE. The oxidative state of vitamin E wear particles may also be different. These potential differences may influence the response *in vivo* to the wear particles therefore this will require further study (Bracco and Oral, 2011). Many studies (Teramura *et al.*, 2009; Vaidya *et al.*, 2011) claim that vitamin E itself reduces wear particle production however, in actuality, it is the crosslinking of UHMWPE that results in reduced wear particle production due to mechanical strengthening of the polymer; crosslinking the polymer chains increases the polymer's toughness. Studies that compare virgin and cross-linked UHMWPE clearly show this relationship; as discussed above, cross-linked UHMWPE produces 80% less wear debris than virgin UHMWPE (Popoola *et al.*, 2010). It is important therefore that the materials used in each study are carefully considered. Gowland (2014) compared the wear rates of GUR 1050 XL (10 MRad) and GUR 1050 XL (10 MRad) VE (1000 ppm) and found no significant difference; 2.5 $mm^3.Nm^{-1}$ and 1.9 $mm^3.Nm^{-1}$ respectively. Vitamin E does, however, prevent oxidative damage, which, in turn, preserves the mechanical properties of the polymer, such as ultimate tensile strength, elongation at break, work to failure and stress factor range at fatigue crack inception (Bracco and Oral, 2011).

In vitro studies with vitamin E doped UHMWPE have shown that vitamin E exhibits anti-inflammatory properties, therefore vitamin E may also exhibit such effects *in vivo*. Studies by Bladen *et al.* (2013b) showed that vitamin E (either alone - at doses of 500 $mg.ml^{-1}$- or contained in UHMWPE wear debris – GUR 1050 containing vitamin E at 1000 ppm) reduced the production of inflammatory and osteolytic cytokines and chemokines, TNF-α, IL-1β, IL-6 and IL-8, in PBMNC's compared to virgin UHMWPE wear particles (Bladen *et al.*, 2013a; Bladen *et al.*, 2013b). Since UHMWPE wear particles cause a sustained inflammatory response in periprosthetic tissue, it is possible that the inclusion of vitamin E into the UHMWPE material may mitigate this response through the reduction in production of osteolytic mediators therefore potentially decreasing osteoclastogenesis. The lack of osteoclastogenesis could therefore, potentially, reduce the risk of osteolysis and aseptic loosening. The reduction in osteolysis potentially may lead to a longer implant lifetime in the patient;

taking orthopaedics one step closer to creating a prosthesis that lasts the lifetime of the patient. This is supported by studies that show that vitamin E has a direct effect on osteoclasts although the effect itself is not clear as there is evidence of both beneficial, such as the inhibition of osteoclast formation, and deleterious effects, such as the upregulation of osteolytic cytokines gene expression, on osteolysis (Roodman, 2012). Bladen *et al.* (2013b) cultured PBMNC's and U937 human macrophages with vitamin E (500 $mg.ml^{-1}$) and cell viability was assessed after 24 hours using the ATP-lite cell viability assay; vitamin E did not affect cell viability except at high concentrations (3mM and 2 mM for PBMNC's and U937 cells respectively) (Bladen *et al.*, 2013b). These studies suggested that vitamin E itself is biocompatible and that vitamin E wear debris is better tolerated than virgin UHMWPE on a cellular level.

Hindered phenols

Hindered phenols are complex molecules with multiple phenol groups which often contain one or more ring structures and several branches. A common example of a hindered phenol compound used to stabilise medical grade UHMWPE is pentaerythritol tetrakis (3,5-di-tert-butyl-4-hydroxyhydrocinnamate) (Figure 1.5) used by DePuy Synthes Joint Reconstruction. Hindered phenols as antioxidant additives in orthopaedic implants are currently in clinical use in total knee replacements (TKR) (AOX 7.5 – 8 MRad) and in development for THR's (10 – 11.5 MRad).

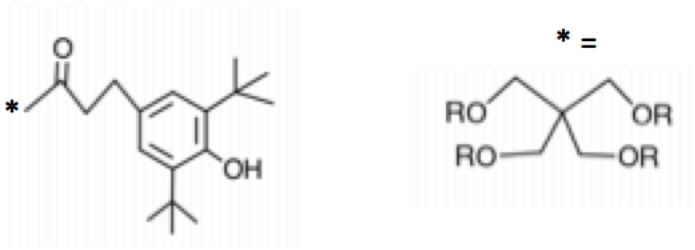

Figure 1.5 Structure of pentaerythritol tetrakis (3,5-di-tert-butyl-4-hydroxyhydrocinnamate).

In vitro studies have shown that pentaerythritol tetrakis (3,5-di-tert-butyl-4-hydroxyhydrocinnamate) is cytotoxic to U937 human histiocytes and human peripheral blood mononuclear cells (PBMNC's), even at low concentrations; with LC_{50} (lethal concentrations that killed 50% of the cells) at 100 µM and 300 µM, respectively. Pentaerythritol tetrakis (3,5-di-tert-butyl-4-hydroxyhydrocinnamate) elicited reduced TNF-α production in LPS stimulated U937 human histiocytes, however it was less effective than vitamin E or europium (III) chloride (a lanthanide salt) at reducing TNF-α production and had no effect on TNF-α production from LPS stimulated PBMNC's (Bladen *et al.*, 2013b). These *in vitro* studies suggest that pentaerythritol tetrakis (3,5-di-tert-butyl-4-hydroxyhydrocinnamate) may have some anti-inflammatory activity, certainly not to the same extent as vitamin E, however this requires further study into

other inflammatory mediators and pathways of inflammation to verify this. These studies also suggest that hindered phenols, such as pentaerythritol tetrakis (3,5-di-tert-butyl-4-hydroxyhydrocinnamate), may have reduced biocompatibility as they may exhibit cytotoxic effects. It is not known if hindered phenol compounds are capable of leaching from UHMWPE, and therefore into the body, so elution studies must also be carried out to determine whether free hindered phenol compounds could leach from the implant into the body and, if so, what biological effects they would have.

In vivo animal studies by King *et al.* (2010), carried out in rats (over 26 weeks) and rabbits (over 12 weeks), assessed the biocompatibility of GUR 1020 highly cross-linked AOX material (containing hindered phenol; Poly-phenol of tetrakis[3-(3,5-di-tert-butyl-4-hydroxyphenyl) propionate]. Haematoxylin and eosin staining of periprosthetic muscle (rabbit) and subcutaneous tissue (rat) after 26 weeks showed no adverse effects on the normal periprosthetic tissue architecture (King, Arscott and Narayan, 2009). This, however, does not conclusively suggest biocompatibility for this material as haematoxylin and eosin stains cellular structures rather than highlighting any change in viability. More specific *in vivo* animal and human studies are required to comment more conclusively on biocompatibility. Studies by Green et al. (2012) used mouse calvarial models to demonstrate that the GUR 1020 highly cross-linked AOX material exhibits a similar osteolytic potential to current clinical UHMWPE orthopaedic materials; suggesting that there may be no improvement in the incidence of osteolysis with the use of hindered phenol UHMWPE materials (Green *et al*, 2012).

Studies by Narayan *et al.* (2009) investigated the effect of hindered phenols, Pentaerythritol tetrakis [3-(3,5-di- tert-butyl-4-hydroxyphenyl) propionate], Octadecyl-3,5-di-tert-butyl-4- hydroxycinnamate, and Isooctyl-3,5-di-tert-butyl-4-hydroxycinnamate, on the wear rate of cross-linked UHMWPE. It was found that increasing the amount of hindered phenol present, from 0 to 0.1%, resulted in an increased wear rate (from around 1 mg per million cycles to around 5 mg per million cycles) due to a reduction in crosslinking as the hindered phenol was blended rather than diffused. However this effect could be overcome by increasing the radiation dose to increase the level of cross-linking (Narayan *et al.*, 2009). The interfering effect of blended antioxidants on the crosslinking process is already known therefore further studies should be carried out on diffused hindered phenol UHMWPE materials.

Lanthanide compounds

Lanthanide compounds are already in use as stabilisers for polyvinyl chloride (PVC) (Peng *et al.*, 2003; Zheng *et al.*, 2005). Lanthanides form complexes with oxygen in high coordination numbers (Gallardo *et al.*, 2011a). Lanthanides have no biological role *in vivo* however they are classified as having low toxicity (McGill, 2005).

Pennekamp *et al.* (2009) suggest that europium may have an anti-inflammatory effect on periprosthetic tissue, based on their initial study using murine macrophages (Pennekamp *et al.*, 2009). This is promising, however, there is a need to do further study in human cells to validate this claim. Some lanthanides, such as cerium and yttrium (oxide nanoparticles), have been found to have an antioxidant effect on neurons. This is also promising, however it is necessary to confirm this effect in periprosthetic tissue and the joint capsule (Schubert *et al.*, 2006).

A pilot study examining the effects of europium (II) stearate on the mechanical properties of UHMWPE was carried out by Gallardo *et al.* (2011a). GUR 1050 UHMWPE powder was blended with europium (II) stearate (375 ppm and 750 ppm), compression moulded and irradiated at 35 kGy. The study showed that the addition of europium (II) stearate at both concentrations reduced the loss of mechanical integrity (ultimate load, ultimate displacement and work to failure) of the polymer under accelerated aging conditions (Gallardo *et al.*, 2011a) . However fatigue strength, the mechanical property most affected by crosslinking, was not assessed. Additionally, the addition of europium (II) stearate resulted in a statistically significantly lower oxidation index after accelerated aging than that of virgin UHMWPE. Europium (II) stearate is a reducing agent and is therefore capable of acting as an antioxidant through the oxidation of the europium ion from Eu^{2+} to Eu^{3+}. However, the study did not examine cross-linked materials which are the most up-to-date form of clinically available UHMWPE for orthopaedic purposes and where antioxidants are more likely to be used to reduce the oxidative damage caused by free radicals. This study did not attempt to make any erroneous claims about the effect of the antioxidant on the wear rate of the material as some studies often do.

Gallardo *et al.* (2011b) carried out a further study with europium (III) stearate specifically examining its antioxidant ability. The study characterised the quantity and nature of the oxidation products, hydroxides, ketones and carboxylic acid, from irradiated and non-irradiated UHMWPE doped with europium (III) stearate at 0, 375 and 3750 ppm after accelerated aging using fourier transform infrared (FTIR) spectroscopy. The concentration of both hydroperoxides and ketones increased over time in all materials however significantly higher concentrations were found in non-doped UHMWPE compared to doped UHMWPE. It seems the presence of europium (III) stearate significantly reduces the rate of oxidation of the material and therefore slows the increase in concentration of oxidation products (Gallardo *et al.*, 2011b). The authors speculated that lanthanides may interact with carboxylate anions and thus stabilise UHMWPE – it is possible that europium is capable of coordinating to carbonyl anions as ligands in the same way as oxygen, thereby reducing their availability in the material for the continuation of the oxidation cycle. The study also suggested that the

stearate chains may be acting symbiotically with the europium to prevent oxidation as the IR spectra showed a change in structure over time with oxidation however a change in structure is not sufficient to claim an antioxidant role. The study did not account for cross-linked UHMWPE – the materials were gamma irradiated for sterilisation purposes, however the irradiation dose could have caused some crosslinking, which could have caused an unknown effect on the mechanism of oxidation.

Bladen *et al.* (2013b) carried out cytotoxicity studies on europium (II) and (III) chloride using U937 human histiocytes and PBMNC's. Europium chloride was not cytotoxic to either cell types except at high concentrations (2.5 mM and 1 mM, respectively). Similarly, both cell types when stimulated with LPS and treated with europium chloride produced reduced levels of inflammatory cytokines, notably TNF-α, in comparison with LPS stimulation alone. This study suggests that lanthanide salts are not cytotoxic and may be well tolerated in vivo therefore further animal and human studies are required to validate this (Bladen *et al.*, 2013b).

Hindered amine light stabilisers

Hindered amine light stabilisers (HALS) are complex molecules containing multiple amine groups and cyclic ring structures (both aromatic and non-aromatic). They often contain triazine aromatic rings and piperidine rings .

Initial studies by Gjisman *et al.* (2010) showed that, compared to vitamin E, HALS did not affect crosslinking efficiency, as the amine form of the antioxidant compounds does not react with the polymer or alkyl radicals. HALS are converted into nitroxides which are then capable of free radical scavenging. The nitroxide radical is capable of regeneration, therefore only a small amount of HALS is needed. These authors showed that a small amount (500 ppm) of HALS compound is as effective an antioxidant as vitamin E at three times the concentration (1500 ppm). The authors suggest that HALS compounds should not leach from implanted UHMWPE, due to their lack of solubility in water and indeed no diffusion of the compounds from low density polyethylene (LDPE) was found after 10 months (Malik, Hrivik and Tomova, 1992), although further testing is required to conclusively assess this (particularly *in vivo* as hydrophobic compounds can reside in fatty tissue). Moreover, this should be assessed in UHMWPE as LDPE is not used in an orthopaedic context and therefore has less clinical relevance. There is no information currently on the biocompatibility of HALS – either *in vitro* or *in vivo* therefore further study is required to investigate their biocompatibility and suitability *in vivo*; in particular, a joint environment context (Gijsman, Smelt and Schumann, 2010).

Polyphenols

A natural source of antioxidants that could be used for oxidative stabilisation of cross-linked UHWMPE is polyphenols. Polyphenols are molecules with multiple phenol groups i.e. aromatic rings with an alcohol moiety (Figure 1.6A). Some examples of naturally occurring polyphenols include gingerol (ginger), curcumin (cumin) and resveratrol (wine).

A study by Fu *et al.* (2013) studied two examples of polyphenols, gallic acid (Figure 1.6A) and dodecyl gallate (Figure 1.6B), which may be promising alternative antioxidant stabilisers for medical grade UHMWPE. Gallic acid and dodecyl gallate, an ester of dodecanol and gallic acid, both delayed the onset of oxidation of UHMWPE compared to vitamin E, at lower concentrations; 0.05 wt% for gallic acid and dodecyl gallate compared to 0.1% for vitamin E. The authors claimed that polyphenols provided a greater oxidative stability than vitamin E. The authors suggested that vitamin E experienced phenol loss, which reduced its effectiveness. In terms of mechanical properties, gallic acid and dodecyl gallate, did not influence the tensile strength of cross-linked UHMWPE, whereas vitamin E improved it. The presence of gallic acid or dodecyl gallate however, ensured that the mechanical properties were not affected by aging. Additionally, the presence of gallic acid and dodecyl gallate in UHMWPE were found to have no effect on wear rate. UHMWPE with gallic acid and dodecyl gallate was found to have a higher crosslinking density compared to vitamin E cross-linked UHWMPE, therefore gallic acid and dodecyl gallate did not interfere with the crosslinking process and therefore its efficiency. Finally, the biocompatibility of cross-linked UHMWPE doped with gallic acid and dodecyl gallate was tested by growing chondrocytes onto both materials – cells were found to adhere, spread and proliferate successfully; indicating biocompatibility (Fu *et al.*, 2013). Further studies are required to verify biocompatibility; in particular in response to wear debris generated from such polyphenol materials. Detailed wear studies are required to assess the wear profiles of these materials – in terms of particle size and volume distribution and morphology as these are important factors in determining a biological response to the wear debris.

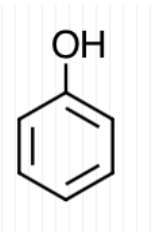

A)

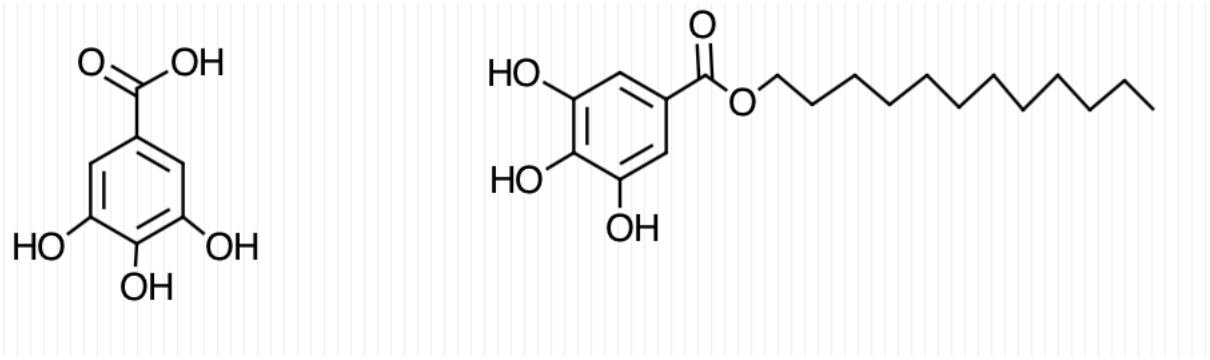

B)

Figure 1.6 A) The general structure of phenol molecule, B) the structure of gallic acid (left) and dodecyl gallate (right).

Nitroxides

There is some interest in the use of nitroxide compounds as alternative antioxidant stabilisers for medical grade UHMWPE. Nitroxides, also called amine oxides, are charged (zwitterionic) nitrogen centred molecules with one oxygen and three alkyl chains bound (Figure 1.7A). Compounds of interest for stabilising orthopaedic UHMWPE include 2,2,6,6-tetramethylpiperidine-1-oxyl (TEMPO) (Figure 1.7B) and 4-hydroxy-2,2,6,6-tetramethylpiperidine-1-oxyl (TEMPOL) (Figure 1.7C) (Chumakov, 2009).

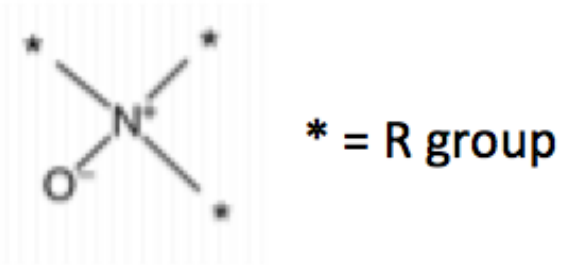

A)

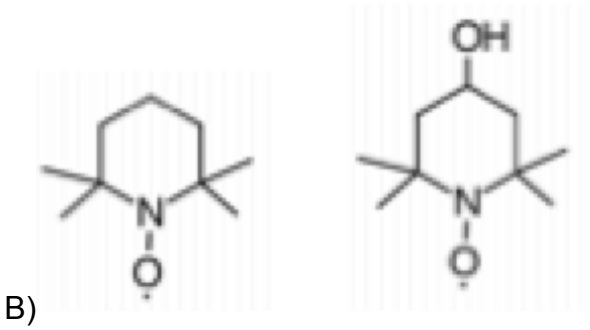

B) C)

Figure 1.7 The general structure of nitroxide compounds (A) and the individual structures of TEMPO (B) and TEMPOL (C).

In vitro studies by Bladen et al (2013) showed that a solution of TEMPO (10 mM in ethanol) was cytotoxic (even at low concentrations – 200 μM and 300 μM, respectively) to U937 human histiocytes and human peripheral blood mononuclear

cells (PBMNC's). The toxicity could not be attributed to ethanol, as ethanol was only present in a very low concentration, which was significantly below its cytotoxicity level. TEMPO did appear to cause a reduction in TNF-α production in LPS stimulated U937 human histiocytes; approximately 75% less than LPS alone. This, however, was less than other antioxidants tested such as vitamin E; approximately 95% less than LPS alone. TEMPO did not reduce the amount of TNF-α produced or exhibit any anti-inflammatory effects in LPS stimulated PBMNC's. The study by Bladen *et al.* (2013b) showed that, although an antioxidant may perform well in terms of material properties, it is vital to consider the biological effects of such antioxidants before approving their use in medical grade UHMWPE; particularly if the compounds are capable of leaching from the implant into the body (Bladen *et al.*, 2013b).

Anthocyanins

Anthocyanins are a well-known class of naturally occurring antioxidants. They consist of a conjugated dual heteroaromatic ring system covalently attached to a functionalised benzene ring (Figure 1.8). They also contain a sugar molecule in the 3 position. There are hundreds of different anthocyanins and they are found naturally in a wide variety of different plants such as blueberries, blackcurrants and beetroots. Anthocyanins are responsible for the colouration of the plants they are found in and their colour depends on the pH of the environment they are in.

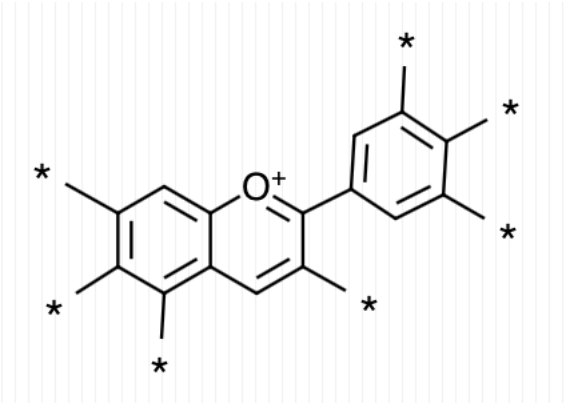

Figure 1.8 Anthocyanin general structure (* may be any alkyl group or hydrogen).

Research is ongoing into the use of anthocyanins as alternative antioxidants to stabilise orthopaedic UHMWPE. Research is in the early stages and there are currently only two existing patents for anthocyanin doped UHMWPE (He *et al.*, 2012, 2013). He *et al.* (2012) performed a study on the wear rates and oxidation of anthocyanin doped UHMWPE acetabular cups in comparison to vitamin E doped UHMWPE acetabular cups. Two types of anthocyanin compounds were used to dope UHMWPE (antho-B – sourced from bilberries – and antho-G – sourced from grapes). The addition of both types of anthocyanins to the polymer showed no impact on

physical and mechanical properties. Both anthocyanins and vitamin E doped UHMWPE showed no oxidation after 2 and 4 weeks of accelerated aging. Both anthocyanin doped UHMWPE cups showed lower wear rates than vitamin E doped UHMWPE at lower concentrations (1.3-1.4 mm^3 per million cycles and 6 mm^3 per million cycles respectively– antho-B was present at 125 ppm and antho-G was present at 40 ppm compared to vitamin E at 500 ppm (He *et al.*, 2009). However, what is not clear from the study is whether the materials used were cross-linked and, if so, whether they were cross-linked to the same as extent as a clinical material would be. Additionally, the level of crosslinking may need to be increased if an antioxidant is blended with the polymer as this can impair the crosslinking process – this is true of vitamin E, which requires a higher dose of radiation to compensate. It was not therefore clear whether the characteristics of the anthocyanin and vitamin E doped materials were consistent, and therefore directly comparable. Anthocyanins may be a promising alternative antioxidant for use in stabilising UHMWPE for orthopaedic use. They are likely to be biocompatible as anthocyanins are naturally occurring antioxidants and are contained in food, such as beetroot (they are the source of purple colour), which is regularly consumed by humans with no ill effects. However, there may be drawbacks similar to blended vitamin E as the patents specify a method which includes anthocyanins with UHMWPE powder before crosslinking and, since the anthocyanins are present during the crosslinking procedure, they may impede the crosslinking process and reduce efficiency in the same way as vitamin E. Further study evaluating crosslinking density to verify the effect on crosslinking efficiency is required. There is no research data on the bulk implant material and the nature of wear particles produced from anthocyanin stabilized cross-linked UHMWPE at the present time. It is unknown how this material would fare on a systemic level *in vivo* and on a cellular level *in vitro* so further study is needed into this potentially promising orthopaedic material to establish its biological reactivity.

1.6.3 Other modifications

There are a number of alternative modifications currently in development for UHMWPE to improve mechanical properties and wear resistance. One such group of alternative materials are UHMWPE composites such as UHMWPE/graphene oxide nanocomposites (Puertolas and Kurtz, 2016; Suñer *et al.*, 2018), UHMWPE-hyaluronan (<5%) microcomposites (James *et al*, 2016), UHMWPE homocomposites (Siskey *et al*, 2016) and UHMWPE hydroxyapatite composites (Puertolas and Kurtz, 2016). Another such group is phospholipid polymer grafter highly cross-linked UHMWPE (Kyomoto, Moro and Ishihara, 2016). These are all still in development and undergoing further testing before clinical release. As such, these modifications will be

discussed no further in this introduction however it is helpful to acknowledge them in the context of UHMWPE modifications.

1.7 *In vivo* and *in vitro* modelling

The inflammatory and osteolytic potential of UHMWPE; both as a bulk material and particulate matter can be modelled *in vivo* and *in vitro*.

1.7.1 *In vivo* modelling

The *in vivo* response to UHMWPE is typically measured using animal models to both the bulk material and its particulate matter. Long term clinical studies in humans do also yield data although the return of data is typically over a much larger time frame (years or decades rather than weeks or months).

1.7.1.1 *In vivo* implantation of bulk material

In terms of assessing the biological response to the bulk UHMWPE material, the material can be implanted subcutaneously or alternatively a full joint replacement can be implanted into the animal.

Several studies in animals have been carried out to verify the biocompatibility of vitamin E doped UHMWPE in an orthopaedic setting. Jarett *et al.* (2010) performed extensive animal studies on vitamin E doped UHMWPE. Vitamin E doped UHMWPE (GUR 1050 virgin material obtained from Orthoplastics, which was then gamma irradiated at 100 kGy and then soaked in vitamin E for 120 hours to provide two different doses of 1.4% and 0.7% by weight) was implanted subcutaneously in rabbits and vitamin E doped UHMWPE acetabular cups were implanted into a canine model to establish the effect of the material on bone and periprosthetic tissue. These studies showed that periprosthetic tissue histology was normal in the canine model and the subcutaneous implantation of the material resulted in a normal fibrous encapsulation response in the rabbit models (there was some initial inflammation, although this was consistent with a standard response to a foreign body) (Jarrett *et al.*, 2010). These animal studies implied that vitamin E UHMWPE is well tolerated in the body in an orthopaedic setting as no adverse effects were observed in either rabbit or canine models. However, it is imperative that such biocompatibility data be established in humans as the response to chemical compounds can vary between species. These studies are useful because they assess the whole body and localised response to the bulk material but fail to account for the response to wear debris (unless the periprosthetic tissue is harvested from a joint implantation study). This study used UHMWPE materials with a clinically relevant dose of vitamin E (0.7% by weight) and a higher than clinical dose (1.4% by weight); both of which were tolerated by the rabbit and canine models.

1.7.1.2 *In vivo* injection or implantation of particulate matter

The biological response to UHMWPE wear debris can be observed by implanting or injecting the wear debris, suspended in water or a water-ethanol solution (Jarrett *et al.*, 2010), into an animal model and, after several weeks, harvesting the animal tissues for histology.

The anti-inflammatory properties of vitamin E may reduce the incidence of osteolysis *in vivo* which is corroborated by studies by Bichara *et al.* (2014)**.** Bichara *et al.* (2014) implanted the vitamin E cross-linked UHWMPE (0.8 % vitamin E by weight, 100 kGy gamma irradiation) wear debris (generated from clinical material obtained from Biomet) periostally in a mouse calvarial model. Bichara *et al.* (2014) showed a reduction in osteolysis in a mouse calvarial model when vitamin E cross-linked UHMWPE was compared to cross-linked UHMWPE with no antioxidant (Bichara *et al.*, 2014). Further study is required however into *in vivo* human biocompatibility. As vitamin E doped UHMWPE was only approved for clinical use in 2007, there is no long term clinical performance data; such studies are still ongoing. Over time, such data will reveal how well tolerated vitamin E doped UHMWPE is *in vivo* in an orthopaedic context as well as any additional effects such as anti-inflammatory effects and their implications. This is useful for gaining an understanding of what the 3D *in vivo* whole body response is to UHMWPE debris however, since it is an animal model, it is less relevant than a human model and somewhat harder to interrogate for specific qualities such as cytokine production. This requires an *in vitro* model.

Jarett *et al.* (2010) injected vitamin E (pure and solubilised) into the knees of rabbits, in order to replicate any elution or leaching of vitamin E from the implant material. This study showed that the tissue histology was normal in response to solubilised vitamin E in the rabbit models (Jarrett *et al.*, 2010). This study implied that vitamin E, unbound to polyethylene, would be well tolerated in the body in an orthopaedic setting as no adverse effects were observed in the rabbit models. However, it is imperative that such biocompatibility data be established in humans as the response to chemical compounds can vary between species.

1.7.2 *In vitro* modelling

The *in vitro* response to UHMWPE is typically measured using animal or human primary cells or cell lines – these can be cultured with or on the bulk material or in the presence of UHMWPE wear debris.

1.7.2.1 *In vitro* modelling of response to bulk material

Studies often culture animal or human primary cells or cell lines on a tablet of UHMWPE bulk material in order to establish biocompatibility and cytotoxicity data. This helps gain an understanding of how cellular qualities such as viability are affected

by cells growing on the bulk material but this situation is much less clinically relevant than subcutaneous implantation as it is only a flat 2D model. Moreover, it, again, fails to account for the impact wear debris has.

Wolf *et al.* (2002) grew L929 murine fibroblasts onto thin sheets of vitamin E doped UHMWPE and showed that vitamin E doped UHMWPE did not have a cytotoxic effect on the cells or affect their behaviour in terms of proliferation, mitochondrial activity or membrane integrity although the study did show a reduction in cell adhesion and spreading (Wolf, Lederer and Muller, 2002). The growth of cells onto the acetabular cup of the prostheses is not directly relevant to the biocompatibility of this material as it is unlikely that cells will colonise the interior of the implant and the growth of tissue here would not be beneficial. It is perhaps more important to assess the response of relevant cells to the wear debris generated from the material and any free vitamin E that may arise from material elution. Additionally, whilst fibroblasts are a relevant cell type in terms of periprosthetic tissue, it is also important to establish biocompatibility in other relevant cells, such as macrophages and osteoclasts. Furthermore, biocompatibility must be established in a human primary cell source as well as cell lines (as the behaviour may differ between the two types of cells). It is also important to use human cells as these may differ from animal cells in their response to vitamin E UHMWPE and such material will ultimately be in humans not animals.

A further study by Wolf *et al.* (2007) did indeed use human cell lines to test for biocompatibility with vitamin E doped UHMWPE. Cells were grown on ‘tablets’ of vitamin E doped UHMWPE. A fibroblastic cell line (HF-SAR) was used in addition to the GSJO cell line (established from a medullary thyroid carcinoma). The studies showed no negative impact on the human cell lines in terms of proliferation, mitochondrial activity and morphology (and where applicable, adherence and spreading) (Wolf *et al.*, 2007). Whilst it is positive that human cell lines experienced no negative impact from growth on vitamin E doped UHMWPE compared to unstabilised UHMWPE, it is important to assess the biocompatibility of the wear debris generated from this material. Any significant biological response to joint implants tends to arise from wear debris, not the bulk implant itself, as the implant tends to be walled off from the rest of the body by a fibrous capsule whereas wear debris can travel away from the joint site (depending on size).

1.7.2.2 *In vitro* modelling of response to particulate matter

The cellular response to wear debris can be modelled by culturing representative cell types with clinically relevant wear debris. The cellular response to metal and ceramic wear debris is studied by directly culturing the cells of interest with the wear debris in cell culture medium. Both metal and ceramic particles are significantly denser than water therefore the wear particles sink to the bottom of the well and are in direct

contact with the cells in 2D culture on the base. Unlike metal or ceramic wear debris, UHMWPE wear debris cannot be directly cultured with cells. Polyethylene is less dense than water so wear debris floats on top of the cell culture medium in the well plates thus never coming into contact with the cells growing on the base of the well therefore simple 2D culture is inappropriate for assessing cellular response to UHMWPE wear debris. There are a number of adapted methods that can be used to culture cells with UHMWPE wear debris such as rotation culture models, inverted 2D culture models and gel encapsulation models.

Rotation culture models

Matsusaki *et al.* (2007) cultured U937 human histiocytes with polyethylene wear debris in a continuously rotating culture flask (Matsusaki *et al.*, 2007). This method would not be suitable for adherent cell types, such as macrophages and fibroblasts, which are commonly used in *in vitro* studies of polyethylene so this method is limited in its application. Additionally, a rotation culture is not clinically representative as the periprosthetic tissue fluid is not experiencing continual rotary forces *in vivo*.

Inversion culture models

Inversion culture model, or cover slip method, involves suspending UHMWPE wear debris in the relevant cell medium and cells are cultured on to a cover slip which is then inverted over the medium so the cells are in contact with the debris floating on the top. Matthews *et al.* (2000b) cultured human PBMNC's with model Ceridust® polyethylene particles using the inverted culture method. PBMNC's were seeded onto a glass cover slip and allowed to adhere before inverting over an IVF dish containing medium with Ceridust® fractionated into the following mean sizes: 0.21 μm, 0.49 μm, 4.3 μm, 7.2 μm and 88 μm. The viability was assessed using the MTT viability assay and the output of osteolytic mediators (IL-1β, IL-6, TNF-α, GM-CSF and PGE_2) was assessed using ELISA. Matthews *et al.* (2000b) found that there was significantly increased osteolytic mediator production in response to the model particles in particular the particles with a mean size of 0.21 μm and 0.49 μm which was consistent with the earlier findings of Green *et al.* (1998) that particles of a critical size range (0.1 – 10 μm) are necessary to activate macrophages. However the results were highly variable due to donor heterogeneity – this is the cost of using primary cells which, although they are more representative, demonstrate significant variability between donors. The inversion method is a reasonable method for evaluating specific *in vitro* responses such as viability and cytokine output as it is easy to set up and use and produces results consistent with existing literature. However, the inversion method is a flat 2D model and does not fully represent the 3D clinical environment. It is also costly in terms of the IV dishes required.

Gel encapsulation models

The agarose gel encapsulation model has been developed and used at the University of Leeds for two decades - the UHMWPE wear debris is encapsulated within an agarose gel matrix, the relevant cells are seeded on top of the gel and the outputs are measured as required.

The first iteration of this model was a 2D model developed by Green *et al.* (1998) – Ceridust® model polyethylene particles and GUR 1120 resin powder were added to the agarose gel and, once the gel plugs were placed into the well plates, the well plate was centrifuged at 800 g. This centrifugation brought the polyethylene particles to the surface of the gel, creating a 2D monolayer upon which C3H primary murine peritoneal macrophages were seeded, in direct contact with the particles. This model effectively traps the wear debris and, as the particles are at the surface of the gel in a monolayer, the cells do not have to penetrate the gel in order to access the debris. This model was 2D rather than 3D, as the particles were centrifuged into a monolayer, which is not clinically representative of the *in vivo* periprosthetic environment. Additionally, Green *et al.* (1998) used primary mouse cells which are less representative as they are not human.

The agarose gel encapsulation model was also used by Liu (2012). Liu (2012) removed the centrifugation step and instead relied upon the low density of polyethylene to allow the UHMWPE wear debris to rise to the surface of agarose gel. Additionally, Liu (2012) used human PBMNC's, which contain macrophages (in addition to lymphocytes which make up the majority of the cell fraction obtained from donated blood) and are more representative than murine peritoneal macrophages. However, PBMNC's are primary human cells and therefore require a human donor for each experiment that they are used for. The donor is often different each time as it is unethical to extract multiple samples from the same donor over a short time frame. This results in significant donor variation so it is difficult to establish a reliable response over multiple studies. Liu (2012) found it difficult to establish a significant donor response to the UHMWPE wear debris – the levels of cytokines produced were very low and often not significantly different from the controls. Additionally, this model is 2D when the periprosthetic environment is 3D and some cells do not remain on the surface of the agarose gel and thus lack contact with the UHMWPE particles; some travel down the sides of the gel or underneath it. This issue cannot be solved by trapping the cells with the particles simultaneously within the agarose gel as agarose gelation is temperature dependent and requires a high temperature (>60°C) to plate it out in its liquid phase (even for low temperature gelling agarose), which would adversely affect any cells present (Liu, 2012).

Gowland (2014) also used the agarose gel model adapted by Liu (2012) with some further modifications. The number of PBMNC's used was increased from 1 x 10^5 to 2 x 10^5 cells per well. The gel plug volume was increased from 200 µl to 300 µl to accommodate a greater wear debris volume. The agarose concentration was decreased from 1% (w/v) to 0.4% (w/v) to facilitate cell penetration of the gel. However it should be noted that agarose gel lacks cell attachment sites so cells would not naturally penetrate the gel. Finally, the volume of particles used was increased from 100 µm^3 per cell to 500 µm^3 per cell to maximise the number of particles in the critical size range for macrophage response: 0.3 – 1.0 µm (Green *et al.*, 1998). Gowland (2014) also briefly trialled a human macrophage cell line – U937 – to overcome the issues associated with PBMNC's. Matthews *et al.* (2001) conducted a study of three different human macrophage cell lines – U937, Monomac-1 and THP-1, to assess which is the most appropriate for assessing cytokine release in response to UHMWPE wear debris. Matthews *et al.* (2001) found that only U937 cells behaved in reliable, reproducible manner. U937 human histiocytes are the closest human cell line equivalent to PBMNC's. However the use of U937 cells is not straightforward. U937 human histiocytes are a cell line so donor variation is no longer an issue however U937 human histiocytes are a suspension culture therefore they must be chemically transformed using phorbol-12-myristate-13-acetate (PMA) in order to become true macrophages – both adherent and activated. Additionally they lack the sensitivity of murine macrophage lines such as RAW 264.7 cells (Matthews *et al.*, 2000c). Ultimately Gowland (2014) returned to using PBMNC's for the remainder of his work.

1.8 Aims and objectives

1.8.1 Hypothesis

It is hypothesised that a 3D *in vitro* model can aid with determining whether the presence of antioxidants, such as vitamin E and hindered phenols, in UHMWPE can reduce osteolytic cytokine production in macrophages exposed to the particulate wear debris.

1.8.2 Aims

The aim of this study was to develop a novel 3D *in vitro* model with which to investigate the cellular response to highly cross-linked, antioxidant doped UHMWPE wear debris in order to assess the effect of antioxidant doping on osteolytic cytokine production.

1.8.3 Objectives

- To test the viability of three different types of cells (PBMNC's, U937 human histiocytes and RAW 264.7 murine macrophages) in two different types of gels

(agarose and type I collagen) using ATP-lite^{TM} luminescence detection assay in order to develop a novel *in vitro* model to measure cellular responses to UHMWPE wear debris.

- To measure the TNF-α output of three different types of cells (PBMNC's, U937 human histiocytes and RAW 264.7 murine macrophages) in two different types of gels (agarose and type I collagen) in response to model polyethylene particles using ELISA in order to develop a novel *in vitro* model to measure cellular responses to UHMWPE wear debris.
- To generate UHMWPE wear debris from both highly cross-linked UHMWPE and highly cross-linked, antioxidant doped UHMWPE using single and six station wear simulator rigs.
- To isolate and characterise the generated wear debris using field emission gun scanning electron microscopy (FEGSEM) and analyse the data using ImageJ in order to assess the size and volume distribution.
- To assess the cellular output of osteolytic cytokines and chemokines (TNF-α, IL-1β, IL-6 and KC) and inflammatory mediators (LTB_4 and PGE_2) in response to generated UHMWPE wear debris using ELISA; both the full unfiltered range of particles and particles that have been filtered into the critical size range of 0.1-1 μm known to activate macrophages.
- To assess intracellular reactive oxygen species production in response to generated UHMWPE wear debris using the cellular reactive oxygen species detection assay; both the full unfiltered range of particles and particles that have been filtered into the critical size range of 0.1-1 μm known to activate macrophages.
- To assess the cellular output in terms of osteolytic cytokine and chemokine production (TNF-α, IL-1β and IL-6) and inflammatory mediators (LTB_4 and PGE_2) in response to LPS-stimulated cells treated with inflammatory pathway inhibitors (indomethacin, bisindolylmaleimide I, calphostin C, MK 886 and REV 5901) and antioxidants (vitamin E and pentaerythritol tetrakis (3,5-di-tert-butyl-4-hydroxyhydrocinnamate)) using ELISA in order to elucidate the pathway of any anti-inflammatory effects from doping orthopaedic UHMWPE with antioxidants.
- To image particle sequestration (of fluorescein treated six station generated particles and model FluoSphere® particles) in the novel *in vitro* model using Lysotracker red to co-localise the particles with the lysosomes inside the macrophage cell line and Hoechst to assess whether particles from antioxidant doped UHMWPE materials are retained about the nucleus as shown previously by Gowland (2014) with GUR 1050 XL wear debris.

Chapter 2
Materials and methods

2.1 Materials

The general materials used throughout this study are detailed throughout Chapter 2.

2.1.1 Chemicals and reagents

The general chemicals and reagents used throughout this study are listed in Table 2.1.

Table 2.1 General chemicals and reagents used throughout this study.

Name	Supplier	Storage and preparation
7X-PF detergent	ICN Biomedicals Inc, Ohio, USA	Stored at room temperature (25°C).
10X Minimum Essential Medium (MEM)	Sigma Aldrich, Dorset, UK.	Stored at 4°C.
ATP-lite™ Luminescence ATP detection assay kit	Perkin Elmer, Cambridge, UK.	Stored at 4°C.
Bovine Serum Albumin (BSA)	Sigma Aldrich, Dorset, UK.	Stored at 4°C
Dimethyl sulfoxide (DMSO)	Sigma Aldrich, Dorset, UK.	Stored at room temperature (25°C) and passed through a 0.2 µm filter unit prior to use.
Distilled deionised water (dH_2O) – ELGA Reservoir 75 L still	ELGA, High Wycombe, UK.	Stored at room temperature (25°C).
Dulbecco's Modified Eagles medium (DMEM)	Sigma Aldrich, Dorset, UK.	Stored at 4°C.

Dulbecco's phosphate buffered saline solution (without calcium and magnesium) (DPBS)	Sigma Aldrich, Dorset, UK.	Stored at room temperature (25°C).
Ethanol - 70% (v/v)	ThermoFisher Scientific UK, Loughborough, UK.	Stored at room temperature (25°C) and mixed with distilled water (7:3).
Fairy liquid detergent (15 – 30% anionic surfactants and 5 – 15% nonanionic surfactants)	Proctor and Gamble, Weybridge, UK.	Stored at room temperature (25°C).
Foetal Bovine Serum (FBS)	Seralab, Haywards Heath, UK.	Stored at -20°C.
4-(2-hydroxyethyl)-1-piperazineethanesulfonic acid (HEPES) (1 M)	Bio-Whittaker, Lonza, Verviers, Belgium	Stored at room temperature (25°C).
Human TNF-α uncoated ELISA kit – 20 x 96 well plates	Diaclone, Besancon Cedex, France	Stored at 4°C.
L-glutamine	Sigma Aldrich, Dorset, UK.	Stored at -20°C.
Lipopolysaccharide (LPS) - from E. coli	Sigma Aldrich, Dorset, UK.	Stored at 4°C and stock solution prepared by adding 1 ml DPBS to 1 mg vial of lyophilised powder and frozen at -20°C until use.
Low melting point agarose	Sigma Aldrich, Dorset, UK	Stored at room temperature (25°C).

Lymphoprep	Fresenius Kabi Norge AS for Axis Shield PoC AS, Oslo, Norway	Stored at room temperature (25°C).
Mouse IL-1β uncoated ELISA kit -10 x 96 well plates	ThermoFisher Scientific UK, Loughborough, UK.	Stored at 4°C.
Mouse IL-6 uncoated ELISA kit – 10 x 96 well plates	ThermoFisher Scientific UK, Loughborough, UK.	Stored at 4°C.
Mouse TNF-α uncoated ELISA kit – 10 x 96 well plates	ThermoFisher Scientific UK, Loughborough, UK.	Stored at 4°C.
Penicillin/Streptomycin	Sigma Aldrich, Dorset, UK.	Stored at -20°C.
Phorbol-12-myristate-13-acetate (PMA)	Cayman Chemical, UK	Stored at -20°C. Reconstituted by dissolving 1 mg powder in 1 ml DMSO.
Rat Tail Collagen Type I, >2mg.ml^{-1} Chloroform Treated	First Link Ltd, Wolverhampton, UK.	Stored at 4°C.
RayBio® Mouse KC ELISA kit – 1 x 96 well plate	RayBio®, Georgia, USA.	Stored at -20°C.
R&D® Parameter ™ LTB_4 assay – 1 x 96 well plate	R&D® Systems, Minneapolis, USA.	Stored at -20°C.

R&D® Parameter ™ PGE_2 assay – 1 x 96 well plate	R&D® Systems, Minneapolis, USA.	Stored at -20°C.
Roswell Park Memorial Institute medium (RPMI) 1640 medium	Sigma Aldrich, Dorset, UK.	Stored at 4°C.
Sodium azide	Sigma Aldrich, Dorset, UK	Stored at room temperature (25°C).
Sodium hydroxide (NaOH) pellets	ThermoFisher Scientific UK, Loughborough, UK.	Stored at 25°C.
Sulfuric acid (H_2SO_4) - 1 M	Sigma Aldrich, Dorset, UK.	Stored at room temperature (25°C).
Trypan blue	Sigma Aldrich, Dorset, UK.	Stored at room temperature (25°C) and passed through a 0.2 µm filter unit prior to use.
Trypsin (0.5% (v/v)) in ethylenediaminetetraacetic acid (EDTA)	Sigma Aldrich Ltd, Dorset, UK	Stored at -20°C.
TWEEN-20 (Polysorbate-20)	Sigma Aldrich, Dorset, UK.	Stored at room temperature (25°C).
Ultrapure water	Baxter Healthcare, Zurich, Switzerland.	Stored at room temperature (25°C).
Vacuum grease	Dow Corning, Michigan, USA.	Stored at room temperature (25°C).

Virkon solution – 1% (w/v)	DuPont, Stevenage, UK.	Stored at room temperature (25°C) and prepared by adding 5 scoops of virkon powder to 5000 ml of distilled water.

2.1.2 Consumables

The general consumables used throughout this study are listed in Table 2.2.

Table 2.2 General consumables used throughout this study.

Item	Size	Supplier
Blue paper roll	N/A	Scientific Laboratory Supplies Ltd, Nottingham, UK.
Cell scraper	N/A	Greiner Bio-One, Kremsmunster, Germany.
Cryovial	1 ml	ThermoFisher Scientific UK, Loughborough, UK.
Dish sponge	N/A	Tesco, Cheshunt, UK.
Falcon tubes	50 ml	Scientific Laboratory Supplies Ltd, Nottingham, UK.
Filter units	0.2 µm	Merck Millipore Ltd, Cork, Ireland.
Flat bottomed tissue culture plates	48 and 96 well	Corning, New York, USA and Nunc, Denmark.
Foil	N/A	Scientific Laboratory Supplies Ltd, Nottingham, UK.
Glass cover slips	22 x 22 mm	Scientific Laboratory Supplies Ltd, Nottingham, UK.

Needles	Various sizes	Scientific Laboratory Supplies Ltd, Nottingham, UK.
Nitrile gloves	Medium	Scientific Laboratory Supplies Ltd, Nottingham, UK.
Nunc maxisorp plates	96 well	Nunc, Denmark
Nunc uncoated F plates	96 well	Nunc, Denmark
Plastic bijoux	N/A	Scientific Laboratory Supplies Ltd, Nottingham, UK.
Plastic petri dishes	Various sizes	Sterilin Ltd, Newport, UK.
Plastic pipette tips	1000 µl, 200 µl and 20 µl	Starlab, Milton Keynes, UK.
Plastic serological pipettes	5 ml, 10 ml and 25 ml	Sarstedt, Numbredt, Germany.
Plastic syringes	1 ml, 2 ml, 5 ml, 10 ml, 20 ml and 50 ml	Appleton Woods, Birmingham, UK.
Plastic universals	N/A	Scientific Laboratory Supplies Ltd, Nottingham, UK.
Plate seals	N/A	Perkin Elmer, Cambridge, UK.
Polycarbonate filter papers	10 µm, 1 µm, 0.1 µm and 0.015 µm pore sizes	Whatman, Maidstone, UK.
Sepmate tubes	50 ml	Stem Cell Technologies, Vancouver, Canada.
Sodium heparinised collection test tubes	14 ml	Scientific Laboratory Supplies Ltd, Nottingham, UK.

Sterile plastic pots	60 ml, 150 ml and 250 ml	ThermoFisher Scientific, Hemel Hempstead, UK.
Tissue culture flask	75 cm^2	Corning, New York, USA and Nunc, Denmark.
Toothbrushes	N/A	Morrisons, Bradford, UK.
Vacuum seal bags	30 cm x 10 cm	Westfield Medical Ltd, Radstock, UK.
Weighing boats	Various sizes	Scientific Laboratory Supplies Ltd, Nottingham, UK.
White optiplates	96 well	Perkin Elmer, Cambridge, UK.
Wide bore pipette tips	1000 µl	Starlab, Milton Keynes, UK.

2.1.3 Equipment

The general equipment used throughout this study is listed in Table 2.3.

Table 2.3 General equipment used throughout this study.

Name	Model	Supplier
Balance	GR200	A & D Instruments Ltd, Oxford, UK.
Balance	GX 2000 EC	Sartorius, Epsom, UK.
Centrifuge	Harrier 15/80	Sanyo, Watford, UK.
Class I laminar flow cabinet	N/A	Bassaire, Southampton, UK
Class II safety cabinet	Heraeus 85	Heraeus Instruments, Hanau, Germany
Fluorescence microscope	Zeiss Axio Imager M2	Carl Zeiss, Oberkochen, Germany.
Freezer (-20°C)	N/A	Labcold, Basingstoke, UK.

Freezer (-80°C)	N/A	Labcold, Basingstoke, UK.
Fridge	N/A	Labcold, Basingstoke, UK.
Fumehood	N/A	Whiteley, Hants, UK.
Gilson pipettes – 1000 µl, 200 µl, 20 µl and 2 µl	N/A	Thermo Scientific, Hemel Hempstead, UK.
Glass Duran bottles (500 ml and 1 L)	N/A	Fisherbrand, Loughborough, UK.
Glass filtration equipment	N/A	Sartorius, Epsom, UK.
Glass petri dish	N/A	Scientific Laboratory Supplies Ltd, Nottingham, UK.
Glass universals	N/A	Glassware Stores, School of Molecular and Cellular Biology, University of Leeds.
Haemocytometer	N/A	Optik Labor, Friedrichshofen, Germany.
Ignitor	N/A	Fisher Scientific UK, Loughborough, UK.
Incubator	MCO-20AIC	Sanyo, Watford, UK.
Light microscope	Olympus CK40-SLP	Olympus Optical Co. Ltd, London, UK.
Metal spatula	N/A	Scientific Laboratory Supplies Ltd, Nottingham, UK.
Metal tweezers	N/A	Fisher Scientific UK, Loughborough, UK.
Microwave	KM19W	Proline, UK

Mr Frosty	N/A	Sigma Aldrich, Dorset, UK.
Orbital shaker	PSU-10i	Fisher Scientific UK, Loughborough, UK.
Oven	N/A	Genlab, Widnes, UK.
Pipette boy	N/A	Scientific Laboratory Supplies Ltd, Nottingham, UK.
Plate reader	Hidex plate chameleon	Hidex, Turku, Finland.
Plate reader	Multiskan spectrum	Thermo Scientific, Hemel Hempstead, UK.
Scissors	N/A	Scientific Laboratory Supplies Ltd, Nottingham, UK.
Sonicating water bath	N/A	VWR, Lutterworth, UK.
Thermometer	N/A	Fisher Scientific UK, Loughborough, UK.
Vacuum pump	N/A	KNF, Neubauer, Germany.
Vacuum sealer	N/A	Hulme-Martin Ltd, Woking, UK.
Vacuum tubing	N/A	Cole-Parmer Instrument Co Ltd, London, UK.
Vortex mixer	Topmix FB15024	ThermoFisher Scientific UK, Loughborough, UK.
Wash bottle	N/A	Scientific Laboratory Supplies Ltd, Nottingham, UK.
Water bath	N/A	Grant Instruments Limited, Cambridge, UK.

White plastic filtration disc	N/A	Scientific Laboratory Supplies Ltd, Nottingham, UK.

2.1.4 Cell lines

The general cell lines used throughout this study are listed in Table 2.4.

Table 2.4 General cell lines used throughout this study.

Cell line	Species	Origin	Supplier
RAW 264.7	Mouse	Ascites of an induced tumour by intraperitoneal injection of Abselon Leukaemia Virus.	European Collection of Animal Cell Cultures.
U937	Human	Histiocytic lymphoma	European Collection of Animal Cell Cultures.

2.1.5 Primary cells

The primary cells used in this study are listed in Table 2.5.

Table 2.5 Primary cells used throughout this study.

Primary cell type	Species	Origin	Supplier
Peripheral Blood Mononuclear Cells (PBMNCs)	Human	Blood	Individual donors

2.1.6 Particles

The general particles used throughout this study are listed in Table 2.6.

Table 2.6 General particles used throughout this study.

Item	Supplier

0.2 µm FluoSpheres® Carboxylate-Modified Microspheres – yellow-green fluorescent (505/515)	Invitrogen Life Technologies Ltd, Paisley, UK.
Ceridust® 3615 resin	Hoescht, Germany.

2.2 Methods

The methods used throughout all chapters of this study are described below.

2.2.1 Equipment sterilisation

Throughout the course of this study, it was necessary to sterilise various equipment and disinfect work surfaces to ensure a sterile working environment. The methods used to do so are detailed below.

2.2.1.1 Aseptic technique

Prior to use, the interior surfaces of the class II safety cabinet were sprayed with 1% Virkon (w/v) followed by 70% ethanol (v/v). All items that entered the cabinet were sprayed with 70% ethanol (v/v). After use, the cleaning process was repeated and the cabinet was disinfected with UV light for one hour prior to shut down.

2.2.1.2 Glassware and plastic-ware sterilisation

All glassware and plastic-ware was washed with fairy liquid and warm water and scrubbed using a toothbrush. The glassware and plastic-ware was then rinsed with distilled water followed by ultrapure water. The glassware was then sterilised using dry heat sterilisation and the plastic-ware was sterilised using moist heat sterilisation.

2.2.1.3 Dry heat sterilisation

All equipment to be sterilised was wrapped in foil after being washed thoroughly and air dried. Equipment was then placed into a hot air oven at 190°C for 4 hours. Items were left to cool before being removed from the oven.

2.2.1.4 Moist heat sterilisation

Items unable to undergo dry heat sterilisation, for example plastic and solutions in glass bottles, were autoclaved. After being washed thoroughly with detergent and air dried, items were sealed in medical packaging and autoclaved at 15 psi and 121°C for 20 minutes. Items were left to cool before being removed from the autoclave.

2.2.1.5 Filter sterilisation

Solutions, such as DMSO and Trypan blue, were filter sterilised using a 0.22 µm sterile filter unit in a sterile class II safety cabinet prior to use. Solutions were drawn up

into a 10 ml syringe, the filter unit was attached and the solution was passed through into a sterile universal.

2.2.2 Microscopy

The methods used to carry out bright field and fluorescence microscopy are detailed below.

2.2.2.1 Bright field

For cell culture observation and counting, an optical Olympus CK040-SLP microscope was used. Köhler illumination was used to view the samples.

2.2.2.2 Fluorescence

A Zeiss Axio Imager M2 fluorescence microscope was used to image fluorescently stained cells and particles in collagen gel. The channels used were: 461 nm (Hoechst; blue), 521 nm (Fluorescein; green) and 590 nm (Lysotracker red; red).

2.2.3 General reagents and solutions preparation

The preparation of the general reagents and solutions used throughout this study are described below. Reagents and solutions specific to particular chapters are described in the relevant methods of Chapters 3, 4 and 5.

2.2.3.1 Cryopreservation medium

Cryopreservation medium for RAW 264.7 murine macrophages was prepared by combining 14 ml DMEM with 4 ml FBS (20% (v/v)) and 2 ml DMSO (10% (v/v)). The cryopreservation medium was heated to 37°C prior to use and stored at 4°C between uses for up to one month.

2.2.3.2 Dulbecco's Modified Eagles Medium cell culture medium

Cell culture medium for RAW 264.7 murine macrophages was prepared by combining 500 ml DMEM with 100 $U.ml^{-1}$ penicillin and 100 $\mu g.ml^{-1}$ streptomycin, 2 mM L-glutamine and 10% (v/v) FBS. Aliquots of 100 $U.ml^{-1}$ penicillin and 100 $\mu g.ml^{-1}$ streptomycin, 2 mM L-glutamine and 10% (v/v) FBS were stored at -20°C and defrosted using a water bath at 37°C. Complete DMEM was heated in a water bath at 37°C for 30 minutes before use and stored in the fridge at 4°C between uses for up to one month.

2.2.3.3 Ethanol

A 10 L stock of 70% (v/v) ethanol was prepared by adding 3 L distilled water to 7 L of ethanol.

2.2.3.4 Lipopolysaccharide

Stock solution preparation

A mass of 1 mg of LPS powder was reconstituted with 1 ml DPBS to produce a 1 $mg.ml^{-1}$ stock solution. This was stored at -20°C between uses and defrosted in a water bath at 37°C when required.

Working solution preparation

A working solution of LPS was prepared by adding 4 µl of LPS stock (4000 ng) to 20 ml medium (either DMEM or RPMI 1640) to give a final working concentration of 200 $ng.ml^{-1}$.

2.2.3.5 Nutrient broth

Nutrient broth powder, 13 g, was weighed out and added to 1 L of distilled water in a sterile glass Duran bottle. The bottle was agitated to dissolve the powder. The bottle was then autoclaved to sterilise the nutrient broth.

2.2.3.6 Roswell Park Memorial Institute 1640 cell culture medium

Cell culture medium for PBMNC's and U937 human histiocytes was prepared by combining 500 ml RPMI 1640 cell culture medium with 100 $U.ml^{-1}$ penicillin and 100 $\mu g.ml^{-1}$ streptomycin, 2 mM L-glutamine and 10% (v/v) FBS as per Section 2.2.3.2.

2.2.3.7 Sodium hydroxide (1.94 M)

Sodium hydroxide pellets (7.76 g) were weighed out and added to a 100 ml glass Duran bottle. The pellets were dissolved in 100 ml ultrapure water. This solution was then sent to autoclave (121°C and 15 psi for 20 minutes).

2.2.3.8 Trigene

A 5 L stock of 1% (w/v) Trigene was prepared by combining 50 ml of Trigene with 5 L distilled water.

2.2.3.9 Virkon

A 5 L stock of 1% (w/v) Virkon was prepared by mixing 50 g of Virkon powder with 5 L distilled water.

2.2.3.10 Wear simulator rig lubricant

FBS was added to RPMI 1640 cell culture medium to create a 25% (v/v) solution in a sterile, aseptically cleaned class II cell culture cabinet. This was prepared either the day before or on the day of the wear test in which it was used and was stored in a sterile plastic pot in the fridge at 4ºC until use.

2.2.4 Isolation of primary cells

The full procedure to isolate PBMNCs from donated human whole blood is detailed below. The blood used herein was collected as per the Faculty of Biological Sciences Ethics Committee approval (BIOSCI 10-018). All donors were healthy and were

between 24 and 60 years of age. Each donor provided informed consent prior to donation.

2.2.4.1 Solution preparation

RPMI 1640 cell culture medium

RPMI 1640 cell culture medium was prepared as described previously in Section 2.2.3.6.

RPMI 1640 transport medium

Transport medium for PBMNCs was prepared by combining 500 ml RPMI 1640 medium with 2 ml of 100 $U.ml^{-1}$ penicillin and 100 $\mu g.ml^{-1}$ streptomycin and 80 µl 1M HEPES. RPMI 1640 transport medium was heated in a water bath at 37°C for 30 minutes before use and stored in the fridge at 4°C between uses for up to one month.

2.2.4.2 Tissue harvesting

Approximately 30 ml of whole blood was taken by venepuncture of an anonymous donor using a 21 G butterfly needle. The donated blood was stored in sodium heparinised collection tubes at room temperature (25°C) until use later that day.

2.2.4.3 Achiever tracking

The blood was recorded and tracked from whole blood donation to PBMNC isolation to disposal using the Achiever tissue tracking system (Leeds Teaching Hospital NHS Trust and University of Leeds) as specified by the Human Tissue Authority and Faculty of Biological Sciences Ethics Committee Approval (BIOSCI 10-018).

2.2.4.4 Isolation of Peripheral Blood Mononuclear Cells from whole blood tissue

PBMNC isolation was carried out in an aseptically cleaned class II safety cabinet. The blood was mixed by gently inverting the tubes. All vials of blood were pooled in a sterile 150 ml pot (approximately 40 ml blood per sample overall) and were immediately diluted 1:1 with RPMI 1640 transport medium and swirled gently to mix. Lymphoprep was pipetted carefully through the filter hole into each Sepmate tube until the filter was covered (approximately 15 ml). Whole blood (between 10 and 15 ml per tube) was then layered over the lymphoprep in each tube. The Sepmate tubes were then centrifuged at 12000 g and brake speed 4 for 10 minutes at room temperature (25°C). The top layer of each Sepmate tube was poured into fresh falcon tubes; leaving behind the red blood cells below the filter. The PBMNC's were washed with RPMI 1640 transport medium and centrifuged at 150 rcf for 10 minutes at brake speed 4 at room temperature (25°C). This was repeated twice more. Finally the cell pellets were resuspended in complete RPMI 1640 cell culture medium and combined. The

cells were counted using the Trypan blue exclusion assay as described in Section 2.2.8.3.

2.2.5 Cell line culture and maintenance

2.2.5.1 Resurrection of cell lines

RAW 264.7 murine macrophages

A cryovial of RAW 264.7 murine macrophages, containing approximately 1 x 10^6 cells, was taken from storage in liquid nitrogen at -196°C and defrosted rapidly (2 to 5 minutes) in a water bath at 37°C. Complete DMEM cell culture medium (8 ml) was added to a Corning T75 tissue culture flask followed by the addition of the cells and cryopreservation medium contained in the cryovial (1 ml). The cryovial was rinsed with a further 1 ml of complete DMEM cell culture medium, which was also added to the tissue culture flask to give a final volume of 10 ml medium inside the flask. The cells were observed using light microscopy to confirm their presence and then the flask was placed inside an incubator at 37°C and 8% (v/v) CO_2 in air overnight. After approximately 12 hours, the flask was observed again using light microscopy to confirm cell adherence. The existing medium in the tissue culture flask was replaced with 10 ml fresh complete DMEM cell culture medium in order to remove any remains of cryopreservation medium. The flask was placed in the incubator at 37°C and 8% (v/v) CO_2 in air for a further 48 hours.

U937 human histiocytes

A cryovial of U937 human histiocytes (containing approximately 1 x 10^6 cells) was prepared as described above. Complete RPMI 1640 cell culture medium (8 ml) was added to a universal in addition to the contents of the cryovial (1 ml) and the medium used to rinse the cryovial (1 ml) to give a final volume of 10 ml medium. The universal was then centrifuged at 150 rcf for 10 minutes in order to separate the cells from the cryopreservation medium. The supernatant was discarded and the cell pellet was resuspended in 10 ml of fresh complete RPMI 1640 cell culture medium. The cells and medium were then transferred to a sterile Nunc T75 tissue culture flask. The flask was observed using light microscopy as above and placed at a 45° angle inside an incubator at 37°C and 5% CO_2 (v/v) in air overnight.

2.2.5.2 Transformation of U937 human histiocytes using Phorbol-12-Myristate-13-Acetate

Phorbol-12-Myristate-13-Acetate (PMA) powder (1 mg) was dissolved in 1 ml DMSO to create a 1 $mg.ml^{-1}$ stock. A volume of 1 µl of stock PMA was added to 1 ml of DPBS to create a 1 $\mu g.ml^{-1}$ stock. A volume of 100 µl of the diluted stock solution (1 $\mu g.ml^{-1}$) was added to 10 ml of complete RPMI 1640 cell culture medium and suspended, non-

transformed U937 human histiocytes in a tissue culture flask to create a 10 $ng.ml^{-1}$ working solution. This was carried out after a medium change (as described below in Section 2.2.5.3) to ensure the transformation medium was fresh. The tissue culture flask was then laid flat and incubated at 37°C and 5% (v/v) CO_2 in air for 24 hours. After 24 hours, cell morphology was inspected using light microscopy to confirm transformation; transformed cells displayed fibroblastic morphology rather than rounded.

2.2.5.3 Medium change of cell lines

RAW 264.7 murine macrophages and transformed U937 human histiocytes

Occasionally, it was necessary to change the medium rather than passage cells in order to maintain cell numbers prior to use. This was achieved by simply aspirating the existing medium and replacing it with 10 ml fresh complete cell culture medium and returning the tissue culture flasks to the incubator at 37°C and 8% (v/v) (RAW 264.7 murine macrophages) or 5% (v/v) (U937 human histiocytes) CO_2 in air.

Non-transformed U937 human histiocytes

The existing U937 human histiocytes and medium were removed from the tissue culture flask and placed into a sterile universal, which was centrifuged at 150 rcf for 10 minutes at room temperature (25°C). The supernatant was discarded and the cell pellet was resuspended in 10 ml fresh complete RPMI 1640 cell culture medium. This was then transferred back into the existing tissue flask. The flask was then incubated at 37°C in 5% (v/v) CO_2 in air overnight at a 45° angle.

2.2.5.4 Passage of cell lines

RAW 264.7 murine macrophages

Following resurrection, the cells were regularly observed using a light microscope to check their confluency, i.e. how much of the observable space was covered with cells expressed as a percentage. Once the confluency was 70% or more, the RAW 264.7 murine macrophages were passaged. RAW 264.7 murine macrophages were passaged at a lower confluency than other cell types (typically >80%) because they are a semi-adherent cell type. This means they can change phenotype and become a suspension cell type if they become overcrowded. Passaging was achieved by first replacing the existing medium with fresh medium. The cells were then detached physically from the tissue flask base using a cell scraper. The base was scraped back and forth from the back of the flask to the front and then in reverse. The medium became cloudy as the cells were detached and their detachment was confirmed using a light microscope. The detached cells were visible as free floating rounded up cells in the medium. The resultant cell:medium mixture was then divided between tissue

culture flasks in the ratio 1:2. Fresh medium was then added to each flask until each flask contained 10 ml complete cell culture medium. The flasks were then replaced in the incubator at 37°C and 8% (v/v) CO_2 in air overnight.

Non-transformed U937 human histiocytes

Passaging was achieved by placing the existing suspension cells and medium from the tissue culture flask into a sterile universal, which was centrifuged at 150 rcf for 10 minutes at room temperature (25°C). The supernatant was discarded and the cell pellet was resuspended in 10 ml fresh complete RPMI 1640 cell culture medium. This was then split 1:3 with each flask having a total volume of 10 ml medium. The flasks were then incubated at 37°C in 5% (v/v) CO_2 in air overnight.

Transformed U937 human histiocytes

The existing medium was removed from the tissue culture flask and discarded. A volume of 3 ml of trypsin (0.5%(v/v)) in EDTA was added to the tissue culture flask such that the monolayer of cells attached to the surface was covered. The tissue culture flask was incubated at 37°C and 5% (v/v) CO_2 in air for 10 minutes. The flasks were then gently tapped and inspected under a light microscope to confirm detachment of the cells. The cells and trypsin were removed from the tissue culture flask and placed into a sterile universal. A volume of 10 ml of fresh complete RPMI 1640 cell culture medium was added to the universal. The universal was then centrifuged at 150 rcf for 10 minutes at brake speed 4 at room temperature (25°C). The supernatant was discarded and the cells were resuspended in 10 ml of fresh complete RPMI 1640 cell culture medium. The cells were not split amongst further flasks but instead went on to be used immediately.

2.2.5.5 Cryopreservation of cell lines

Cells were passaged as described in Section 2.2.5.4 and counted using Trypan blue exclusion assay as described in Section 2.2.8.3. The cells were then centrifuged at 150 rcf for 10 minutes at brake speed 4. The supernatant was discarded and the cell pellet was resuspended in cryopreservation medium made with either DMEM or RPMI 1640 culture medium according to the cell line used. Frozen cell stocks were created by adding 1 ml of cryopreservation medium to 1 x 10^6 cells in a cryovial. The cryovial was then placed into a controlled rate freezer (Mr Frosty) at -80°C for 24 hours. After 24 hours, the cryovial was moved to permanent storage in liquid nitrogen at -196°C.

2.2.5.6 Disposal of cell lines

All cell containing waste was disposed of by adding 1% (w/v) Virkon solution, incubating at room temperature (25°C) for 30 minutes followed by disposal into the waste water system.

2.2.6 Particle preparation

Both Ceridust® and FluoSpheres® were used as model particles throughout this study in addition to artificially generated UHMWPE wear debris. The preparation of all types of particles to be seeded with cells are detailed herein.

2.2.6.1 Ceridust®

Ceridust 3615® resin (Hoechst, Germany) is a low molecular weight polyethylene powder which is commercially available and often used to used to initially model cellular response to polyethylene particles in place of clinically relevant wear debris in cases where yields may be low and thus particle stock is limited. Ceridust 3615® resin is known to induce the production of inflammatory cytokines associated with osteolysis in both human (Matthews *et al.*, 2000a; Matthews *et al.*, 2001) and murine (Green *et al.*, 1998) macrophage cells. In this study, Ceridust 3615® resin was filtered into three different size ranges (>10 μm, 1 – 10 μm and 0.1 – 1 μm) to assess the inflammatory response to defined particle sizes as size is known to be an important factor for the production of inflammatory cytokines by macrophage cells (Green *et al.*, 1998).

Preparation

A mass of 100 mg of Ceridust® was weighed out. In a sterile environment, the Ceridust® was placed in a sterile glass petri dish. A volume of 1 ml of either RPMI 1640 medium (for use with U937 human histiocytes and PBMNCs) or DMEM (for use with RAW 264.7 murine macrophages) was added drop-wise and used to blend the particles. Further volumes of medium (1 ml at a time drop-wise) were added until the particles were fully blended and a final volume of 20 ml was achieved. The particles and medium mixture was placed into a sterile glass universal. The universal was then sonicated for 40 minutes.

Filtration

Polycarbonate filter papers (10 μm, 1 μm and 0.1 μm pore sized) were rinsed with 70% (v/v) ethanol and air dried then weighed. The filtration equipment was cleaned and sterilised in an oven at 190°C. The filtration equipment was set up in a sterile class II safety cabinet and then Ceridust® suspension was filtered sequentially through the 10 μm, 1 μm and 0.1 μm filters. The filter papers were then left to air dry overnight in the class II safety cabinet, in order to evaporate any moisture present which may affect mass readings, and then weighed again. The mass of Ceridust® for each size range (>10 μm, 1 - 10μm and 0.1 - 1 μm) was calculated:

$$
\begin{aligned}
&Mass\ of\ Ceridust\ (g) \\
&= Mass\ of\ Ceridust\ and\ filter\ paper\ (after\ filtration\ and\ air\ drying)(g) \\
&- Mass\ of\ dry\ filter\ paper\ prior\ to\ filtration\ (g)
\end{aligned}
$$

The filter papers were then cut into small pieces and placed in 10 ml of medium as before. The suspensions were stored at -20°C between use and, when required, defrosted and sonicated for 40 minutes prior to use.

The particle dose for Ceridust® was calculated as follows. Each experiment required a dose of 100 μm^3 particles.cell^{-1}. The final cell seeding density chosen was 1 x 10^5 cells.ml^{-1}. These quantities are used to calculate the required volume of particles.ml^{-1}:

$$1 \times 10^5 \text{ cells.ml}^{-1} \times 100 \ \mu m^3 \text{ particles.cell}^{-1} = 1 \times 10^7 \ \mu m^3 \text{ particles.ml}^{-1}$$

The relationship between density and volume was then used to calculate the mass of particles needed per well:

$$Mass = Volume \times Density$$

$$(1 \times 10^7 \ \mu m^3) \times (1 \times 10^{-6} \ \mu g. \ \mu m^{-3}) = 10 \ \mu g \text{ particles per well}$$

This mass was then used to calculate the volume of the prepared Ceridust® suspension required to encapsulate in either agarose or collagen gel.

$$\frac{Mass\ of\ particles\ required\ per\ condition\ (6\ repeats)}{Mass\ of\ ceridust\ on\ filter\ paper}\ x\ 100$$

$$= \%\ volume\ of\ particle\ suspension\ to\ use$$

for example - 0.06 mg/14.7 mg x 100 = 0.41%

therefore 0.41% of 5 ml (20.5 µl) of the >10 µm Ceridust® suspension was used.

2.2.6.2 FluoSpheres®

FluoSpheres® (Invitrogen Life Technologies Ltd, Paisley, UK) are latex particles that are commercially available in a variety of sizes and with a variety of fluorescent tags. FluoSpheres® are known to induce an inflammatory response in human PBMNCs (Richards, 2008; Liu, 2012). For this study, 0.2 µm FluoSpheres® Carboxylate-Modified Microspheres yellow-green fluorescent (505/515) were used.

The volume of FluoSpheres® required per ml was calculated as follows:

$$1 \times 10^5 \text{ cells.ml}^{-1} \times 100 \ \mu m^3 \text{ particles.cell}^{-1} = 1 \times 10^7 \ \mu m^3 \text{ particles.ml}^{-1}$$

The total volume of the stock FluoSpheres® was then divided by the volume of FluoSpheres® required in order to yield the dilution factor:

$$1.905 \times 10^{10} \ \mu m^3 / 1 \times 10^7 \ \mu m^3 = 1905$$

Therefore 1/1905th of the total volume of FluoSpheres® (1 ml) was required per well, i.e. 0.5 µl.

2.2.6.3 Single and six station pin-on-plate multidirectional wear simulator rig generated UHMWPE wear debris

Polycarbonate filter papers (10 μm, 1 μm and 0.1 μm pore sized) were rinsed with 70% (v/v) ethanol and air dried then weighed. The filtration equipment was cleaned and sterilised in an oven at 190°C. The six station wear test lubricants to be used were removed from storage at -20°C, allowed to defrost at room temperature (25°C) and sonicated for 40 minutes. The filtration equipment was set up in a sterile class II safety cabinet and then each six station pin-on-plate (POP) wear test serum (GUR 1020 XL, GUR 1020 XL AOX, GUR 1050 XL and GUR 1050 XL VE) was filtered sequentially through the 10 μm, 1 μm and 0.1 μm pore sized polycarbonate filters. The polycarbonate filter papers were then left to air dry overnight in the class II safety cabinet and the 0.1 μm pore sized polycarbonate filter paper was weighed again. The mass of UHMWPE wear debris for the size range 0.1 - 1 μm was calculated:

$$Mass\ of\ UHMWPE\ wear\ debris\ (g) = Mass\ of\ UHMWPE\ wear\ debris\ and\ filter\ paper\ after\ filtration\ (g) - Mass\ of\ filter\ paper\ prior\ to\ filtration\ (g)$$

Once dry, the filter papers were then cut into small pieces and placed in 1 ml of medium. The suspensions were used immediately with sonication for 40 minutes prior to use.

The mass of particles required per condition was calculated:

$$\frac{Mass\ of\ particles\ required\ per\ condition\ (12\ repeats)}{Mass\ of\ generated\ wear\ debris\ in\ suspension}\ x\ 100 = \%\ volume\ of\ particle\ suspension\ to\ use$$

for example - 0.12 mg/88.8 mg x 100 = 0.14%

therefore 0.14% of 20 ml (28 μl) of the single station POP generated GUR 1020 XL AOX suspension was used.

2.2.7 Preparation of gels

The methods used to prepare both the agarose and collagen gels used in this study are described below.

2.2.7.1 Agarose gel preparation

A stock solution of 2% (w/v) agarose was prepared which was then used to prepare the final 0.4% (w/v) agarose gel solution. The preparation of both is detailed below.

Stock agarose gel preparation – 2% (w/v)

A mass of 6 g of low melting point agarose powder was added to 30 ml of medium (either DMEM or RPMI 1640 depending on the cell type to be seeded within it) in a

sterile glass Duran bottle. The contents were then mixed and the glass Duran bottle underwent moist heat sterilisation as described in Section 2.2.1.4.

Working concentration agarose gel preparation – 0.4% (w/v)

The glass Duran bottle containing 2% (w/v) agarose gel stock was heated in the microwave until molten (approximately 1 minute). Stock agarose gel (2 ml) was added to preheated (37°C) medium (8 ml) – either DMEM or RPMI 1640 medium – to create a 10 ml stock solution. Gels were prepared in 48 well plates as follows. A volume of 200 µl of the 0.4 % (w/v) agarose gel was pipetted into either Corning Co-Star (for RAW 264.7 murine macrophages) or Nunc coated 48 well tissue culture plates (for U937 human histiocytes and PBMNCs). The gels were left to set at room temperature (25°C) for 10 to 15 minutes, sealed with a plastic film cover and stored at 4°C until use.

2.2.7.2 Type I rat tail collagen

Initially 80% (v/v) type I rat tail collagen gel was added to a sterile universal followed by 10% (v/v) 10X MEM which was added slowly to avoid generating bubbles and mixed gently. The mixture was not aspirated in order to avoid the generation of bubbles. A peach/orange colour was observed. Once the collagen and 10X MEM was mixed, 1.94 M sodium hydroxide was added drop-wise to the gel in order to begin the pH dependent process of setting the gel until a light pink colour was achieved. Finally, 4.2% (v/v) cells/medium/particles was added to the gel; again pipetted carefully into the gel mixture and mixed gently. A volume of 200 µl gel was added to each well of a Corning CoStar 48 well tissue culture plate and the plate was placed into the incubator until set (approximately 10 to 15 minutes). This volume was kept the same as that of agarose gel in order to generate gels of the same depth in the 48 well plates. This process was repeated for each batch. Finally, a volume of 1 ml complete DMEM was added to each well and the plates were incubated at 37°C and 8% (v/v) CO_2 in air.

Working example

To create 3 ml of collagen gel for use *in vitro*, 2.4 ml (80% (v/v)) of type I rat tail collagen gel was added to a sterile universal followed by 300 µl (10% (v/v)) 10X MEM and mixed gently. Once the collagen and 10X MEM were mixed, 1.94 M sodium hydroxide was added drop-wise to the gel until a light pink colour was achieved. Finally, 126 µl (4.2% (v/v)) cells/medium/particles was added to the gel and mixed gently. A volume of 200 µl gel was added to each well of a Corning 48 well tissue culture plate and the plate was placed into the incubator until set.

2.2.8 Biochemical assays

Below are detailed the methods of the general biochemical assays used throughout this project: ATP-lite™ luminescence ATP detection assay, ELISA and Trypan blue exclusion assay.

2.2.8.1 ATP-lite™ luminescence ATP detection assay

Adenosine triphosphate (ATP) is one of many markers of cell viability as it is present in healthy, metabolically active cells in abundance but declines when cells are undergoing apoptosis or necrosis. The ATP-lite™ luminescence ATP detection assay utilises the reaction of D-luciferin with ATP and oxygen, catalysed by luciferase, to produce detectable luminescence. This light is detected by a scintillation counter and is proportional to the amount of ATP present in the sample.

$$ATP + D - Luciferin + O_2 \xrightarrow[Mg^{2+}]{Luciferase} Oxyluciferin + AMP + PPi + CO_2 + light$$

This assay was chosen in place of the traditional colorimetric MTT assay as previous studies at the University of Leeds (Lee, 2016; Smith, 2016) have shown that the reduction reaction required for the MTT assay is disrupted by collagen gel, which causes the formazan product to turn brown instead of purple. As the MTT assay relies on a general reduction reaction, this is easily interfered with by the presence of other redox reagents.

ATP-lite™ luminescence ATP detection assay kit components

The components of the ATP-lite™ luminescence ATP detection assay kit are listed in Table 2.7.

Table 2.7 List of ATP-lite™ luminescence detection assay kit components.

ATP-lite™ luminescence detection assay kit components	**Supplier**	**Storage**
Mammalian cell lysis solution (MCL)	Perkin Elmer, Cambridge, UK.	Stored at 4°C.
ATP-lite™ substrate	Perkin Elmer, Cambridge, UK.	Stored at 4°C.
ATP-lite™ substrate buffer	Perkin Elmer, Cambridge, UK.	Stored at 4°C.

Preparation of ATP-lite™ substrate

ATP-lite™ substrate solution was prepared by adding 25 ml ATP-lite™ buffer solution to pre-weighed, lyophilised ATP-lite™ substrate, divided into 5 ml aliquots and frozen at -20°C until use. The aliquots were defrosted in a water bath at 37°C when required.

ATP-lite™ luminescence detection *assay procedure*

The supernatant was removed and 50 µl of MCL was added to each well. The plate was then placed on the orbital shaker for 5 minutes at 700 rpm at room temperature (25°C). Following this, 50 µl of ATP-lite™ substrate was added to each well in the dark. The plate was wrapped in foil and placed on the shaker as before. The contents of each well were then transferred to the corresponding wells of a white optiplate. The plate was checked for bubbles and any present were removed with a sterile needle. The plate was then sealed with a clear plastic cover, wrapped in foil and read using a Hidex plate chameleon plate reader; initially dark adapting each plate for 10 minutes prior to measuring luminescence output. On day 0, the assay was performed 2 hours post seeding to allow for cells to adhere to the tissue culture plate.

Adapted procedure for agarose and collagen gels in 48 well tissue culture plates

The manufacturers instructions were adapted in order to allow the reagents to fully penetrate the agarose and collagen gels. The volumes of MCL and ATP-lite substrate were increased four-fold from 50 µl to 200 µl. The shaking times were increased four fold from 5 minutes to 20 minutes. The contents of each well were therefore increased to 400 µl rather than 100 µl. Only 100 µl from each well was transferred to the white optiplate and measured. To account for this, the luminescence counts were multiplied by four during statistical analysis.

2.2.8.2 Enzyme Linked Immunosorbent Assay

A variety of both human and murine enzyme linked immunosorbent assays (ELISAs) were carried out during this study overall. The general kits used are detailed in the materials section of this chapter (Section 2.1.1) whereas the specific reagents associated with each kit are detailed in Tables 2.8, 2.9, 2.10, 2.11 and 2.12 below. In addition, a general method for both human and murine kits is described below and any details specific to a particular inflammatory cytokine or mediator tested are listed separately. Where the kit used differed significantly from the general method described, the specific method associated with a particular kits use is described in full.

General assay components

Human

Table 2.8 Human TNF-α ELISA kit reagents, storage and preparation instructions.

Reagent	Storage and preparation
Human TNF- α capture antibody	Stored at 4°C and prepared by adding 100 µl of capture antibody to 10 ml of coating buffer.
Human TNF-α standard (800 pg.ml^{-1})	Stored at 4°C and prepared by reconstituting with 0.87 ml of RPMI 1640 cell culture medium and inverted to mix.
Biotinylated anti-hTNF-α detection antibody	Stored at 4°C and reconstituted with 550 µl of reconstitution buffer prior to use. A volume of 100 µl of reconstituted biotinylated anti-hTNF-α detection antibody was added to 5 ml of secondary antibody buffer.
Streptavidin-HRP	Stored at 4°C and prepared by adding 150 µl of vortexed streptavidin-HRP to 10 ml streptavidin-HRP diluent in a glass universal.
TMB substrate	Stored at 4°C.
Reconstitution buffer	Stored at 4°C and prepared by adding 0.09% (v/v) sodium azide to 1X PBS.
Coating buffer	Stored at 4°C and prepared by decanting 1X PBS into a sterile glass Duran bottle.
Wash buffer	Prepared by adding 0.05% (v/v) TWEEN-20 to 1X PBS. Not stored after use.
Blocking buffer	Stored at 4°C and prepared by adding 5% (v/v) BSA to 1X

	PBS.
Standard dilution buffer	RPMI 1640 medium was used as the standard dilution buffer.
Secondary antibody dilution buffer	Stored at 4°C and prepared by adding 1% (v/v) BSA to 1X PBS.
HRP-dilution buffer	Stored at 4°C and prepared by adding 1% (v/v) BSA and 0.1% (v/v) TWEEN-20 to 1X PBS.

Mouse

Table 2.9 Murine TNF-α, IL-1β and IL-6 ELISA kit reagents, storage and preparation instructions.

Murine TNF-α uncoated 10 x 96 well ELISA kit components	**Supplier**	**Storage and preparation**
Anti mouse TNF-α/IL-1β /IL-6 Capture antibody	ThermoFisher Scientific UK, Loughborough, UK	Stored at 4°C and prepared by diluting 1:250 with 1X coating buffer.
mTNF-α (1000 $pg.ml^{-1}$)/IL-1β (1000 $pg.ml^{-1}$)/IL-6 (500 $pg.ml^{-1}$)standard	ThermoFisher Scientific UK, Loughborough, UK	Stored at 4°C and prepared by reconstituting with DMEM and inverted to mix.
ELISA diluent	ThermoFisher Scientific UK, Loughborough, UK	Stored at 4°C and prepared by diluting 1:5 in deionised water.
Biotinylated anti-mTNF-α/IL-1β/IL-6 detection antibody	ThermoFisher Scientific UK, Loughborough, UK	Stored at 4°C and prepared by diluting 1:250 in ELISA diluent. The detection antibody was allowed to

		reconstitute for 10 – 30 minutes with gentle swirling prior to use.
Streptavidin-HRP	ThermoFisher Scientific UK, Loughborough, UK	Stored at 4°C and prepared by diluting 1:250 in ELISA diluent.
TMB substrate	ThermoFisher Scientific UK, Loughborough, UK	Stored at 4°C.
Coating buffer	ThermoFisher Scientific UK, Loughborough, UK	Stored at 4°C and prepared by diluting 1:10 with deionised water
Wash buffer	N/A	Prepared by adding 0.05% (v/v) TWEEN-20 to DPBS and stored at 4°C for up to one month.
Stop solution – Sulfuric acid 1 M	Sigma Aldrich, Dorset, UK.	Stored at room temperature (25°C).

General assay procedure

Detailed below are the methods used to carry out quantitation of human and mouse TNF-α, IL-1β and IL-6 ELISA after stimulation with particles and/or controls.

Human

A volume of 100 µl of diluted capture antibody was added to each well of a 96 well Nunc maxisorp plate. The plate was sealed and incubated at 4°C overnight. The cover was then removed and the plate was washed by aspirating the plate, filling each well with wash buffer and aspirating the wells again. This procedure was repeated once more. A volume of 100 µl of blocking buffer was then added to each well and the plate was sealed again and incubated at room temperature (25°C) for 2 hours. Following this incubation, the plate was washed a further three times as described previously. The plates were typically used immediately and thus preparation for storage was not necessary. During the previous incubation, the reagents were brought to room temperature (25°C) before use. The standards were added to the plate (100 µl per well) in serial dilution at the following concentrations: 800 $pg.ml^{-1}$, 400 $pg.ml^{-1}$, 200

$pg.ml^{-1}$, 100 $pg.ml^{-1}$, 50 $pg.ml^{-1}$, 25 $pg.ml^{-1}$ and 0 $pg.ml^{-1}$. The samples were also added to each well - 100 µl per well. Standards and zeros were included in duplicate alongside duplicated cell culture supernatant samples. Once all standards and samples were added to the plate, 50 µl of dilute detection antibody was then added to each well and the plate was sealed and incubated at room temperature for 3 hours. After the incubation, the plate was washed as above twice. Following washing, 100 µl of dilute streptavidin-HRP was added to each well. The plate was sealed and incubated at room temperature for 30 minutes. The plates were then washed twice. A volume of 100 µl of TMB substrate was added to each well and the plates were sealed and wrapped in foil. The plates were incubated in the dark for between 5 and 15 minutes. After approximately 10 minutes, 100 µl of 1 M sulfuric acid (stop reagent) was added to each well. The plate was then read immediately using the Multiskan plate reader at 450 nm and 630 nm. The 630 nm readings were subtracted from the 450 nm readings prior to analysis.

Mouse

The plates of supernatant and the murine TNF-α/IL-1β/IL-6 ELISA kit components were defrosted at room temperature (25°C). The ELISA reagents were prepared as detailed above (Table 2.9). A volume of 100 µl of diluted capture antibody was added to each well of a Corning CoStar 96 well plate. The plates were sealed and incubated overnight at 4°C. Following this, the wells were aspirated and washed 3 times with wash buffer. The plate was then blotted dry and all wells were blocked with 200 µl ELISA diluent. The plate was sealed and then incubated at room temperature for 1 hour. The standard was prepared as described in Table 2.9. The plate was then aspirated and washed once as before. A serial dilution of the standard was performed within the plate in order to generate a standard curve. A volume of 100 µl of each sample or each standard were added to the relevant wells. The plate was sealed and incubated at room temperature for 2 hours. The detection antibody was prepared as described above. The plate was aspirated and washed 3 times. A volume of 100 µl of detection antibody was added to each well and the plate was sealed and incubate at room temperature (25°C) for one further hour. Streptavidin-HRP was prepared as described above. The plate was aspirated and washed three times. A volume of 100 µl of Streptavidin-HRP was added to each well. The plate was then sealed and incubated at room temperature (25°C) for 30 minutes. The plate was then aspirated and washed five times. A volume of 100 µl TMB substrate was added to each well. The plate was sealed and wrapped in foil. The plate was incubated for 10 – 15 minutes after which 50 µl of stop solution (1 M sulfuric acid) was added to each well. The contents of the well plate were then immediately read at 450 and 570 nm using a

Multiskan plate reader. The 570 nm readings were subtracted from the 450 nm readings prior to analysis.

TNF-α

Human

A serial dilution of the TNF-α standard was performed within the plate in order to generate a standard curve from the following concentrations: 800 $pg.ml^{-1}$, 400 $pg.ml^{-1}$, 200 $pg.ml^{-1}$, 100 $pg.ml^{-1}$, 50 $pg.ml^{-1}$, 25 $pg.ml^{-1}$, 12.5 $pg.ml^{-1}$ and 0 $pg.ml^{-1}$ (i.e. RPMI cell culture medium only).

Mouse

A serial dilution of the TNF-α standard was performed within the plate in order to generate a standard curve from the following concentrations: 1000 $pg.ml^{-1}$, 500 $pg.ml^{-1}$, 250 $pg.ml^{-1}$, 125 $pg.ml^{-1}$, 62.5 $pg.ml^{-1}$, 31.25 $pg.ml^{-1}$, 15.625 $pg.ml^{-1}$ and 0 $pg.ml^{-1}$ (i.e. DMEM cell culture medium only).

IL-1β

A serial dilution of the IL-1β standard was performed within the plate in order to generate a standard curve from the following concentrations: 1000 $pg.ml^{-1}$, 500 $pg.ml^{-1}$, 250 $pg.ml^{-1}$, 125 $pg.ml^{-1}$, 62.5 $pg.ml^{-1}$, 31.25 $pg.ml^{-1}$, 15.625 $pg.ml^{-1}$ and 0 $pg.ml^{-1}$ (i.e. DMEM cell culture medium only).

IL-6

A serial dilution of the IL-6 standard was performed within the plate in order to generate a standard curve from the following concentrations: 500 $pg.ml^{-1}$, 250 $pg.ml^{-1}$, 125 $pg.ml^{-1}$, 62.5 $pg.ml^{-1}$, 31.63 $pg.ml^{-1}$, 15.81 $pg.ml^{-1}$, 7.41 $pg.ml^{-1}$ and 0 $pg.ml^{-1}$ (i.e. DMEM cell culture medium only).

KC

Table 2.10 Murine KC ELISA kit reagents, storage and preparation instructions.

Murine KC coated 1 x 96 ELISA kit component	**Storage and preparation**
KC 96 well microplate coated with anti-mouse KC	Stored at 4°C for one month.
Wash buffer concentrate (20X) – 25 ml	Diluted 20 ml of wash buffer with 400 ml deionised water to prepare a 1X solution, Stored at 4°C for one month.

Standard protein (Mouse KC x 2 vials)	Stored at -80°C for one week. Each vial was diluted with 400 µl 1X assay diluent to prepare a 50 $ng.ml^{-1}$ standard solution. This was further diluted to a 150 $pg.ml^{-1}$ by adding 3 µl of 50 $ng.ml^{-1}$ standard solution to 997 µl 1X assay diluent.
Detection antibody (KC) x 2 vials	Each vial was diluted with 100 µl 1X assay diluent. This was then diluted further (1:80) with 1X assay diluent prior to use. Stored at 4°C for five days.
HRP-Streptavidin concentrate (200X) – 200 µl	Diluted 50 µl of HRP-Streptavidin concentrate with 10 ml 1X assay diluent. Not stored.
TMB one step substrate reagent – 12 ml	Not stored.
Stop solution – 0.2 M sulfuric acid – 8ml	Not stored.
Assay diluent (5X) – 15 ml	Diluted with 60 ml deionised water. Stored at 4°C for one month.

The plates of supernatant and the murine KC ELISA kit components were defrosted at room temperature (25°C). The ELISA reagents were prepared as detailed above (Table 2.10). Each cell culture supernatant sample was diluted prior to use: 33 µl sample was added to 67 µl assay diluent. A serial dilution of the KC standard was performed within the plate in order to generate a standard curve from the following concentrations: 150 $pg.ml^{-1}$, 60 $pg.ml^{-1}$, 24 $pg.ml^{-1}$, 9.6 $pg.ml^{-1}$, 3.84 $pg.ml^{-1}$, 1.54 $pg.ml^{-1}$, 0.614 $pg.ml^{-1}$ and 0 $pg.ml^{-1}$ (i.e. DMEM cell culture medium only). A volume of 100 µl of each diluted sample or each standard were added to the relevant wells. The plate was sealed and incubated at room temperature (25°C) for 2.5 hours with gentle shaking. The plate was aspirated and washed four times. A volume of 100 µl of

detection antibody was added to each well and the plate was sealed and incubate at room temperature (25°C) for one further hour with gentle shaking. The plate was aspirated and washed four times. A volume of 100 µl of Streptavidin-HRP was added to each well. The plate was then sealed and incubated at room temperature for 45 minutes with gentle shaking. The plate was then aspirated and washed four times. A volume of 100 µl TMB substrate was added to each well. The plate was sealed and wrapped in foil. The plate was incubated for 30 minutes with gentle shaking after which 50 µl of stop solution (1 M sulfuric acid) was added to each well. The contents of the well plate were then immediately read at 450 and 570 nm using a Multiskan plate reader. The 570 nm readings were subtracted from the 450 nm readings prior to analysis.

LTB_4

Table 2.11 Murine LTB_4 ELISA kit reagents, storage and preparation instructions.

Murine LTB_4 coated 1 x 96 ELISA kit component	**Storage and preparation**
LTB_4 (coated with rabbit anti-chicken polyclonal antibody) 96 well microplate	Stored at 4°C for one month.
LTB_4 conjugate – 1 vial (6 ml)	Stored at -20°C for one month.
LTB_4 standard – 1 vial	Stored at -20°C for one month. Reconstituted with deionised water to create a 50 $ng.ml^{-1}$ stock solution,
Primary antibody (chicken polyclonal) solution -1 vial (6 ml)	Stored at 4°C for one month.
Calibrator diluent – 1 vial (21 ml)	Stored at 4°C for one month.
Wash buffer concentrate 25X – 1 vial (21 ml)	Diluted 20 ml wash buffer concentrate with 500 ml deionised water. Stored at 4°C for one month.
Colour reagent A -1 vial (12 ml) stabilised hydrogen peroxide	Stored at 4°C for one month. Mixed with colour reagent B in equal volumes immediately prior to use.
Colour reagent B – 1 vial (12 ml) stabilised chromogen, tetramethylbenzidine.	Stored at 4°C for one month. Mixed with colour reagent B in equal volumes immediately prior to use.
Stop solution – 1 vial (11 ml) 2N (1M)	Stored at 4°C for one month.

sulphuric acid	
Adhesive plate sealers x 4	N/A

A serial dilution of the LTB_4 standard was performed within the plate in order to generate a standard curve from the following concentrations: 2500 $pg.ml^{-1}$, 833 $pg.ml^{-1}$, 278 $pg.ml^{-1}$, 92.6 $pg.ml^{-1}$, 30.9 $pg.ml^{-1}$, 10.3 $pg.ml^{-1}$ and 0 $pg.ml^{-1}$ (i.e. calibration diluent only). A volume of 50 µl of each standard and sample was added to the corresponding wells of the microplate (n=3). A volume of 50 µl of primary antibody solution was added to each well (except the non-specific binding wells). A volume of 100 µl of calibrator diluent was added to the non-specific binding well. The plate was then sealed and incubated at room temperature (25°C) with shaking at 500 rpm for one hour. A volume of 50 µl of conjugate was added to each well. The plate was then sealed and incubated at room temperature (25°C) with shaking at 500 rpm for 3 hours. The plate was then aspirated and washed four times then blotted. A volume of 200 µl of substrate solution (colour reagents A and B) was added to each well and the plate was wrapped in foil. The plate was incubated at room temperature (25°C) for 30 minutes. A volume of 100 µl of stop solution was added to each well. The contents of the well plate were then immediately read at 450 and 570 nm using a Multiskan plate reader. The 570 nm readings were subtracted from the 450 nm readings prior to analysis.

PGE_2

The components for the PGE_2 ELISA were the same as the LTB_4 ELISA in Table 2.11 with any different components outlined in Table 2.12.

Table 2.12 Murine PGE_2 ELISA kit reagents, storage and preparation instructions.

Murine PGE_2 coated 1 x 96 ELISA kit component	**Storage and preparation**
PGE_2 (coated with goat anti-mouse polyclonal antibody) 96 well microplate	Stored at 4°C for one month.
PGE_2 standard	Stored at -20°C for one month.
PGE_2 conjugate	Stored at 4°C for one month.

A serial dilution of the PGE_2 standard was performed within the plate in order to generate a standard curve from the following concentrations: 2500 $pg.ml^{-1}$, 1250 $pg.ml^{-1}$, 625 $pg.ml^{-1}$, 313 $pg.ml^{-1}$, 156 $pg.ml^{-1}$, 78 $pg.ml^{-1}$, 39 $pg.ml^{-1}$ and 0 $pg.ml^{-1}$ (i.e. calibration diluent only). The assay was carried out as per the LTB_4 ELISA method.

2.2.8.3 Trypan blue exclusion assay

Cell numbers were assessed by adding a 90 µl sample of cells/medium from an existing tissue culture flask to 10 µl of trypan blue in a sterile bijou. A volume of 20 µl of the resultant mixture was pipetted underneath the cover slip of a Neubauer haemocytometer and all the cells in the grid were counted. The number of cells was calculated as follows:

$$\textit{No. of cells per ml} = \textit{No. of cells counted} \times 10/9 \times (1 \times 10^4)$$

$$\textit{*Dilution factor} = 1 \times 10^4$$

*** 10/9 = correction for dilution factor when adding trypan blue to cell suspension*

2.2.9 Statistical analysis

All data where n>1 was analysed using one-way or two-way ANOVA as appropriate (Statplus) and the Tukey-Kramer post-hoc test at a significance level $p<0.05$ (Microsoft Excel). The 95% confidence limits were also displayed on the subsequent graphs.

Chapter 3
Development of a novel 3D *in vitro* model for measuring cellular responses to model polyethylene particles

3.1 Introduction

There is a need for a 3D method for modelling *in vitro* responses to UHMWPE wear debris as there is currently no working 3D model, only 2D models. A 3D model is more representative of the periprosthetic *in vivo* environment than a 2D model. The model needs to be simple to use and reliable in terms of inflammatory cytokine release. Significant time and resources were used in previous 2D studies to attempt to yield a consistent level of cytokine release from cells with particles in agarose gel. The cell types used, i.e. PBMNCs, have issues, such as donor heterogeneity and supply, associated with them so a more reliable and easy to use cell type should be chosen. The agarose gels used by previous 2D studies is not naturally found in the periprosthetic environment and lacks cell attachment sites therefore the gel type could be improved. The use of a gel must be continued to achieve a 3D culture model as UHMWPE wear debris floats in cell culture medium if not trapped in a gel matrix. However, it is possible to use inverted cell culture methods successfully to create a 2D cell-particle model.

This study aimed to develop a novel 3D *in vitro* model by testing an alternative cell type – RAW 264.7 murine macrophages – alongside the existing PBMNCs and U937 human histiocytes in addition to testing a new gel type – type I rat tail collagen – alongside the existing agarose gel. RAW 264.7 murine macrophages are a cell line derived from the ascites of an induced tumour by intraperitoneal injection of Abselon Leukaemia Virus. RAW 264.7 murine macrophages are a semi-adherent cell type; in culture, some cells are adherent and some cells are in suspension. As they are a cell line, there is no issue with donor supply or variation. The cells also do not require chemical transformation. RAW 264.7 murine macrophages are not human cells which is not ideal, as animal cells may behave differently in response to UHMWPE wear debris than human cells, however this is somewhat mitigated by the simplicity of both their use and their ability to generate vast cell numbers quickly without the need for a human donor. Furthermore, Matthews *et al.* (2000) compared the responses of primary murine macrophages and a human histiocyte cell line (U937) to UHMWPE wear debris and suggested that murine macrophages were an appropriate cell type for use in modelling cellular responses to UHMWPE wear debris. Additionally, as RAW 264.7 murine macrophages are a cell line, their use is less representative of the *in*

vivo environment as the behaviour of cell lines in culture will differ from primary cells in the periprosthetic environment. However, primary cells, such as PBMNCs, introduce problematic donor variation so a compromise must be made. Type I rat tail collagen gel was chosen as the material for the gel as it has previously been successfully used to model neural cell responses to metal wear debris (Lee, 2016). Type I rat tail collagen gel includes cell attachment sites; making it more appropriate for 3D culture models than agarose. Collagen also uses a pH dependent gelling mechanism, rather than the temperature dependent gelling mechanism of agarose, and therefore does not affect the viability of any cells encased within it, so both wear debris and cells can be encapsulated within the gel simultaneously. Additionally, type I rat tail collagen is more representative of the 3D *in vivo* environment, i.e. the extracellular matrix which typically consists of collagen, elastin and proteoglycans to support the local cells, experienced by the macrophages in the body.

3.2 Aims and objectives

3.2.1 Aims

The overall aim of this chapter was to develop a 3D *in vitro* model to assess the cellular responses to model polyethylene particles in order to provide a more accurate representation of the periprosthetic environment in comparison to earlier 2D models.

3.2.2 Objectives

The objectives of this chapter were as follows:

- To determine the working seeding density of a number of different cells (RAW 264.7, U937 and PBMNC's) in both gel types (agarose and type I rat tail collagen) using the ATP-lite™ luminescence detection assay.
- To investigate the effect of changing gel type on cell viability of a number of different cells (RAW 264.7, U937 and PBMNC's) using the ATP-lite™ luminescence detection assay.
- To assess the TNF-α release of each different cell type (RAW 264.7, U937 and PBMNC's) in both gel types (agarose and type I rat tail collagen) in response to model polyethylene particles (Ceridust®) and FluoSpheres® using ELISA.
- To assess the suitability of RAW 264.7 murine macrophages and U937 human histiocytes for use in an inverted 2D *in vitro* model using cell viability (ATP-lite™ luminescence detection assay) and TNF-α release (ELISA) as indicators.

3.3 Materials

The materials used throughout Chapter 3 are detailed below.

3.3.1 Chemicals and reagents

All chemicals and reagents used throughout Chapter 3 are listed in Chapter 2, Section 2.1.1.

3.3.2 Consumables

All consumables used throughout Chapter 3 are listed in Chapter 2, Section 2.1.2.

3.3.3 Equipment

All equipment used throughout Chapter 3 is listed in Chapter 2, Section 2.1.3.

3.3.4 Cell lines and primary cells

All cell lines and primary cells used throughout Chapter 3 are listed in Chapter 2, Sections 2.1.4 and 2.1.5, respectively.

3.3.5 Particles

All particles used throughout Chapter 3 are listed in Chapter 2, Section 2.1.6.

3.4 Methods

The specific experimental methods used throughout Chapter 3 are described below. General methods can be found in Chapter 2, Section 2.2.

3.4.1 Determining working cell seeding densities of RAW 264.7 murine macrophages in 48 well tissue culture plates

The agarose method of culturing cells in 3D with polyethylene wear debris in 48 well tissue culture plates used at the University of Leeds was developed using PBMNC's at a density of 1 x 10^5 cells in 1 ml of cell culture medium (Green *et al.*, 1998). This seeding density was later increased to 2 x 10^5 cells in 1 ml of cell culture medium as the centrifugation step was removed and the cells were presumed to penetrate the gel (Gowland, 2014). Additionally, Gowland (2014) used U937 human histiocytes at a seeding density of 2 x 10^5 cells.ml^{-1} in agarose gel in 48 well tissue culture plates. The seeding density of RAW 264.7 murine macrophages in 2D was determined by carrying out a cell viability assay in 48 well tissue culture plates in order to suggest a suitable range of seeding densities to assess in 3D.

RAW 264.7 murine macrophages were cultured, passaged and counted as described in Chapter 2, Section 2.2.5.4. Cells were seeded into 48 well tissue culture plates at densities of 1 x 10^3, 5 x 10^3, 1 x 10^4, 5 x 10^4 and 1 x 10^5 cells.ml^{-1}. Each well contained 1 ml medium. Cells plus DMSO (200 µl.ml^{-1}) positive controls and medium only negative controls were included (n=6). Plates were incubated at 37°C and 8% (v/v) CO_2 in air. Plates were assessed using the ATP-lite^{TM} viability assay on days 0,

1, 2, 3 and 5 as described in Chapter 2, Section 2.2.8.1. The results were analysed statistically using two-way ANOVA and the Tukey-Kramer post-hoc test as described in Chapter 2, Section 2.2.9.

3.4.2 Determining cell viability and TNF-α release of PBMNC's, RAW 264.7 murine macrophages and U937 human histiocytes following model particle treatments in agarose and collagen gel

The viability of PBMNC's, U937 human histiocytes and RAW 264.7 murine macrophages in both agarose and collagen gels was assessed over three days. The viability was assessed up to day 3, as the chosen cell type was only used for 24 hours as a maximum in the chosen gel type in later work therefore extending the viability assay significantly beyond this time frame was redundant.

3.4.2.1 Cell viability of PBMNC's, RAW 264.7 murine macrophages and U937 human histiocytes in agarose and collagen gel

RAW 264.7 murine macrophages and U937 human histiocytes, transformed (i.e. treated with PMA to become adherent and chemically activated macrophages) and non-transformed (i.e. untreated cells in a suspension culture), were cultured, passaged and counted as described in Chapter 2, Section 2.2.5.4 and 2.2.8.3 respectively. PBMNC's (donor 2) were isolated as described in Chapter 2, Section 2.2.4. Agarose gels (0.4% (w/v)) were prepared in 48 well tissue culture plates as described in Chapter 2, Section 2.2.7.1. Cells were seeded on top of the agarose gels at densities of 1×10^4, 5×10^4 and 1×10^5 cells.ml^{-1}. Cells were assembled in collagen gels as described in Chapter 2, Section 2.2.7.2. Cells were seeded at densities of 1×10^4, 5×10^4 and 1×10^5 cells.ml^{-1}. Each well contained 1 ml of medium (DMEM for RAW 264.7 murine macrophages and RPMI 1640 cell culture medium for PBMNCs and U937 human histiocytes). Cells plus DMSO (200 µl.ml^{-1}) acted as the positive control and a medium only negative control was included (n=6). All conditions were assessed using the ATP-lite™ viability assay on days 0, 1 and 3 as described in Chapter 2, Section 2.2.8.1. The results were analysed statistically using two-way ANOVA and the Tukey-Kramer post-hoc test as described in Chapter 2, Section 2.2.9.

RAW 264.7 murine macrophage viability was assessed in agarose gels both with and without a rinse step. A rinse step was included to remove any cells that had not penetrated the agarose gel and therefore would not be exposed to particle treatments in subsequent studies. For those assessed with a rinse step, this involved changing the medium in all wells 12 hours post seeding and then performing the ATP-lite™ viability assay as described in Chapter 2, Section 2.2.8.1.

3.4.2.2 TNF-α release from PBMNC's, RAW 264.7 murine macrophages and U937 human histiocytes following model particle treatments in agarose and collagen gel

RAW 264.7 murine macrophages and U937 human histiocytes (transformed and non-transformed) were cultured, passaged and counted as described in Chapter 2, Section 2.2.5.4 and 2.2.8.3 respectively. PBMNC's (donor 2) were isolated as described in Chapter 2, Section 2.2.4. Agarose gels (0.4% (w/v)) were prepared with particle treatments as described in Chapter 2, Section 2.2.7.1. Collagen gels were prepared with cells and particle treatments as described in Chapter 2, Section 2.2.7.2. The following particle treatments were prepared as described in Chapter 2, Section 2.2.6.1: >10 μm Ceridust®, 1 – 10 μm Ceridust®, 0.1 -1 μm Ceridust® and 0.2 μm FluoSpheres® at volumes of 100 μm^3 particles per cell. Cells were seeded on top of the agarose gels at a density of 1 x 10^5 cells.ml^{-1}. Each well contained 1 ml of medium (DMEM for RAW 264.7 murine macrophages and RPMI 1640 cell culture medium for PBMNCs and U937 human histiocytes). Cells plus LPS (200 ng.ml^{-1}) acted as a positive control and cells only acted as a negative control for ELISA (n=4). Cells plus DMSO acted as a positive control and medium only acted as a negative control for cell viability (n=6). The plates were assessed at 12 and 24 hours post seeding using the ATP-lite™ viability assay as described in Chapter 2, Section 2.2.8.1. Prior to performing the ATP-lite™ viability assay, the supernatants from each plate were placed in the corresponding wells of a Nunc F uncoated plate and were frozen at -80°C until required for ELISA. When ELISA was performed, the required supernatants were defrosted at room temperature (25°C). Subsequently, ELISA was performed on supernatants in duplicate for TNF-α quantification as described in Chapter 2, Section 2.2.8.2. The results were analysed statistically using two-way ANOVA and the Tukey-Kramer post-hoc test as described in Chapter 2, Section 2.2.9.

3.4.3 Determining working cell seeding densities of RAW 264.7 murine macrophages and U937 human histiocytes in 96 well tissue culture plates for use in inverted 2D culture

Previous studies at the University of Leeds cultured PBMNC's with polyethylene wear debris in a novel inverted 2D model. PBMNCs are seeded at a density of 2 x 10^4 cells in 200 μl of cell culture medium on the base of a 96 well tissue culture plate and medium containing polyethylene particles is loaded on top of the cells. The plate is then carefully inverted, allowing the particles floating on the surface of the medium to come into contact with the cells seeded on the base of the plate. During the present study, RAW 264.7 murine macrophages and U937 human histiocytes were trialled in this novel inverted 2D model. A seeding density of 1 x 10^4 in 200 μl of cell culture medium was recommended for cell lines and this was verified by performing cell

viability assays of both cell types in 96 well tissue culture plates at a variety of cell seeding densities over five days.

RAW 264.7 murine macrophages and U937 human histiocytes were cultured, passaged and counted as described in Chapter 2, Section 2.2.5.4 and 2.2.8.3 respectively. Cells were seeded into 96 well tissue culture plates at densities of 5 x 10^3, 1 x 10^4, 5 x 10^4, 1x 10^5 and 5 x 10^5 cells.ml^{-1} (n=6). Each well contained 200 µl medium (DMEM for RAW 264.7 murine macrophages and RPMI 1640 cell culture medium for U937 human histiocytes). Cells plus DMSO (200 µl.ml^{-1}) positive controls and medium only negative controls were included (n=6). Plates were incubated at 37°C and 5% (U937 human histiocytes) or 8% (RAW 264.7 murine macrophages) (v/v) CO_2 in air. Plates were assessed using the ATP-lite^{TM} viability assay on days 0, 1, 2, 3 and 5 as described in Chapter 2, Section 2.2.8.1. The results were analysed statistically using two-way ANOVA and the Tukey-Kramer post-hoc test as described in Chapter 2, Section 2.2.9.

3.4.4 Determining TNF-α release from RAW 264.7 murine macrophages and U937 human histiocytes following particle treatments in an inverted 2D culture model

RAW 264.7 murine macrophages and U937 human histiocytes, transformed (i.e. treated with PMA to become adherent and chemically activated) and non-transformed (i.e. untreated cells in a suspension culture), were cultured, passaged and counted as described in Chapter 2, Section 2.2.5.4 and 2.2.8.3 respectively. Using a pipette, 1 x 10^4 cells in 100 µl medium was slowly and carefully placed into the centre of each well of a 96 well tissue culture plate. The plates were then incubated at 37°C and 5% (RAW 264.7 murine macrophages) or 8% (U937 human histiocytes) (v/v) CO_2 in air for 3 hours to allow the cells to adhere to the tissue culture plate. After 3 hours, the medium was removed and replaced with 150 µl medium per well containing particle treatments, prepared as described in Chapter 2, Section 2.2.6.1, as follows: >10 µm Ceridust® particles, 1 – 10 µm Ceridust® particles, 0.1 – 1 µm Ceridust® particles and 0.2 µm FluoSpheres®. Cells plus LPS (200 ng.ml^{-1}) acted as a positive control and cells only acted as a negative control for ELISA (n=4). Cells plus DMSO acted as a positive control and medium only acted as a negative control for cell viability (n=6). The plates were then deliberately inverted – neither too quickly or slowly – and the medium was then held in place by surface tension. Since polyethylene is less dense than water, the particles float at the surface of the medium, which was in contact with the monolayer of cells when the plate was inverted. The plates were then incubated at 37°C and 5% (RAW 264.7 murine macrophages) or 8% (U937 human histiocytes) (v/v) CO_2 in air. The cells were assessed at 12 and 24 hours post particle exposure using the ATP-lite^{TM} viability assay as described in Chapter 2, Section 2.2.8.1. Prior to

performing the ATP-lite™ viability assay, the supernatants from each plate were placed in the corresponding wells of a Nunc F uncoated plate and were frozen at -80°C until required for ELISA. When ELISA was performed, the required supernatants were defrosted at room temperature (25°C). Subsequently, ELISA was performed on supernatants in duplicate for TNF-α quantification as described in Chapter 2, Section 2.2.8.2. The results were analysed statistically using two-way ANOVA and the Tukey-Kramer post-hoc test as described in Chapter 2, Section 2.2.9.

3.5 Results

The viability of PBMNC's, U937 human histiocytes and RAW 264.7 murine macrophages at different seeding densities (1 x 10^4 cells.ml^{-1}, 5 x 10^4 cells.ml^{-1} and 1 x 10^5 cells.ml^{-1}) was assessed over three days in agarose and collagen gels. The ability of PBMNC's, U937 human histiocytes and RAW 264.7 murine macrophages to produce the inflammatory cytokine, TNF- α, in response to model debris in both agarose and collagen gels was assessed using ELISA at 12 and 24 hour time points. ATP-lite™ luminescence detection assays were also carried out at these time points to assess cell viability and the results reported alongside ELISA analysis. Cells were seeded at 1 x 10^5 cells.ml^{-1} and particles were seeded at 100 μm^3 per cell. The following conditions were examined : >10 μm Ceridust® 1 -10 μm Ceridust®, 0.1-1 μm Ceridust®, 0.2 μm FluoSpheres®, cells only, medium only (for ATP-lite™ luminescence detection assay only), cells plus DMSO (200 μl.ml^{-1}) (for ATP-lite™ luminescence detection assay only) and cells plus LPS (200 ng.ml^{-1}). Cells plus LPS was included as a positive control as LPS is known to produce an intense cytokine response (Cho *et al.*, 2002). The cells only condition acted as the negative control.

Viability and ELISA data was analysed using ANOVA and the Tukey-Kramer post-hoc test. Error bars, using 95% confidence intervals, were displayed on the resultant graphs. It should be noted that, as 100 μl of supernatant from the total 1 ml volume was used for each ELISA – the results represent 1/10^{th} of the volume of cytokine produced. Since this is the same for all experiments, the results have not been multiplied upwards.

3.5.1 Cell viability and inflammatory response of PBMNCs to model particles in agarose and collagen gels

The viability of PBMNC's was assessed in both agarose and collagen gels over three days using the ATP-lite™ luminescence detection assay. PBMNC's were cultured with model particles, Ceridust® and FluoSpheres®, in agarose and collagen gel. The viability was measured at 12 and 24 hours using the ATP-lite™ luminescence

detection assay. The supernatants at these time points were then used to assess the levels of TNF-α cytokine released using ELISA.

3.5.1.1 Cell viability and response of PBMNCs to model particles in agarose gels

The viability of PBMNC's (donor 2) at three seeding densities (1 x 10^4, 5 x 10^4 and 1 x 10^5 cells.ml^{-1}) in agarose gel was assessed at days 0, 1, 2 and 3 using the ATP-lite^{TM} luminescence detection assay. Isolated PBMNC's were then cultured with Ceridust® and FluoSpheres® model particles in agarose gel. Cells were seeded at 1 x 10^5 cells.ml^{-1} with 100 μm^3 particles per cell in a 48 well tissue culture plate. The contents of each well were assessed using the ATP-lite^{TM} luminescence detection assay and ELISA for quantitation of TNF-α at 12 and 24 hours post particle exposure.

Viability of PBMNCs in agarose gel

The viability of PBMNC's (Figure 3.1) at all densities tested remained relatively constant over the three days, whereas cells cultured with DMSO (200 μl.ml^{-1}) demonstrated a significant decrease in viability over the three days (ANOVA; $p<0.05$).

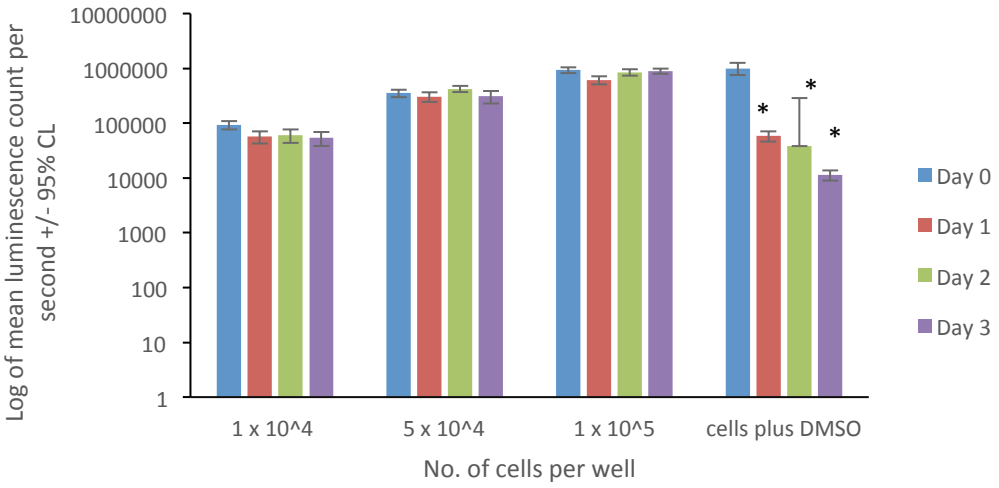

Figure 3.1 Cell viability of PBMNC's seeded at different densities in agarose gel over three days at 37°C in 5% (v/v) CO_2 in air. Cells were seeded at densities of 1 x 10^4, 5 x 10^4 and 1 x 10^5 cells.ml^{-1} in a 48 well tissue culture plate. Cells plus DMSO (200 μl.ml^{-1}) acted as a positive control. Cell viability was assessed using the ATP-lite^{TM} luminescence detection assay. * designates a statistically significant data point relative to the seeding densities assessed (ANOVA, $p<0.05$). Error bars represent 95% confidence intervals, n=6.

Viability of PBMNCs after exposure to model particles in agarose gels

None of the treatments had a significant effect on the viability of PBMNC's (Figure 3.2A) compared to the cells only negative control at 12 hours post particle exposure (ANOVA; p>0.05). Cells cultured with 1 – 10 µm Ceridust®, 0.1 – 1 µm Ceridust® and 0.2 µm FluoSpheres® exhibited significantly reduced viability when compared to the cells only control at 24 hours post particle exposure (ANOVA; p>0.05).

TNF-α release from PBMNCs after exposure to model particles in agarose gels

After 12 hours, cells cultured with >10 µm Ceridust®, 0.2 µm FluoSpheres® and LPS produced significantly elevated levels of TNF-α (Figure 3.2B) compared to the cells only negative control (ANOVA: p>0.05). None of the remaining Ceridust® treatments had any significant effect on TNF-α release.

After 24 hours, only PBMNC's treated with LPS (positive control) produced a significant release of TNF-α when compared to the cells only negative control (ANOVA: p<0.05). None of the Ceridust® or FluoSphere® particle treatments had a significant effect on the release of TNF-α.

A)

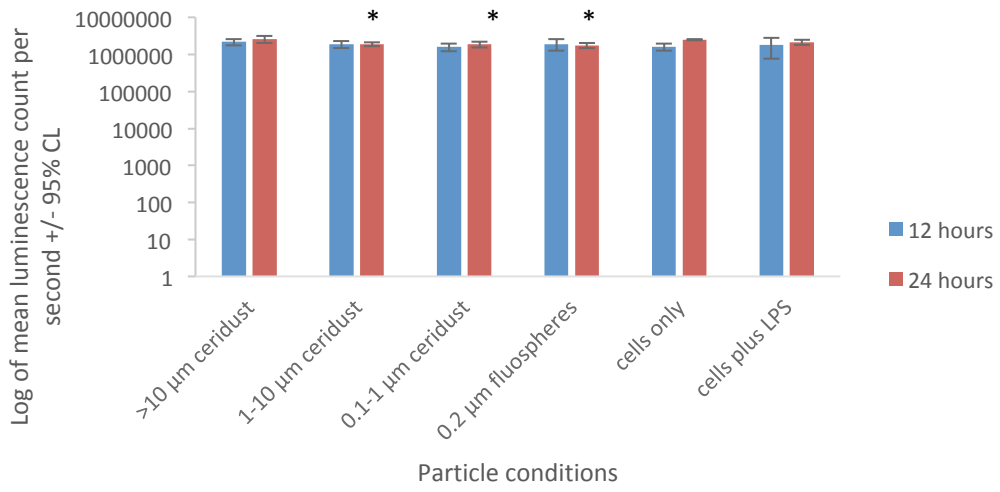

B)

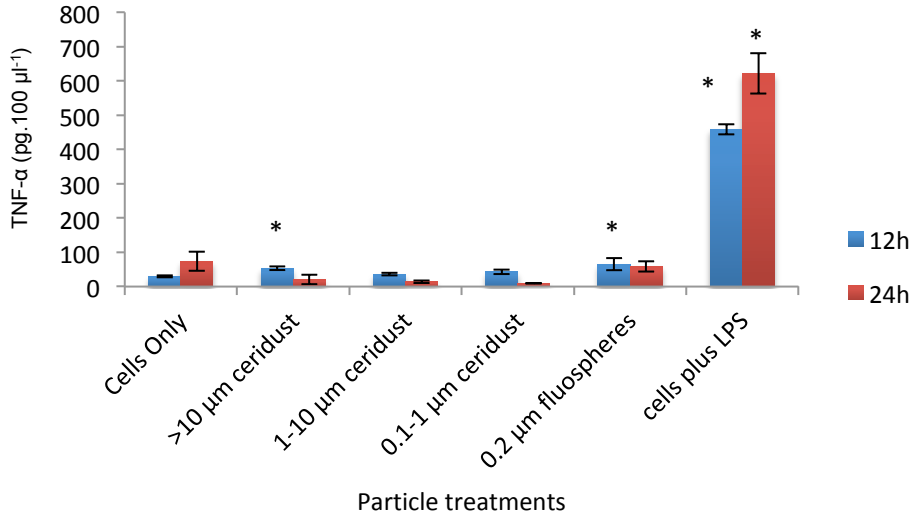

Figure 3.2– A) Cell viability and B) TNF-α release from PBMNC's (donor 2) incubated with Ceridust® and FluoSpheres® model particles at a concentration of 100 μm^3 particles per cell in agarose gel at 12 and 24 hours post particle exposure at 37°C in 5% (v/v) CO_2 in air. Cells were seeded at a density of 1 x 10^5 cells.ml^{-1} with particle treatments in a 48 well tissue culture plate. A cells only negative control and LPS positive control (200 ng.ml^{-1}) were included in the conditions. * designates a statistically significant data point compared to the cells only negative control (ANOVA, $p<0.05$). Error bars represent 95% confidence intervals, n=4.

3.5.1.2 Cell viability and response of PBMNCs to model particles in collagen gels

The viability of PBMNCs (donor 2) at three seeding densities (1 x 10^4, 5 x 10^4 and 1 x 10^5 cells.ml^{-}) in collagen gel was assessed at days 0, 1, 2 and 3 using the ATP-lite™ luminescence detection assay. Isolated PBMNC's were cultured with Ceridust® and FluoSpheres® model particles in collagen gel. Cells were seeded at 1 x 10^5 cells.ml^{-1} with 100 μm^3 particles per cell in 48 well tissue culture plates. The contents of each well was assessed using the ATP-lite™ luminescence detection assay and ELISA for TNF-α at 12 and 24 hours post particle exposure.

The cell viability of PBMNC's (Figure 3.3) at all cell seeding densities remained relatively constant over the three days whereas cells cultured with DMSO (200 µl.ml^{-1}) demonstrated a significant decrease over three days (ANOVA; $p<0.05$).

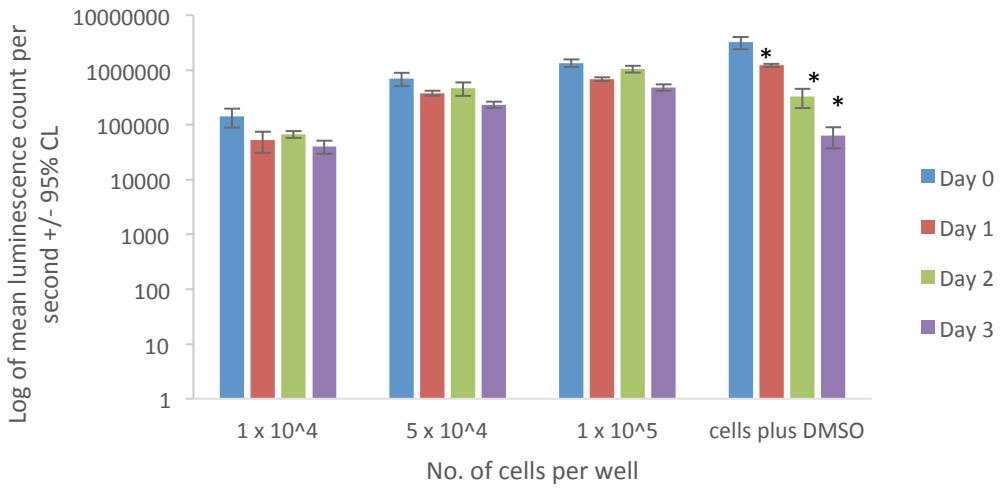

Figure 3.3 Cell viability of PBMNC's seeded at different densities in collagen gel over three days at 37°C in 5% (v/v) CO_2 in air. Cells were seeded at densities of 1 x 10^4, 5 x 10^4 and 1 x 10^5 cells.ml^{-1} in a 48 well tissue culture plate. A cells plus DMSO (200 µl.ml^{-1}) positive control was included in the conditions. Cell viability was assessed using the ATP-lite^{TM} luminescence detection assay. * designates a statistically significant data point compared to the seeding densities assessed (ANOVA, $p<0.05$). Error bars represent 95% confidence intervals, n=6.

Viability of PBMNCs after exposure to model particles in collagen gels

None of the treatments had a significant effect on the viability of PBMNC's (Figure 3.4A) compared to the cells only negative control at 12 and 24 hours post particle exposure with the exception of cells treated with LPS (200 ng.ml^{-1}) at 24 hours post particle exposure (ANOVA; $p<0.05$).

TNF-α release from PBMNCs after exposure to model particles in collagen gels

After 12 hours, none of the treatments produced a significant release of TNF-α (Figure 3.4B) when compared to the cells only negative control (ANOVA: $p>0.05$).

After 24 hours, only PBMNC's treated with the LPS (200 ng.ml^{-1}) positive control produced a significant release of TNF-α (Figure 3.4B) when compared to the cells only negative control (ANOVA: $p<0.05$). None of the Ceridust® or FluoSphere® particle treatments had a significant effect on the release of TNF-α.

A)

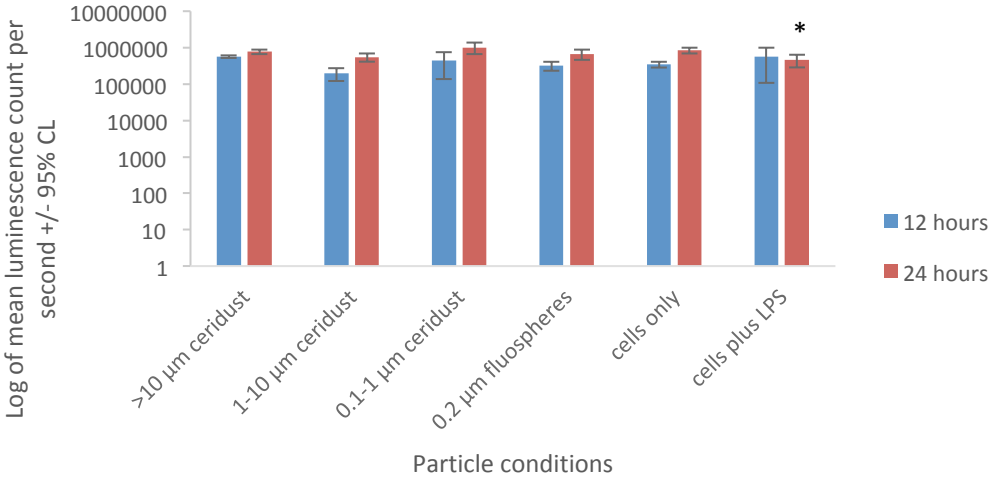

B)

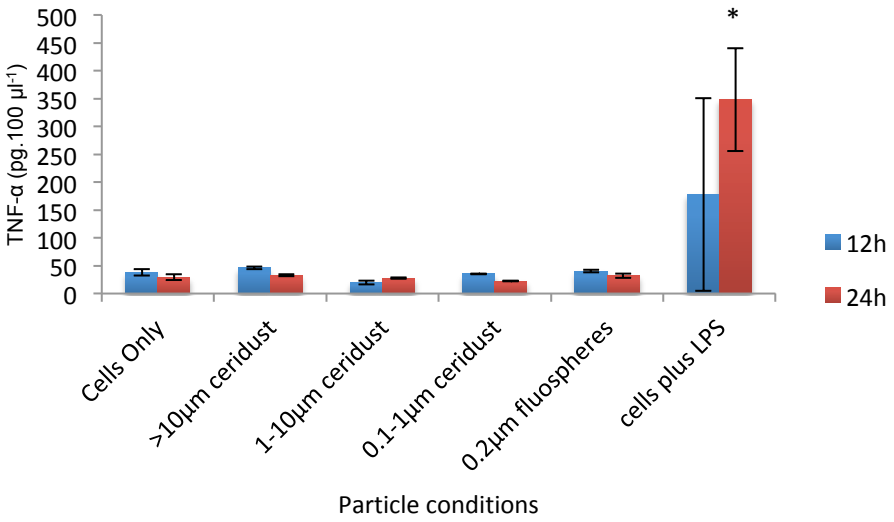

Figure 3.4 – A) Cell viability and B) TNF-α release from PBMNC's (donor 2) incubated with Ceridust® and FluoSpheres® model particles at a concentration of 100 μm^3 particles per cell in collagen gel at 12 and 24 hours post particle exposure at 37°C in 5% (v/v) CO_2 in air. Cells were seeded at a density of 1 x 10^5 cells.ml^{-1} with particle treatments in a 48 well tissue culture plate. A cells only negative control and LPS (200 ng.ml^{-1}) positive control were included in the conditions. * designates a statistically significant data point compared to the cells only negative control (ANOVA, $p<0.05$). Error bars represent 95% confidence intervals, n=4.

3.5.2 Cell viability and inflammatory response of RAW 264.7 murine macrophages to model particles in agarose and collagen gels and inverted 2D culture

The viability of RAW 264.7 murine macrophages was assessed in both agarose and collagen gels over three days using the ATP-lite™ luminescence detection assay. RAW 264.7 murine macrophages were cultured with model particles, Ceridust® and FluoSpheres®, in agarose gel (1 x 10^5 cells.ml^{-1}), collagen gel (1 x 10^5 cells.ml^{-1}) and in inverted 2D culture (1 x 10^4 cells in 200 µl of cell culture medium). The viability was measured at 12 and 24 hours using the ATP-lite™ luminescence detection assay. The supernatants at these time points were then used to assess the levels of TNF-α cytokine release using ELISA.

3.5.2.1 RAW 264.7 murine macrophage cell viability and response to model particles in agarose gels

The optimal cell seeding density of RAW 264.7 murine macrophages in 48 well tissue culture plates in 2D was initially assessed to provide a suitable range of seeding densities for use in the subsequent viability assays. The viability of RAW 264.7 murine macrophages at three seeding densities (1 x 10^4, 5 x 10^4 and 1 x 10^5 cells.ml^{-}) in agarose gel was assessed at days 0, 1, 2 and 3 using the ATP-lite™ luminescence detection assay. RAW 264.7 murine macrophages were cultured with Ceridust® and FluoSpheres® model particles in agarose gels. Cells were seeded at 1 x 10^5 cells.ml^{-1} with 100 µm^3 particles per cell in a 48 well tissue culture plate. The contents of each well was assessed using the ATP-lite™ luminescence detection assay and ELISA for TNF-α at 12 and 24 hours post particle exposure.

Viability of RAW 264.7 murine macrophages over time

All cell seeding densities except 1 x 10^5 cells.ml^{-1} displayed a continual increase in viability for up to three days (Figure 3.5) and remained at a constant level of viability on day 5 (ANOVA; $p<0.05$). Cells seeded at 1 x 10^5 cells.ml^{-1} exhibited a significant increase in viability on day 1 and remained at a consistently high levels of viability throughout the course of the assay (ANOVA; $p<0.05$). The cells seeded at 2 x 10^5 cells.ml^{-1} treated with DMSO (200 µl.ml^{-1}) exhibited a significant decrease in viability every time point post seeding (ANOVA; $p<0.05$).

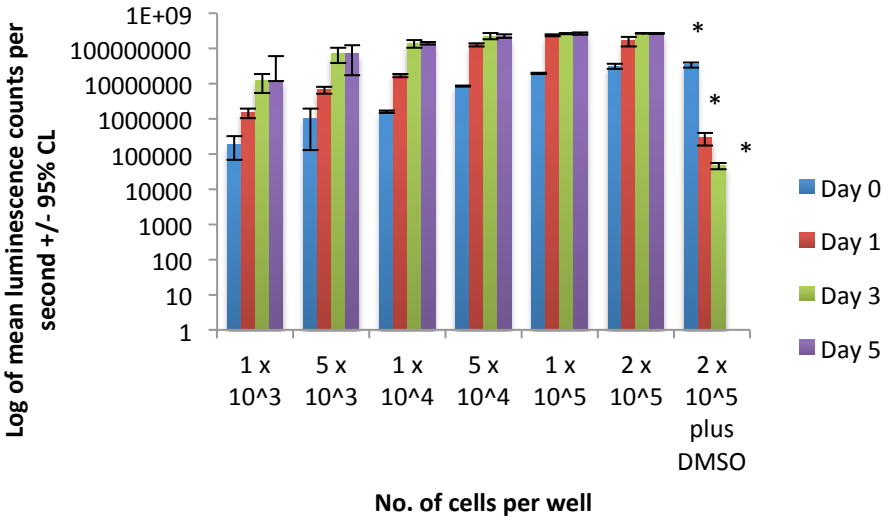

Figure 3.5 Cell viability of RAW 264.7 murine macrophages seeded at different densities over five days at 37°C in 5% (v/v) CO_2 in air. Cells were seeded at densities of 5 x 10^3, 1 x 10^4, 5 x 10^4, 1 x 10^5 and 5 x 10^5 cells.ml^{-1} in a 48 well tissue culture plate. A cells plus DMSO (200 µl.ml^{-1}) positive control was included in the conditions. * designates a statistically significant data point compared to the seeding densities assessed (ANOVA, $p<0.05$). Error bars represent 95% confidence intervals, n=6.

RAW 264.7 murine macrophage viability in agarose gel

The viability of RAW 264.7 murine macrophages in agarose gel was assessed using the ATP-lite™ luminescence detection assay. The assay was repeated both with and without a rinse step as it was observed, using light microscopy, that many cells were failing to penetrate the gel and were clumped together on the surface of the agarose gel. The rinse step removed the cells that had failed to penetrate the gel so that they would not affect subsequent experiments.

RAW 264.7 murine macrophages cultured with no rinse step (Figure 3.6A) show a general increase in cell viability in agarose gels over three days, whereas the positive control, cells plus DMSO (200 µl.ml^{-1}), showed a significant decrease in viability after day 0 (ANOVA; $p<0.05$ for day 0 and $p>0.05$ for days 1 and 3). However RAW 264.7 murine macrophages cultured in agarose gel with a rinse step (Figure 3.6B) exhibited an increase in viability after 12 hours until day 2, followed by a decrease in viability on day three (ANOVA; $p<0.05$).

A)

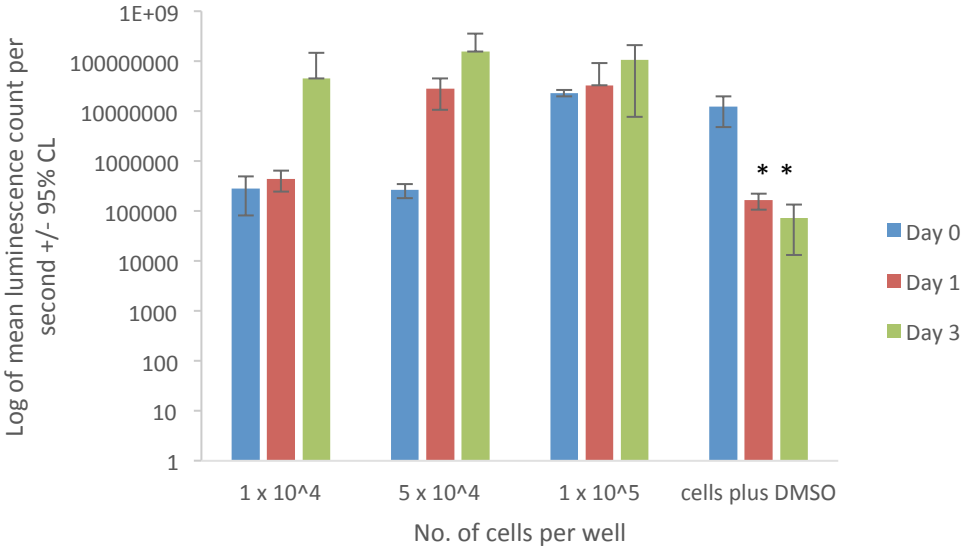

B)

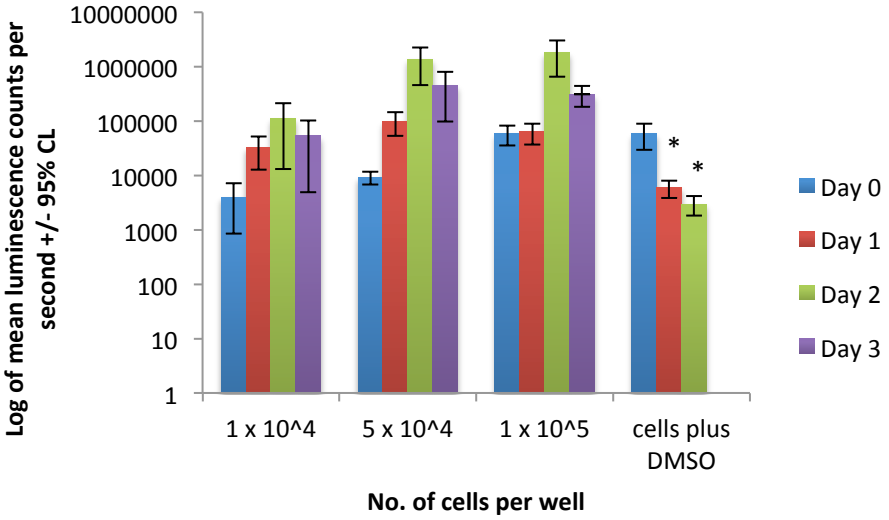

Figure 3.6 Cell viability of RAW 264.7 murine macrophages seeded at different densities in agarose gel over three days at 37°C in 8% (v/v) CO_2 in air. Cells were seeded at densities of 1 x 10^4, 5 x 10^4 and 1 x 10^5 cells.ml^{-1} in a 48 well tissue culture plate. A cells plus DMSO (200 µl.ml^{-1}) positive control was included in the conditions. Cells viability was assessed using the ATP-lite^{TM} luminescence detection assay both without (A) and with (B) a rinse step 12 hours post seeding to remove any cells that had not penetrated the gel. * designates a statistically significant data point compared to the seeding densities assessed (ANOVA, $p<0.05$). Error bars represent 95% confidence intervals, n=6.

Viability of RAW 264.7 murine macrophages after exposure to model particles in agarose gels

None of the particle treatments had any effect on cell viability (Figure 3.7A) when compared to the cells only negative control (ANOVA; $p<0.05$).

TNF-α release from RAW 264.7 murine macrophages after exposure to model particles in agarose gels

After 12 hours, cells cultured with >10 µm Ceridust®, 0.2 µm FluoSpheres® and LPS produced significantly elevated levels of TNF-α (Figure 3.7B) compared to the cells only negative control (ANOVA; $p>0.05$). None of the remaining treatments had any significant effect on TNF-α release from RAW 264.7 murine macrophages (ANOVA; $p<0.05$).

After 24 hours, cells cultured with LPS (200 $ng.ml^{-1}$) produced significantly elevated levels of TNF-α (Figure 3.7B) compared to the cells only negative control (ANOVA; $p>0.05$). None of the remaining treatments had any significant effect on the TNF-α release of RAW 264.7 murine macrophages (ANOVA; $p<0.05$).

A)

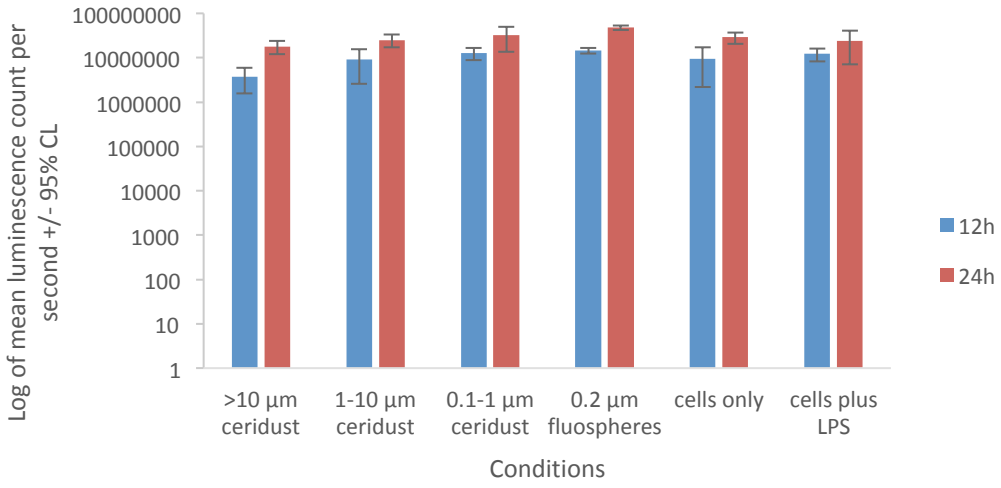

B)

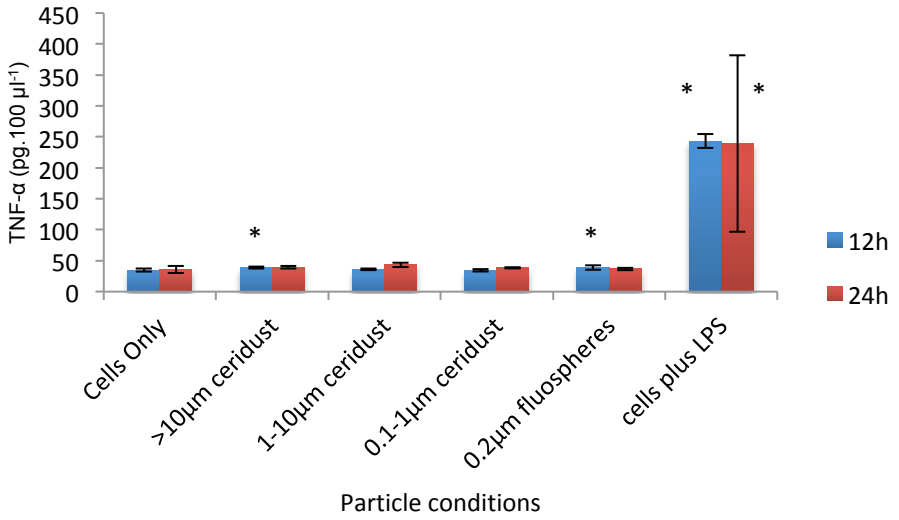

Figure 3.7 – A) Cell viability and B) TNF-α release from RAW 264.7 murine macrophages incubated with Ceridust® and FluoSpheres® model particles at a concentration of 100 µm^3 particles per cell in agarose gel at 12 and 24 hours post particle exposure at 37°C in 8% (v/v) CO_2 in air. Cells were seeded at a density of 1 x 10^5 cells.ml^{-1} with particle treatments in a 48 well tissue culture plate. A cells only negative control and LPS (200 ng.ml^{-1}) positive control were included in the conditions. * designates a statistically significant data point compared to the cells only negative control (ANOVA, $p<0.05$). Error bars represent 95% confidence intervals, n=4.

3.5.2.2 RAW 264.7 murine macrophage cell viability and response to model particles in collagen gels

The viability of RAW 264.7 murine macrophages in collagen gel was assessed using the ATP-lite™ luminescence detection assay. RAW 264.7 murine macrophages were cultured with Ceridust® and FluoSpheres® model particles in collagen gel. Cells were seeded at 1 x 10^5 cells.ml^{-1} with 100 µm^3 particles per cell in a 48 well tissue culture plate. The contents of each well were assessed using the ATP-lite™ luminescence detection assay and ELISA for TNF-α at 12 and 24 hours post particle exposure.

RAW 264.7 murine macrophage viability in collagen gels

RAW 264.7 murine macrophages in collagen gel exhibit a general increase in cell viability (Figure 3.8) over three days with the exception of cells seeded at 1 x 10^5 cells.ml^{-1}, which declined in viability on day 3 (ANOVA; $p<0.05$). The positive control, cells plus DMSO (200 µl.ml^{-1}), showed a significant decrease in viability beyond day 0.

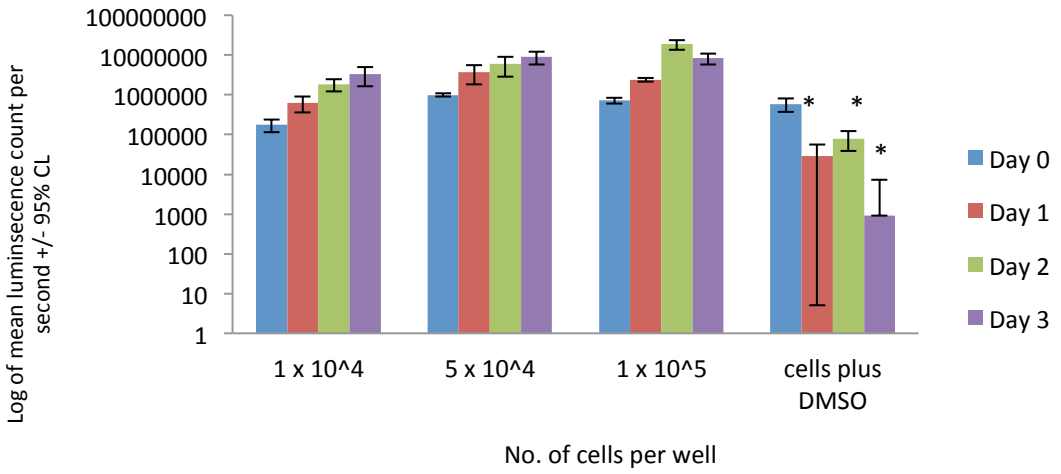

Figure 3.8 Cell viability of RAW 264.7 murine macrophages seeded at different densities in collagen gel over three days at 37°C in 8% (v/v) CO_2 in air. Cells were seeded at densities of 1 x 10^4, 5 x 10^4 and 1 x 10^5 cells.ml^{-1} in a 48 well tissue culture plate. A cells plus DMSO (200 µl.ml^{-1}) positive control was included in the conditions. * designates a statistically significant data point compared to the range of seeding densities assessed (ANOVA, $p<0.05$). Error bars represent ± the 95% confidence level, n=6.

Viability of RAW 264.7 murine macrophages after exposure to model particles in collagen gels

Cells treated with 0.1 - 1 µm Ceridust®, 0.2 µm FluoSpheres® and LPS (200 ng.ml^{-1}) exhibited a significant increase in cell viability at both 12 and 24 hours post particle exposure (Figure 3.9A) when compared to the cells only negative control (ANOVA; $p<0.05$). None of the remaining treatments had any effect on cell viability when compared to the cells only negative control (ANOVA; $p<0.05$).

TNF-α release from RAW 264.7 murine macrophages after exposure to model particles in collagen gels

After 12 hours, none of the treatments have any significant effect on the TNF-α release of RAW 264.7 murine macrophages (Figure 3.9B) except cells cultured with LPS (ANOVA; $p>0.05$).

After 24 hours, cells cultured with >10 µm Ceridust® and LPS (200 ng.ml^{-1}) produced a significantly elevated TNF-α (Figure 3.9B) compared to the cells only negative control (ANOVA; $p>0.05$). None of the remaining treatments had any significant effect on the TNF-α release of RAW 264.7 murine macrophages (ANOVA; $p<0.05$). These results were unexpected so this assay was repeated (Figure 3.9C and Figure 3.9D) which confirmed the same findings i.e. cells cultured with >10 µm Ceridust® and LPS

(200 ng.ml^{-1}) produced a significantly elevated TNF-α (Figure 3.9B) compared to the cells only negative control (ANOVA; p>0.05). In addition, the repeated study showed that 0.2 µm FluoSpheres® also produced a significantly elevated TNF-α (Figure 3.9B) compared to the cells only negative control (ANOVA; p>0.05).

A)

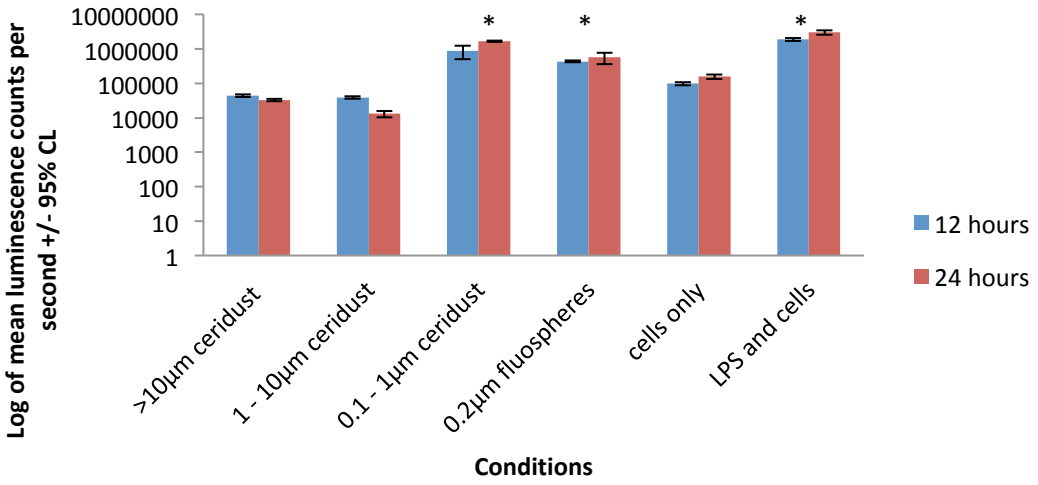

B)

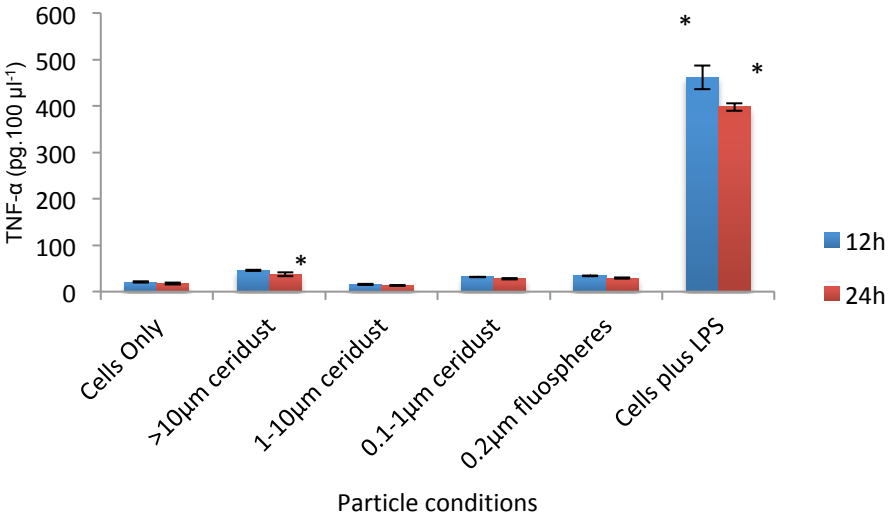
600
500
400
300
200
100
0
TNF-α (pg.100 µl⁻¹)
*
*
*
12h
24h
Cells Only
>10µm ceridust
1-10µm ceridust
0.1-1µm ceridust
0.2µm fluospheres
Cells plus LPS
Particle conditions

C)

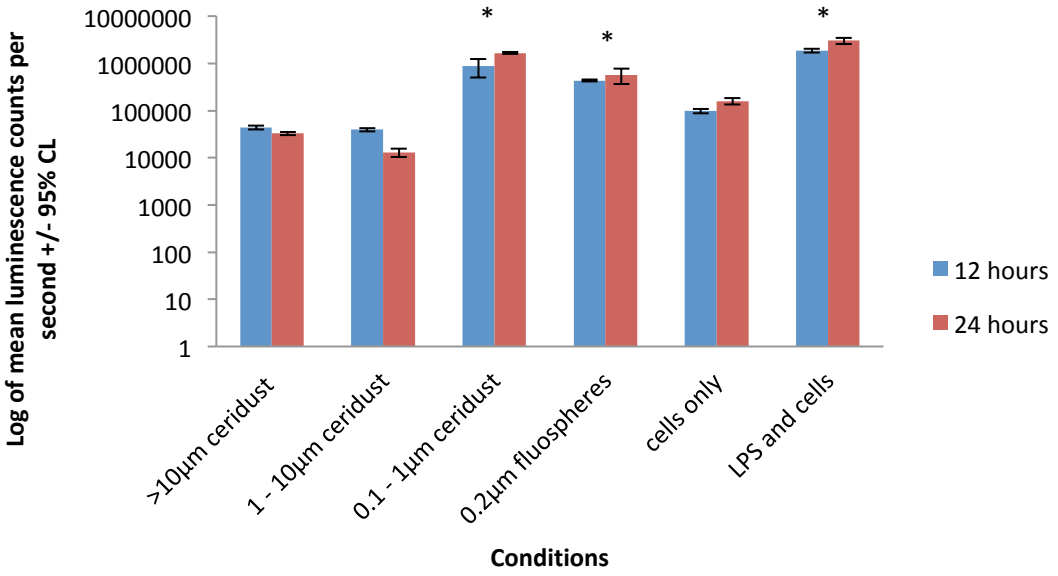
10000000
1000000
100000
10000
1000
100
10
1
Log of mean luminescence counts per second +/- 95% CL
*
*
*
12 hours
24 hours
>10µm ceridust
1 - 10µm ceridust
0.1 - 1µm ceridust
0.2µm fluospheres
cells only
LPS and cells
Conditions

D)

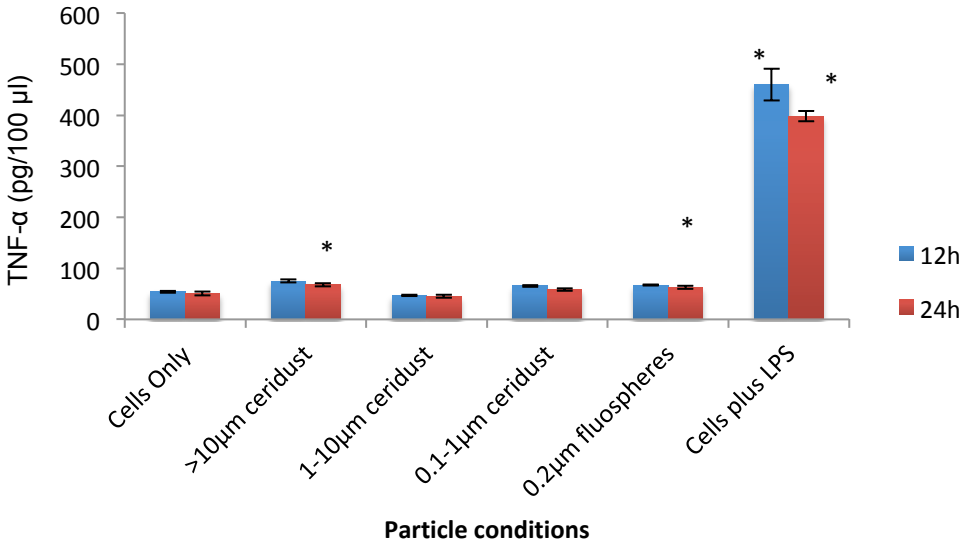

Figure 3.9 – A) Cell viability and B) TNF-α release from RAW 264.7 murine macrophages incubated with Ceridust® and FluoSpheres® model particles at a concentration of 100 µm^3 particles per cell in collagen gel at 12 and 24 hours post particle exposure at 37°C in 8% (v/v) CO_2 in air. Cells were seeded at a density of 1 x 10^5 cells.ml^{-1} with particle treatments in a 48 well tissue culture plate. A cells only negative control and LPS (200 ng.ml^{-1}) positive control were included in the conditions. * designates a statistically significant data point compared to the cells only negative control (ANOVA, $p<0.05$). Error bars represent 95% confidence intervals, n=4. C) and D) show a repeat of the above in order to confirm the results were repeatable.

3.5.2.3 Response of RAW 264.7 murine macrophage cells to model particles in an inverted culture model

The optimal cell seeding density of RAW 264.7 murine macrophages in 96 well tissue culture plates in 2D was initially assessed over five days to provide a suitable range of densities for use in the subsequent inverted culture model. RAW 264.7 murine macrophages were cultured with Ceridust® and FluoSpheres® model particles in an inverted 2D culture model. Cells were seeded at 5 x 10^4 cells.ml^{-1} with 100 µm^3 particles per cell in a 96 well tissue culture plate. The contents of each well was assessed using the ATP-lite™ luminescence detection assay and TNF-α ELISA at 12 and 24 hours post seeding.

Viability of RAW 264.7 murine macrophages over time

Cells seeded at densities of 1 x 10^3, 5 x 10^3 and 1 x 10^4 cells.ml^{-1} display a pattern of continual increase in viability (Figure 3.10) over the course of five days (ANOVA;

p<0.05). Cells seeded at densities of 5 x 10^4 and 1 x 10^5 cells.ml^{-1} displayed relatively constant levels of viability over two days, experienced a significant increase in viability on day 3 and then a significant decrease in viability on day 5 (ANOVA; p<0.05).

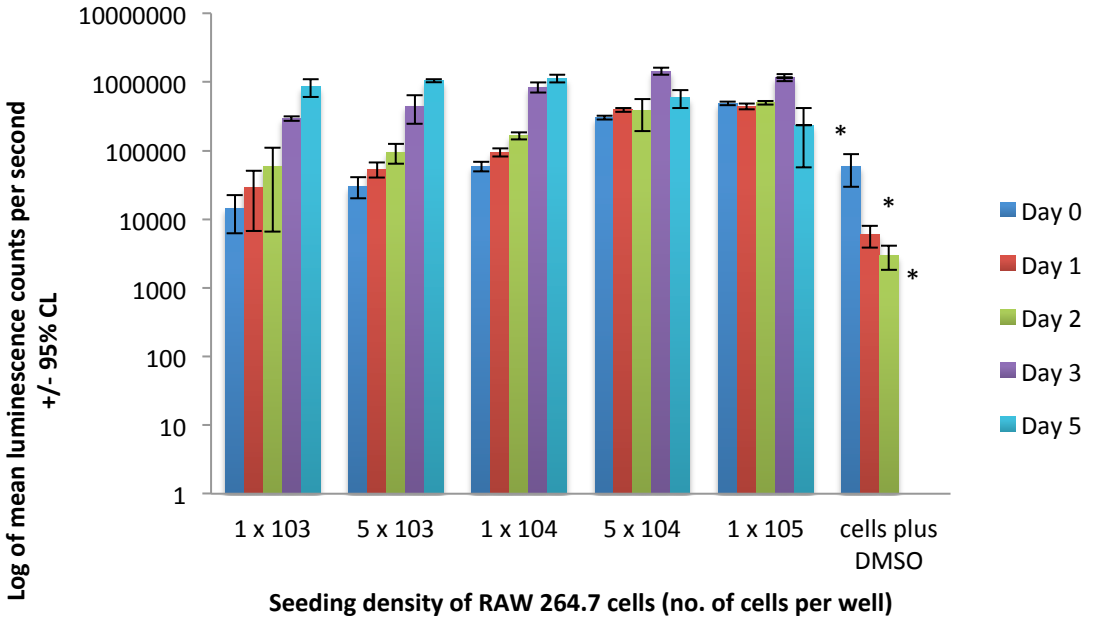

Figure 3.10 Cell viability of RAW 264.7 murine macrophages seeded at different densities over five days at 37°C in 5% (v/v) CO_2 in air. Cells were seeded at densities of 5 x 10^3, 1 x 10^4, 5 x 10^4, 1 x 10^5 and 5 x 10^5 cells.ml^{-1} in a 96 well tissue culture plate. A cells plus DMSO (200 µl.ml^{-1}) positive control was included in the conditions. * designates a statistically significant data point compared to the seeding densities assessed (ANOVA, p<0.05). Error bars represent 95% confidence intervals, n=6.

Viability of RAW 264.7 murine macrophages after exposure to model particles in inverted 2D culture

None of the treatments had a significant effect on the viability of RAW 264.7 murine macrophages (Figure 3.11A) compared to the cells only negative control at 12 hours post particle exposure, except cells cultured with >10 µm Ceridust®. The majority of treatments had no significant effect on the viability of RAW 264.7 murine macrophages compared to the cells only negative control at 24 hours post particle exposure except cells cultured with cells cultured with >10 µm Ceridust® and LPS (200 ng.ml^{-1}) (ANOVA; p<0.05).

TNF-α release from RAW 264.7 murine macrophages after exposure to model particles in inverted 2D culture

After 12 hours, none of the treatments have any significant effect on the TNF-α release (Figure 3.11B) of RAW 264.7 murine macrophages (ANOVA; p>0.05).

After 24 hours, none of the treatments have any significant effect on the TNF-α release (Figure 3.11B) of RAW 264.7 murine macrophages (ANOVA; p>0.05).

A)

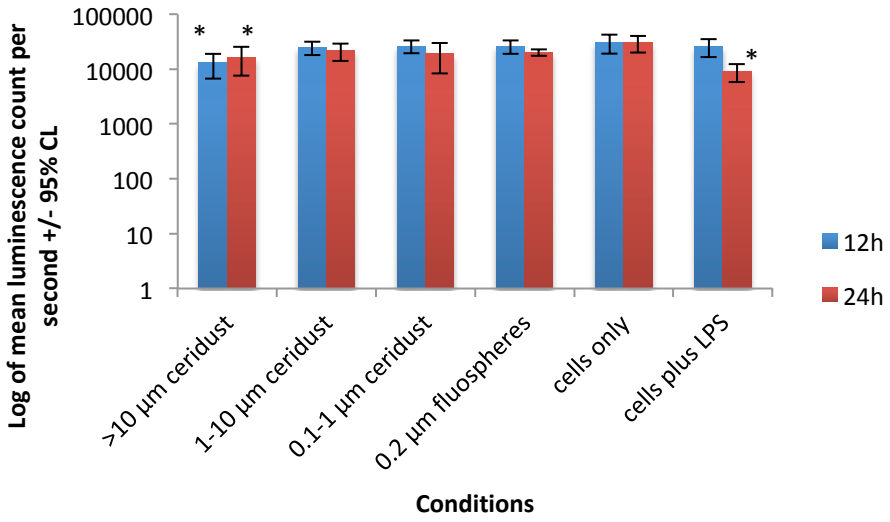

B)

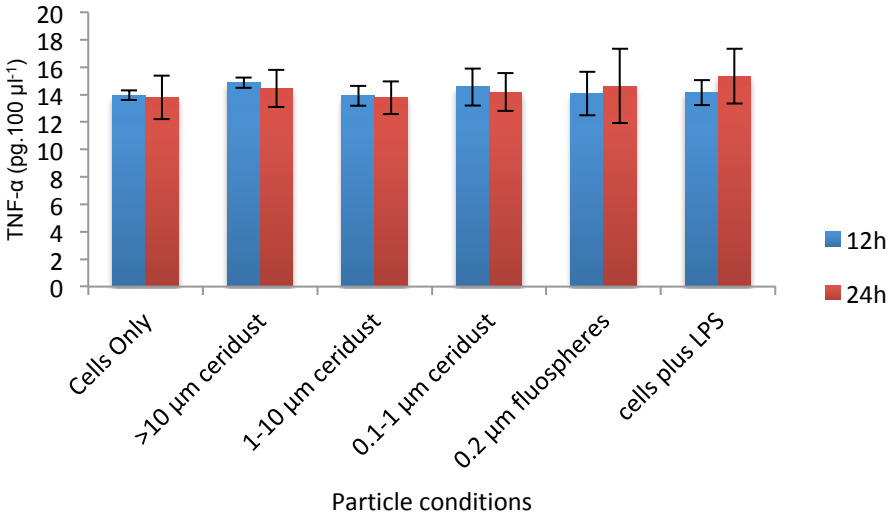

Figure 3.11– A) Cell viability and B) TNF-α release from RAW 264.7 murine macrophages incubated with Ceridust® and FluoSpheres® model particles at a concentration of 100 μm^3 particles per cell at 12 and 24 hours post particle exposure at 37°C in 8% (v/v) CO_2 in air. Cells were seeded at a density of 1 x 10^5 cells.ml^{-1} whilst inverted with particle treatments in a 48 well tissue culture

plate. A cells only negative control and LPS (200 ng.ml^{-1}) positive control were included in the conditions. * designates a statistically significant data point compared to the cells only negative control (ANOVA, $p<0.05$). Error bars represent 95% confidence intervals, n=3.

3.5.3 Cell viability and inflammatory response of U937 human histiocytes to model particles in agarose and collagen gels and inverted 2D culture

The viability of U937 human histiocytes was assessed in both agarose and collagen gels over three days using the ATP-lite™ luminescence detection assay. U937 human histiocytes were cultured with model particles, Ceridust® and FluoSpheres®, in agarose gel, collagen gel and in inverted 2D culture. In agarose gel, only adherent cells were used as suspension cells are inappropriate in agarose gel as they do not penetrate or adhere to the gel. Similarly, in inverted 2D culture, only adherent cells were used as suspension cells are inappropriate for use in this context as they are incapable of adhering to the tissue culture plate prior to inversion. For the collagen gel, both adherent and suspension cells were assessed. The viability was measured at 12 (and 24 hours for the inverted model) using the ATP-lite™ luminescence detection assay. The supernatants at these time points were then used to assess the levels of TNF- α cytokine released using ELISA. Unfortunately, the data for U937 human histiocytes in agarose and collagen gels with Ceridust® 24 hours post particle exposure was lost due to experimental error and the candidate made the decision not to repeat the assay for this time point due to time pressures and that this cell type was not being carried forward to the remaining parts of the study.

3.5.3.1 U937 human histiocyte cell viability and response to model particles in agarose gels

The viability of U937 human histiocytes was assessed in agarose gel over three days using the ATP-lite™ luminescence detection assay. Transformed U937 human histiocytes were cultured with Ceridust® and FluoSpheres® model particles in agarose gel. Cells were seeded at 1 x 10^5 cells.m^{l-1} with 100 μm^3 particles per cell in a 48 well tissue culture plate. The contents of each well was assessed using the ATP-lite™ cell viability assay (at 12 and 24 hours post particle exposure) and TNF-α ELISA (at 12 hours post particle exposure). Unfortunately, the data for U937 human histiocytes in agarose gels with Ceridust® 24 hours post particle exposure was lost due to experimental error and the candidate made the decision not to repeat the assay for this time point.

Non-transformed U937 human histiocytes viability in agarose gel

Non-transformed U937 human histiocytes (i.e. untreated cells in a suspension culture) exhibited a general increase in cell viability over three days (Figure 3.12). Cell seeded at 5 x 10^4 and 1 x 10^5 cells.ml^{-1} remained constant in terms of their viability between days 1 and 3. Cells cultured with DMSO (200 µl.ml^{-1}) demonstrated a significant decrease in viability from day 0 onwards (ANOVA; $p<0.05$).

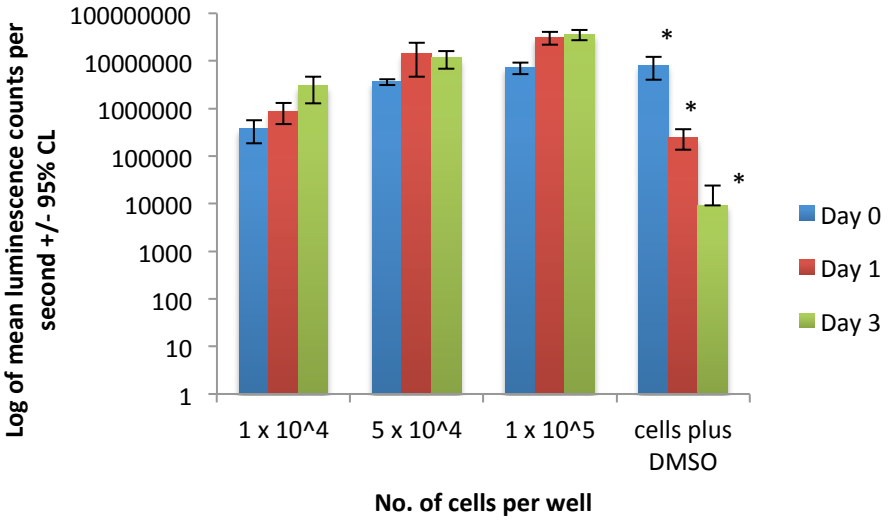

Figure 3.12 Cell viability of **non-transformed** U937 human histiocytes seeded at different densities in **agarose gel** over five days at 37°C in 5% (v/v) CO_2 in air. Cells were seeded at densities of 5 x 10^3, 1 x 10^4, 5 x 10^4, 1 x 10^5 and 5 x 10^5 cells.ml^{-1} in a 48 well tissue culture plate. A cells plus DMSO (200 µl.ml^{-1}) positive control was included in the conditions. * designates a statistically significant data point compared to the seeding densities assessed (ANOVA, $p<0.05$). Error bars represent 95% confidence intervals, n=6.

Transformed U937 human histiocytes viability in agarose gel

Transformed U937 human histiocytes (i.e. cells treated with PMA to become adherent and activated) exhibited a general increase in cell viability in agarose gel over three days (Figure 3.13) for all seeding densities (days 0 and 1 ANOVA; $p<0.05$, day 3 ANOVA; $p>0.05$).

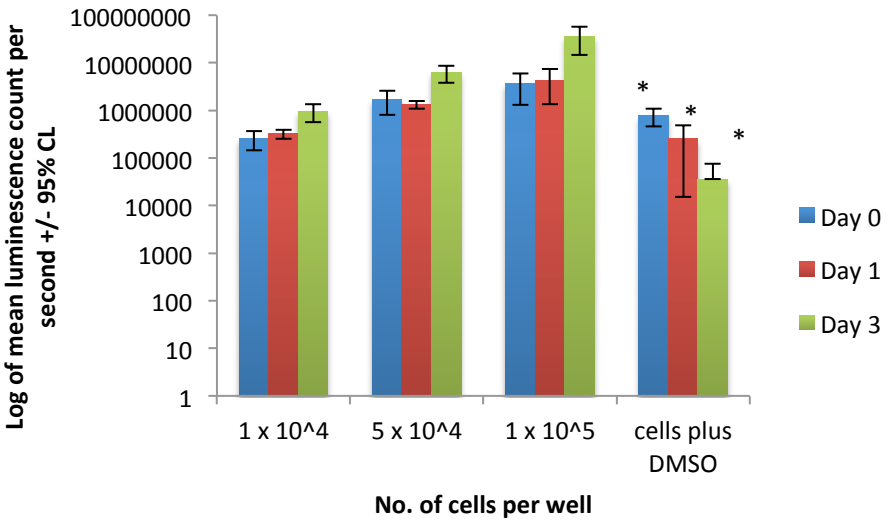

Figure 3.13 Cell viability of **transformed** U937 human histiocytes seeded at different densities in **agarose gel** over five days at 37°C in 5% (v/v) CO_2 in air. Cells were seeded at densities of 5 x 10^3, 1 x 10^4, 5 x 10^4, 1 x 10^5 and 5 x 10^5 cells.ml^{-1} in a 48 well tissue culture plate. A cells plus DMSO (200 µl.ml^{-1}) positive control was included in the conditions. * designates a statistically significant data point compared to the seeding densities assessed (ANOVA, $p<0.05$). Error bars represent 95% confidence intervals, n=6.

Viability of transformed U937 human histiocytes after exposure to model particles in agarose gels

None of the treatments except LPS (200 ng.ml^{-1}) (12 hours post particle exposure only) had a significant effect on the viability of transformed U937 human histiocytes (Figure 3.14A) compared to the cells only negative control at 12 and 24 hours post particle exposure (ANOVA; $p<0.05$).

TNF-α release from transformed U937 human histiocytes after exposure to model particles in agarose gels

After 12 hours, non-transformed U937 human histiocytes treated with 0.2 µm FluoSpheres® in addition to LPS (200 ng.ml^{-1}) treated positive control cells produced significantly elevated levels of TNF-α (Figure 3.14B), when compared to the cells only negative control (ANOVA: $p<0.05$). None of the remaining Ceridust® particle treatments had a significant effect on the release of TNF-α. Unfortunately, the data for U937 human histiocytes in agarose gels with Ceridust® 24 hours post particle exposure was lost due to experimental error and the candidate made the decision not to repeat the assay for this time point.

A)

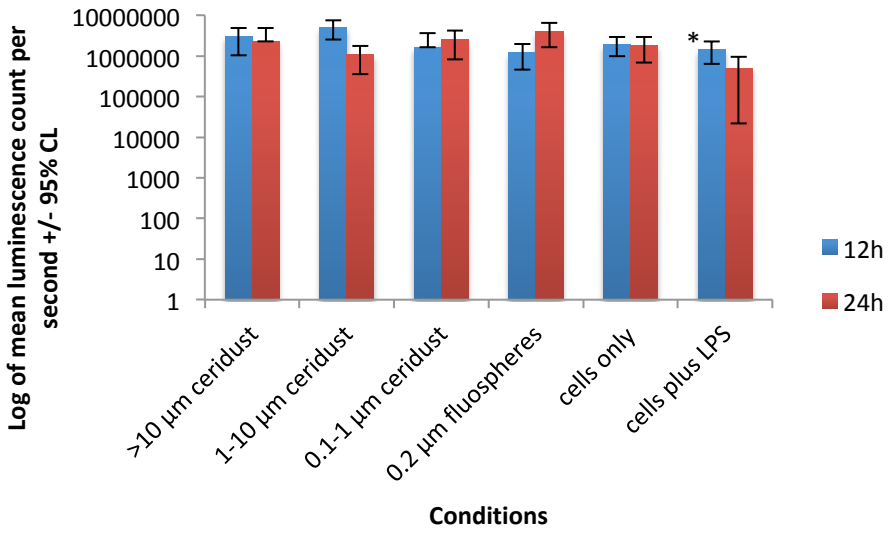

B)

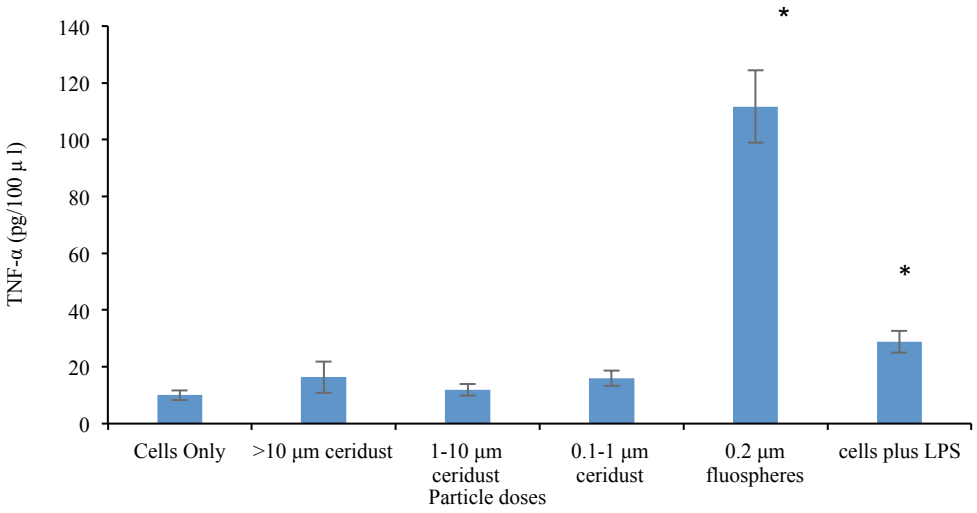

Figure 3.14– A) Cell viability and B) TNF-α release from **transformed** U937 human histiocytes incubated with Ceridust® and FluoSpheres® model particles at a concentration of 100 μm^3 particles per cell in **agarose gel** at 12 hours post particle exposure at 37°C in 5% (v/v) CO_2 in air. Cells were seeded at a density of 1 x 10^5 cells.ml^{-1} with particle treatments in a 48 well tissue culture plate. A cells only negative control and LPS (200 ng.ml^{-1}) positive control were included in the conditions. * designates a statistically significant data point compared to the cells only negative control (ANOVA, $p<0.05$). Error bars represent 95% confidence intervals, n=4.

3.5.3.2 U937 human histiocyte cell viability and response to model particles in collagen gels

The viability of U937 human histiocytes was assessed in collagen gel over three days using the ATP-lite™ luminescence detection assay. Transformed and non-transformed U937 human histiocytes were cultured with Ceridust® and FluoSpheres® model particles in collagen gels. Cells were seeded at 1 x 10^5 cells.ml^{-1} with 100 µm^3 particles per cell in a 96 well tissue culture plate. The contents of each well was assessed using the ATP-lite™ luminescence detection assay (at 12 and 24 hours post particle exposure) and TNF-α ELISA (at 12 hours post particle exposure). Unfortunately, the data for U937 human histiocytes in collagen gels with Ceridust® 24 hours post particle exposure was lost due to experimental error and the candidate made the decision not to repeat the assay for this time point.

Transformed U937 human histiocytes

Transformed U937 human histiocytes remain at a relatively constant level of cell viability at all densities in collagen gel (Figure 3.15) on days 0 and 1 however, on day 3, a decrease in cell viability is observed although this is not significant (days 0 and 1 ANOVA; $p<0.05$, day 3 ANOVA; $p>0.05$). Cells cultured with DMSO (200 µl.ml^{-1}) exhibited a significant decrease in viability from day 0 onwards.

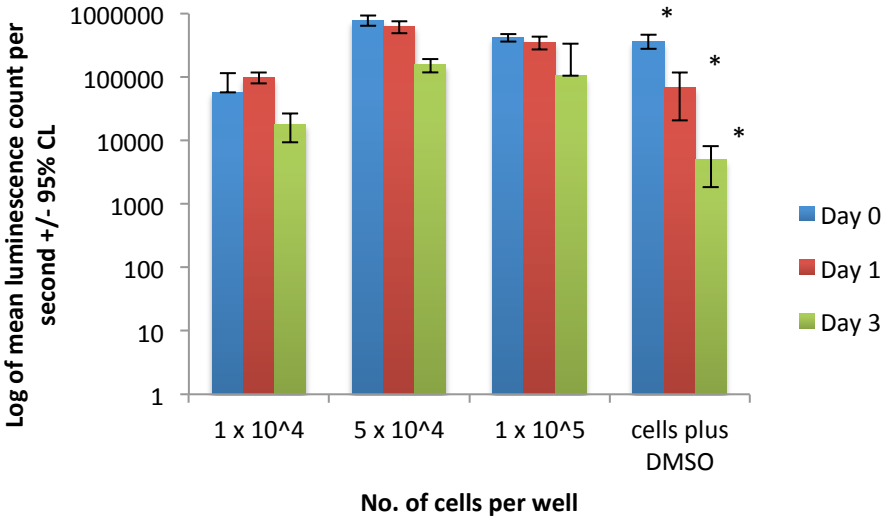

Figure 3.15 Cell viability of **transformed** U937 human histiocytes seeded at different densities in **collagen gel** over five days at 37°C in 5% (v/v) CO_2 in air. Cells were seeded at densities of 5 x 10^3, 1 x 10^4, 5 x 10^4, 1 x 10^5 and 5 x 10^5 cells.ml^{-1} in a 48 well tissue culture plate. A cells plus DMSO (200 µl.ml^{-1}) positive control was included in the conditions. * designates a statistically significant data point compared to the seeding densities assessed (ANOVA, $p<0.05$). Error bars represent 95% confidence intervals, n=6.

Viability of transformed U937 human histiocytes after exposure to model particles in collagen gels

All of the treatments except >10 µm Ceridust® had a significant effect on the viability of transformed U937 human histiocytes (Figure 3.16A) compared to the cells only negative control at 12 hours post seeding (ANOVA; $p<0.05$).

TNF-α release from transformed U937 human histiocytes after exposure to model particles in collagen gels

After 12 hours, non-transformed U937 human histiocytes treated with 0.2 µm FluoSpheres® in addition to LPS (200 $ng.ml^{-1}$) treated cells produced a significantly higher level of TNF-α (Figure 3.16B) when compared to the cells only negative control (ANOVA: $p<0.05$). None of the remaining Ceridust® particle treatments had a significant effect on the release of TNF-α. Unfortunately, the data for U937 human histiocytes in collagen gels with Ceridust® 24 hours post particle exposure was lost due to experimental error and the candidate made the decision not to repeat the assay for this time point.

A)

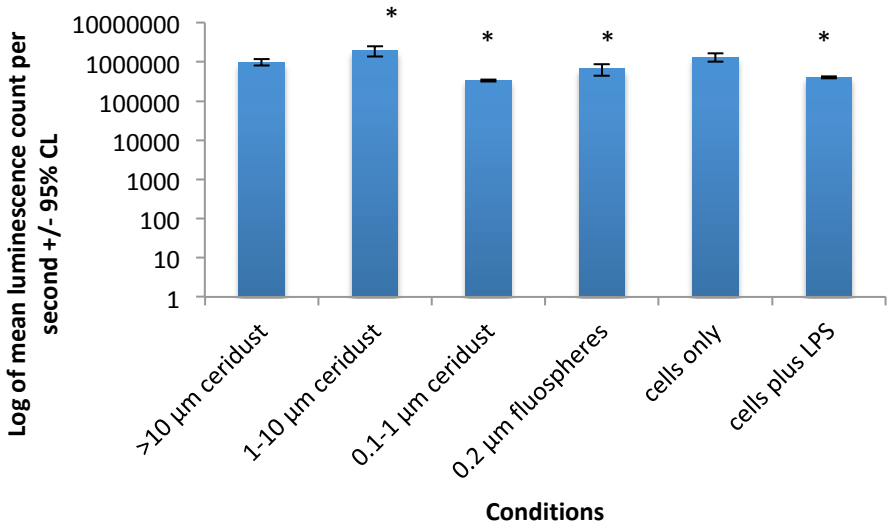

B)

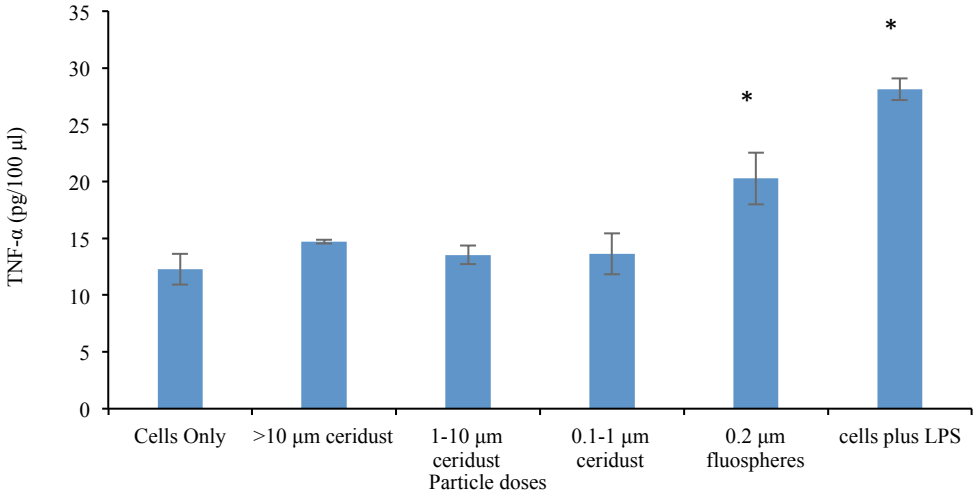

Figure 3.16– A) Cell viability and B) TNF-α release from **transformed** U937 human histiocytes incubated with Ceridust® and FluoSpheres® model particles at a concentration of 100 μm^3 particles per cell in **collagen gel** at 12 hours post particle exposure at 37°C in 5% (v/v) CO_2 in air. Cells were seeded at a density of 1 x 10^5 cells.ml^{-1} with particle treatments in a 48 well tissue culture plate. A cells only negative control and LPS (200 ng.ml^{-1}) positive control were included in the conditions. * designates a statistically significant data point compared to the cells only negative control (ANOVA, $p<0.05$). Error bars represent 95% confidence intervals, n=4.

Non-transformed U937 human histiocytes

Transformed U937 human histiocytes showed a general increase in cell viability over three days in collagen gel (Figure 3.17) whereas cells cultured with DMSO demonstrated a significant decrease in viability over three days (ANOVA; $p<0.05$).

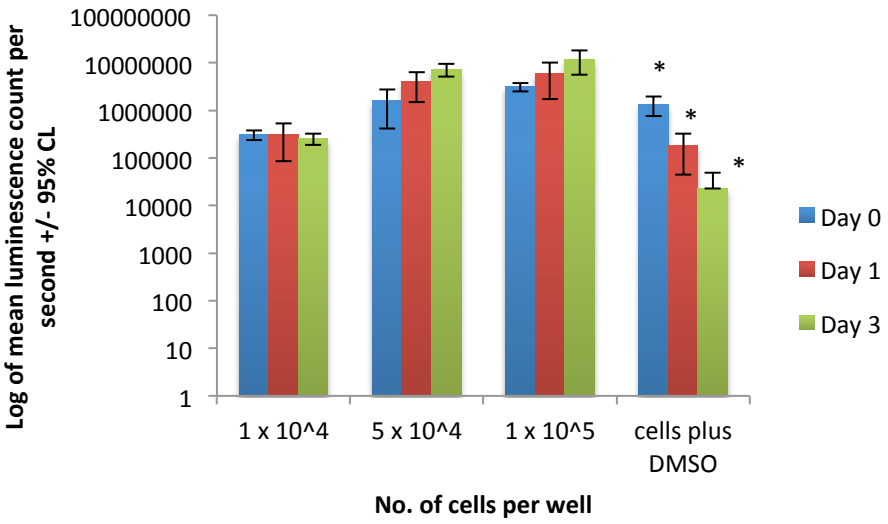

Figure 3.17 Cell viability of non-transformed U937 human histiocytes seeded at different densities in collagen gel over three days at 37°C in 5% (v/v) CO_2 in air. Cells were seeded at densities of 5 x 10^3, 1 x 10^4, 5 x 10^4, 1 x 10^5 and 5 x 10^5 cells.ml^{-1} in a 48 well tissue culture plate. A cells plus DMSO (200 µl.ml^{-1}) positive control was included in the conditions. * designates a statistically significant data point compared to the seeding densities assessed (ANOVA, $p<0.05$). Error bars represent 95% confidence intervals, n=6.

Viability of non-transformed U937 human histiocytes after exposure to model particles in collagen gels

All of the treatments had a significant effect on the viability of non-transformed U937 human histiocytes (Figure 3.18A) compared to the cells only negative control at 12 hours post particle exposure (ANOVA; $p<0.05$).

TNF-α release from non-transformed U937 human histiocytes after exposure to model particles in collagen gels

After 12 hours, non-transformed U937 human histiocytes treated with >10 µm Ceridust®, 0.2 µm FluoSpheres® in addition to LPS (200 ng.ml^{-1}) treated positive control cells produced a significantly elevated release of TNF-α (Figure 3.18B) when compared to the cells only negative control (ANOVA: $p<0.05$). None of the remaining Ceridust® particle treatments had a significant effect on the release of TNF-α. Unfortunately, the data for U937 human histiocytes in collagen gels with Ceridust® 24 hours post particle exposure was lost due to experimental error and the candidate made the decision not to repeat the assay for this time point.

A)

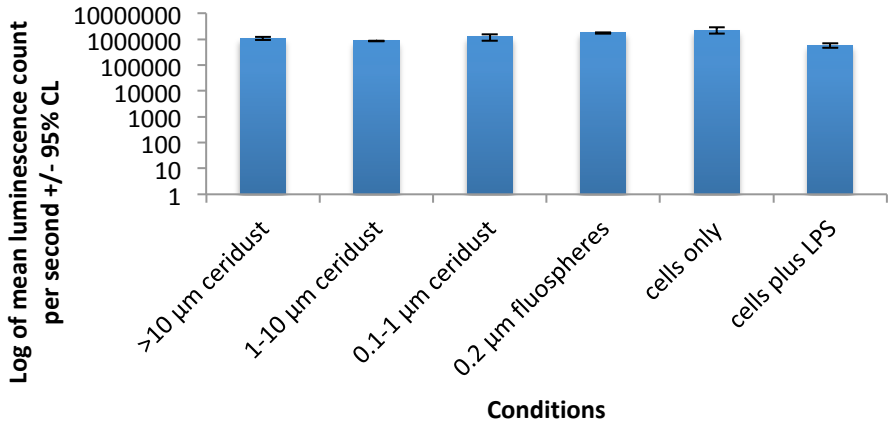

B)

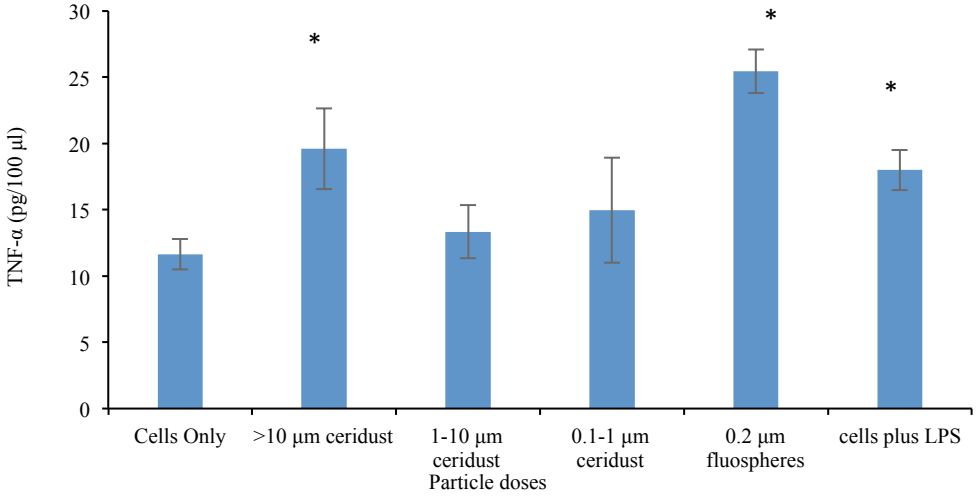

Figure 3.18– A) Cell viability and B) TNF-α release from **non-transformed** U937 human histiocytes incubated with Ceridust® and FluoSpheres® model particles at a concentration of 100 μm^3 particles per cell in **collagen gel** at 12 hours post particle exposure at 37°C in 5% (v/v) CO_2 in air. Cells were seeded at a density of 1 x 10^5 cells.ml^{-1} with particle treatments in a 48 well tissue culture plate. A cells only negative control and LPS (200 ng.ml^{-1}) positive control were included in the conditions. * designates a statistically significant data point relative to the cells only negative control (ANOVA, $p<0.05$). Error bars represent 95% confidence intervals, n=4.

3.5.3.3 Response of transformed U937 human histiocyte cells to model particles in an inverted culture model

The optimal cell seeding density of U937 human histiocytes in 96 well tissue culture plates in 2D was initially assessed over five days to provide a suitable range of densities for use in the forthcoming inverted culture model. Transformed U937 human

histiocytes were cultured with Ceridust® and FluoSpheres® model particles in an inverted 2D culture model. Cells were seeded at 5 x 10^4 cells.ml^{-1} with 100 µm^3 particles per cell in a 96 well tissue culture plate. The contents of each well was assessed using the ATP-lite^{TM} luminescence detection assay and TNF-α ELISA at 12 and 24 hours post particle exposure.

Viability of transformed U937 human histiocytes over time

Cells seeded at densities of 1 x 10^3, 5 x 10^3 and 1 x 10^4 cells per ml displayed relatively constant levels of viability (Figure 3.19) over two days, experienced a significant increase in viability on day 3 and then a significant decrease in viability on day 5 (ANOVA; $p<0.05$). Cells seeded at densities of 5 x 10^4 and 1 x 10^5 cells.ml^{-1} experienced a significant decrease in viability on day 1, remained constant on day 2, experienced a significant increase in viability on day 3 followed by a decrease in viability on day 5, although the latter was not significant (ANOVA; $p<0.05$).

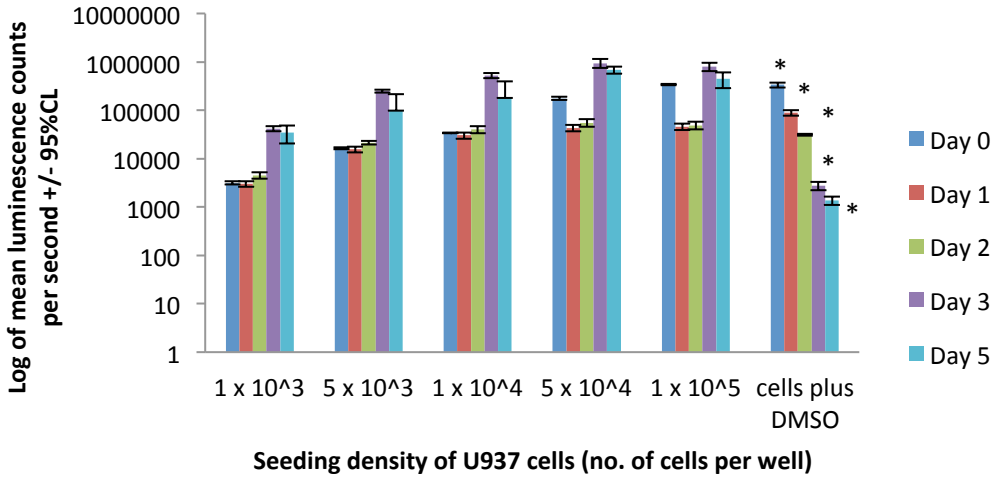

Figure 3.19–Cell viability of **transformed** U937 human histiocytes seeded at different densities over five days at 37°C in 5% (v/v) CO_2. Cells were seeded at densities of 5 x 10^3, 1 x 10^4, 5 x 10^4, 1 x 10^5 and 5 x 10^5 cells.ml^{-1} in a 48 well tissue culture plate. A cells plus DMSO (200 µl.ml^{-1}) positive control was included in the conditions. * designates a statistically significant data point compared to the seeding densities assessed (ANOVA, $p<0.05$). Error bars represent 95% confidence intervals, n=6.

Viability of U937 human histiocytes after exposure to model particles in inverted 2D culture

None of the Ceridust® treatments had a significant effect on the viability of U937 human histiocytes (Figure 3.20A) compared to the cells only negative control at 12 and 24 hours post particle exposure. However, cells cultured with 0.2 µm

FluoSpheres® and LPS (200 ng.ml^{-1}) (positive control) did exhibit a significant reduction in viability 12 hours post particle exposure (ANOVA; $p<0.05$) but not at 24 hours post particle exposure.

TNF-α release from U937 human histiocytes after exposure to model particles in inverted 2D culture

After 12 hours, transformed U937 human histiocytes treated with 0.2 µm FluoSpheres® in addition to LPS treated positive control cells produced a significant release of TNF-α (Figure 3.20B) when compared to the cells only negative control (ANOVA: $p<0.05$). None of the Ceridust® particle treatments had a significant effect on the release of TNF-α.

After 24 hours, transformed U937 human histiocytes treated with 0.2 µm FluoSpheres® in addition to LPS (200 ng.ml^{-1}) treated positive control cells produced a significant release of TNF-α (Figure 3.20B) when compared to the cells only negative control (ANOVA: $p<0.05$). None of the Ceridust® particle treatments had a significant effect on the release of TNF-α.

A)

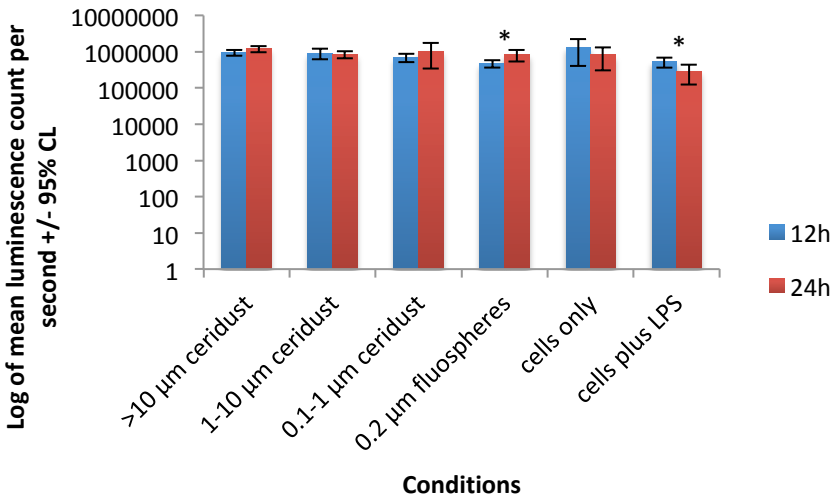

B)

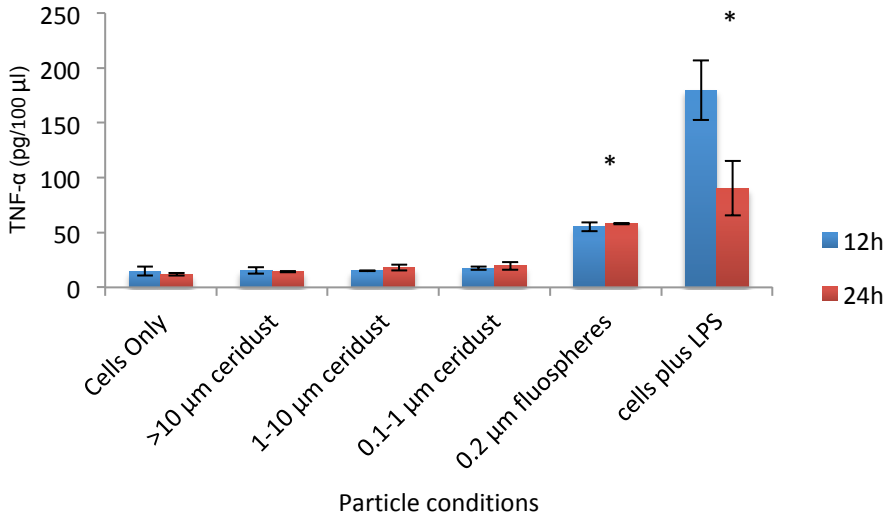

Figure 3.20 – A) Cell viability and B) TNF-α release from **transformed** U937 human histiocytes incubated with Ceridust® and FluoSpheres® model particles at a concentration of 100 μm^3 particles per cell at 12 and 24 hours post particle exposure at 37°C in 5% (v/v) CO_2. Cells were seeded at a density of 1 x 10^4 cells.ml^{-1} whilst **inverted** with particle treatments in a 96 well tissue culture plate. A cells only negative control and LPS (200 ng.ml^{-1}) positive control were included in the conditions. * designates a statistically significant data point compared to the cells only negative control (ANOVA, $p<0.05$). Error bars represent 95% confidence intervals, n=3.

3.6 Discussion

Aim of the present study

The aim of the chapter was to develop a 3D *in vitro* model to assess the cellular response to model polyethylene particles in order to provide a more accurate representation of the periprosthetic environment in comparison to earlier 2D models.

In vitro modelling of the biological response to polyethylene using gel encapsulation

Green *et al.* (1998) encapsulated polyethylene particles (Ceridust®) in 1% (w/v) agarose gel and centrifuging the gel at 800 g to create a monolayer of polyethylene particle on the surface of the gel and seeding murine peritoneal macrophages on top of the gel (Green *et al.*, 1998). This method was adapted and used by Liu (2012); the percentage of agarose in the gel was reduced from 1% to 0.4% (w/v) to increase porosity of the gel and the centrifugation step was removed, leaving polyethylene particles dispersed throughout the gel (Liu, 2012). Liu (2012) also used human PBMNC's, rather than murine peritoneal macrophages. As both of these cell types are

primary, they demonstrate donor heterogeneity which can reduce the reliability and repeatability of the results obtained. Gowland (2014) also used this model and adapted it further by increasing the cell seeding density of PBMNC's from 1 x 10^5 cells.ml^{-1} to 2 x 10^5 cells.ml^{-1} and increasing the volume of particles used from 100 μm^3 particles.cell^{-1} to 500 μm^3 particles.cell^{-1}. This increased the proportion of polyethylene particles within the critical size range required to cause a biological response from macrophages. Gowland (2014) also trialled the use of transformed U937 human histiocytes in this setting and found their response comparable to PBMNC's (Gowland, 2014). As U937 human histiocytes are a cell line, the issue of donor heterogeneity was removed, although Gowland (2014) did not continue their use.

The agarose gel encapsulation method created a 2D culture system and overcame the issues associated with culturing cells with particles with a lower density than cell culture medium. However, as this is a 2D culture system, this model is not representative of the 3D periprosthetic environment.

Development of a novel 3D model to measure cellular response to polyethylene wear debris

In order to address the lack of a 3D model of the periprosthetic environment, this study sought to develop a novel 3D model to measure the cellular response to polyethylene wear debris to enhance reliability and repeatability of future studies. In order to improve the reliability of the model developed, alternative cell types and alternative gel types were investigated in different combinations in terms of their viability and ability to produce an inflammatory response when stimulated with model polyethylene wear debris.

Initially the viability of PBMNC's, U937 human histiocytes and RAW 264.7 murine macrophages in both agarose and collagen gels was examined using the ATP-lite™ luminescence detection assay. PBMNC's were used as they represent the original primary cell type used in this model setting. U937 human histiocytes were chosen as they had been highlighted by a previous study by Matthews *et al.* (2001) as a human monocytic cell line capable of responding in a manner akin to PBMNC's to polyethylene particles (Matthews *et al.*, 2001). Moreover, Gowland (2014) briefly trialled their use and their responses to UHMWPE wear debris were promising (Gowland, 2014). Finally, RAW 264.7 murine macrophages were chosen as previous studies (Green *et al.*, 1998; Matthews *et al.*, 2000a) have routinely used murine peritoneal macrophages with success to model cellular response to UHMWPE wear debris. A cell line alternative, RAW 264.7 murine macrophages, as used in previous studies such as Musib and Saha (2010), was chosen in place of primary cells to avoid

donor heterogeneity. Agarose gel was chosen as it was the original type of gel used in this type of model. Collagen gel was chosen as previous studies by Lee (2016) and Smith (2016) had demonstrated its use in modelling cellular response to neural injuries in a 3D environment (Lee, 2016; Smith, 2016). Moreover, the gelation of collagen is pH dependent, allowing for simultaneous cell and particle encapsulation, whereas agarose gelation is heat dependent and it is therefore impossible to simultaneously encapsulate cells with particles as the high temperature required to plate the gel (>60°C) would adversely affect any cells present. Whereas, collagen gel allows for the simultaneous encapsulation of both cells and particles. Finally, agarose lacks cell attachment sites, such as RGD motifs, unlike collagen gel. The ATP-lite^{TM} luminescence detection assay was chosen rather than the MTT viability assay as previous studies (Lee, 2016; Smith, 2016) found that MTT interacted with collagen gel, forming a brown precipitate; these authors instead used the live-dead assay to count viable cells in microscopic z stacks. The ATP-lite^{TM} luminescence detection assay protocol was modified previously at the University of Leeds to account for its use with gels; the volume of reagents used was multiplied by four and the incubation and shaking times for each step were increased from 5 minutes to 20 minutes to allow the reagents sufficient time to penetrate the gels fully. A positive control, 1 x 10^5 cells.ml^{-1} treated with DMSO (200 µl.ml^{-1}), was included for comparative purposes. Additionally a medium only control was included to correct for background created by the cell culture medium itself.

Neither the agarose or collagen gels adversely affected the viability of either the PBMNC's, U937 human histiocytes or RAW 264.7 murine macrophages. This is consistent with previous studies carried out in agarose (Green *et al.*, 1998, 2000; Matthews *et al.*, 2001; Liu, 2012; Gowland, 2014) and collagen (Lee, 2016; Smith, 2016). It was determined that the working cell seeding density for use in 48 well tissue culture plates was 1 x 10^5 cell.ml^{-1} as opposed to the increased cell seeding density, 2 x 10^5 cells.ml^{-1}, used by Gowland (2014); although it should be noted that Gowland (2014) used this cell seeding density in agarose gel rather than simple 2D culture on the base of a 48 well plate. When comparing the two seeding densities (1 x 10^5 cell.ml^{-1} and 2 x 10^5 cells.ml^{-1}) in simple 2D culture, there appeared to be a decrease in viability experienced by cells seeded at 2 x10^5 cells.ml^{-1} on day 1 which was not experienced by cells seeded at 1 x 10^5 cells.ml^{-1} on day 1. As cells were to be used within 24 hours, this seeding density was not carried forwards. When RAW 264.7 murine macrophages were initially cultured in agarose gels, it was observed, using light microscopy, that the majority of cells were not penetrating the gel and were instead clumping together on the surface of the gel. The viability assay was therefore repeated with the addition of a rinse step after 12 hours to remove any cells that had failed to penetrate the gel. However the addition of this step resulted in significantly

lower cells numbers; too low for future studies so this step was discontinued. No images were obtained of each cell type in each gel type which would, in hindsight, have provided useful evidence whether the cells and particles in each type of gel had been able to penetrate the gel or not and, where penetration of the gel had occurred, how the cells and particles were distributed throughout the gel. For example, imaging the cells in the gels would have clearly shown the RAW 264.7 murine macrophages failing to penetrate the agarose gel and added evidence to the claims of this study.

Once the viability of each cell type in each gel type had been established, the ability of each cell type to produce TNF-α in response to model particles, Ceridust® and FluoSpheres® in each gel environment was assessed using ELISA. The inflammatory response to model polyethylene particles of each combination tested is summarised in Table 3.1. TNF-α was chosen as the pro-inflammatory/osteolytic cytokine to assess as it has several roles in the inflammatory cascade and osteolysis. Moreover, it is one of the first cytokines to be released upon initial contact with a foreign material in the innate immune response (Janeway *et al.*, 2001). It was decided not to use UHMWPE wear debris generated artificially using a wear simulator rig as the yield of particles can often be low and these particles were reserved for later inflammatory studies. Instead, it was decided to use model polyethylene particles, Ceridust®, as these had successfully been used previously to demonstrate the inflammatory and osteolytic response to polyethylene particles in both PBMNC's (Matthews *et al.*, 2000a; Matthews *et al.*, 2001; Liu, 2012) and murine peritoneal macrophages (Green *et al.*, 1998). FluoSpheres® were also included as a particle control as these had also been proven to induce an inflammatory response in PBMNC's (Liu, 2012; Gowland, 2014). LPS was included as a positive control as it is known to induce an extreme inflammatory response (Liu, 2012; Gowland, 2014). Cells were seeded in a 200 µl gel plug in a 48 well tissue culture plate rather than a 96 well tissue culture plate. Although, a 96 well tissue culture plate would be more economical in terms of the cell numbers and particle volumes required, the 1 ml of supernatant in a 48 well tissue culture plate would allow multiple ELISA's to be performed from the supernatant of one experiment compared to 200 µl in 96 well plates. This would also preserve time and remove the need to set up multiple experiments to achieve the same results in 96 well plates. Finally, it was also decided to report the cytokine data as pg.100 μl^{-1} rather than specific activity as this is consistent with previous studies by Liu (2012) and Gowland (2014) thus allowing a direct comparison between the data obtained in this study and the data obtained in the studies by Liu (2012) and Gowland (2014).

The overall findings of this study were not consistent with previous studies conducted by Green *et al.* (1998) and Matthews *et al.* (2000a, 2001) which found that non-cross-linked polyethylene particles (artificially generated GUR 1120 UHMWPE wear debris

and commercially available Ceridust®) between 0.1 and 10 μm generated a significant inflammatory cytokine response in comparison to particles greater than 10 μm in both PBMNC's (Matthews *et al.*, 2000b), U937 human histiocytes (Matthews *et al.*, 2001) and murine peritoneal macrophages (Green *et al.*, 1998). This study only found an inflammatory response to Ceridust® particles greater than 10 μm. It is not immediately clear why this was the case. This result was unexpected and the experiment was repeated for the cell type and gel type chosen to proceed with (RAW 264.7 murine macrophages and collagen gel) in order to confirm repeatability. As the 3D cell culture is very different to 2D cell culture, it is possible that this reproducible effect is valid rather than an error. It is hypothesised that the particles in the critical size range were trapped in the >10 μm particle fraction, as this did thickly coat the filter paper, and failed to fully pass through the filter paper membrane upon rinsing with ultrapure water however, since size distribution data was not obtained, it is not possible to verify this hypothesis. Unfortunately, neither size distribution data nor images were obtained of the Ceridust® particles obtained. Upon reflection, this was an oversight as it would have provided useful data as to the true size range of each Ceridust® particle fraction tested which may have accounted for the unexpected results. Similarly, the repeatability of this effect in other cell and gel combinations (PBMNC's and agarose gel, RAW 264.7 murine macrophages and agarose gel and non-transformed U937 human histiocytes and collagen gel) ought to have been confirmed in order to validate the legitimacy of this effect in 3D culture. In most cases, all cell and gel combinations, except PBMNC's in agarose, produced a significant TNF-α response to 0.2 μm FluoSpheres® in comparison to the cells only control. This was consistent with previous studies by Liu (2012) and Gowland (2014). It should be noted that the levels of TNF-α produced by the various cells types in response to >10 μm Ceridust® and 0.2 μm FluoSpheres®, although statistically significant, were very low (only slightly higher than the cells only control) (Table 3.1). It is therefore difficult to assess the biological significance of these responses. The low levels of TNF-α produced in response to polyethylene wear debris is however consistent with previous studies by Liu (2012) and Gowland (2014); both of whom found it difficult to produce a significantly higher levels of TNF-α in PBMNC's. For example, Liu (2012) produced values <100 $pg.ml^{-1}$ from PBMNC's treated with 100 μm^3 0.2 μm FluoSpheres® and this study produced responses ranging from 20 to 120 $pg.100\ \mu l^{-1}$. Similarly, Gowland (2014) treated PBMNC's with 100 μm^3 GUR 1050 XL UHMWPE and GUR 1050 XL VE and produced TNF-α levels ranging between 3 and 19 $pg.ml^{-1}$ (GUR 1050 XL) and 1 and 9 $pg.ml^{-1}$; none of which were significantly increased compared to the cells only control. All cell types in all gel types were able to produce significantly elevated levels of TNF-α in response to the LPS positive control. This was consistent with previous studies by Liu (2012) and Gowland (2014). In this study, both RAW 264.7 murine

macrophages and PBMNC's produced between 400 and 500 pg.100 μl^{-1} of TNF-α in response to the LPS positive control. Although U937 human histiocytes did produce an increased TNF-α response, they failed to produce a significantly higher response consistent with previous studies so their use was discontinued. Gowland (2014) achieved TNF-α levels of around 1400 $pg.ml^{-1}$ in response to the LPS positive control. In order to remove to issue of donor heterogeneity, the use of PBMNCs was discontinued. In order to create a 3D model, i.e. one allowing simultaneous encapsulation of cells and particles to ensure adequate cell-particle contact and allow for cell attachment to the gel, collagen gel was chosen to replace agarose gel as the encapsulation medium. Finally, as subsequent study examined the effect of antioxidants on inflammatory pathways such as the PKC pathway, RAW 264.7 murine macrophages were chosen rather than U937 human histiocytes as PMA, used to transform U937 human histiocytes, is an inhibitor of PKC. PMA is necessary to stimulate the differentiation of U937 human histiocytes into activated macrophages; without this stimulation, non-transformed U937 human histiocytes may not be an appropriate alternative to PBMNCs as their reactivity may be different to transformed U937 human macrophages. RAW 264.7 murine macrophages, however, do not require this chemical activation step. Overall, the combination of RAW 264.7 murine macrophages in collagen gels was chosen as the novel model and carried forward to subsequent chapters.

Trialling an alternative inverted 2D culture with RAW 264.7 murine macrophages and U937 human histiocytes with model polyethylene particles

An alternative inverted 2D culture method was developed at the University of Leeds by PDRA, Dr Saurabh Lal. PBMNC's were seeded on the base of a 96 well tissue culture plate and UHMWPE wear debris was suspended in cell culture medium. The tissue culture plate was then inverted and the cells were then in contact with the model polyethylene particles at the cell culture medium interface. The cell culture medium was held in place by surface tension. As part of this study, the candidate trialled the use of RAW 264.7 murine macrophages and U937 human histiocytes in this novel inverted 2D culture model. RAW 264.7 murine macrophages failed to respond to any of the conditions, including the LPS positive control. The U937 human histiocytes produced significantly increased levels of TNF-α when treated with 0.2 μm FluoSpheres® and LPS in comparison to the cells only control. The inherent limitation and weakness of this novel method is that the plate itself is inverted and, if the plate is disturbed, the surface tension of the cell culture medium is destroyed and the cells will no longer be in contact with the particles or the medium. This may have been the case for RAW 264.7 murine macrophages. In comparison, the inverted cover slip method,

as carried out by Matthews *et al.* (2000a), is more robust as it is not sensitive to loss of surface tension and may be preferable to use for initial 2D culture studies.

Table 3.1 Table of different cell and gel combinations treated with varying sizes of Ceridust® model polyethylene particles (>10 µm, 1 – 10 µm and 0.1 – 1 µm), 0.2 µm FluoSpheres® and LPS to assess TNF-α release using ELISA. ✔ indicates a significant release of TNF-α and ✖ indicates no significant release of TNF-α in comparison to the cells only negative control.

Cell and gel combination tested	**Particle treatment**				
	>10 µm Ceridust®	**1 – 10 µm Ceridust®**	**0.1 – 1 µm Ceridust®**	**0.2 µm FluoSpheres®**	**LPS (200 ng.ml^{-1})**
PBMNCs in agarose	✔ <50 pg	✖	✖	✔ <50 pg	✔ 550 pg
PBMNCs in collagen	✖	✖	✖	✖	✔ 330 pg
RAW cells in agarose	✔ <50 pg	✖	✖	✔ <50 pg	✔ 230 pg
RAW cells in collagen	✔ <50 pg	✖	✖	✖	✔ 450 pg
Transformed U937 cells in agarose	✖	✖	✖	✔ 120 pg	✔ <50 pg
Transformed U937 cells in collagen	✖	✖	✖	✔ 20 pg	✔ <50 pg
Non-transformed U937 cells in collagen	✔ 20 pg	✖	✖	✔ 25 pg	✔ 20 pg

3.7 Conclusions

- This study showed that agarose and collagen gels do not cause any adverse effects on the viability of PBMNC's, U937 human histiocytes and RAW 264.7 murine macrophages.

- The combination of RAW 264.7 murine macrophages in collagen gel was chosen to proceed forwards with for further studies. RAW 264.7 murine macrophages were capable of responding to Ceridust® and FluoSphere® particles, do not require a donor or demonstrate donor heterogeneity and do not require chemical transformation. Collagen gel also simultaneously encapsulates cells and particles, allowing for a 3D model rather than a 2D model, in addition to providing cell attachment sites.

Chapter 4
Generation, isolation and characterisation of antioxidant doped, highly cross-linked ultra-high molecular weight polyethylene wear debris

4.1 Introduction

Multidirectional reciprocating pin-on-plate (POP) wear simulator rigs have been successfully used to produce clinically relevant UHMWPE wear particles that resemble those found *in vivo* (Lancaster *et al.*, 1997; Endo *et al.*, 2001; Ingram *et al.*, 2004; Galvin *et al.*, 2006; Affatato *et al.*, 2008). In a multidirectional reciprocating POP wear simulator rig, the plate moves forwards and backwards whilst the pin rotates; this combination simulates the movement of the femoral head in the acetabulum of the hip joint. Both single and six station multidirectional reciprocal POP wear simulators are used at the University of Leeds. Galvin *et al.* (2006) produced clinically relevant cross-linked and non-cross-linked UHMWPE wear debris using a six station multidirectional POP wear simulator rig operated using kinematics known to reproduce similar conditions to the hip in normal gait. Liu (2012) went on to use a six station multidirectional POP wear simulator rig to produce sterile nanometre sized UHMWPE wear debris. Ingram *et al.* (2004) used a single station multidirectional POP wear simulator aseptically to produce sterile, endotoxin-free UHMWPE wear debris. Multidirectional POP wear simulators may be used with rough (R_a 0.08 – 0.09 μm) or smooth (R_a 0.01 – 0.02 μm) CoCr plates. Smooth plates replicate the surface roughness of clinical implants *in vivo,* whereas rough plates are used to generate a large volume of wear debris for *in vitro* cell culture studies, as the wear factor is typically increased. The size distribution of particles produced differs between the types of plates: rough plates tend to produce larger particles (Endo *et al.*, 2001). Both types of plates produce UHMWPE wear debris of similar particle size ranges and morphologies observed in retrieval studies (Endo *et al.*, 2001; Ingram *et al.*, 2004). The morphology and size and volume distribution of the particles generated was assessed at the University of Leeds using KOH digestion method developed by Tipper *et al.* (2000, 2006) with both retrieved periprosthetic tissue (Tipper *et al.*, 2000) and simulator rig serum lubricants (Tipper *et al.,* 2006) to isolate the particles which were then imaged using FEGSEM.

The size and shapes of UHMWPE wear particles is important for *in vitro* studies in order to accurately assess the osteolytic cytokine production of representative cell types (usually macrophages) in response to UHMWPE wear debris. The size

distribution of wear particles is important for assessing the biological response to wear debris. Green *et al.* (1998) found the size range of polyethylene particles necessary to produce a biological response to be between 0.3 and 10 μm. Moreover, Ingham *et al.* (2000) found that polyethylene particles between 0.2 and 0.8 μm activated macrophages. The size of UHMWPE wear debris dictates how the body responds to it. Larger particles (>10 μm) are unable to be phagocytosed and are walled off by foreign body giant cells and granulomatous tissue. Local macrophages uptake UHMWPE particles less than 10 μm are uptaken and the macrophages attempt to phagocytose them. However, as polyethylene is chemically inert, phagocytosis is not possible and the macrophages become frustrated; releasing further pro-inflammatory cytokines and recruiting more macrophages to the periprosthetic tissue. The pro-inflammatory cytokines (such as TNF-α, IL-1β and IL-6) stimulate osteoclastogenesis and an increase in osteoclastic activity. Osteoclasts begin to resorb bone surround the THR and, over time, the fixation of the implant is loosened. This results in pain and, ultimately, revision surgery. It is therefore important to have representative UHMWPE wear debris in order to accurately reproduce this effect *in vitro*.

UHMWPE has been modified from the original virgin material to reduce the volume of wear debris produced and therefore the incidence of osteolysis. Cross-linked UHMWPE produces lower volumes of wear debris and exhibits lower wear factors than virgin (non-cross-linked) UHMWPE (Endo *et al.*, 2001; Ingram *et al.*, 2004). Antioxidant (vitamin E) doped, highly cross-linked UHMWPE does not exhibit a significantly different wear factor or a significantly different distribution of particle sizes in comparison to highly cross-linked UHMWPE (Gowland, 2014). The addition of antioxidants, such as vitamin E, does however quench free radicals and prevents the reduction in mechanical properties associated with oxidative embrittlement (Wannomae *et al.*, 2006).

The aim of this study was to produce UHMWPE wear debris from GUR 1020 XL, GUR 1020 XL AOX, GUR 1050 XL, GUR 1050 XL VE using both the six and single station multidirectional wear simulators. The single station multidirectional POP wear simulator was used to generate the full range (nm to mm) of sterile UHMWPE wear debris that would be produced *in vivo,* whereas the six station multidirectional POP wear simulator was used to generate a greater volume of UHMWPE wear debris that was then filtered in to the critical size range specified by Matthews *et al.* (2001) as activating macrophages (0.1 to 1 μm) to produce osteolytic cytokines for later use in the novel *in vitro* model developed in Chapter 3. Rough (R_a 0.08 – 0.09 μm) ASTM 1537 low carbon CoCr plates were used to produce a larger volume of UHMWPE over a short time frame (compared to smooth plates). The samples for each material on each type of wear simulator rig were then pooled and isolated using the digestion

method developed by Tipper *et al.* (2000, 2006) and modified by Richards *et al.* (2008). The particles were then imaged using FEGSEM and the images were analysed using Image J to assess the size and volume distribution of wear debris generated from each material on each type of rig in order to compare to previous studies.

4.2 Aims and objectives

4.2.1 Aims

The overall aim of this chapter was to aseptically generate, isolate and characterise both highly cross-linked and antioxidant-doped, highly cross-linked UHMWPE wear debris using both the single and six station wear simulator rigs to culture with RAW 264.7 murine macrophages in collagen gels to assess inflammatory and oxidative cellular response.

4.2.2 Objectives

The objectives of this chapter were as follows:

- Generation of GUR 1020 XL, GUR 1020 XL AOX, GUR 1050 XL and GUR 1050 XL VE UHMWPE wear debris using single and six station pin on plate wear simulator rigs under hip kinematic conditions for later use in *in vitro* studies throughout the subsequent chapters.
- Microbiological and endotoxin testing of all wear debris samples obtained on each wear rig to confirm sterility in terms of whole organism and LPS contamination, which may have adversely affected later *in vitro* studies.
- Isolation of a sample of wear debris from each material on each type of rig using the digestion method as previously validated by Tipper *et al.* (2000, 2006) and Richards *et al.* (2008).
- To image and characterise a full, unfractionated sample of wear debris from each material on each type of rig using FEGSEM to image the particles at various magnifications and ImageJ to analyse the subsequent images and characterise them according to size and volume frequency distribution.

4.3 Materials

The materials used throughout Chapter 4 are detailed below.

4.3.1 Chemicals and reagents

The chemicals and reagents used throughout Chapter 4 are listed in Table 4.1. Any general chemicals and reagents used can be found in Chapter 2, Section 2.1.1.

Table 4.1 Chemicals and reagents used throughout Chapter 4.

Chemicals and reagents	Supplier	Storage and preparation
Bleach (<5% sodium hypochlorite)	Tesco, Cheshunt, UK.	Stored at room temperature (25°C).
Carbon paste	Agar Scientific, Stanstead, Essex, UK.	Stored at room temperature (25°C).
Chloroform	VWR International Ltd, Poole, UK.	Stored at room temperature (25°C).
Ethanol absolute	Fisher Scientific UK, Loughborough, UK.	Stored at room temperature (25°C).
Heated blood agar (HBA) plates	Fisher Scientific UK, Loughborough, UK.	Stored at 4°C.
Isopropanol (70% (v/v))	Acros Organics, Geel, Belgium.	Prepared by adding 100% (v/v) isopropanol to distilled water (7:3) and stored at room temperature (25°C).
LAL chromogenic endotoxin quantitation kit	ThermoFisher Scientific, Hemel Hempstead, UK.	Stored at 4°C.
Methanol	Atom Scientific Ltd, Hyde, UK.	Stored at room temperature (25°C).
Nutrient agar (NA) plates	Fisher Scientific UK, Loughborough, UK.	Stored at 4°C.
Nutrient broth powder	Oxoid Limited, Basingstoke, Hampshire, UK.	Stored at room temperature (25°C).
Potassium hydroxide pellets	Fluka Analytical, Buchs, Switzerland.	Stored at room temperature (25°C).

Sabouraud dextrose agar (SAB) plates	Fisher Scientific UK, Loughborough, UK.	Stored at 4°C.
Trigene (1% (v/v))	Scientific Laboratory Supplies Ltd, Nottingham, UK.	Stored at room temperature (25°C) and a 1% solution is prepared by adding 100% Trigene (v/v) to distilled water.
Vaseline (petroleum jelly) – anti-fretting lubricant	Unilever, Leatherhead, UK.	Stored at room temperature (25°C).

4.3.2 Consumables

The consumables used throughout Chapter 4 are listed in Table 4.2. Any general consumables used can be found in Chapter 2, Section 2.1.2.

Table 4.2 Consumables used throughout Chapter 4.

Materials and consumables	Supplier
Disposable aprons	PAL International, Lutterworth, UK.
Endotoxin free 1.5 ml microcentrifuge tubes	Starlab, Milton Keynes, UK.
Endotoxin free 96 well plates	Associates of Cape Cod, Massachusetts, USA.
Endotoxin free pipette tips	Starlab, Milton Keynes, UK.
Face masks	Alpha Solway Ltd, Annan, UK.
Foil packets	Westfield Medical Ltd, Radstock, UK.
Glass Pasteur pipettes	Glassware Stores, School of Molecular and Cellular Biology, University of Leeds.
Glass serological pipettes (10ml and	MBL, UK.

25ml)	
Oversleeves	PAL International, Lutterworth, UK.
Short aluminium stubs	Electron Optics, School of Chemical and Process Engineering, University of Leeds.
Sterile latex surgical gloves	Bioclean™, Newmarket, UK.
Tupperware box	Tesco, Cheshunt, UK.

4.3.3 Equipment

The equipment used throughout Chapter 4 are listed in Table 4.3. Any general equipment used can be found in Chapter 2, Section 2.1.3.

Table 4.3 Equipment used throughout Chapter 4.

Equipment and model (where relevant)	Manufacturer
Balance – XP26	Mettler Toledo, Ohio, USA.
Bunsen burner	Fisher Scientific UK, Loughborough, UK.
Calibration load cell - 444N	RDP Electronics
Carbon coater – Quorum Q150T E	Quorum, Lewes, UK.
Centrifuge – Mistral 3000E	Sanyo, Watford, UK.
Compressed air dispenser	Manufactured in house, School of Mechanical Engineering, University of Leeds.
Field emission gun scanning electron microscope – Hitachi SU8230 Cold-FEGSEM	Hitachi, Maidenhead, UK.
Heat sealer	Hulme Martin Heat Sealers Ltd, Woking, UK.
Heating block	Eppendorf, Stevenage, UK.
High speed Sorvall Evolution RC	Thermo Scientific, Hemel

centrifuge and SLA-1500 rotor	Hempstead, UK.
Ignitor	Fisher Scientific UK, Loughborough, UK.
Infrared lamp	Phillips, Guildford, UK.
Plastic tweezers	Mettler Toledo, Ohio, USA.
Platinum inoculation loop and holder	Fisher Scientific UK, Loughborough, UK.
Single station pin on plate wear simulator 1	Manufactured in house, School of Mechanical Engineering, University of Leeds.
Single station pin on plate wear simulator 2	Manufactured in house, School of Mechanical Engineering, University of Leeds.
Six station pin on plate wear simulator B	Manufactured in house, School of Mechanical Engineering, University of Leeds.
Sonicator – RS Pro	RS Components, Leeds, UK.
Sorvall 250ml dry spin centrifuge bottles and sealing lids	Thermo Scientific, Hemel Hempstead, UK.
Stirrer bar	Fisher Scientific UK, Loughborough, UK.
Stirrer plate	Stuart, Stone, UK.
Stub storage and transport box	Electron Optics, School of Chemical and Process Engineering, University of Leeds.
Syringe driver	Manufactured in house, School of Mechanical Engineering, University of Leeds.
Timer	Scientific Laboratory Supplies, Nottingham, UK

4.3.4 Pins and plates

The UHMWPE pin and cobalt chromium (CoCr) plate materials used throughout Chapter 4 are listed in Table 4.4.

Table 4.4 Pins and plates used throughout Chapter 4.

Pins and plates	Supplier
GUR 1050 vitamin E (1000ppm) highly cross-linked (10 MRad) UHMWPE pins	Bar stock supplied by Meditech medical polymers (Pennsylvania, USA). Machined in house, School of Mechanical Engineering, University of Leeds.
GUR 1050 highly cross-linked (9.39 MRad) UHMWPE pins	Bar stock supplied by DePuy Synthes Joint Reconstruction (Leeds, UK; Warsaw, USA). Machined in house, School of Mechanical Engineering, University of Leeds. Pins sent for gamma irradiation treatment by Synergy Health PLC at a dose range of 9 – 11.5 MRad with an actual dose of 9.39 MRad.
GUR 1020 AOX (hindered phenol - 700 ppm) highly cross-linked (8 MRad) UHMWPE pins	Bar stock supplied by DePuy Synthes Joint Reconstruction (Leeds, UK; Warsaw, USA). Machined in house, School of Mechanical Engineering, University of Leeds.
GUR 1020 highly cross-linked (9.39 MRad) UHMWPE pins	Bar stock supplied by DePuy Synthes Joint Reconstruction (Leeds, UK; Warsaw, USA). Machined in house, School of Mechanical Engineering, University of Leeds. Pins sent for gamma irradiation treatment by Synergy Health PLC at a dose range of 9 – 11.5 MRad with an actual dose of 9.39 MRad.
Rough (Ra 0.08 – 0.09 μm) ASTM 1537 low carbon CoCr plates	Raw material supplied by DePuy Synthes Joint Reconstruction (Leeds, UK; Warsaw, USA). Manufactured in

	house, School of Mechanical Engineering, University of Leeds.

4.3.5 Software

The software used throughout Chapter 4 is detailed in Table 4.5.

Table 4.5 Software used throughout Chapter 4.

Software	***Supplier***
Image J	Fiji – open source

4.4 Methods

The methods used throughout this study to generate, isolate and characterise wear debris from highly cross-linked UHMWPE pins with and without antioxidant doping are detailed in the following sections.

4.4.1 Preparation of pins and plates for wear testing

4.4.1.1 UHMWPE pin preparation

4.4.1.1.1 Manufacture of UHMWPE pins

The cylindrical UHMWPE pins were machined to be 12mm in diameter with a contact face of 10mm (Figure 4.1).

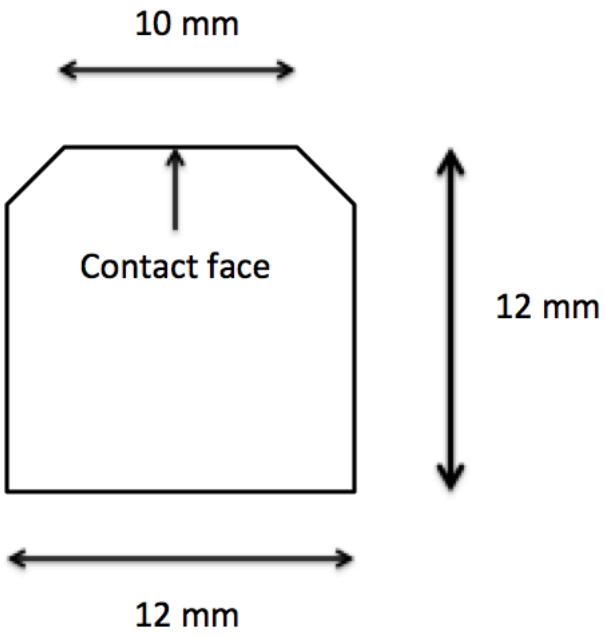

Figure 4.1 UHMWPE cylindrical pin dimensions.

4.4.1.1.2 UHMWPE pin characteristics

The details of the UHMWPE pins used throughout this study are listed in Table 4.6.

Table 4.6 UHMWPE materials used throughout this study; including details of resin, irradiation dose, antioxidant dose and supplier.

Name	Resin	Gamma irradiation dose	Antioxidant	Supplier	Abbreviation
GUR 1050 highly cross-linked UHMWPE	GUR 1050	9.39 MRad	No	DePuy Synthes	GUR 1050 XL
GUR 1050 highly cross-linked vitamin E UHMWPE	GUR 1050	10 MRad	Vitamin E 1000 ppm	Meditech Polymers	GUR 1050 XL VE
GUR 1020 highly cross-linked UHMWPE	GUR 1020	9.39 MRad	No	DePuy Synthes	GUR 1020 XL
GUR 1020 highly cross-linked AOX UHMWPE	GUR 1020	8 MRad	Hindered phenol 700 ppm	DePuy Synthes	GUR 1020 XL AOX

4.4.1.1.3 Cleaning of UHMWPE pins for use in wear rig simulators

All UHMWPE pins were cleaned by scrubbing with a toothbrush and household detergent with warm water. The pins were then transferred to sterile glass universals

containing bleach (>5% sodium hypochlorite) and placed on an orbital shaker at 180 rpm for 20 minutes. Following this, in the presence of a Bunsen burner flame to maintain sterility, the pins were transferred to nutrient broth. The pins in nutrient broth were then incubated at 37ºC for 48 hours in order to confirm sterility. Once the pins were confirmed as sterile, the pins were either transferred to ethanol (70% (v/v)) if their use was imminent or to sterile ultrapure water for longer-term storage as carried out by Gowland (2014).

4.4.1.2 Manufacture of rough cobalt chromium plates

The low carbon CoCr alloy plates were prepared with a surface roughness of (0.08 – 0.09 µm) (Figure 4.2).

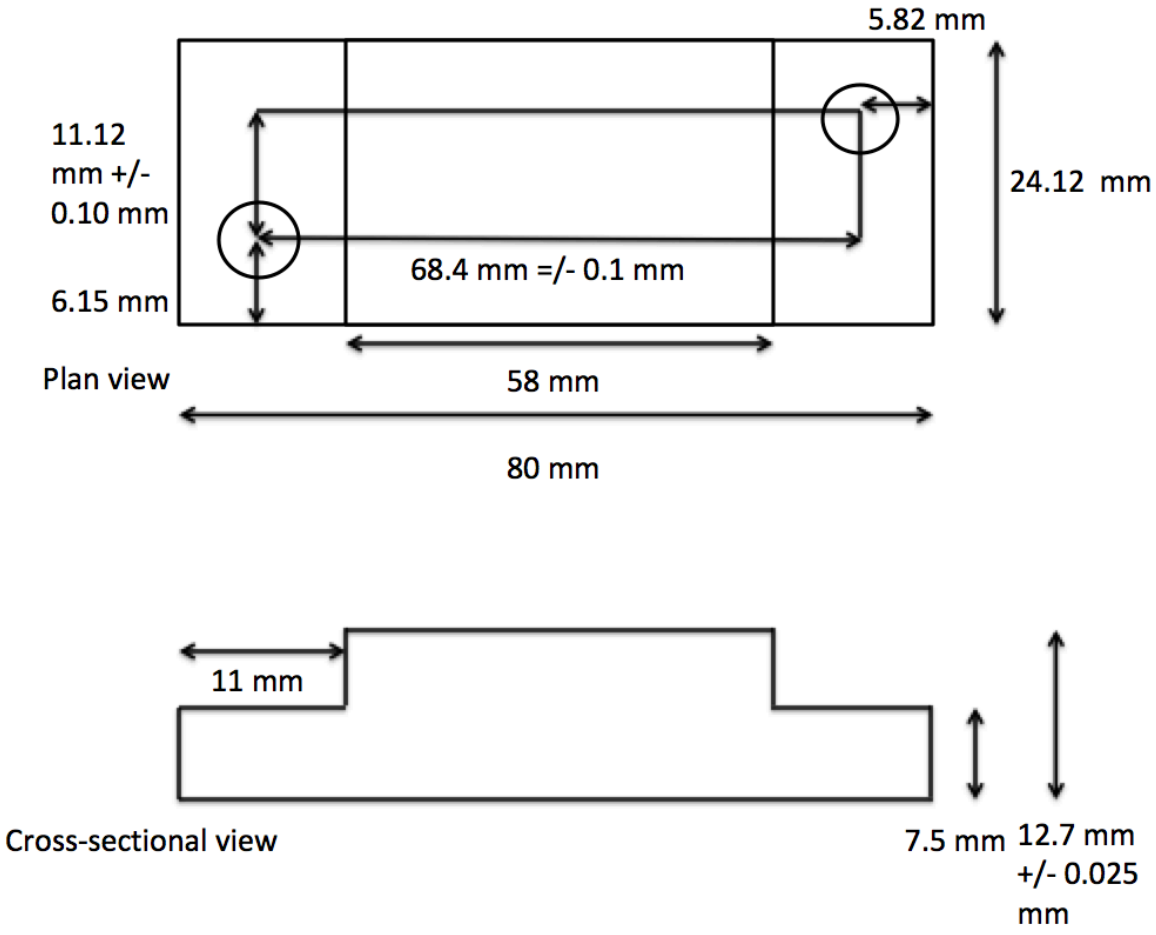

Figure 4.2 Schematic diagram of rough (R_a 0.08 – 0.09µm) low carbon (ASTM 1537) cobalt chromium plate.

4.4.2 Determination of mass of UHMWPE pins

In order to calculate the volume of wear debris generated, the UHMWPE pins were weighed before and after each test in the wear simulator. The pins were incubated in

the measurements lab for 48 hours prior to weighing in order to acclimatise to a constant temperature, pressure and humidity. The pins were then weighed at least five times to generate five measurements that were within 10 µg of each other. It was first necessary to take into account any increase in mass caused by the UHMWPE pin absorbing the lubricant. In order to do this, the additional mass was calculated using the soak control pin as follows:

$$\boldsymbol{Increase\ in\ mass\ due\ to\ soak} = \boldsymbol{weight\ of\ soak\ control\ pin\ after\ run} - \boldsymbol{weight\ of\ soak\ control\ pin\ before\ run}$$

The amount of wear debris created (i.e. the mass lost) was then calculated as follows (allowing for the soak control correction):

$$\boldsymbol{Mass\ of\ wear\ debris} = (\boldsymbol{weight\ of\ pin\ before\ run} + \boldsymbol{increase\ in\ mass\ due\ to\ soak}) - \boldsymbol{weight\ of\ pin\ after\ run}$$

The mass lost by the pin (or mass of wear debris) was used to calculate the volume generated as follows:

$$\boldsymbol{Volume\ of\ wear\ generated}\ (\boldsymbol{mm^3}) = \frac{\boldsymbol{weight\ loss\ of\ UHMWPE\ pin}}{\boldsymbol{density}\ (\boldsymbol{g.mm^3})}$$

Then the sliding distance was calculated as follows:

$$\boldsymbol{Sliding\ distance}\ (\boldsymbol{m}) = \boldsymbol{operation\ time}\ (\boldsymbol{hours})\ \boldsymbol{x\ distance\ travelled\ by\ pin\ in\ one\ cycle}\ (\boldsymbol{2\ x\ 0.028m})\ \boldsymbol{x\ frequency}\ (\boldsymbol{1\ Hz})\ \boldsymbol{x\ 60}$$

Both the volume lost and the sliding distance were then used to calculate the wear factor for each material in each test as follows:

$$\boldsymbol{Wear\ factor}\ (\boldsymbol{mm^3.Nm^{-1}}) = \frac{\boldsymbol{Wear\ volume}\ (\boldsymbol{mm^3})}{\boldsymbol{sliding\ distance}\ (\boldsymbol{m})\boldsymbol{x\ load}\ (\boldsymbol{N})}$$

4.4.3 Generation of highly cross-linked and antioxidant doped, highly cross-linked ultra-high molecular weight polyethylene wear debris

In order to measure any response of relevant cells to wear debris that is generated by THR's, it was first necessary to generate wear debris with which to dose cells for further study. Previous studies (Galvin *et al.*, 2006) examined the size and volume distribution and morphology of UHMWPE particles produced and showed that clinically relevant wear debris can be generated using both single and six station pin on plate wear simulators. The single station multidirectional reciprocating POP wear simulator rig was operated under aseptic conditions at the kinematic conditions specified in Table 4.7 as the wear particles generated were to be used in future cell

studies and must therefore be free of any biological contaminants which may affect any results later obtained.

Table 4.7 Kinematic conditions, to replicate hip conditions during normal gait, under which the single station wear simulator was run to create UHMWPE wear debris for cell culture studies.

Wear simulator condition	Hip kinematics value
Stroke length	28 mm
Rotation	+/-30°
Load	160 N
Frequency	1 Hz

4.4.2.1 Generation of highly cross-linked and antioxidant doped, highly cross-linked ultra-high molecular weight polyethylene wear debris using single station pin-on-plate multidirectional wear simulator rigs

The methods used to set up, maintain and disassemble both single station wear simulator rigs used (labelled 1 and 2 in this study) are detailed in the following sections.

4.4.2.1.1 Preparation of single station pin-on-plate wear simulator components

The single station wear simulator metal components (*Figures 4.3 and 4.5*) were prepared by scrubbing with a toothbrush in warm water and household detergent followed by sonicating in 70% (v/v) isopropanol for 20 minutes. The components were then rinsed with distilled water, dried and wrapped in foil before being placed into an oven at 190°C for 4 hours to sterilise the components and remove any endotoxin present. The vacuum tubing was by sterilised by autoclaving in a heat sealed packet.

4.4.2.1.2 Setting up the single station pin-on-plate multidirectional wear simulator rig

The methods used to set up each individual single station wear simulator rig (1 and 2) are detailed in the following sections.

4.4.2.1.2.1 Single station pin-on-plate multidirectional wear simulator rig 1

Prior to set up, stroke length and load were calibrated. Stroke length was measured with a ruler. Load was assessed by placing the load cell disc in the bridge (in place of the pin holder) and loading the cantilever arm with the 5.37 kg weight at a particular load (e.g. 160 N). The load was measured using the load cell to ensure accuracy between the load marked on the cantilever arm. The simulator, its components (*Figure*

4.3) and the class II laminar flow cabinet were all sterilised or cleaned before use. The simulator was assembled under sterile conditions using sterile gloves and sterile hex keys and components were held on sterile foil. The simulator was operated in a class II safety cabinet in order to maintain a sterile air flow and sterile environment. Prior to simulator assembly; the simulator (*Figure 4.4*) and the class II safety cabinet were cleaned with household detergent and warm water followed by 1% (v/v) Trigene and finally all components were sprayed with 70% (v/v) ethanol.

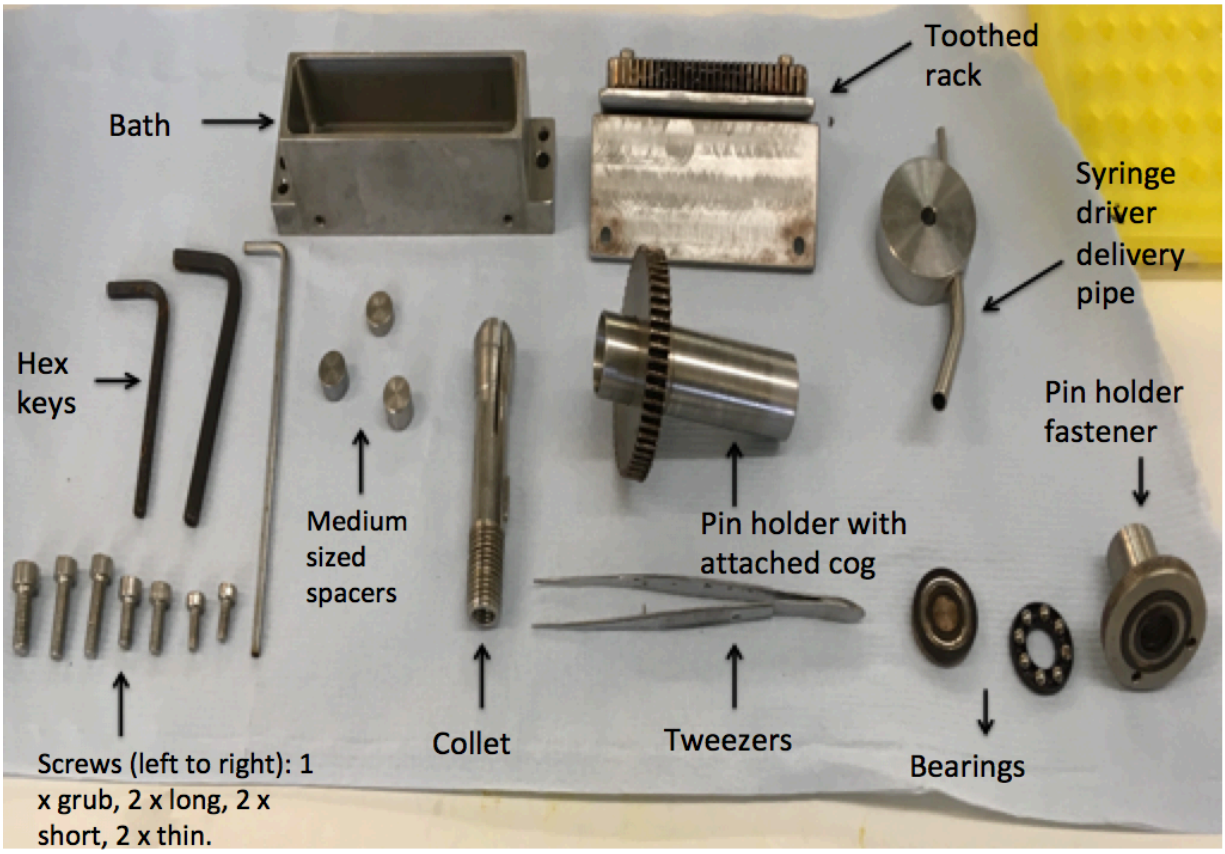

Figure 4.3 Components of single station multidirectional reciprocating POP wear simulator 1 and components used to assemble the rig: Hex keys x 3 (used to assemble the rig), bath, toothed rack, medium sized spacers x 3, Screws (1 x grub, 2 x long (used to fix bath to rig), 2 x short (used to fix plate to bath) and 2 x thin (used to fix rack to bath)), tweezers (used to assemble the rig), collet, pin holder fastener, pin holder with attached cog, syringe driver delivery pipe and bearings. This image does not include the bridge, which remains with the rig itself.

The simulator was then set up as follows: the plate was fixed to the bath using the two short screws and a hex key. The toothed rack was then fixed to the side of the bath using the two thin screws and a hex key. The bath was then fixed to the rig using the two long screws and a hex key. A metal spacer followed by the relevant UHMWPE pin (with the 10 mm contact face facing outwards) was placed into the collet using the

sterile tweezers. The collet was then placed into the cog in the correct alignment (ensuring the notch on the outside of the collet lined up with the notch on the inside of the pin holder) and tightened in place using the pin holder fastener. The pin was fixed into place in the pin holder ensuring that the pin was protruding at least 3-4 mm from the holder. The pin holder was inverted over a sterile surface to verify that the pin was securely in place before proceeding. The pin holder was placed into position in the bridge. A volume of 30 ml of previously prepared sterile RPMI 1640 cell culture medium containing 25% (v/v) FBS was placed into the bath using a sterile plastic syringe. The pin holder was lifted up slightly to allow the lubricant underneath the pin and then the bridge was secured in place. The bearings (lightly coated in anti-fretting lubricant) were placed into position atop the pin holder. Anti-fretting lubricant was also added to the toothed rack and cog attached to the pin holder. The cantilever arm was then lowered and the motor was switched on. A 5.37 kg weight was loaded at a set distance on the cantilever arm to provide a load of 160N and fixed in place. The stroke speed was adjusted to 7 on the motor – approximately 1 Hz (one complete cycle back and forth per second). The single station pin on plate wear simulator was operated under the kinematic conditions outlined in *Table 4.7*. A spare pre-weighed UHMWPE pin of the relevant material was placed into a sterile pot with 30ml RPMI 1640 cell culture medium with 25% FBS (v/v) to act as a soak control.

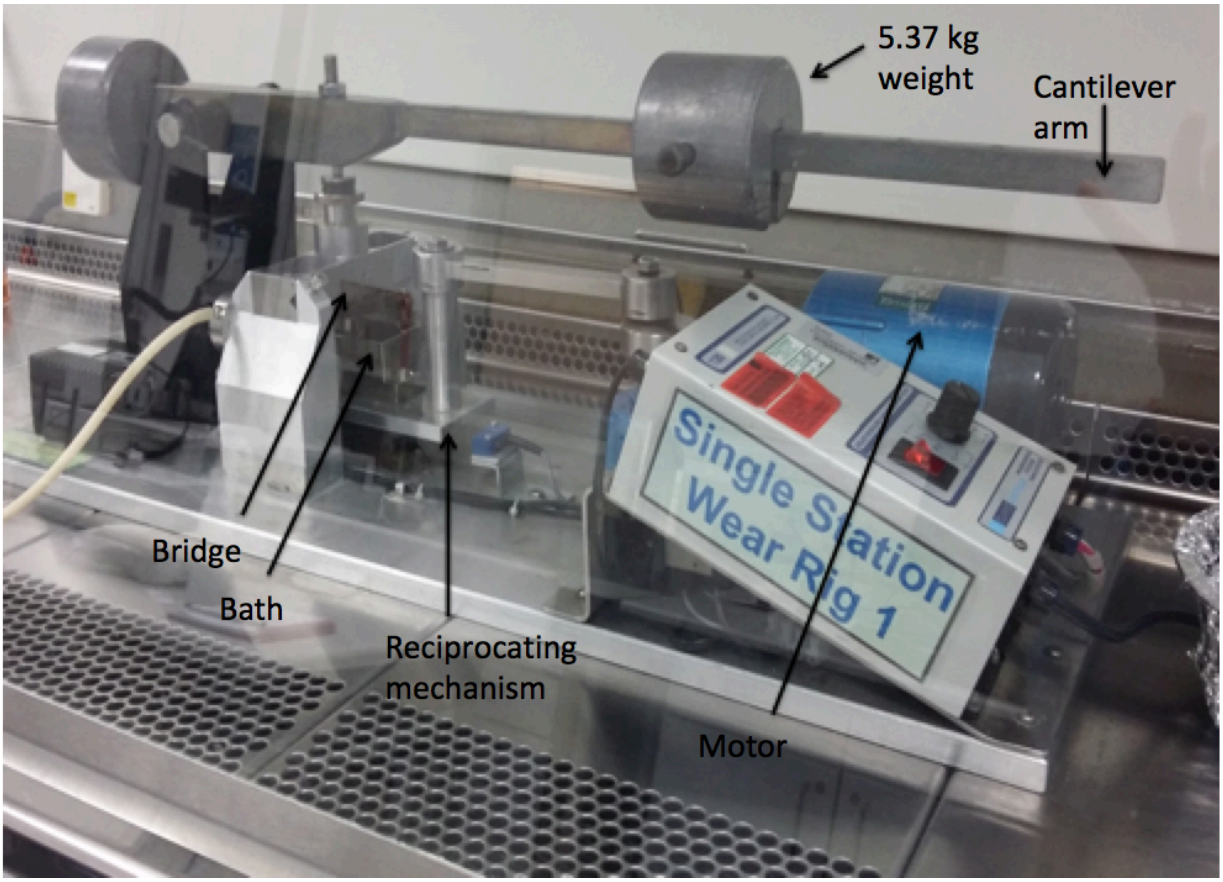

Figure 4.4 Single station multidirectional reciprocating POP wear simulator rig 1 -

complete set up (photo kindly taken and used with permission of Pirkko-Liisa Muhonen).

4.4.2.1.2.2 Single station pin-on-plate multidirectional wear simulator rig 2

The initial set up was identical to single station wear simulator rig 1. The components for single station wear simulator rig 2 are shown in Figure 4.5.

Single station wear simulator rig 2 was set up in the same manner as single station wear simulator rig 1 with some minor differences. The pin holder was assembled by placing the O-ring inside the pin holder followed by a metal spacer and the relevant UHMPWPE pin (with the 10 mm contact face facing outwards). The pin was fixed into place in the pin holder ensuring that the pin was protruding at least 3-4 mm from the holder and the pin holder screw was tightened using the smallest hex key. Anti-fretting lubricant was also placed on the rotating mechanism housing the pin holder.

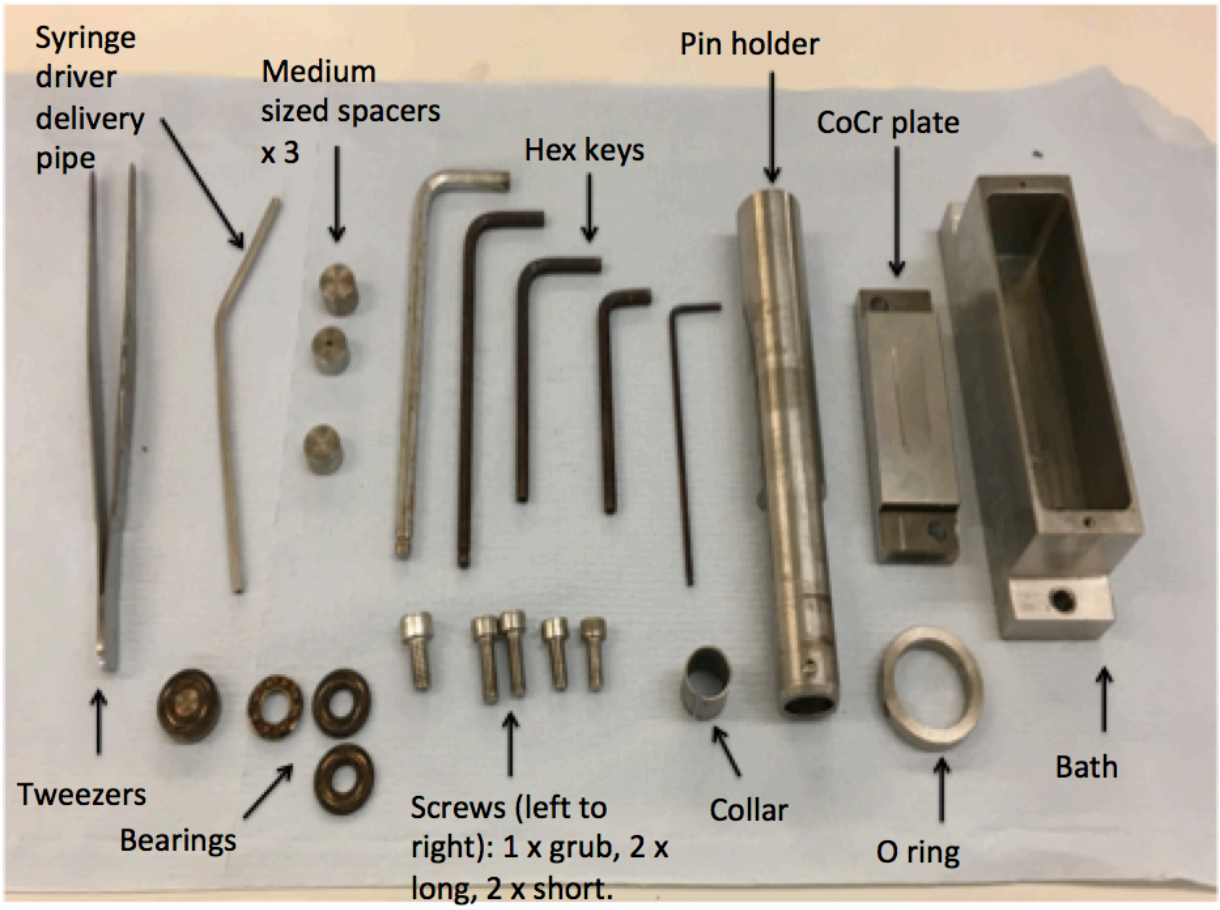

Figure 4.5 Components for single station multidirectional reciprocating POP wear simulator 2 and the components used to set up the wear rig: syringe driver delivery pipe, tweezers (used to set up the rig), bearings, medium sized spacers x 3, screws (left to right: 1 x grub, 2 x long (to fix bath to rig), 2 x short (to fix plate to bath)), hex keys, pin holder, collar, O ring and bath. Image also shows a CoCr plate. However the bridge holder is not shown as it is remains with the rig itself.

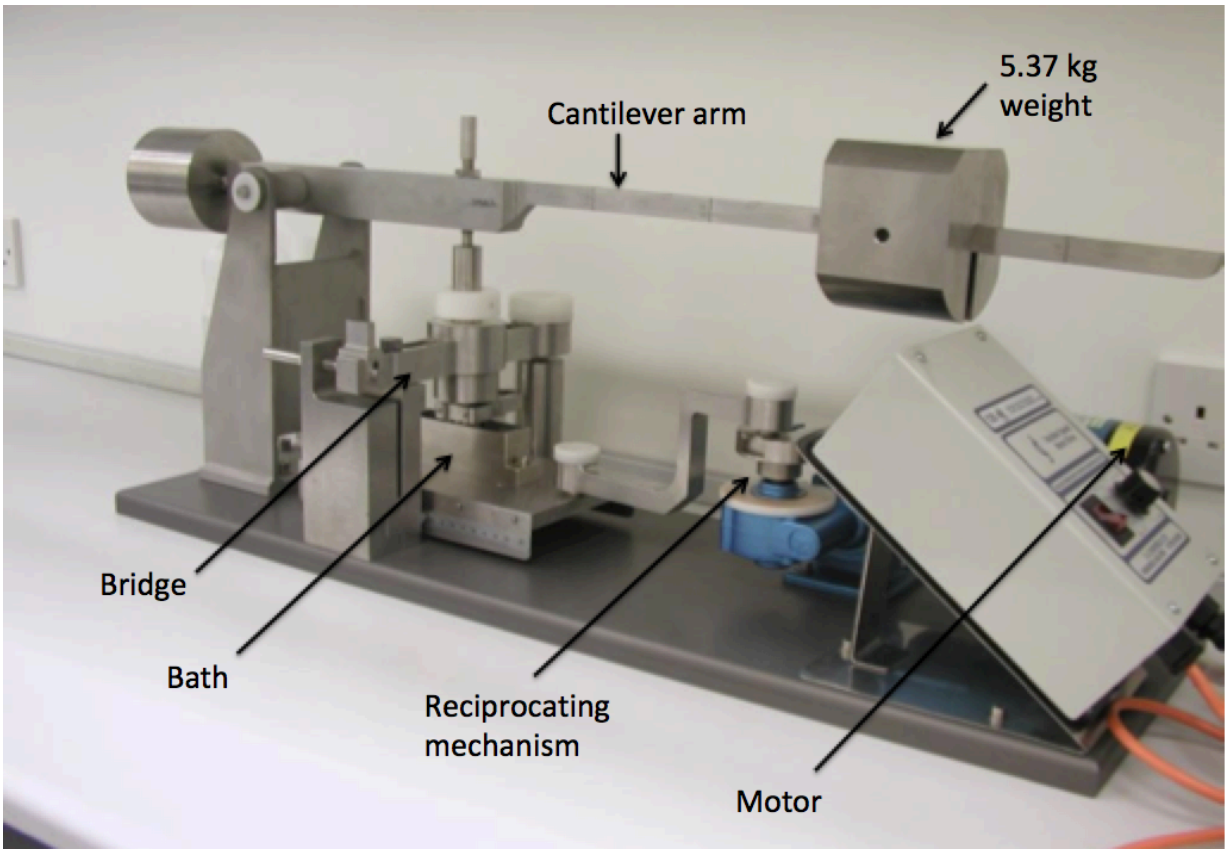

Figure 4.6 Single station multidirectional reciprocating POP wear simulator 2 – complete set up.

4.4.2.1.2.3 Setting up the syringe driver

The syringe driver is designed to deliver a constant supply of sterile water droplets to the bath via the delivery pipe to prevent total loss of lubricant through evaporation. The stainless steel delivery pipe was fixed to the rig using the grub screw. A 60 ml sterile plastic syringe was filled with water and attached to one end of the vacuum tubing whilst the other end of the vacuum tubing was attached to the stainless steel delivery pipe fixed to the rig. The syringe was fixed in place in the motorised syringe driver. The syringe was slowly depressed over time in order to replenish the bath and prevent evaporation of the lubricant. Finally, the speed of the syringe driver (the speed at which water is delivered to the lubricant bath) was set at 1 (the lowest speed).

4.4.2.1.3 Maintenance of the single station pin-on-plate multidirectional wear simulator rig

Each single station wear simulator rig was operated for up to five days in a sterile environment. The syringe driver was replenished every day with sterile ultrapure water and the motorised arm wound backwards such that the driver may have room to

depress the syringe plunger. The maintenance of sterility was verified throughout by daily microbiological testing.

4.4.2.1.4 Disassembling the single station pin-on-plate multidirectional wear simulator rig

After five days, the rig and syringe driver were switched off and disassembled. Sterility was maintained during disassembly until the lubricant and wear debris were contained within a sterile plastic container. Firstly, the lubricant was removed from the bath using a sterile plastic syringe and placed into a sterile plastic container along with 5 ml of ultrapure water that was used to rinse the remaining particles from the bath. The rig was washed with household detergent and warm water followed by 1% (v/v) Trigene and 70% (v/v) ethanol. The metal components of the simulator were washed with household detergent and warm water. The UHMWPE pins were cleaned with a paper tissue and placed into the metrology lab for 48 hours prior to weighing.

4.4.2.2 Generation of highly cross-linked and antioxidant doped, highly cross-linked ultra-high molecular weight polyethylene wear debris using six station pin-on-plate multidirectional wear simulator rig

The methods used to prepare, set up, maintain and disassemble the six station pin-on-plate wear simulator rig B under aseptic conditions are detailed in the following sections.

4.4.2.2.1 Preparation of six station pin-on-plate multidirectional wear simulator rig components

Prior to use, the stroke length and load were calibrated by a lab technician. Sterile gloves, oversleeves, a face mask and a disposable apron were worn throughout preparation and use of the six station wear simulator rig. All were sprayed with ethanol regularly and changed when necessary throughout. All rig components were immersed in warm water and household detergent for 15 minutes and then scrubbed individually with a toothbrush. The hex keys, plates, screws and ball bearings were sonicated for 10 minutes in 70% (v/v) isopropanol. All rig components (Figure 4.7) were then immersed in 1% (v/v) trigene for 30 minutes. The baths were assembled as follows: the plates were fixed onto the bath using the short screws and a hex key. The polymer baffles were then inserted into the baths and fixed in placed using the thin short screws. The stainless steel toothed rack were then fixed to the side of each bath using the thin, medium length screws and a hex key. The pin holders were assembled as follows: medium sized spacers followed by UHMWPE pins of the relevant material (with the 10 mm contact face facing outwards) were placed into the collet. The collet was then fitted into place in the pin holder – taking care to align the notches on the exterior of the collet and the interior of the pin holder. The pin holder was then fed

through the opening in the relevant numbered bridge and the pin fastener was screwed tightly in place to ensure the pin was securely held. The security of the pin was tested over a sterile surface. The assembled baths and bridges were then placed back into 1% (v/v) Trigene for a further 30 minutes. All components were then rinsed in deionised water and air-dried. The rig itself was cleaned using 1% (v/v) Trigene followed by 70% (v/v) ethanol.

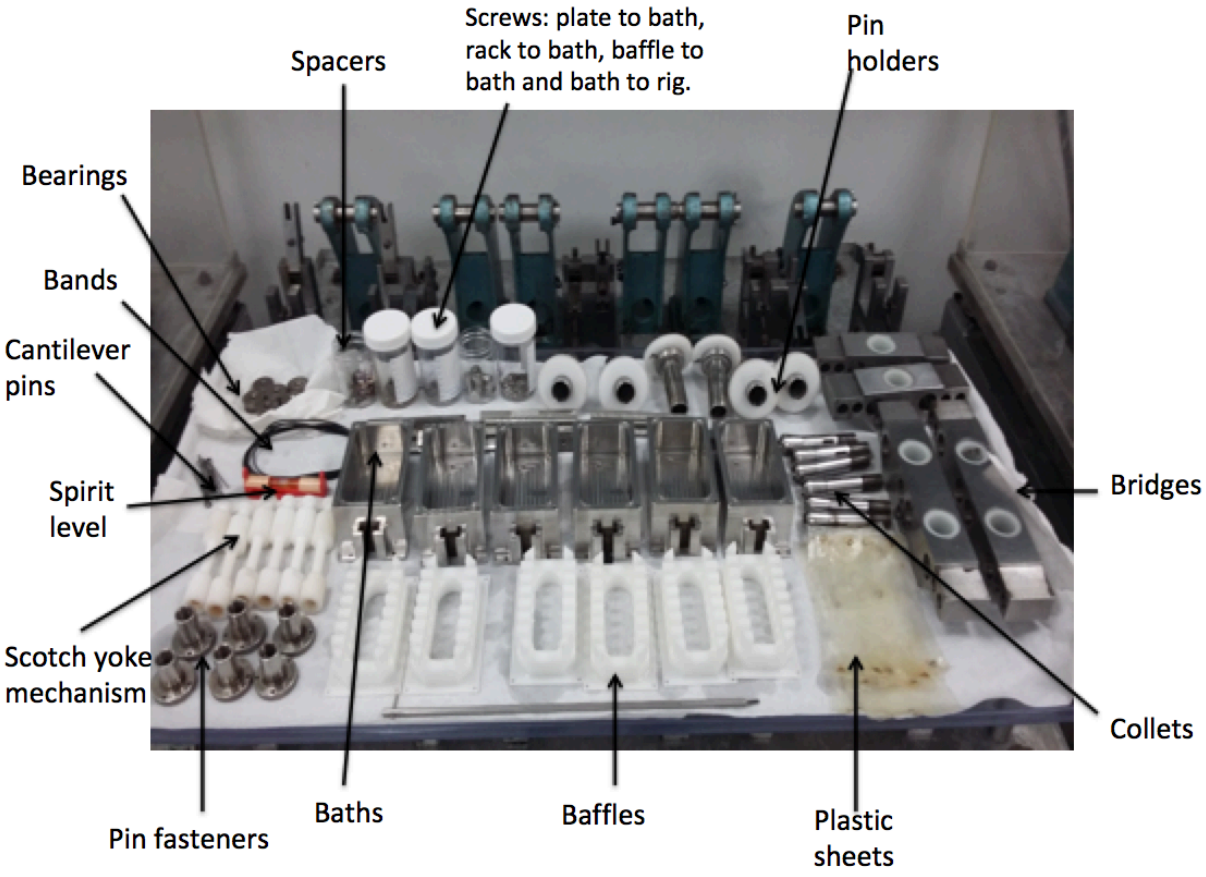

Figure 4.7 Components of six station multidirectional reciprocating POP wear simulator rig B (photo kindly taken and used with permission of Pirkko-Liisa Muhonen).

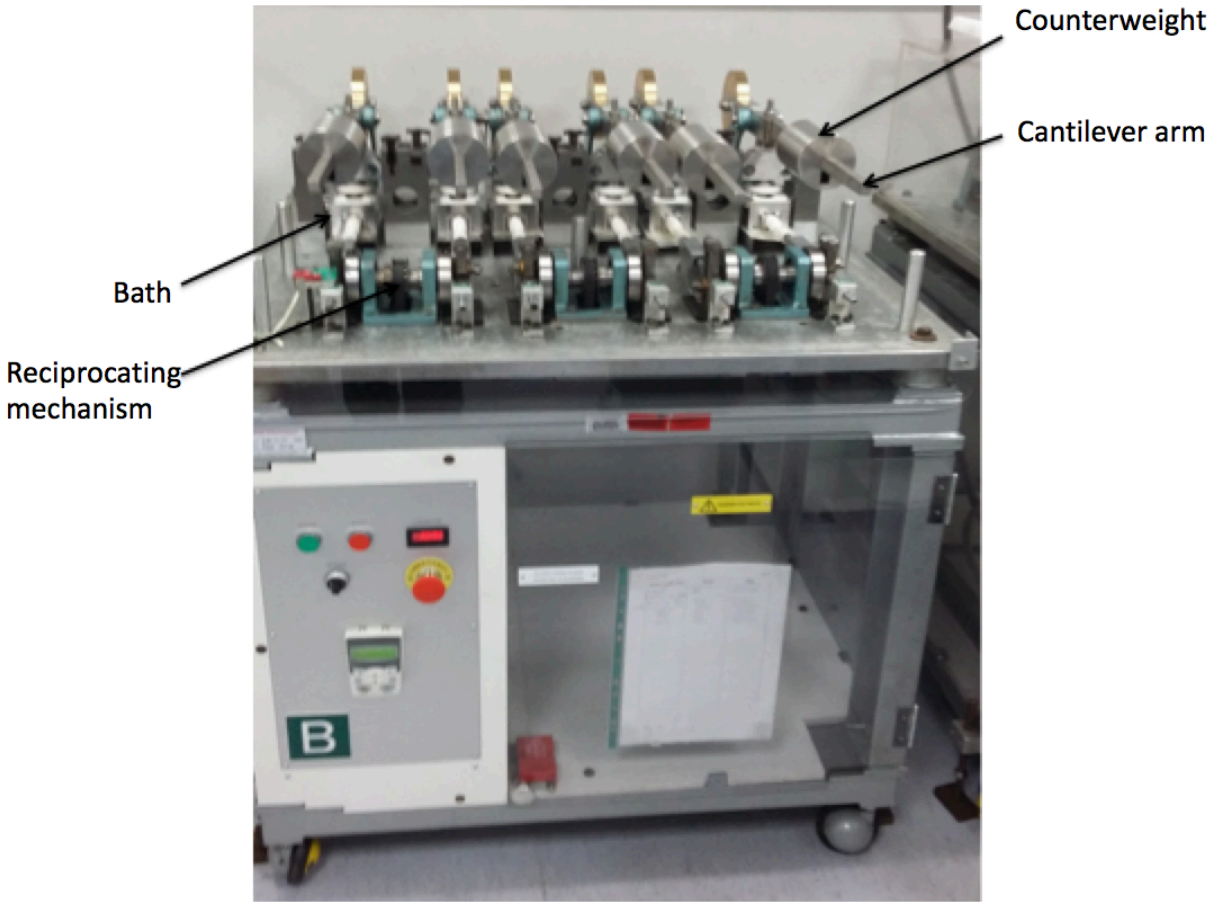

Figure 4.8 Complete set up of six station multidirectional reciprocating POP wear simulator rig (photo kindly taken and used with permission of Pirkko-Liisa Muhonen).

4.4.2.2.2 Assembly of six station pin-on-plate multidirectional wear simulator rig

Following sterile preparation, the six station wear simulator rig was assembled as follows. The baths were fixed to the rig using the thin, long screws and a hex key. The baths were placed on top of plastic sheets to protect the metal base from leaks. The baths were then filled with RPMI 1640 cell culture medium and bridges were then fixed in place. The white scotch yoke mechanisms were then screwed into place. The cantilever arms were then fixed to each station. The cycle counter was reset and the rig was switched on at low speed. The weights were loaded onto each cantilever arm at 160 N. The speed of the rig was then adjusted to 1 Hz (one complete cycle back and forth per second). A spare pre-weighed UHMWPE pin of the relevant material was placed into a sterile pot with 30 ml RPMI 1640 cell culture medium to act as a soak control.

4.4.2.2.3 Maintenance of six station pin-on-plate multidirectional wear simulator rig B

Each day, the rig speed was slowed down and the baths were topped up with sterile ultrapure water using a sterile plastic syringe. The speed of the reciprocation of the paths was increased back to 1 Hertz.

4.4.2.2.4 Disassembling the six station pin-on-plate multidirectional wear simulator rig B

The six station wear simulator rig was disassembled as follows. The rig was slowed down and the weights were removed from the cantilever arms. The rig was then turned off completely. The cantilever arms were removed and the scotch yoke mechanisms disconnected. The bridges and pin holders were removed – the pin holders were disassembled and the pins removed and cleaned prior to weighing. The baths were unscrewed from the rig and the lubricant was removed using a sterile syringe and placed into sterile labelled pots. Aseptic conditions were maintained up until this point. All rig components were then cleaned with household detergent and warm water, soaked in 1% (v/v) Trigene for 10 minutes and rinsed with deionised water. All pins and plates were sonicated in isopropanol for 10 minutes, rinsed with deionised water and air-dried. All dry components were then replaced neatly in the rig.

4.4.4 Microbiological testing of wear simulator lubricant

A volume of 0.5 ml was taken daily from the lubricant in the bath (having first switched off the simulator) for use in microbiological tests to ensure sterility was maintained. The lubricant sample was streaked (*Figure 4.9*) onto three types of agar plates using a platinum innoculation loop in the presence of Bunsen burner flame (to main sterility). The agar plates used were: heated blood agar (HBA) (to test for fastidious, haemolytic bacteria), sabouraud dextrose agar (SAB) (to test for non-fastidous fungi and dermatophytes) and nutrient agar (NA) (to test for non-fastidious bacteria). The plates were incubated at 37°C (HBA and NA) and 30°C (SAB) for up to 5 days and assessed for contamination daily.

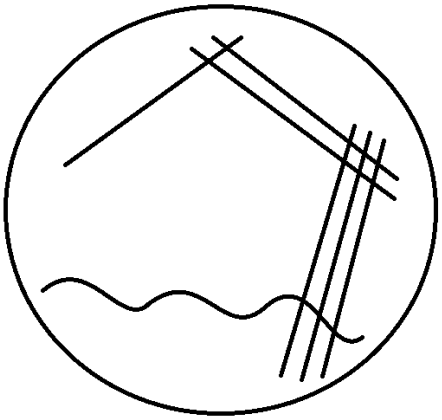

Figure 4.9 A schematic of a petri dish showing how a microbiological sample is streaked through the agar to test for biological contamination.

4.4.5 Endotoxin testing of generated UHMWPE wear debris

4.4.4.1 Endotoxin kit components

Table 4.8 Endotoxin assay kit components

Pierce LAL chromogenic endotoxin quantitation kit contents	**Storage and preparation**
E. coli endotoxin standard (20 EU.ml^{-1})	Stored at 4°C and reconstituted with 20 ml endotoxin free water.
LAL lyophilised 1.4 ml x 2 vials	Stored at 4°C and reconstituted with 1.4 ml endotoxin free water.
Chromogenic substrate lyophilised 6.5 ml	Stored at 4°C and reconstituted with 6.5 ml endotoxin free water.
Endotoxin free water 30 ml	Stored at 4°C.

4.4.4.2 Sample preparation

Each wear debris sample was defrosted and 500 µl from each sample was taken and placed in a labelled eppendorf whilst the remainder of the samples were returned to storage in the freezer. All eppendorfs were then heated to 75°C in a water bath for 30 minutes. All eppendorfs were then vortexed for 1 minute and then centrifuged at 13,000 g for 10 minutes. A volume of 0.5 µl supernatant in each eppendorf was transferred to a fresh labelled eppendorf and diluted with 49.5 µl endotoxin free water to achieve a 1:100 dilution as per the manufacturers instructions.

4.4.4.3 Reagent preparation

The reagents of the endotoxin assay kit were prepared as described below.

4.4.4.3.1 Endotoxin standard

The endotoxin assay kit was equilibrated to room temperature (25°C). The endotoxin standard was reconstituted with 1 ml endotoxin free water and vortexed for 15 minutes. This stock endotoxin standard was used to prepare standard as follows:

- 1 $EU.ml^{-1}$: 0.95 ml endotoxin free water + 50 µl stock
- 0.5 $EU.ml^{-1}$: 0.25 ml 1 $EU.ml^{-1}$ standard + 0.25 ml endotoxin free water
- 0.25 $EU.ml^{-1}$: 0.25 ml 1 $EU.ml^{-1}$ standard + 0.75 ml endotoxin free water
- 0.1 $EU.ml^{-1}$: 0.1 ml 1 $EU.ml^{-1}$ standard + 0.9 ml endotoxin free water

All standards were then vortexed for 1 minute at room temperature (25°C).

4.4.4.3.2 Limulus Amebocyte Lysate reagent

Limulus Amebocyte Lysate (LAL) was reconstituted by adding 1.4 ml endotoxin free water to the vial and the vial was swirled gently to mix.

4.4.4.3.3 Chromogenic substrate

Chromogenic substrate was reconstituted by adding 6.5 ml endotoxin free water to the vial which was kept at 37°C until use.

4.4.4.3.4 Stop reagent

25% (v/v) acetic acid was prepared by adding 1.5 ml 100% (v/v) glacial acetic acid to 4.5 ml endotoxin free water.

4.4.4.4 Assay procedure

An endotoxin-free 96 well plate was placed in the incubator at 37°C. The safety cabinet and heating block were cleaned with 1% (v/v) Trigene followed by 70% (v/v) ethanol and the heating block was placed inside the class II safety cabinet. Sterile, empty labelled eppendorfs were placed in the heating block and heated to 37°C for 10 minutes. A volume of 50 µl of either diluted sample, standard or blank (endotoxin free water only and RPMI 1640 medium only blanks were included) was added to an eppendorf. The timer was started and 50 µl of LAL reagent was added to each eppendorf tube. Once added, each tube was removed from the heating block briefly, tapped to mix and returned to the heating block. After 10 minutes, 100 µl chromogenic substrate was added to each tube. Again, once added each tube was removed, tapped to mixed and then returned to the heating block. After a total of 16 minutes, 100 µl 25% (v/v) acetic acid was added to each tube and tapped to mix as before. The contents of each tube were then added to the corresponding labelled well in the

heated endotoxin free 96 well plate. The plate was then read at 405 nm using the Multiskan plate reader.

4.4.4.5 Analysis

The optical densities of the standards were plotted against $EU.ml^{-1}$ (1, 0.5, 0.25 and 0.1 $EU.ml^{-1}$) to generate a standard curve. Linear regression was then used to calculate the concentration of endotoxin in each test sample.

4.4.6 Long term storage of UHMWPE wear particles

The wear debris generated in RPMI 1640 cell culture medium (with or without FBS) was stored in the freezer at -20°C until required for isolation or cell culture.

4.4.7 Isolation of UHMWPE wear debris from wear test lubricants

Each sample of wear debris in RPMI 1640 cell culture medium with 25% (v/v) FBS was taken from storage at -20°C and defrosted at room temperature. A small volume from each sample was taken and added to a sterile glass vial. The samples for each material from each type of rig (single and six station wear simulators) were pooled such that eight samples of at least 1 mm^3 wear debris in total were isolated – wear debris from four different materials produced on two types of wear simulators. Pellets of potassium hydroxide (6.72 g per 10 ml of serum lubricant) were added to the sterile glass vials containing each sample to form a 12 M solution. The samples were then incubated in a water bath at 60°C for five days as the serum proteins were digested. The water level in the bath was topped up and each vial gently agitated each day. After five days, the vials were removed from the water bath and placed into the cold room at 4°C for a minimum of 30 minutes. The vials were removed from the cold room and 10 ml of chloroform:methanol (2:1) mixture was added to each vial using a glass pipette in a fumehood in order to separate the particles from any lipids present. The vials were then incubated at room temperature (25°C) in the fumehood for 48 hours. After 48 hours, the vials were then centrifuged at 2000 g for 20 minutes at room temperature. After centrifugation, the top layer was removed from each vial into a new vial using a glass Pasteur pipette. The separation process was repeated twice more. Upon the final separation, ice-cold 100% (v/v) ethanol (previously prepared by freezing at -20°C for several hours) was added to each vial containing the isolated top layer in order to precipitate any remaining proteins. The vials were then centrifuged at 1000 g for 10 minutes at 4°C. The supernatants were decanted into a clean glass Duran bottle and an equal volume of ultrapure water was added. A stirrer bar was added to the bottle which was then placed on a stirrer plate in the cold room at 4°C overnight. The particle suspension was then decanted into a Sorvall bottle and centrifuged at 10,000 g at 4°C without the brake engaged for 2 hours. After centrifugation, the supernatant was decanted into a clean 1 litre glass Duran bottle

and an equal volume of ultrapure water was added. The sample was then stored at 4°C until filtration.

4.4.8 Filtration of isolated UHMWPE wear debris

The methods for preparing the filtration equipment and carrying out the particle filtration are detailed below.

4.4.8.1 Preparation of filtration units and filters

All glass filtration equipment was washed thoroughly with household detergent and warm water before use, rinsed with distilled water followed by ultrapure water and dried at 180°C in the oven overnight (wrapped in foil). The plastic filter manifold was packaged and autoclaved before use.

4.4.8.2 Filter coating for electron microscopy analysis

The glass filtration equipment was assembled in a class I laminar flow cabinet and attached to the vacuum pump as below (*Figure 4.10*). Particular care was taken placing the filter paper correctly upon the plastic filter manifold (*Figure 4.11*).

The particle suspension was filtered sequentially through 10 µm, 1 µm and 0.015 µm pore sized filter papers. Each filter paper was then carefully removed with tweezers and placed into a sterile petri dish. The filter papers were then placed under an infra-red lamp for a minimum of 4 hours to dry.

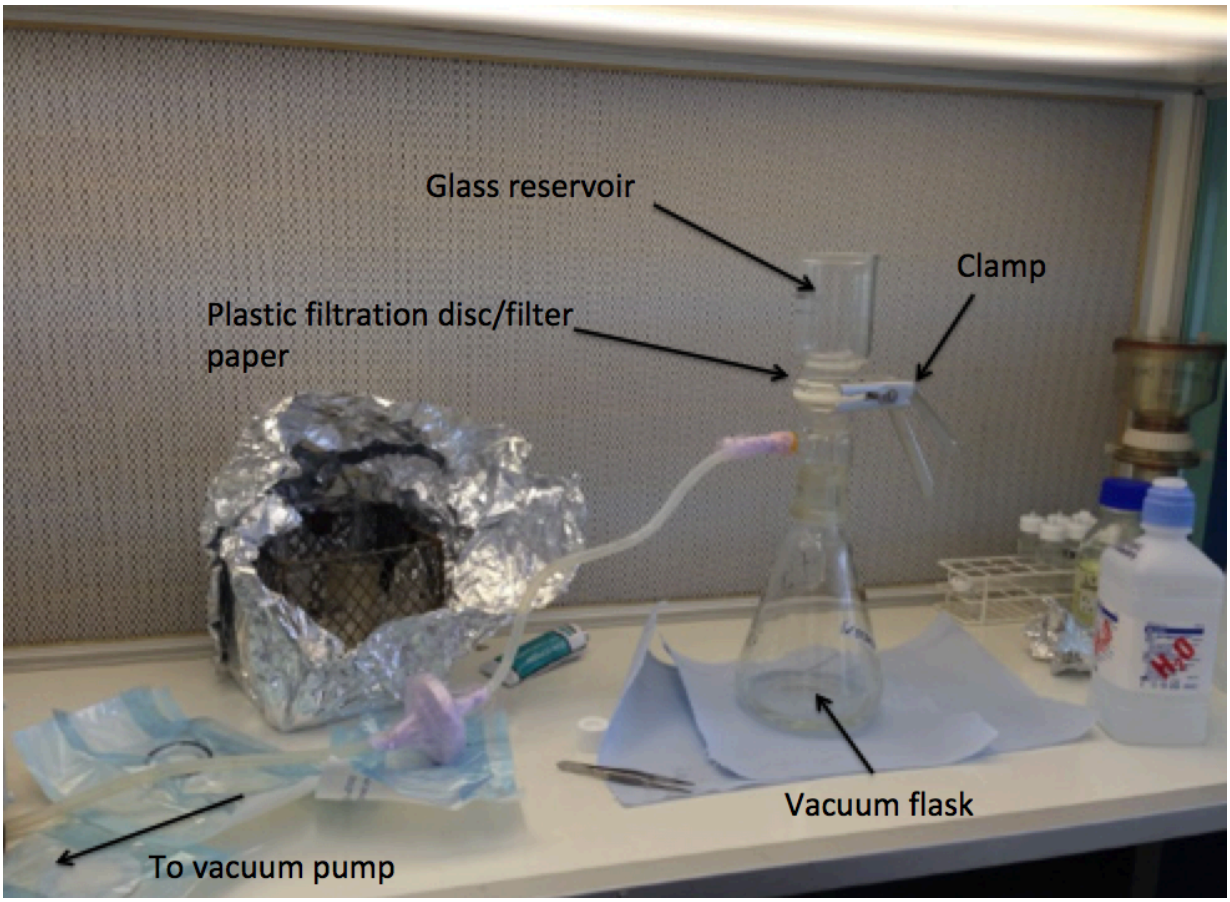

Figure 4.10 UHMWPE particle filtration set up: vacuum flask, clamp, glass reservoir, plastic filtration disc, filter paper and tubing leading to vacuum pump.

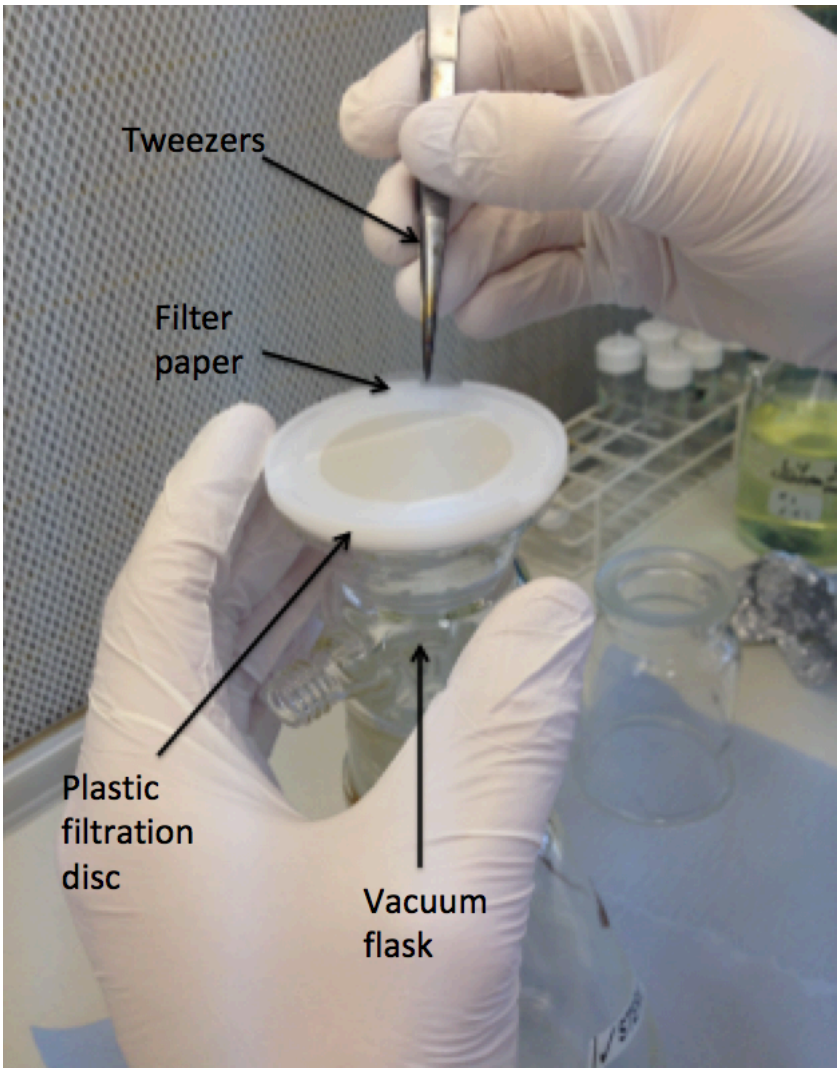

Figure 4.11 UHMWPE particle filtration set up showing the candidate lifting the filter paper of the plastic filtration disc.

4.4.9 Imaging

The method for imaging the isolated UHMWPE wear particles using FEGSEM is detailed below.

4.4.9.1 Imaging UHMWPE wear particles using Field Emission Gun Scanning Electron Microscopy

The stubs for scanning electron microscope (SEM) analysis were prepared by cutting a small section from each filter paper and placing it on a SEM aluminium stub followed by sealing the edges with carbon paint. Prior to viewing, the stubs were coated with carbon (10 nm coating thickness). The stubs were then viewed using a field emission gun electron microscope (FEGSEM) (Hitachi SU8230 Cold-FEGSEM**)**. For each stub, three random fields of view were captured over seven different magnifications (*Table*

4.9). A total of 62 images were taken for each material on each different rig (496 images in total).

Table 4.9 FEGSEM magnifications used to observe 10 µm, 1 µm and 0.015 µm pore sized filter stubs containing POP generated GUR 1020 XL, GUR 1020 XL AOX, GUR 1050 XL and GUR 1050 XL VE UHMWPE wear debris.

Magnifications taken of 10 µm pore sized filter stub	**Magnifications taken of 1 µm pore sized filter stub**	**Magnifications taken of 0.015 µm pore sized filter stub**
400X	1500X	10kX
700X	5kX	20kX
1500X	10kX	30kX
3kX	20kX	60kX
8kX	30kX	70kX
12kX	40kX	90kX
15kX	60kX	N/A

4.4.10 Characterisation

The methods for analysing the images of the UHMWPE wear debris using Image J software and utilising the resultant data to assess size and volume distribution are detailed in the following sections.

4.4.10.1 ImageJ

All images were then analysed using the Image J software package. Each UHMWPE wear particle was selected by the candidate and drawn around. For each material in each rig, approximately 100 random particles were analysed. The following measurements were calculated by the software for each particle: area, shape descriptors, perimeter, Ferets diameter (the longest dimension of the particle) and aspect ratio. The roundness was calculated manually from the equation below as set out in ASTM standard F1877-05 (2010) for particle isolation. A value of 1 indicates a perfectly round or circular particle.

$$\boldsymbol{Roundness\ (R) = (4A)/(\pi {d_{max}}^2)}$$

Where A = aspect ratio and d_{max} = Ferets diameter.

4.4.10.2 Analysis

The above data was then placed into an Excel spreadsheet and used to calculate size and volume distribution by placing each particle within a defined range (or bin) which included: 0 – 0.1μm, 0.1 - 1μm, 1 - 10 μm and >10 μm.

4.5 Results

Highly cross-linked and antioxidant doped, highly cross-linked UHMWPE wear debris (GUR 1020 XL, GUR 1020 XL AOX, GUR 1050 Xl and GUR 1050 XL VE) was generated using single and six station multidirectional POP wear simulators under aseptic conditions. The serum lubricants were tested for microbiological and endotoxin contamination to ensure sterility prior to use in *in vitro* cell culture studies. Samples of the serum lubricants generated from each material and each type of wear simulator were pooled and the wear particles isolated using the digestion method. The resultant filter papers were imaged using FEGSEM and the images were analysed using Image J to generate size and volume distribution data in order to compare to previous studies.

4.5.1 Microbiological testing of wear test lubricant from single and six station multidirectional Pin-On-Plate wear simulator rigs

Samples of each serum lubricant were streaked onto NA, SAB and HBA plates in order to assess biological contamination from non-fastidious bacteria, fungi and fastidious, haemolytic bacteria respectively. Plates were incubated for up to five days to assess any potential contaminant growth.

All agar plates used to test wear debris lubricant for the presence of any microbiological organisms were free of contamination. No signs of growth were present on any of the plates at any time point (Figure 4.12).

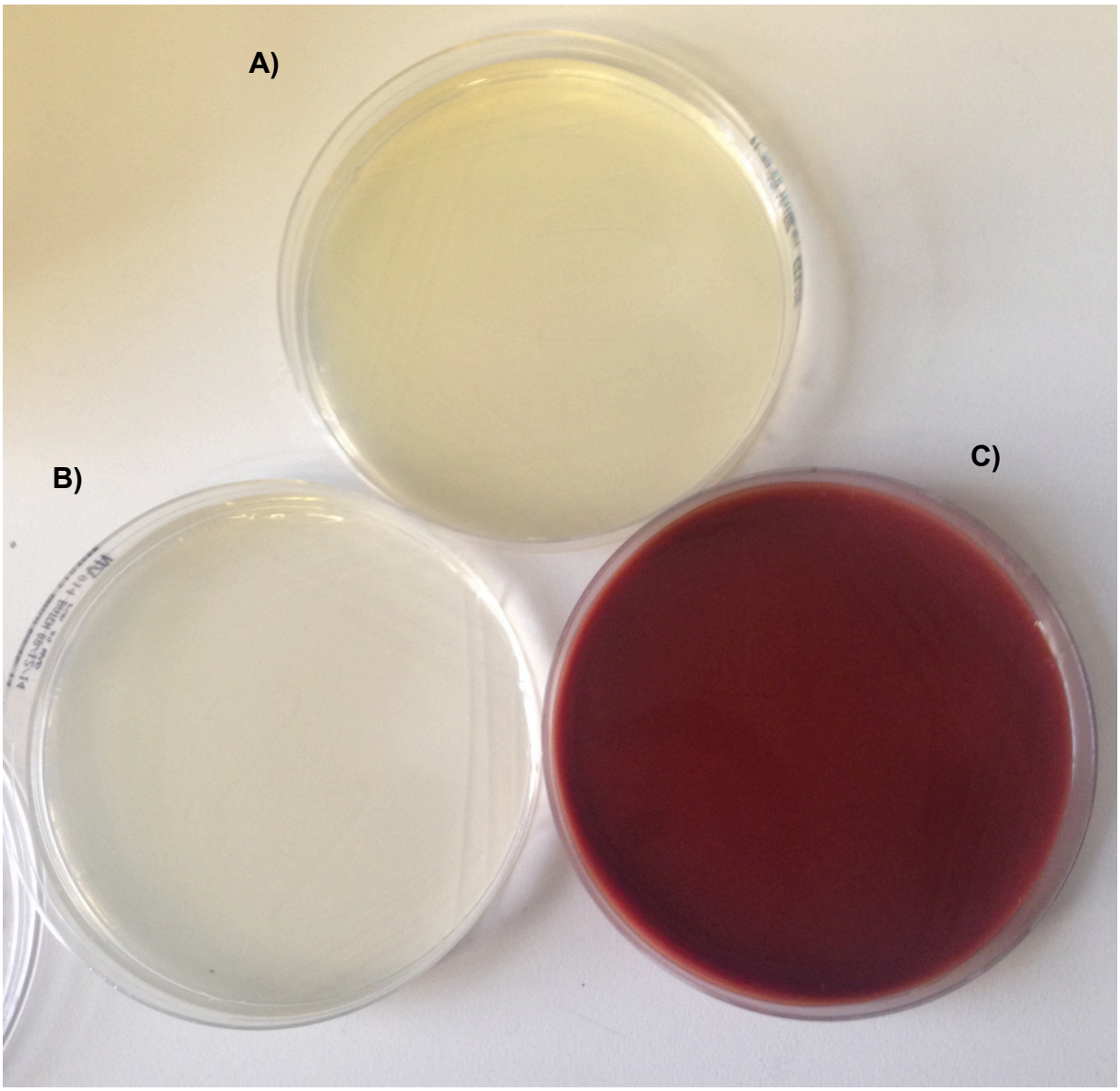

Figure 4.12 An example of nutrient agar (A), sabouraud dextrose agar (B) and heated blood agar (C) plates streaked with serum lubricant after five days showing no signs of microbial growth and therefore no biological contamination.

4.5.2 Endotoxin testing of wear test lubricant

The following section reports the results of the Pierce LAL endotoxin quantitation assay for both single and six station wear simulator rig generated wear debris for all materials. The optical density values for the standards were used to generate a standard curve (Figure 4.13). Linear regression of the equation for the standard curve was then used to calculate the endotoxin concentration in each test sample. Previous studies (Liu, 2012) and the pharmaceutical industry for injectable pharmaceuticals (FDA regulatory affairs, 1985) state that any value below 5 $EU.ml^{-1}$ is considered acceptable.

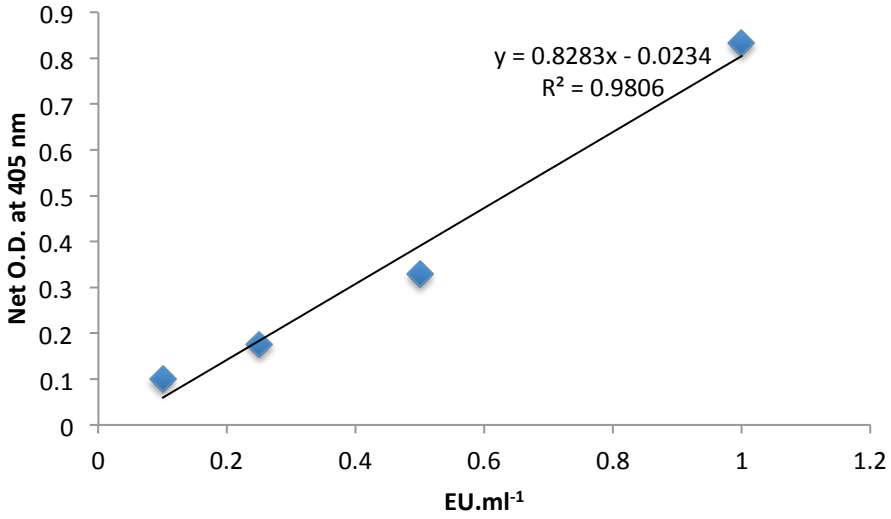

Figure 4.13 Standard curve for the quantitation of endotoxin in wear simulator lubricant. The line of best fit was calculated using linear regression. The coefficient of determination (R^2) and the line equation are reported on the graph. The line equation was then used to calculate the amount of endotoxin present in each sample analysed based on the optical density acquired.

4.5.2.1 Determination of endotoxin concentration in single station pin-on-plate multidirectional wear simulator lubricant

The endotoxin concentration values for each wear debris sample generated using the single station wear simulator rigs are shown in Table 4.10. All values were below the required standard of 5 $EU.ml^{-1}$.

Table 4.10 Endotoxin concentrations of wear debris samples generated with single station wear simulator rigs using GUR 1020 XL, GUR 1020 XL AOX, GUR 1050 XL and GUR 1050 XL VE UHMWPE.

GUR 1020 XL optical density at 405 nm	$EU.ml^{-1}$	GUR 1020 XL AOX optical density at 405 nm	$EU.ml^{-1}$
0.087	0.133	0.09	0.137
0.082	0.127	0.127	0.182
0.09	0.137	0.078	0.122
0.084	0.130	0.087	0.133

GUR 1050 XL optical density at 405 nm	EU.ml^{-1}	GUR 1050 XL VE optical density at 405 nm	EU.ml^{-1}
0.088	0.135	0.089	0.136
0.088	0.135	0.085	0.131
0.091	0.138	0.087	0.133
0.186	0.253	0.113	0.165

4.5.2.2 Determination of endotoxin concentration in six station pin-on-plate multidirectional wear simulator lubricant

The endotoxin concentration values for each wear debris sample generated using the six station wear simulator rigs are shown in Table 4.11. All values were below the required standard of 5 EU.ml^{-1} previously used by Liu (2012) and Gowland (2014).

Table 4.11 Endotoxin concentrations of wear debris samples generated with the six station wear simulator rig using GUR 1020 XL, GUR 1020 XL AOX, GUR 1050 XL and GUR 1050 XL VE UHMWPE.

Rig station number	GUR 1020 XL optical density at 405 nm	EU.ml^{-1}	Rig station number	GUR 1020 XL AOX optical density at 405 nm	EU.ml^{-1}
B1	0.098	0.147	B1	0.089	0.136
B2	0.109	0.160	B2	0.12	0.173
B3	0.086	0.132	B3	0.088	0.135
B4	0.083	0.129	B4	0.198	0.267
B5	-	-	B5	0.087	0.133
B6	0.109	0.160	B6	0.096	0.144
Rig station number	**GUR 1050 XL optical density at 405 nm**	**EU.ml^{-1}**	**Rig station number**	**GUR 1050 XL VE optical density at 405 nm**	**EU.ml^{-1}**
B1	0.092	0.139	B1	0.095	0.143
B2	0.091	0.138	B2	0.088	0.135

B3	0.091	0.138	B3	0.101	0.150
B4	0.096	0.144	B4	-	-
B5	0.104	0.154	B5	0.086	0.132
B6	0.105	0.155	B6	0.091	0.138

4.5.3 Calculation of volume of wear debris generated

The primary aim of this chapter was to generate sterile UHMWPE (GUR 1020 XL, GUR 1020 XL AOX, GUR 1050 XL, GUR 1050 XL VE) wear debris using both the single and six station multidirectional wear simulator rigs. The volume of wear debris generated for each material was therefore reported as a primary output. Individual measurements from individual runs were combined to create a mean volume value and this was reported. The standard error with respect to the mean was reported to show the variation in the range of results obtained.

4.5.3.1 Volume of wear debris generated in the single station pin-on-plate multidirectional wear simulators

The UHMWPE wear debris volumes – range and mean – are reported in Table 4.12 for all materials used in single station wear rig simulators 1 and 2. The mean wear debris volume values and the associated standard errors are reported in Figure 4.14. The antioxidant doped highly cross-linked UHMWPE materials generated the most debris in comparison to the highly cross-linked only materials and exhibited a large variation in range – this was particularly true of GUR 1020 XL AOX. Although statistical analysis revealed no significant difference between the mean wear debris volumes (ANOVA; $p>0.05$). Standard error of the mean (SEM) is reported.

Table 4.12 UHMWPE wear debris volumes generated on single station wear rig simulators 1 and 2 - range and mean values alongside SEM are reported. UHMWPE pins (10 mm contact face) were articulated against rough (Ra 0.08 – 0.09 µm) ASTM 1537 low carbon CoCr plates at 160 N load, 28 mm stroke length and +/- 30° rotation at a speed of 1 Hz over five days.

Material	Range (mm^3)	Mean ± SEM (mm^3)
GUR 1020 XL	0.34 – 4.82	1.72 ± 1.06
GUR 1020 XL AOX	8.45 – 95.11	37.48 ± 28.82
GUR 1050 XL	0.47 – 1.52	0.94 ± 0.22
GUR 1050 XL VE	0.47 – 14.79	9.61 ± 4.59

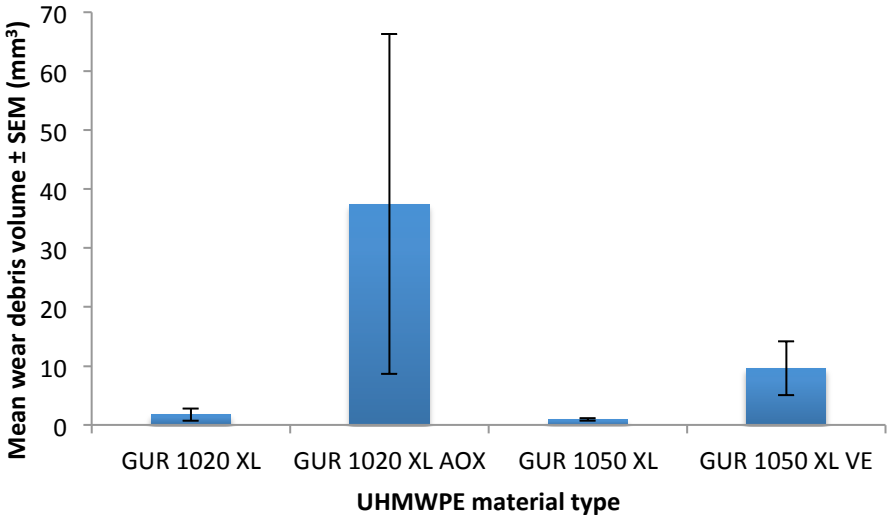

Figure 4.14 Mean wear debris volume ± SEM (mm^3) from UHMWPE pins articulated against rough plates (R_a 0.08 – 0.09 µm) ASTM 1537 low carbon CoCr plates at 160 N load, 28 mm stroke length and +/- 30° rotation at a speed of 1 Hz over five days in single station pin-on-plate wear simulator rigs for each material tested: GUR 1020 XL, GUR 1020 XL AOX, GUR 1050 XL and GUR 1050 XL VE. The error bars represent +/- standard error; n=4. (ANOVA; $p>0.05$)

4.5.3.2 Volume of wear generated in the six station pin-on-plate multidirectional wear simulator

The volumes of UHMWPE wear debris (range and mean) are reported below (Table 4.13) for all materials used in the six station POP multidirectional wear simulator. The mean wear debris volume values and the associated standard errors are reported below (Figure 4.15). The wear debris volumes were much greater than those generated on the single station rig for the same materials. In this case, the GUR 1020 XL material generated the largest volume of wear debris, with the other materials generating similar lower volumes. Although statistical analysis revealed no significant differences between the mean wear debris volumes generated by the different materials (ANOVA; $p>0.05$). Standard error of the mean (SEM) is reported.

Table 4.13 UHMWPE wear debris volumes generated on six station wear rig simulators B - range and mean values alongside SEM are reported. UHMWPE pins (10 mm contact face) were articulated against rough (R_a 0.08 – 0.09 µm) ASTM 1537 low carbon CoCr plates at 160 N load, 28 mm stroke length and +/- 30° rotation at a speed of 1 Hz over three days.

Material	Range (mm^3)	Mean ± SEM (mm^3)
GUR 1020 XL	17.59 – 464.22	201.24 ± 74.69
GUR 1020 XL AOX	41.00 – 148.13	99.56 ± 16.63

GUR 1050 XL	25.55 – 142.11	79.89 ± 20.58
GUR 1050 XL VE	81.71 – 158.53	129.17 ± 13.72

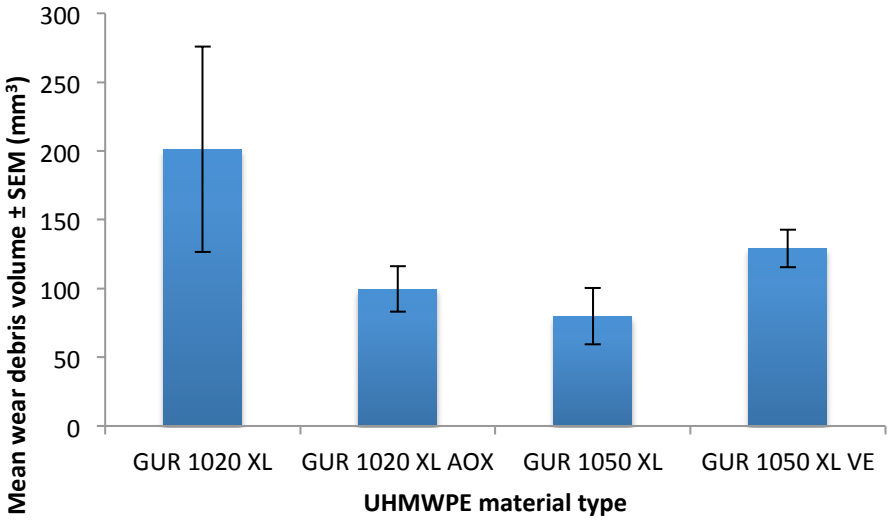

Figure 4.15 Mean wear debris volume (mm^3) from UHMWPE pins tested in the six station pin-on-plate wear simulator rig for each material tested: GUR 1020 XL, GUR 1020 XL AOX, GUR 1050 XL and GUR 1050 XL VE. The error bars represent +/- standard error; n=4. (ANOVA; p>0.05)

4.5.4 Calculation of wear factors from each material tested on each type of wear simulator

The wear factor is defined as an indication of how resistant a material is to wear – this is calculated as a function of volume lost, load and the sliding distance. Wear factor is reported in order to compare wear resistance between different types of material when assessing mechanical behaviour.

4.5.4.1 Wear factors from each material tested on the single station pin-on-plate multidirectional wear simulators

The UHMWPE wear factor values (range and mean) are reported below (Table 4.14) for all materials used in single station wear rig simulators 1 and 2. The mean wear factor values and the associated standard errors are reported below (Figure 4.16). The antioxidant doped highly cross-linked UHMWPE materials exhibited the highest wear factors in comparison to the highly cross-linked only materials and exhibited a large variation in range; this was particularly true of GUR 1020 XL AOX. Although statistical analysis revealed no significant differences between the mean wear factors (ANOVA; p>0.05). Standard error of the mean (SEM) is reported.

Table 4.14 UHMWPE wear factors generated on single station wear rig simulators 1 and 2 - range and mean values alongside SEM are reported. UHMWPE pins (10 mm contact face) were articulated against rough (R_a 0.08 – 0.09 µm) ASTM 1537 low carbon CoCr plates at 160 N load, 28 mm stroke length and +/- 30° rotation at a speed of 1 Hz over five days.

Material	Range ($mm^3.Nm^{-1}$)	Mean ± SEM ($mm^3.Nm^{-1}$)
GUR 1020 XL	$5.9 \times 10^{-7} – 1.2 \times 10^{-5}$	$3.9 \times 10^{-6} \pm 2.7 \times 10^{-6}$
GUR 1050 XL	$9.7 \times 10^{-7} – 3.4 \times 10^{-6}$	$2.4 \times 10^{-6} \pm 4.9 \times 10^{-5}$
GUR 1020 XL AOX	$1.8 \times 10^{-5} – 1.7 \times 10^{-4}$	$6.7 \times 10^{-5} \pm 5.4 \times 10^{-7}$
GUR 1050 XL VE	$6.9 \times 10^{-7} – 3.5 \times 10^{-5}$	$2.1 \times 10^{-5} \pm 1.0 \times 10^{-5}$

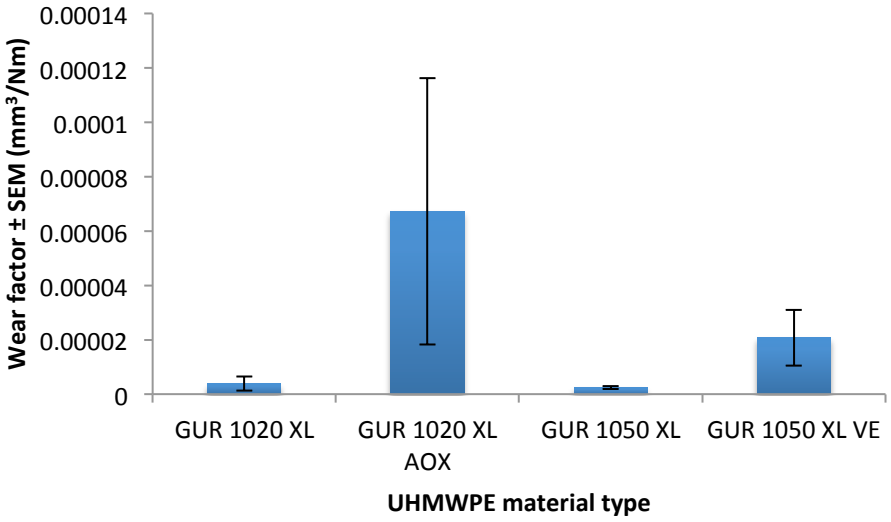

Figure 4.16 Mean wear factors for UHMWPE pins articulated against rough (R_a 0.08 – 0.09 µm) ASTM 1537 low carbon CoCr plates at 160 N load, 28 mm stroke length and +/- 30° rotation at a speed of 1 Hz over five days on single station pin-on-plate wear simulator rigs for each material tested: GUR 1020 XL, GUR 1020 XL AOX, GUR 1050 XL and GUR 1050 XL VE. The error bars represent +/- standard error; n=4. (ANOVA; $p>0.05$)

4.5.4.2 Wear factors from each material tested on the six station pin-on-plate multidirectional wear simulators

The UHMWPE wear factor values (range and mean) are reported in Table 4.15 for all materials used in six station rig B. The mean wear factor values and the associated standard errors are reported below (Figure 4.17). The wear factors were much greater than those generated using the single station POP multidirectional wear simulator for the same materials. In this case, the GUR 1020 XL material generated the highest

wear factor, with the other materials generating similar lower values. Although statistical analysis revealed no significant difference between the mean wear factors (ANOVA; p>0.05). Standard error of the mean (SEM) is reported.

Table 4.15 UHMWPE wear factors generated on six station wear rig simulators B - range and mean values alongside SEM are reported. UHMWPE pins (10 mm contact face) were articulated against rough (R_a 0.08 – 0.09 µm) ASTM 1537 low carbon CoCr plates at 160 N load, 28 mm stroke length and +/- 30° rotation at a speed of 1 Hz over three days.

Material	Range ($mm^3.Nm^{-1}$)	Mean ± SEM ($mm^3.Nm^{-1}$)
GUR 1020 XL	$1.3 \times 10^{-5} – 3.3 \times 10^{-4}$	$1.4 \times 10^{-4} \pm 5.3 \times 10^{-5}$
GUR 1020 XL AOX	$3.1 \times 10^{-5} – 1.1 \times 10^{-4}$	$7.5 \times 10^{-5} \pm 1.3 \times 10^{-5}$
GUR 1050 XL	$2.1 \times 10^{-5} – 1.2 \times 10^{-4}$	$6.5 \times 10^{-5} \pm 1.7 \times 10^{-5}$
GUR 1050 XL VE	$7.7 \times 10^{-5} – 1.5 \times 10^{-4}$	$1.2 \times 10^{-4} \pm 1.3 \times 10^{-5}$

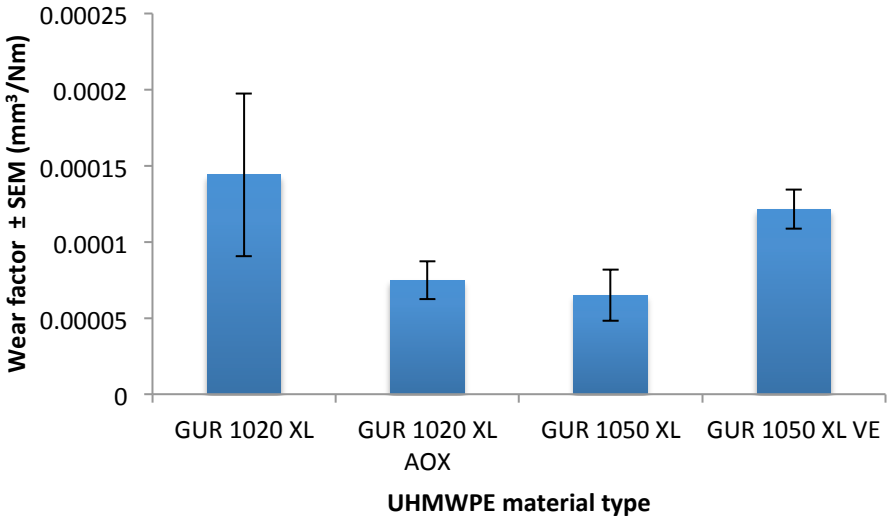

Figure 4.17 Wear factors for UHMWPE pins articulated against rough (R_a 0.08 – 0.09 µm) ASTM 1537 low carbon CoCr plates at 160 N load, 28 mm stroke length and +/- 30° rotation at a speed of 1 Hz over three days on all stations combined on six station pin-on-plate wear simulator rig for each material tested: GUR 1020 XL, GUR 1020 XL AOX, GUR 1050 XL and GUR 1050 XL VE. The error bars represent +/- standard error; n=4. (ANOVA; p>0.05)

4.5.5 Size and morphology of UHMWPE wear debris generated using the single and six station POP multidirectional wear simulators

The following section includes a selection of images taken using FEGSEM of the wear debris generated from GUR 1020 XL, GUR 1020 XL AOX, GUR 1050 XL and GUR 1050 XL VE UHMWPE pins using both the single and six station wear simulators. The

particles were isolated as reported in Section 4.4.7 and filtered onto three different sizes of filter papers (10 μm, 1 μm and 0.015 μm pore sized). Images were taken at varying magnifications from 400X to 90kX. Images display the range of morphologies found – typically UHMWPE can display morphologies including plates, flakes, fibrils and granules.

4.5.5.1 Size and morphology of UHMWPE wear debris generated using the single station pin-on-plate multidirectional wear simulators

A total of 62 images per material per rig were taken using FEGSEM. A selection of the images taken with the FEGSEM of GUR 1020 XL, GUR 1020 XL AOX, GUR 1050 XL and GUR 1050 XL VE UHMWPE wear debris generated on the single station wear simulator rig against rough CoCr plates at 160 N, 28 mm stroke length and 30° rotation at 1 Hz over five days are reported in Figure 4.18: one image per material per rig. The UHMWPE wear debris was subsequently isolated, filtered and imaged as detailed in Sections 4.4.7, 4.4.8, 4.4.9 and 4.4.10 respectively.

A number of the different morphologies possible for UHMWPE wear debris were observed such as large platelet shaped particles (Figure 4.18A and C), smaller granular particles (Figure 4.18B) and aggregated particles (Figure 4.18D). This assortment of images shows that the same range of shapes are generated by all the UHMWPE materials tested in this study.

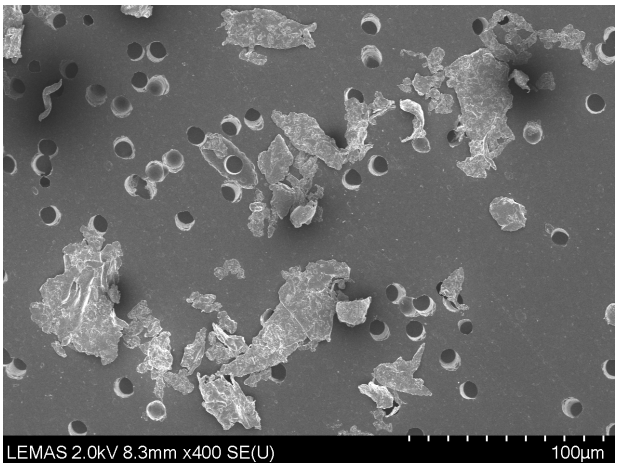

A1)

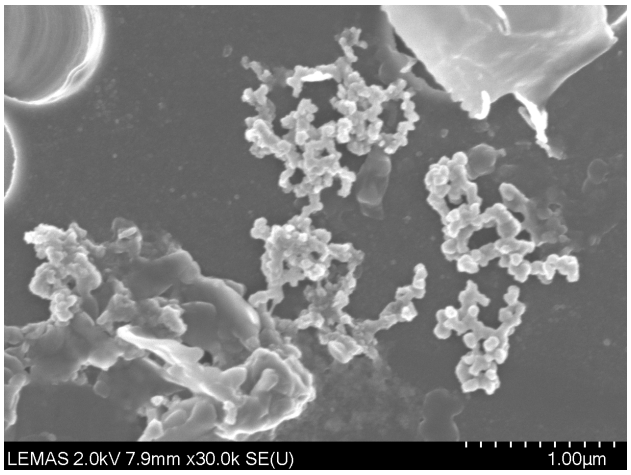

A2)

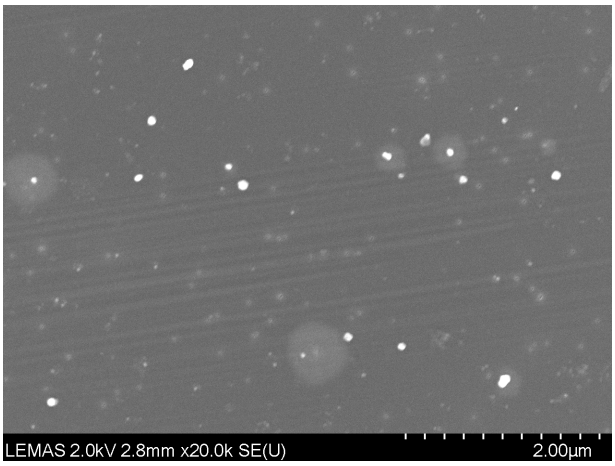

A3)

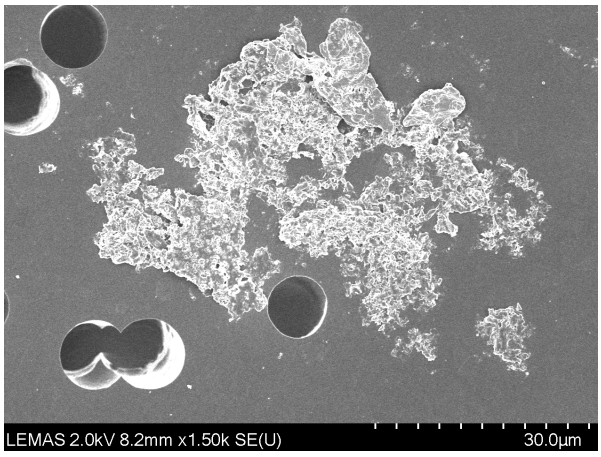

B1)

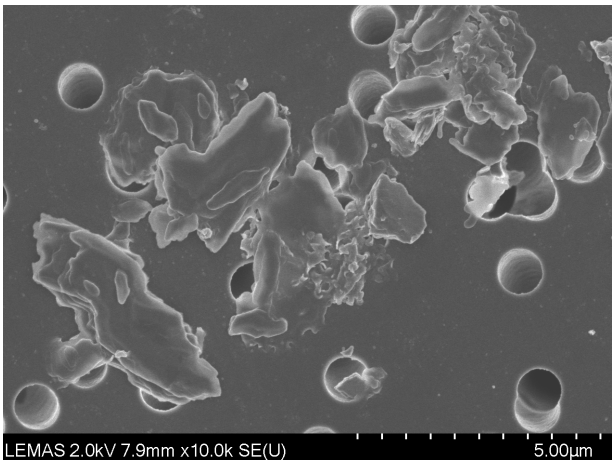

B2)

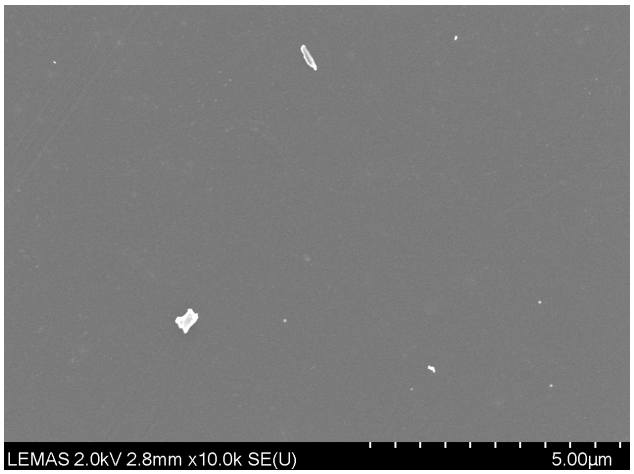

B3)

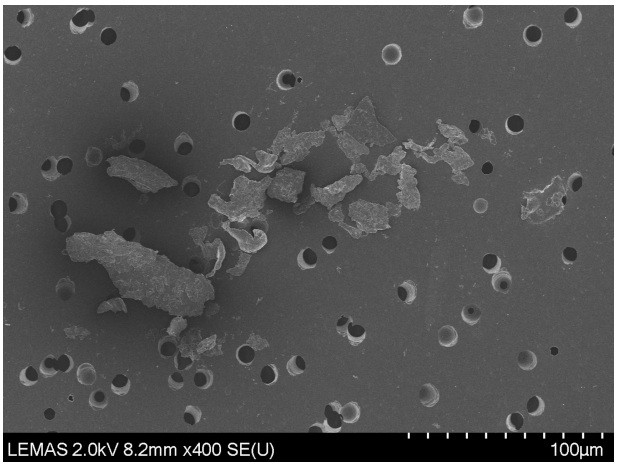

C1)

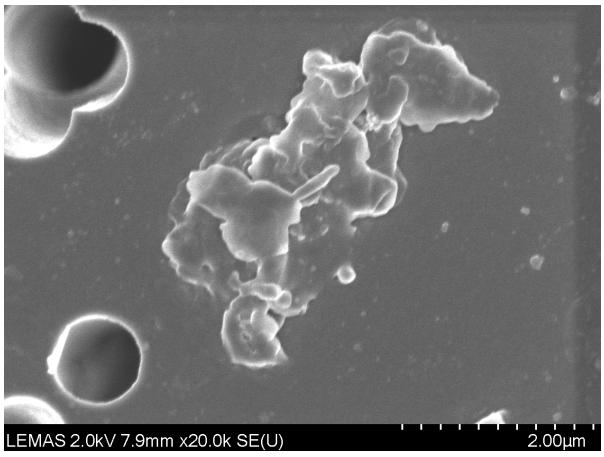

C2)

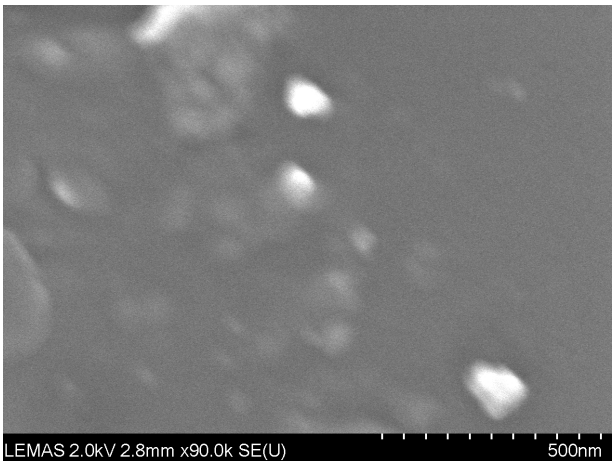

C3)

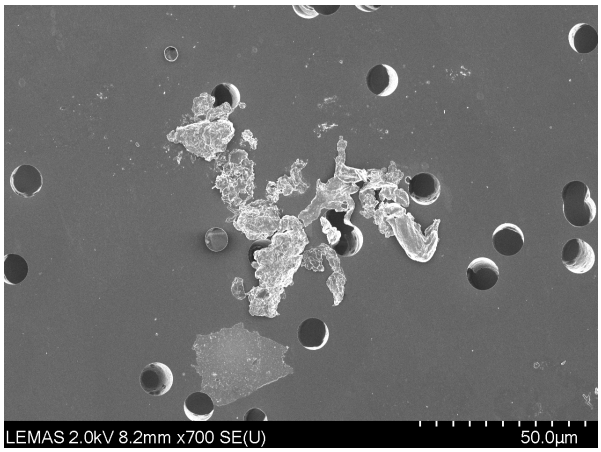

D1)

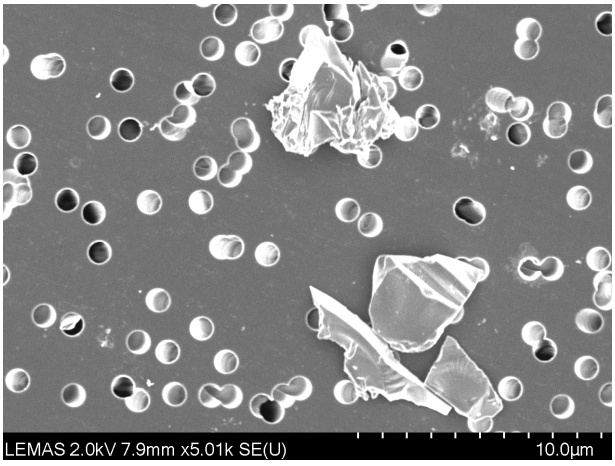

D2)

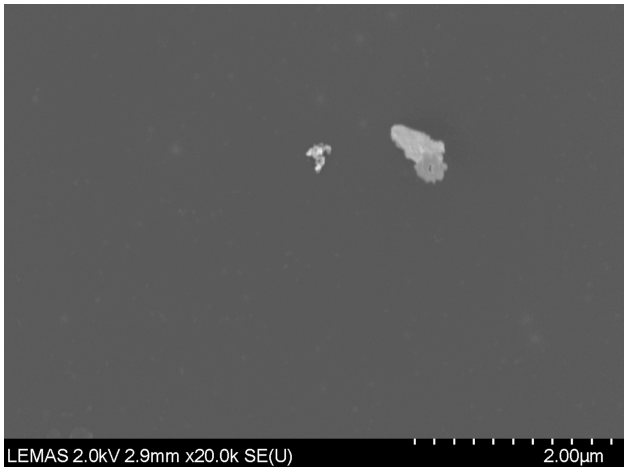

D3)

Figure 4.18 A selection of images depicting UHMWPE wear debris generated against rough CoCr plates using single station multidirectional POP wear simulator rigs 1 and 2. A1) GUR 1020 XL on a 10 µm pore sized filter paper taken at 400X magnification. Multiple large platelet shaped particles can clearly be seen. A2) GUR 1020 XL on a 1 µm pore sized filter paper taken at 30kX magnification. A3) GUR 1020 XL on a 0.015 µm pore sized filter paper taken at 20kX magnification. B1) GUR 1020 XL AOX on a 10 µm pore sized filter paper taken at 1.5kX magnification. B2) GUR 1020 XL AOX on a 1 µm pore sized filter paper taken at 10kX magnification. B3) GUR 1020 XL AOX on a 0.015 µm pore sized filter paper taken at 10kX magnification. Two platelet shaped particles are visible along with several small granular particles. C1) GUR 1050 XL on a 10 µm pore sized filter paper taken at 400X magnification. Multiple large platelet shaped particles can clearly be seen. C2) GUR 1050 XL on a 1 µm pore sized filter paper taken at 20kX magnification. C3) GUR 1050 XL on a 0.015 µm pore sized filter paper taken at 90kX magnification. D1) GUR 1050 XL VE on a 10 µm pore sized filter paper taken at 700X magnification. D2) GUR 1050 XL VE on a 1 µm pore sized filter paper taken at 5kX magnification. D3) GUR 1050 XL VE on a 0.015 µm pore sized filter paper taken at 10kX magnification. One platelet shaped particle is visible on the right and a aggregate of small particles is visible on the left.

4.5.5.2 Size and morphology of UHMWPE wear debris generated using the six station pin-on-plate multidirectional wear simulators

A selection of images taken with the FEGSEM of GUR 1020 XL, GUR 1020 XL AOX, GUR 1050 XL and GUR 1050 XL VE UHMWPE wear debris generated on the six station wear simulator rig against rough CoCr plates at 160 N, 28 mm stroke length and 30° rotation at 1 Hz over three days are reported in Figure 4.19. The UHMWPE wear debris was subsequently isolated, filtered and imaged as detailed in Sections 4.4.7, 4.4.8, 4.4.9 and 4.4.10 respectively.

A number of the different morphologies possible for UHMWPE wear debris were observed such as large platelet shaped particles (Figure 4.19D), groups of aggregated particles (Figure 4.19A) and small granule particles (Figure 4.19C). Figure 4.19C shows several of these morphologies. This assortment of images shows that the same range of shapes are generated by all the UHMWPE materials tested in this study. Some salt contamination was present on Figure 4.19B (long needle-like crystals on the left of the image). The isolation procedure is designed to remove salts as much as possible however occasionally there are some residual salt crystals present.

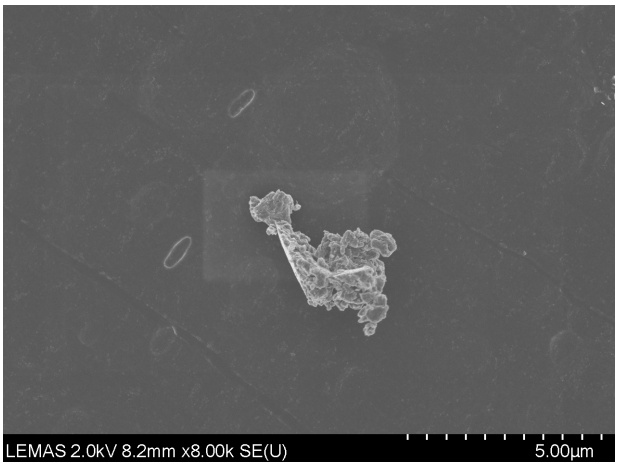

A1)

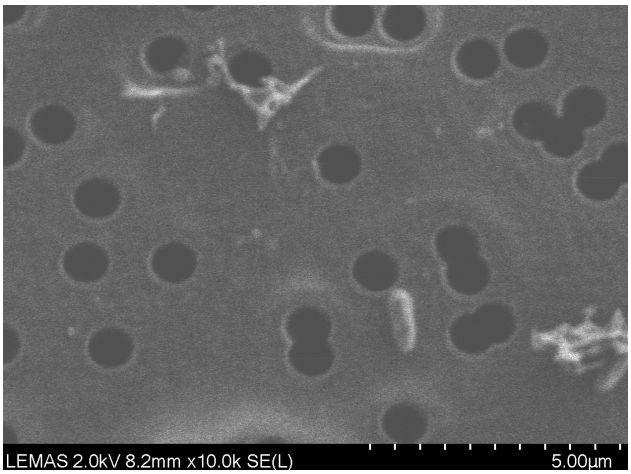

A2)

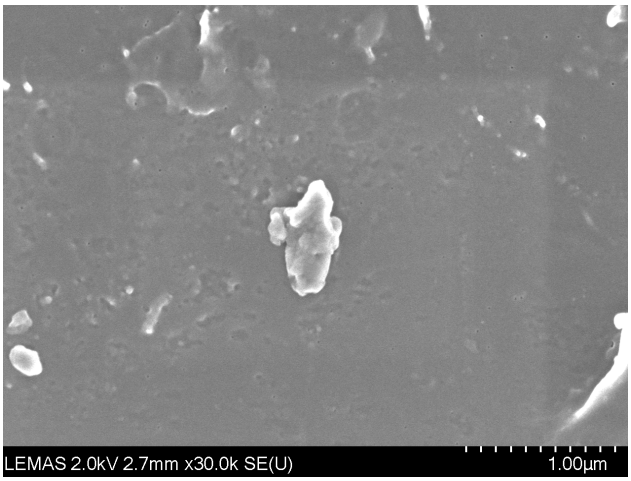

A3)

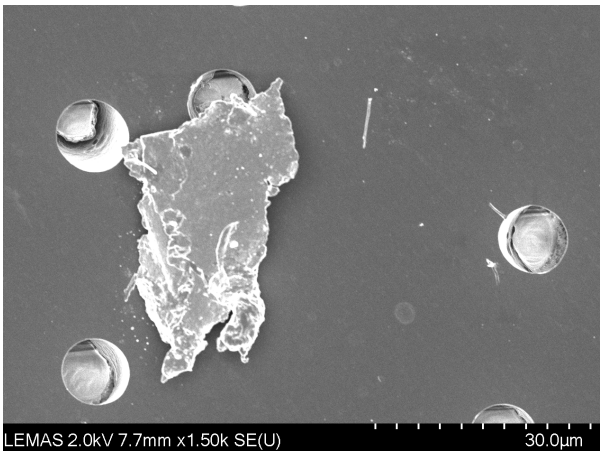

B1)

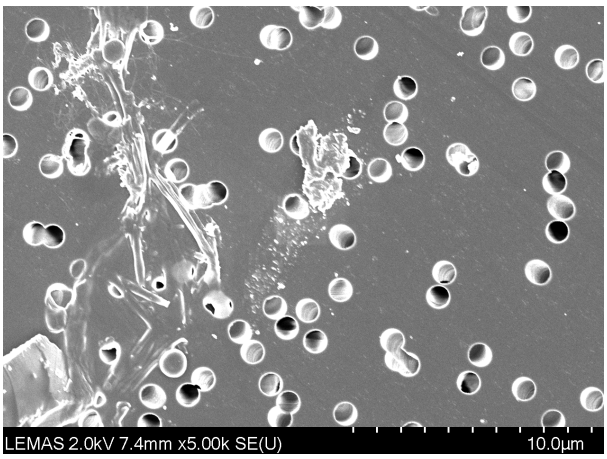

B2)

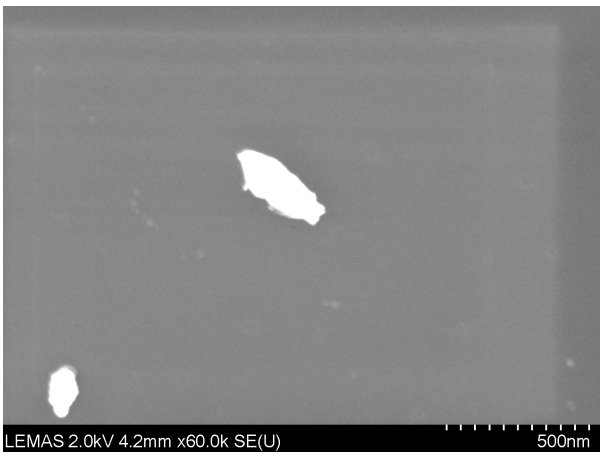

B3)

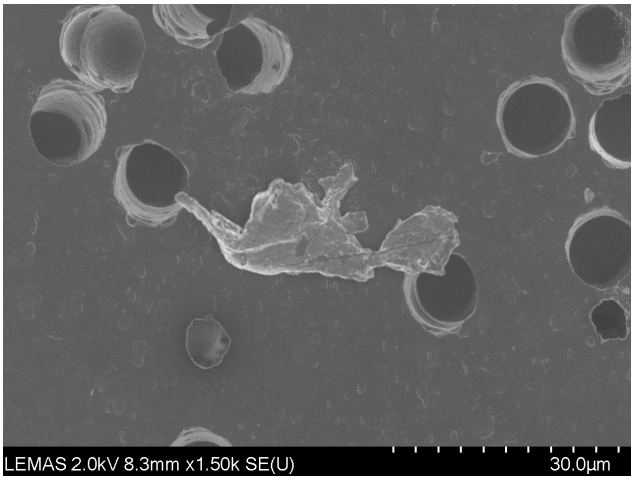

C1)

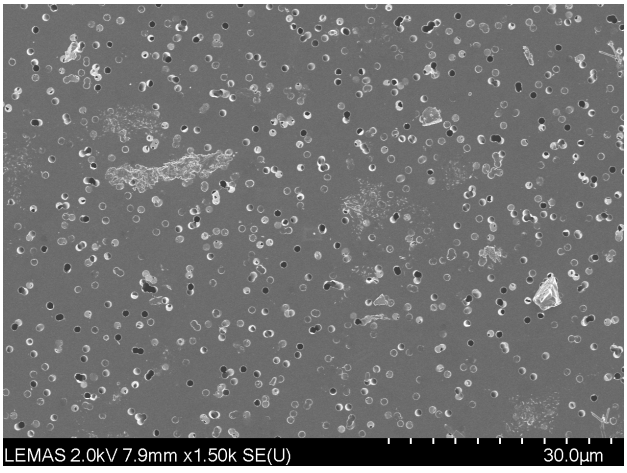

C2)

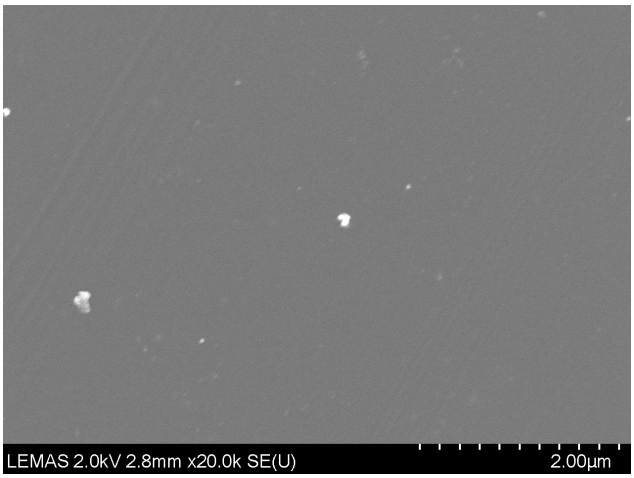

C3)

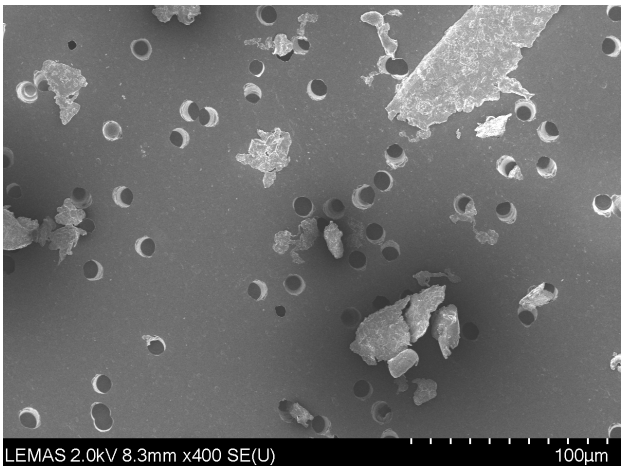

D1)

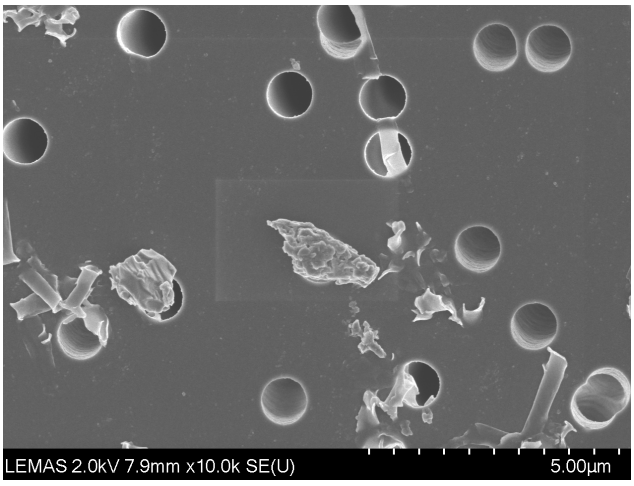

D2)

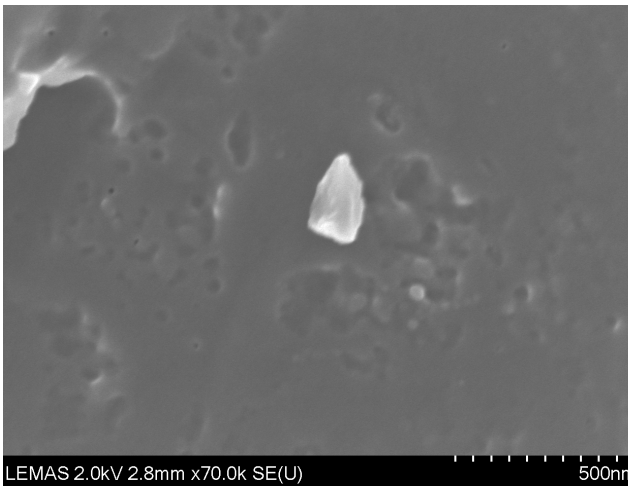

D3)

Figure 4.19 A selection of images depicting UHMWPE wear debris generated against rough CoCr plates using the six station multidirectional POP wear simulator: A1) GUR 1050 XL VE UHMWPE wear debris on a 10 µm pore sized filter paper taken at 8kX magnification. A large aggregated UHMWPE wear particle can clearly be seen in the centre of the image. The particle is approximately 4 µm in diameter. A2) GUR 1050 XL VE UHMWPE wear debris on a 1 µm pore sized filter paper taken at 10kX magnification. A3) GUR 1050 XL VE UHMWPE wear debris on a 0.015 µm pore sized filter paper taken at 30kX magnification. B1) GUR 1050 XL UHMWPE wear debris on a 10 µm pore sized filter paper taken at 1.5kX magnification. B2) GUR 1050 XL UHMWPE wear debris on a 1 µm pore sized filter paper taken at 5kX magnification. In the centre a large platelet shaped particle is clearly visible – approximately 4 µm in diameter – which is surrounded by many much smaller granular particles. There are also some needle-like salt crystals visible on this filter paper. B3) GUR 1050 XL UHMWPE wear debris on a 0.015 µm pore sized filter paper taken at 60kX magnification. C1) GUR 1020 XL AOX UHMWPE wear debris on a 10 µm pore sized filter paper taken at 1.5kX magnification. C2) GUR 1020 XL AOX UHMWPE wear debris on a 1 µm pore sized filter paper taken at 1.5kX magnification. This image shows a range of platelet shaped and granular particles. C3) GUR 1020 XL AOX UHMWPE wear debris on a 0.015 µm pore sized filter paper taken at 20kX magnification. D1) GUR

1020 XL UHMWPE wear debris on a 10 µm pore sized filter paper taken at 400X magnification. This image shows a range of large platelet shaped particles. D2) GUR 1020 XL UHMWPE wear debris on a 1 µm pore sized filter paper taken at 10kX magnification. D3) GUR 1020 XL UHMWPE wear debris on a 0.015 µm pore sized filter paper taken at 70kX magnification.

4.5.6 Characterisation of UHMWPE wear debris particles

Using Image J, particle sizes and volumes were assessed. No statistical analysis was carried out as the samples for each material generated on each rig were pooled therefore n=1.

4.5.6.1 Size distribution, volume distribution and roundness of UHMWPE wear debris generated using the single station multidirectional pin-on-plate wear simulator rigs

Particles generated on the single station multidirectional wear simulator rigs displayed a range of sizes (Figure 4.20). GUR 1050 XL and GUR 1050 XL VE demonstrated particles in all size ranges. GUR 1050 XL particles were most commonly in the range >10 µm, whereas the most common size range of GUR 1050 XL VE particles was 0.1 - 1 µm. For both materials, >10 µm particles represented the largest volume of particles. GUR 1020 XL particles however only exhibited particles in the size ranges 1 – 10 µm and >10 µm with the latter representing the largest volume of particles; none of the particles analysed were in the size ranges <0.1 µm and 0.1 – 1 µm. GUR 1020 XL AOX particles also only exhibited particles in the ranges 0.1 - 1 µm, 1 – 10 µm and >10 µm, with the latter representing the largest volume of particles; none of the particles analysed were found in the range <0.1 µm.

A)

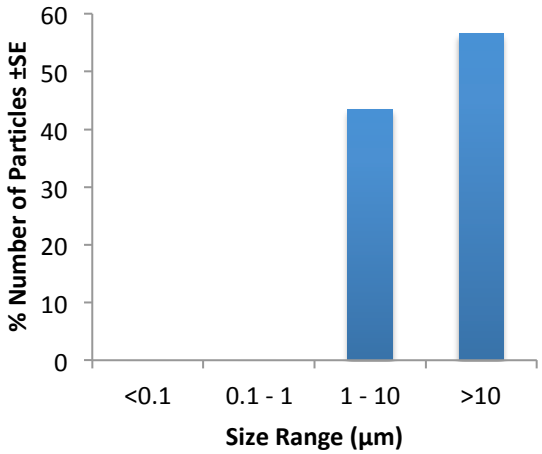

B)

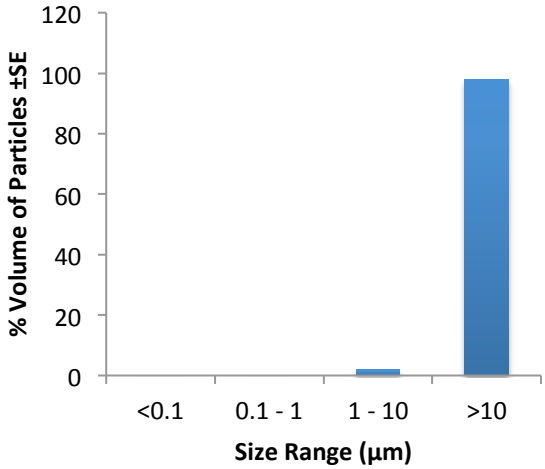

C)

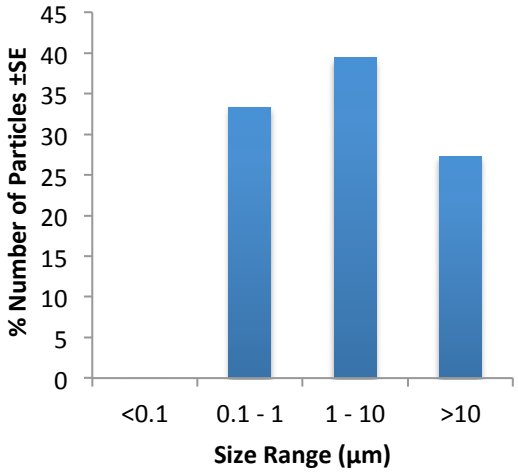
% Number of Particles ±SE
45
40
35
30
25
20
15
10
5
0
<0.1
0.1 - 1
1 - 10
>10
Size Range (µm)

D)

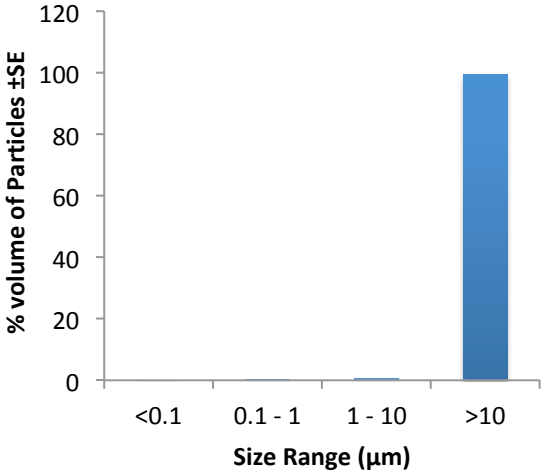
% volume of Particles ±SE
120
100
80
60
40
20
0
<0.1
0.1 - 1
1 - 10
>10
Size Range (µm)

E)

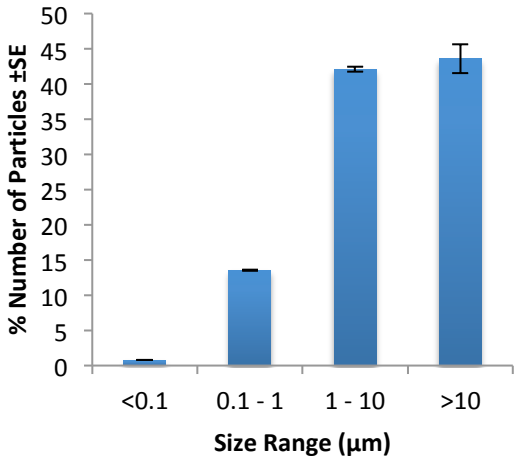
% Number of Particles ±SE
50
45
40
35
30
25
20
15
10
5
0
<0.1
0.1 - 1
1 - 10
>10
Size Range (µm)

F)

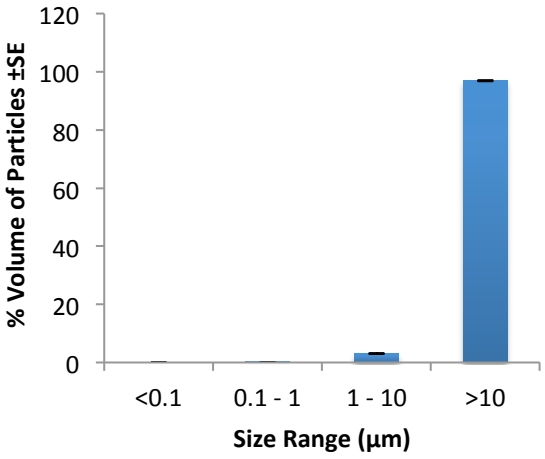
% Volume of Particles ±SE
120
100
80
60
40
20
0
<0.1
0.1 - 1
1 - 10
>10
Size Range (µm)

G)

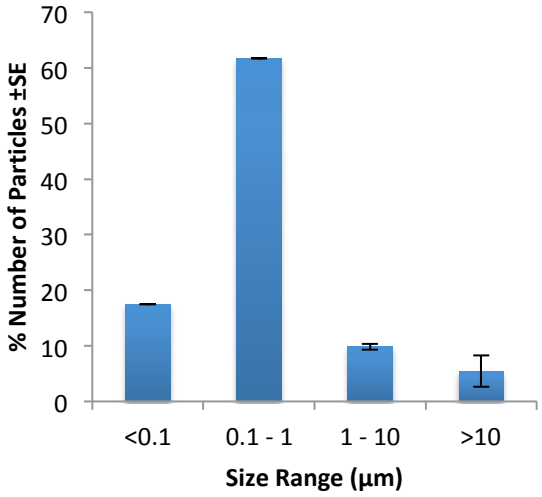

H)

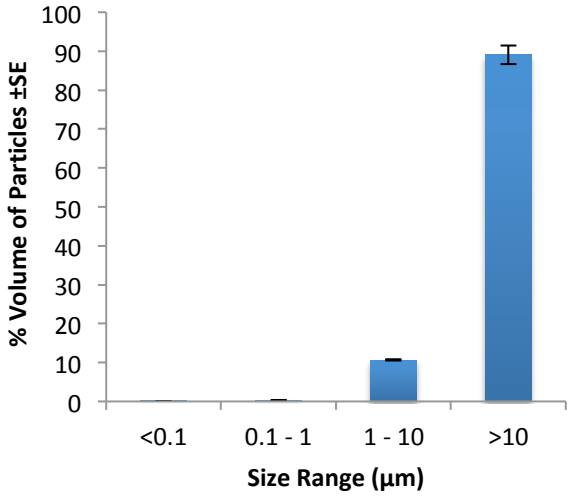

Figure 4.20 The percentage frequency and the percentage volume size distribution of GUR 1020 XL (A, B), GUR 1020 XL AOX (C, D), GUR 1050 XL (E, F) and GUR 1050 XL VE (G, H) UHMWPE particle generated on the single station multidirectional POP wear simulator.

The roundness of approximately 100 particles per material were calculated and an average value for each material was reported. A value of 1.0 indicates a perfectly circular particle. Table 4.16 shows that all materials generated particles of a similar roundness, suggesting that there is little difference in the morphology of particles between highly cross-linked UHMWPE wear particles and highly cross-linked, antioxidant doped UHMWPE wear particles.

Table 4.16 Roundness values of UHMWPE wear debris generated on single station wear rig simulators 1 and 2 – approximately 100 particles per material were analysed and an average roundness value reported.

Rig	Material	Roundness (average)
SS	GUR 1020 XL	0.67
SS	GUR 1020 XL AOX	0.63
SS	GUR 1050 XL	0.61
SS	GUR 1050 XL VE	0.65

4.5.6.2 Size distribution, volume distribution and roundness of UHMWPE wear debris generated using the six station multidirectional pin-on-plate wear simulator rig

Particles generated on the six station multidirectional wear simulator rigs displayed a range of sizes (Figure 4.21). GUR 1020 XL AOX, GUR 1050 XL and GUR 1050 XL VE demonstrated particles in all size ranges except >10 µm and 0.1 – 1 µm particles were the most common; with particles in the size range 1 – 10 µm representing the largest volume. GUR 1020 XL AOX particles however only exhibited particles in the size ranges <0.1 µm and 0.1 – 1 µm with the latter representing the largest volume of particles; none of the particles analysed were found in the ranges 1 - 10 µm and >10 µm.

A)

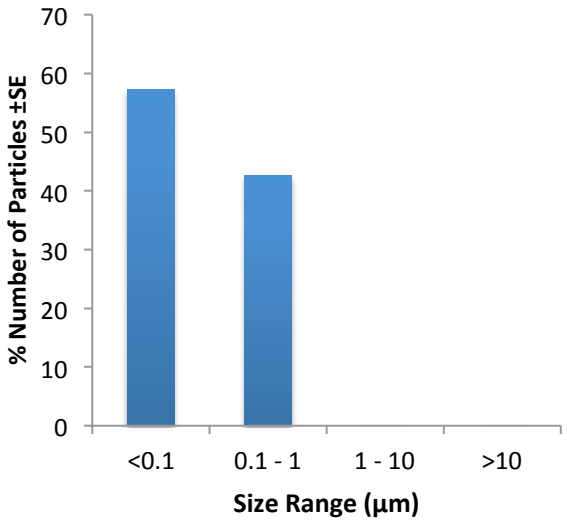

B)

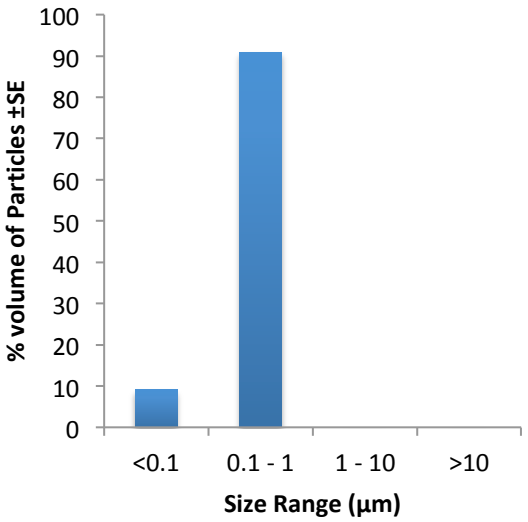

C)

D)

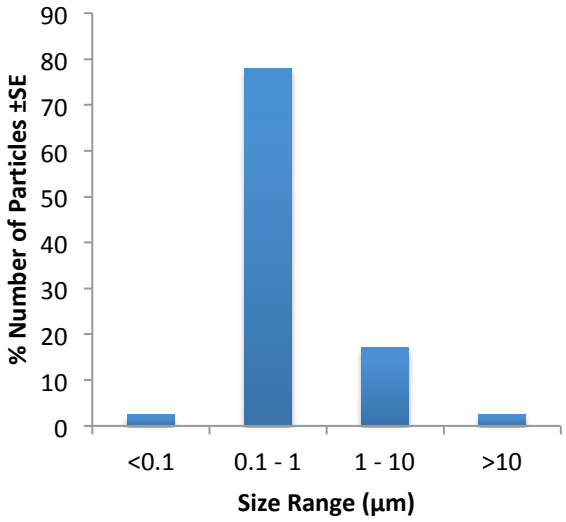
% Number of Particles ±SE
90
80
70
60
50
40
30
20
10
0
<0.1
0.1 - 1
1 - 10
>10
Size Range (µm)

E)

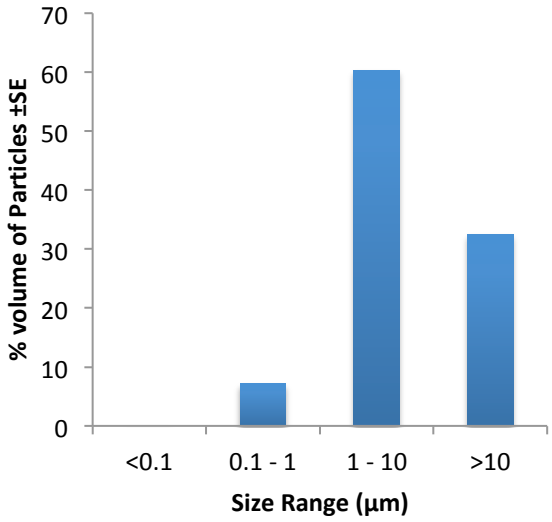
% volume of Particles ±SE
70
60
50
40
30
20
10
0
<0.1
0.1 - 1
1 - 10
>10
Size Range (µm)

F)

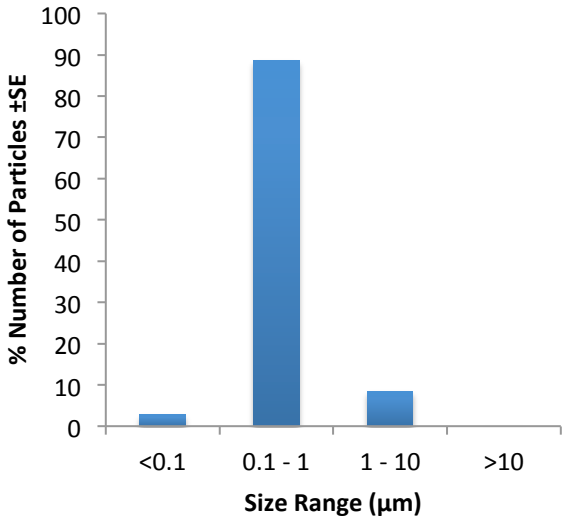
% Number of Particles ±SE
100
90
80
70
60
50
40
30
20
10
0
<0.1
0.1 - 1
1 - 10
>10
Size Range (µm)

G)

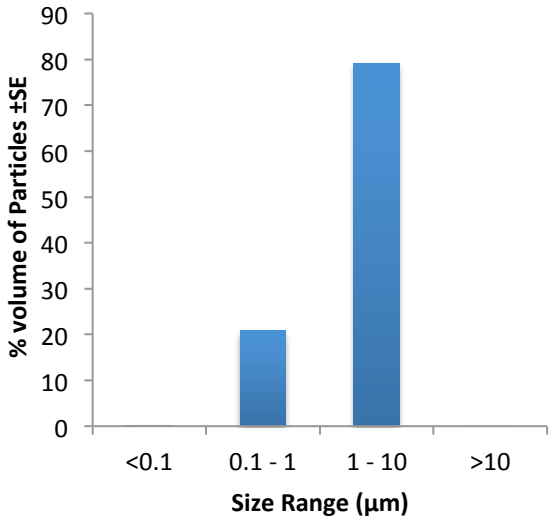
% volume of Particles ±SE
90
80
70
60
50
40
30
20
10
0
<0.1
0.1 - 1
1 - 10
>10
Size Range (µm)

H)

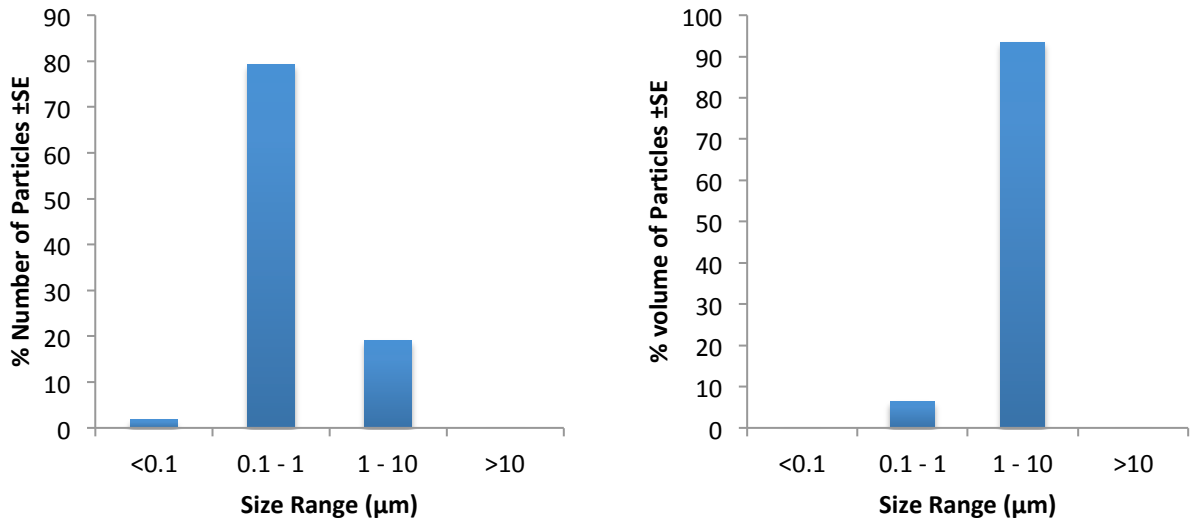

Figure 4.21 The percentage frequency and the percentage volume size distribution of GUR 1020 XL (A, B), GUR 1020 XL AOX (C, D), GUR 1050 XL (E, F) and GUR 1050 XL VE (G, H) UHMWPE particle generated on the six station multidirectional POP wear simulator.

The roundness of approximately 100 particles per material were calculated and an average value for each material was reported. A value of 1.0 indicates a perfectly circular particle. Table 4.17 shows that all materials generated particles of a similar roundness, suggesting that there is little difference in the morphology of particles between highly cross-linked UHMWPE wear particles and highly cross-linked, antioxidant doped UHMWPE wear particles.

Table 4.17 Roundness values of UHMWPE wear debris generated on six station wear rig simulator B – approximately 100 particles per material were analysed and an average roundness value reported.

Rig	Material	Roundness (average)
6S	GUR 1020 XL	0.59
6S	GUR 1020 XL AOX	0.55
6S	GUR 1050 XL	0.66
6S	GUR 1050 XL VE	0.59

4.5.6.3 Comparison of size distribution, volume distribution and roundness of UHMWPE wear debris generated using the single and six station multidirectional pin-on-plate wear simulator rigs

The above size distribution, volume distribution and roundness data for the UHMWPE wear particles generated using the single and six station wear rig simulators is

summarised in Table 4.18. It can clearly be seen that the single station wear rig simulators generally produced wear particles over 1 μm (with the exception of GUR 1050 XL VE) whereas the six station wear rig simulator typically produced particles less than 1 μm. Table 4.18 also shows that particles over 10 μm accounted for the largest volume of particles produced on the single station wear rig simulators whereas the particles between 1 and 10 μm accounted for the largest volume of particles produced on the six station wear rig simulator (with the exception of GUR 1020 XL).

Table 4.18 Comparison of size distribution, volume distribution and roundness values of UHMWPE wear debris generated on single and six station wear rig simulators.

	Rig: SS Material:			
% number of particles in size range:	GUR 1020 XL	GUR 1020 XL AOX	GUR 1050 XL	GUR 1050 XL VE
<0.1 μm	0	0	0.8	17.5
0.1 - 1 μm	0	33.3	13.5	61.7
1 - 10 μm	43.5	39.4	42.1	9.8
>10 μm	56.5	27.3	43.6	5.5
% volume of particles in size range:				
<0.1 μm	0	0	0	0.2
0.1 - 1 μm	0	0.02	0.02	0.2
1 - 10 μm	2.1	0.48	3	10.6
>10 μm	97.9	99.5	96.98	89
Roundness	0.67	0.63	0.61	0.65
	Rig: 6S Material:			
% number of particles in size range:	GUR 1020 XL	GUR 1020 XL AOX	GUR 1050 XL	GUR 1050 XL VE
<0.1 μm	57.3	2.4	2.8	1.7
0.1 - 1 μm	42.7	78	88.7	79.3
1 - 10 μm	0	17.1	8.5	19
>10 μm	0	2.5	0	0
% volume of particles in size range:				
<0.1 μm	9.1	0.2	0.01	0.02
0.1 - 1 μm	90.9	7.1	20.9	6.48
1 - 10 μm	0	60.3	79.09	93.5
>10 μm	0	32.5	0	0
Roundness	0.59	0.55	0.66	0.59

4.5.6.4 Comparison of size distribution, volume distribution and roundness of UHMWPE wear debris generated using the single and six station multidirectional pin-on-plate wear simulator rigs to literature values

The size and volume distribution data from the UHMWPE wear debris produced using the single station wear rig simulator during this study was compared, where possible, to identical data achieved in previous study by Ingram *et al.* (2004). Unfortunately, the author was unable to obtain like-for-like data for all materials except one (GUR 1050 XL). The study by Ingram *et al.* (2004) obtained size and volume distribution data for GUR 1050 XL 10 MRad against smooth (Ra ≈ 0.02 μm) and scratched (Ra ≈ 1 μm) CoCr plates. As there was no rough plate (Ra ≈ 0.08 – 0.09 μm) data available for direct comparison so the data for scratched plates was used. The study by Ingram *et al.* (2004) generated GUR 1050 XL UHMWPE wear debris with the majority of particles between 0.1 and 1 μm however the present study generated the majority of particles between 1 and 10 μm and >10 μm therefore the wear debris generated in the present study was significantly larger than the previous study by Ingram *et al.* (2004).

Table 4.19 Comparison of size distribution, volume distribution and roundness values of UHMWPE wear debris generated on single station wear rig simulators to literature values. In this case, N/A indicates that the data is not available.

	Rig: SS Material:			
% number of particles in size range:	GUR 1020 XL	GUR 1020 XL AOX	GUR 1050 XL	GUR 1050 XL VE
<0.1 μm	0	0	0.8	17.5
0.1 - 1 μm	0	33.3	13.5	61.7
1 - 10 μm	43.5	39.4	42.1	9.8
>10 μm	56.5	27.3	43.6	5.5
% volume of particles in size range:				
<0.1 μm	0	0	0	0.2
0.1 - 1 μm	0	0.02	0.02	0.2
1 - 10 μm	2.1	0.48	3	10.6
>10 μm	97.9	99.5	96.98	89
Roundness	0.67	0.63	0.61	0.65
	Literature Material:			
% number of particles in size range:	GUR 1020 XL	GUR 1020 XL AOX	GUR 1050 XL – 10 MRad – against a scratched plate (Ingram *et*	GUR 1050 XL VE

			al., 2004)	
<0.1 µm	N/A	N/A	0	N/A
0.1 - 1 µm	N/A	N/A	87	N/A
1 - 10 µm	N/A	N/A	13	N/A
>10 µm	N/A	N/A	0	N/A
% volume of particles in size range:				
<0.1 µm	N/A	N/A	0	N/A
0.1 - 1 µm	N/A	N/A	7	N/A
1 - 10 µm	N/A	N/A	56	N/A
>10 µm	N/A	N/A	37	N/A
Roundness	N/A	N/A	N/A	N/A

The size and volume distribution data from the UHMWPE wear debris produced using the six station wear rig simulator during this study was compared to identical data achieved in a previous study by Gowland (2014). Unfortunately, Gowland (2014) only provided size and volume distribution for GUR 102 XL AOX and GUR 1050 XL VE so no comparative data was obtained for GUR 1020 XL and GUR 1050 XL. Table 4.20 shows that GUR 1020 XL AOX materials in both studies yielded similar size and volume distribution data i.e. in both cases the majority of the particles were between 0.1 and 1 µm. However, Table 4.20 shows that the majority of GUR 1050 XL VE wear debris produced by Gowland (2014) was <0.1 µm whereas, in the present study, the majority of the wear debris was between 0.1 and 1 µm.

Table 4.20 Comparison of size distribution, volume distribution and roundness values of UHMWPE wear debris generated on six station wear rig simulators to literature values. In this case, N/A indicates that the data is not available.

	Literature			
	Material:			
% number of particles in size range:	GUR 1020 XL	GUR 1020 XL AOX (Gowland, 2014)	GUR 1050 XL	GUR 1050 XL VE (Gowland, 2014)
<0.1 µm	N/A	9	N/A	62
0.1 - 1 µm	N/A	68	N/A	35
1 - 10 µm	N/A	22	N/A	3
>10 µm	N/A	<1	N/A	<1
% volume of particles in size range:				
<0.1 µm	N/A	<1	N/A	<1
0.1 - 1 µm	N/A	5	N/A	26
1 - 10 µm	N/A	62	N/A	57
>10 µm	N/A	32	N/A	17
Roundness	N/A	N/A	N/A	N/A
	Rig: 6S			

	Material:			
% number of particles in size range:	GUR 1020 XL	GUR 1020 XL AOX	GUR 1050 XL	GUR 1050 XL VE
<0.1 μm	57.3	2.4	2.8	1.7
0.1 - 1 μm	42.7	78	88.7	79.3
1 - 10 μm	0	17.1	8.5	19
>10 μm	0	2.5	0	0
% volume of particles in size range:				
<0.1 μm	9.1	0.2	0.01	0.02
0.1 - 1 μm	90.9	7.1	20.9	6.48
1 - 10 μm	0	60.3	79.09	93.5
>10 μm	0	32.5	0	0
Roundness	0.59	0.55	0.66	0.59

4.6 Discussion

The aim of the chapter was to aseptically generate sterile UHMWPE wear debris (GUR 1020 XL, GUR 1020 XL AOX, GUR 1050 XL and GUR 1050 XL VE) for use in a novel *in vitro* model developed in Chapter 3 in order to assess the inflammatory and oxidative response to highly cross-linked and antioxidant doped, highly cross-linked UHMWPE wear debris. The secondary aim of this chapter was to compare the particle morphology and size and volume distribution of the particles generated to previous studies.

UHMWPE wear debris (GUR 1020 XL, GUR 1020 XL AOX, GUR 1050 XL and GUR 1050 XL VE) was aseptically generated using single and six station multidirectional POP wear simulators. UHMWPE pins (10 mm contact face) were articulated against rough (Ra 0.08 – 0.09 μm) ASTM 1537 low carbon CoCr plates at 160 N load, 28 mm stroke length and +/- 30° rotation at a speed of 1 Hz over five and three days; for single and six station multidirectional POP wear simulators, respectively. Rough plates were used to increase the wear factor and therefore maximise the volume of wear debris available for *in vitro* studies. The single station multidirectional POP wear simulator was chosen to generate the full size range of UHMWPE particles possible with which to dose cells. The six station multidirectional POP wear simulator rig was chosen to maximise the volume of debris produced in order to filter the debris and obtain a sufficient volume of particles within the critical size range necessary to activate macrophages (0.1 – 1 μm). All serum lubricants were assessed for microbiological and endotoxin contamination to ensure sterility for *in vitro* studies. Samples from each serum lubricant were pooled for each material produced on each type of rig and isolated using the digestion method established by Tipper *et al.* (2000,

2006) and Richards *et al.* (2008). The particles were then filtered onto 10 μm, 1 μm and 0.015 μm pore sized filter papers which were then imaged using FEGSEM. The images were subsequently analysed with ImageJ to assess the size and volume distribution of the particles generated.

Previous studies have shown that highly cross-linked UHMWPE materials produce significantly lower volumes of wear debris compared to their virgin, non-cross-linked counterparts (Endo *et al.*, 2001). Moreover, Gowland (2014) found that there was no significant difference in the wear performance between highly cross-linked UHMWPE materials and the equivalent materials that have been doped with antioxidants. Gowland (2014) demonstrated that the presence of antioxidants had no impact on the resistance of the material to wear.

Gowland (2014) generated UHMWPE using smooth (R_a <0.01 μm) CoCr plates in the six station multidirectional POP wear simulator. However, in order to maximise the volume of wear debris available for *in vitro* studies, this study utilised rough (R_a 0.08 – 0.09 μm) plates in the six station multidirectional POP wear simulator. Although Gowland used the same UHMWPE materials (with the exception of GUR 1020 XL), a direct comparison between the two studies is not possible due to the difference in surface roughness of the plates used. However, Ingram *et al.* (2004) compared the wear factors produced by various UHMWPE materials articulated against scratched (R_a 1 μm) and smooth (R_a 0.02 μm) CoCr plates on a single station multidirectional POP wear simulator and found that the wear factor of GUR 1050 XL UHMWPE (10 MRad) articulated against a scratched CoCr plate was 1 x 10^{-7} $mm^3.Nm^{-1}$. This wear factor is 10 times lower than the equivalent mean wear factor observed for GUR 1050 XL against a rough (R_a 0.07 – 0.08 μm) plate on the single station multidirectional POP wear simulator. It is known that the use of rough rather than smooth plates increases the volume of wear debris produced and may impact the size and volume distribution of the particles produced (Endo *et al.*, 2001). Additionally Endo *et al.* (2001) found that cross-linked UHMWPE produced significantly higher wear rates against rough CoCr plates than non-cross-linked UHMWPE.

Previous studies have found that wear debris volumes and wear factors produced by the different UHMWPE materials on each type of rig were similar however this was not consistent with the values observed during this study. The volume of wear debris produced was higher than expected. This was particularly true for GUR 1020 XL AOX UHMWPE wear debris generated on the single station multidirectional POP wear simulator (mean 37.48 ± 28.82). This was also the case for all wear debris volumes for all materials generated on the six station multidirectional POP wear simulator, which were between 10 and 100 times higher than the volumes observed on the single station multidirectional POP wear simulator. There was no similarity or consistency

between the values for each material on different rigs or each material when compared to each other material; although there were no significant differences between the values from the single (ANOVA; $p > 0.05$) and six station multidirectional POP wear simulators (ANOVA; $p > 0.05$). The standard error bars on Figures 4.14 and 4.15 were large and may account for this lack of significance. Similarly, the wear factors observed during this study were higher than expected and there was no similarity or consistency between the values for each material on different rigs or each material when compared to each other material. Again, there was a large margin of error for all mean wear factor values which may account for the lack of consistency. Gowland (2014) reported wear factor values between 1.9 and 2.5 x 10^{-7} $mm^3.Nm^{-1}$ for GUR 1050 XL, GUR 1050 XL VE and GUR 1020 XL AOX UHMWPE pins on smooth CoCr plates on the six station multidirectional POP wear simulator. This study demonstrated wear factors between 100 and 1000 times higher (1.2 x 10^{-4} and 7.5 x 10^{-5} $mm^3.Nm^{-1}$) for UHMWPE pins on rough CoCr plates on the six station multidirectional POP wear simulator. The wear factor values obtained from the single station multidirectional POP wear simulator were lower than those obtained on the six station multidirectional POP wear simulator although these values were still between 10 and 100 times higher (2.1 x 10^{-5} and 3.9 x 10^{-6} $mm^3.Nm^{-1}$) than those reported by Gowland (2014). It was not possible to compare wear factor values for GUR 1020 XL as Gowland (2014) did not include this material in the study due to lack of availability.

Although statistical analysis showed that the differences between the wear debris volumes and wear factors of each material on each type of rig were not significantly different when compared to each other (ANOVA; $p > 0.05$), there is a large margin of error for each of the values. There are several possible explanations for the higher volumes of wear debris, increased wear factors and large margins of error observed in this study.

It is possible that there may have been some differences between the roughness of individual plates used in the study, however the range of surface roughness used was small, so this is unlikely. Surface roughness measurements were not obtained as the primary aim was to produce wear debris for *in vitro* studies rather than a detailed investigation into the mechanical properties of the materials involved. This was a potential oversight and such measurements may have contributed to an explanation for the unusual material behaviour observed in this study.

The age and storage of the UHMWPE bar stock used to create the pins may have impacted the wear debris volumes and wear factors observed during this study. Since there was no industrial collaborator for this study, the bar stocks used to cut the pins were remnants of previous studies stored on the shelf in the Technicians Office in the School of Mechanical Engineering. Each material had been stored in air this way for

several years; for example, the GUR 1050 XL VE bar stock was sourced in 2009. Storage in air, i.e. oxidising conditions, is sub-optimal and may lead to oxidative embrittlement of the UHMWPE (Besong *et al.*, 1997). Oxidative embrittlement reduces the wear resistance of UHMWPE, thus increasing the wear factor and volume of wear debris produced, as free radicals trapped within the polymer structure from cross-linking irradiation, such as ROS, can cause polymer chain scission (Wannomae *et al.*, 2006). Bar stock stored this way may exhibit differences when pins are cut from the edge of the bar stock (exposed to the air) and the centre of the bar stock (somewhat protected from the air). UHMWPE bar stock should be vacuum packed and stored at – 80 °C to prevent oxidation.

As highly cross-linked GUR 1020 and GUR 1050 bar stock was not directly available for this study, the virgin, non-cross-linked GUR 1020 and GUR 1050 available was sent to be commercially irradiated to provide highly cross-linked UHMWPE materials. Pins were cut from the virgin bar stock and vacuum packaged at the University of Leeds prior to being sent to Synergy Health PLC for commercial gamma irradiation. The dose range was specified as 9 – 11.5 MRad and the pins received an approximate dose of 9.39 MRad in order to provide UHMWPE comparable to clinical materials GUR 1050 XL (10 MRad) and GUR 1020 XL (8 MRad). A food grade vacuum sealer was used to package the pins. As the apparatus was not adapted for this purpose, it was difficult for the candidate to achieve a good seal. This may have resulted in the presence of air during the irradiation process which may have lead to oxidation of the pins. Moreover, post-irradiation annealing or remelting was not carried out to remove any free radicals present. It was not known whether the GUR 1020 XL AOX and GUR 1050 XL VE materials underwent post-irradiation annealing or remelting. Remelting involves taking the UHMWPE above its melting point in order to allow the removal of any residual free radicals. Since the temperature is above the materials melting point, all the different regions of the polymer, including the crystalline regions, are melted and it is made certain that the polymer does not contain any free radicals (Wang *et al.*, 2006). However this is at a detriment to the wear resistance of the material which is related to the level of crystallinity of the polymer. Whereas, annealing only exposes the polymer to temperatures below its melting point so does not have this detrimental impact on mechanical properties. However the crystalline regions remain during this process so any residual free radical trapped here will remain in the material and may continue to propagate and react oxidatively with the polymer after irradiation (Wang *et al.*, 2006). Since, it is not known which of these processes, if any, the GUR 1020 XL AOX and GUR 1050 XL VE materials have been exposed to, it is difficult to pinpoint their effects. However it is clear that remelting impacts the mechanical properties of UHMWPE and therefore could impact the resistance to wear resulting in higher wear factors than expected. Additionally,

annealing preserves mechanical properties and therefore the resistance to wear but this may be negated by the continued existence of highly oxidising species within the polymers crystalline structure which can go on to react with polymer well beyond irradiation over the course of years of being stored on the shelf. The deterioration of the material in this way would also reduce the materials resistance to wear over time.

Finally the differences between the wear debris volumes and wear factors from the same materials across the single and six station multidirectional POP wear simulators may be explained by the difference in lubrication regimes between the two types of simulators. The single station multidirectional POP wear simulator is run with RPMI cell culture medium with 25% (v/v) FBS. The presence of FBS mimics the proteins present in synovial fluid that coat wear particles. Whereas the six station multidirectional POP wear simulator is run with RPMI cell culture medium only; i.e. no proteins are added. Sodium azide is often added in such studies to prevent microbial contamination however sodium azide is highly toxic to cells and was not used during this study. Although it is not ideal for replicating conditions *in vivo*, UHMWPE wear debris was generated without FBS to allow fluorescent staining of the particles for microscopy. The presence of FBS changes the lubrication regime of the single station multidirectional POP wear simulator compared to the six station multidirectional POP wear simulator. In RPMI with 25% (v/v) FBS, proteins coat the UHMWPE pin and produce a protective effect i.e. the pin becomes more resistant to wear as the protein layer is sheared prior to the pins contact face (Fröhlich *et al.*, 2014). This reduces the wear factor and volume of wear debris produced. Whereas the six station multidirectional POP wear simulator is operated without the presence of FBS so there is no protective effect created by protein adhesion to the pins. This results in larger volumes of wear debris produced and increased wear factors; similar to UHMWPE pins run in water (the UHMWPE pins become fractured and fatigued). This may account for the differences between the volumes of wear debris and wear factor values observed for each material on each different type of rig.

All UHMWPE wear debris generated was free from microbiological contamination and contained sufficiently low levels of endotoxin (>0.5 $EU.ml^{-1}$); >5 $EU.ml^{-1}$ is recommended by FDA regulatory affairs (1985) for injectable pharmaceuticals to be declared endotoxin-free and sterile. This is consistent with previous studies that have operated both the single and six station multidirectional POP wear simulators under aseptic conditions to generate UHMWPE wear debris (Liu, 2012; Gowland, 2014) This step is necessary to ensure that any cellular response *in vitro* is caused by the particles only rather than any other contaminating material. Previous studies have shown that endotoxin contamination of orthopaedic particulates can induce an increased release of pro-inflammatory cytokines, such as TNF-α (Brooks, Wimhurst

and Rushton, 2002). However, some of the optical density values were below the lowest endotoxin standard and should have been re-assayed in order to be certain that the wear debris produced was indeed free of endotoxin contamination.

FEGSEM images of the UHMWPE wear particles produced on both the single and six station multidirectional POP wear simulators displayed various particle morphologies across all the different types of UHMWPE used: platelet-like particles, small granules and aggregated particles. The particle morphologies observed were consistent from both types of wear simulators. These particle morphologies were consistent with those observed in the previous study by Gowland (2014) using both wear simulators and identical UHMWPE materials (except GUR 1020 XL). Although the particle morphologies observed in this study are consistent with the particle morphologies observed by Tipper *et al.* (2000) in UHMWPE wear debris from retrieved Charnley hip prostheses, the full range of different shapes demonstrated by Tipper et al. (2000) was not observed. For example, no fibril particles were observed. Most materials used to generate particles on the single station multidirectional wear simulator rig demonstrated particles in all size ranges as was demonstrated by Tipper et al (2000) in the retrieval study of Charnley prostheses, however no particles were found in the ranges <0.1 and 0.1 -1 μm for the GUR 1020 XL material. Similarly, no particles were found in the range <0.1 μm for the GUR 1020 XL AOX material. This lack of representation of these size ranges indicates that the samples may not be representative of the wide range of particles sizes produced *in vivo*. Endo *et al.* (2001) demonstrated that UHMWPE pins articulated against rough CoCr plates produced larger particles which may explain why the materials used generated less or no particles in the smaller size ranges. Particles generated on the six station multidirectional wear simulator rig also demonstrated a lack of >10 μm particles for all materials except GUR 1020 XL AOX and a lack of 1 – 10 μm particles for GUR 1020 XL. Since particles generated using the six station multidirectional wear simulator rig went on to be filtered into the range 0.1 – 1 μm, the lack of representation for larger sizes was not a relevant issue. It is not clear why larger particle sizes were not observed using the six station multidirectional wear simulator rig compared to the single station multidirectional wear simulator rig which demonstrated a lack of smaller particles. It is possible that the difference in lubrication regime between the rigs was a contributory factor. The single station multidirectional wear simulator rig used RPMI medium and 25% (v/v) FBS whereas the six station multidirectional wear simulator rig used RPMI medium only. The presence of proteins in FBS change the lubrication regime as discussed before and may contribute to the size of particles produced (Fröhlich *et al.*, 2014).

There were a number of limitations to this study. Since the primary objective of this chapter was not to determine wear performance data for the materials used, certain measurements were not obtained. The surface roughness of the CoCr plates used were not obtained using Talysurf before and after runs. This may have provided further insight as to the unusually high wear debris volumes and wear factors observed during this study. Moreover, EDX analysis of the UHMWPE wear debris was not performed when obtaining FEGSEM images of the particles. The primary limitations to this study were the age and storage conditions of the UHMWPE materials used. The shelf aging in oxidative conditions over several years could have decreased the wear resistance of the UHMWPE materials and resulted in the high volume of wear debris and large wear factors observed. It would have been useful to compare the wear volumes of the UHMWPE pins used in this study before and after irradiation treatment, in order to assess whether the irradiation treatment contributed to the high wear volumes or not. Similarly, it would have been useful to compare wear volumes generated using rough and smooth CoCr plates in order to assess the impact of plate roughness on the high wear volumes seen in this study. Future studies would be improved by obtaining fresh UHMWPE bar stock or pins from industrial collaborators. Additionally, the correct storage of UHMWPE materials in vacuum packaging at -80°C to prevent oxidation would remove shelf aging and oxidation as a potential variable in future studies.

The size and volume distribution values generated by each material on each type of rig simulator were compared, where possible, to data available in the literature or previous studies for wear debris from the same materials on the same type of rig simulator. However, much of the necessary comparative data was not available; meaning a full comparison was not always possible and thus it was difficult to ascertain a full picture of how the wear debris produced in this study compared to previous work. In order to assess the clinical relevance of the wear debris produced in this study, it would be necessary to compare the wear debris produced here to the wear debris from identical materials isolated during retrieval studies. However, as both cross-linked and (in particular) antioxidant doped cross-linked UHMWPE are relatively new clinically and retrieval studies are long term (>10 years), the necessary retrieval data is not available for comparison. As such, it is not possible to comment on the clinical relevance of the wear debris produced in this study.

4.7 Conclusions

- Sufficient volumes of GUR 1020 XL, GUR 1020 XL AOX, GUR 1050 XL and GUR 1050 XL VE UHMWPE wear debris were generated using both the single and six station multidirectional POP wear simulator rigs for use in the *in vitro*

cell culture studies to be performed later in the study. This was confirmed by the high volumes of wear debris and large wear factors reported in Section 4.5.

- Microbiological and endotoxin testing of the serum lubricants produced confirmed particle sterility, i.e. the particles did not exhibit any biological or endotoxin contamination.
- A pooled sample of each material (GUR 1020 XL, GUR 1020 XL AOX, GUR 1050 XL and GUR 1050 XL VE) from each rig was isolated and imaged to assess particle morphology. Typical particle morphologies, such as large platelets, small granules and aggregate particles, were observed across all samples although all possible morphologies found in previous retrieval studies were not found during this study. Particles produced on the single station multidirectional wear simulator were generally larger than those produced on the six station multidirectional wear simulator although larger particles represented a significant volume of the particles produced in both cases. The size and volume distribution of the particles produced in this study did not match the literature values of equivalent materials (where possible to obtain).

Chapter 5
Assessing the anti-inflammatory and antioxidant effects of antioxidant doped, highly cross-linked ultra-high molecular weight polyethylene wear debris using a novel 3D *in vitro* model

5.1 Introduction

Metal on polyethylene (MOP) remains the gold standard THR to the present day and represent 30.4% of all primary THR's (National Joint Registry, 2017). It is well documented that the biological response to polyethylene wear debris produced by MOP THR's is linked to osteolysis and, ultimately, aseptic loosening which is responsible for 50.1% of all revision surgeries in 2017 (National Joint Registry, 2017). Polyethylene has since been modified by cross-linking in order to reduce the volume of wear debris produced (Galvin *et al.*, 2006). Antioxidants, such as vitamin E and hindered phenols, can also be added to quench free radicals and remove the need for remelting or annealing which can reduce the mechanical properties (such as strength and fatigue resistance) of polyethylene (Oral, Malhi and Muratoglu, 2006). Vitamin E is known for its well documented anti-inflammatory effects in cardiovascular disease (Devaraj, Li and Jialal, 1996) and rheumatoid arthritis (De Bandt *et al.*, 2002). Singh and Jialal (2004) showed that treatment of monocytes with vitamin E reduced the release of pro-inflammatory cytokines linked to osteolysis; TNF-α, IL-1β, IL-6. Another study by Devaraj and Jialal (1999) examined the effects of vitamin E on the production of common inflammatory mediators, LTB_4 and PGE_2, in PBMNC's. Devaraj and Jialal (1999) showed that the presence of vitamin E significantly reduced the production of LTB_4 but had no effect of the production of PGE_2 in LPS-stimulated PBMNC's. Devaraj and Jialal (1999) utilised Calphostin C, Bisindolylmaleimide I, Indomethacin, MK 886 and REV 5901 to examine the effects of vitamin E on the inhibition of IL-1β production via the interaction with one of three possible inflammatory pathways: cyclooxygenase (COX), lipooxygenase (5-LO) or protein kinase C (PKC). COX and 5-LO are enzymes involved the production of prostaglandins and leukotrienes, respectively, which are mediators in the cascade of reactions that constitute inflammation. Similarly PKC, which is a family of enzymes that catalyse phosphorylation, also has a role in inflammation (Devaraj and Jialal, 1999). Calphostin C and Bisindolylmaleimide I are inhibitors of PKC, Indomethacin is an inhibitor of COX and MK 886 and REV 5901 are inhibitors of 5-LO.

Bladen *et al.* (2013b) showed that the release of TNF-α, IL-1β and IL-6 were significantly increased (there was no significant effect on the release of IL-8) in

PBMNC's in response to GUR 1050 non-cross-linked UHMWPE compared to the cells only control. However, the release of these cytokines was significantly reduced in response to GUR 1050 VE (3000 and 30,000 ppm) UHMWPE wear debris when compared to GUR 1050 UHMWPE wear debris. However, Bladen *et al.* (2013a) used non-clinical doses of vitamin E to assess cytokine release. Bladen *et al.* (2013b) subsequently showed that GUR 1050 VE (1000 ppm), a clinically relevant dosed material, did exhibit the same reduction in TNF-α however the effect on IL-1β and IL-6 was not assessed with the clinically relevant dose of vitamin E. Moreover, Bladen *et al.* (2013a) did not test highly cross-linked material so it is unclear whether these responses would be repeated with a clinically relevant GUR 1050 XL VE material (1000 ppm). Bladen *et al.* (2013b) also stimulated both PMA-activated U937 human histiocytes and PBMNC's with LPS and, after 3 hours, treated the cells with antioxidant compounds vitamin E (800 μM) and hindered phenol (25 μM) to observe the effect on TNF-α release. Bladen *et al.* (2013a) found that both vitamin E and hindered phenol significantly reduced the release of TNF-α in U937 human histiocytes but only vitamin E significantly reduced the release of TNF-α in PBMNC's. This study demonstrated the potential of antioxidant compounds to exhibit anti-inflammatory activity in a periprosthetic environment however, this study used the antioxidant compounds in isolation rather than blended or diffused UHMWPE as is clinically revelant. There is some debate as to whether vitamin E is freely available in blended UHMWPE (as it is added prior to consolidation and can be grafted into the polymer backbone) in addition to how much vitamin E is capable of leaching from a diffused UHMWPE material (as the consolidated UHMWPE is soaked in a concentrated vitamin E solution).

This study has developed a novel 3D *in vitro* model (RAW 264.7 murine macrophages simultaneously encapsulated with polyethylene particles in collagen gel) as a more accurate representation of the periprosthetic environment than previous 2D models. The novel model requires comparison to the outcomes of previous studies in order to attempt to assess how much value it has for future studies. Liu (2012) used UHMWPE wear debris in the size range 0.1 – 0.6 μm to produce significant TNF-α release in PBMNC's which was consistent with the critical size range necessary for macrophage response demonstrated by Green *et al.* (1998) whereas Gowland (2014) used the full size range of particles generated as this was more clinically representative of the particles found in the *in vivo* periprosthetic environment (Tipper *et al.*, 2000). The aim of this study was to challenge the novel 3D model with both representations of particle sizes: the full size range generated using the single station multidirectional POP wear simulator known to successfully produce representative, sterile UHMWPE wear debris (Ingram *et al.*, 2004) and particles filtered into the critical size range 0.1 – 1 μm, known to activate macrophages, generated using the six station multidirectional POP

wear simulator known to successfully produce representative, sterile UHMWPE wear debris (Liu, 2012). This study aimed to assess the impact of both of these particle size ranges on known inflammatory and osteolytic mediators: TNF-α, IL-1β, IL-6, IL-8 (KC), LTB_4 and PGE_2. Mice do not express IL-8 but they do express a homologue known as keratinocyte derived chemokine (KC) which was measured instead. This study also aimed to assess the impact of both of these particle size ranges on the intracellular concentrations of ROS. Additionally, this study intended to compare the ability of RAW 264.7 murine macrophages to uptake and sequester UHMWPE wear particles to the known ability of PBMNC's to uptake and sequester UHMWPE particles around the nucleus. Finally, the study aimed to use the novel model to assess the effect of inflammatory pathway inhibitors (Calphostin C, Bisindolylmaleimide I, Indomethacin, MK 886 and REV 5901) and antioxidant compounds (Vitamin E and Pentaerythritol tetrakis (3,5-di-*tert*-butyl-4-hydroxyhydrocinnamate)) on the release of osteolytic mediators: TNF-α, IL-1β, IL-6, LTB_4 and PGE_2 in order to ascertain by which pathway any potential anti-inflammatory activity, displayed in previous studies, may be acting.

5.2 Aims and objectives

5.2.1 Aims

The overall aim of this chapter was to use the novel 3D *in vitro* model generated in Chapter 3 (RAW 264.7 murine macrophages in collagen gel) to measure the cellular response to antioxidant doped, highly cross-linked ultra-high molecular weight polyethylene wear debris and compare this data to data generated using previous 2D *in vitro* models. The model was tested in a number of circumstances from previous studies in order to ascertain whether the model was capable of reproducing their effects and may therefore be of future use.

5.2.2 Objectives

The objectives of this chapter were as follows:

- To assess the production of TNF-α, IL-1β, IL-6, IL-8 (KC), LTB_4 and PGE_2 in response to the full range of particle sizes of antioxidant-doped, highly cross-linked UHMWPE generated on the single station wear simulator rig and antioxidant-doped, highly cross-linked UHMWPE particles generated on the six station wear simulator rig which had been filtered into the critical size range necessary for macrophage activation (0.1 μm – 1 μm).
- To assess the cellular oxidative stress response to the full range of particle sizes of antioxidant-doped, highly cross-linked UHMWPE generated on the single station wear simulator rig and antioxidant-doped, highly cross-linked UHMWPE particles generated on the six station wear simulator rig which had

been filtered into the critical size range necessary for macrophage activation (0.1 µm – 1 µm).

- To stimulate the novel *in vitro* model with LPS and then, after 3 hours, dose the novel *in vitro* model with inhibitors of the COX pathway (indomethacin), 5-LO pathway (MK 886 and REV 5901) and PKC pathway (Calphostin C and Bisindolylmaleimide I) and antioxidant compounds (Vitamin E and Pentaerythritol tetrakis(3,5-di-*tert*-butyl-4-hydroxyhydrocinnamate)) in order to assess the resultant cytokine output of TNF-α, IL-1B, IL-6, LTB_4 and PGE_2.
- To assess the internal sequestration of UHMWPE wear debris in RAW 264.7 murine macrophages in the novel *in vitro* model compared to PBMNC's used in the previous model.

5.3 Materials

The materials used throughout Chapter 5 are detailed in the following section. Any general materials used are listed in Chapter 2.

5.3.1 Chemicals and reagents

The chemicals and reagents used throughout Chapter 5 are detailed in Table 5.1. Any general chemicals and reagents are detailed in Chapter 2, Section 2.1.1.

Table 5.1 Chemicals and reagents used throughout Chapter 5.

Chemical/reagent	Supplier	Storage and preparation
Bisindolylmaleimide I	AdipoGen life sciences, California, USA.	Stored at -20°C and prepared by dissolving 1 mg in 1 ml DMSO.
Calphostin C	Santa Cruz Biotechnology Inc., Texas, USA.	Stored at -20°C and prepared by dissolving 100 µg in 1 ml DMSO.
DCFDA cellular ROS detection assay kit	Abcam, Cambridge, UK.	Stored at 4°C.
DMEM – phenol red free	Sigma Aldrich, Dorset, UK.	Stored at 4°C.
Hoechst® 33342	ThermoFisher Scientific UK, Loughborough, UK.	Stored at -20°C and prepared by dissolving 100 mg in 10 ml

		deionised water.
Indomethacin	Sigma Aldrich, Dorset, UK.	Stored at 25°C and prepared by dissolving 10 mg in 1 ml DMSO.
Lysotracker red DND-99	ThermoFisher Scientific UK, Loughborough, UK.	Stored at -20°C.
MK 886	Cayman chemical, Michigan, USA.	Stored at -20°C and prepared by dissolving 1 mg in 1 ml DMSO.
Pentaerythritol tetrakis(3,5-di-*tert*-butyl-4-hydroxyhydrocinnamate)	Sigma Aldrich, Dorset, UK.	Stored at 25°C.
RayBio® Mouse KC ELISA kit – 1 x 96 well plate	RayBio®, Georgia, USA.	Stored at -20°C.
R&D® Parameter ™ LTB_4 assay – 1 x 96 well plate	R&D® Systems, Minneapolis, USA.	Stored at -20°C.
R&D® Parameter ™ PGE_2 assay – 1 x 96 well plate	R&D® Systems, Minneapolis, USA.	Stored at -20°C.
REV 5901	Cayman chemical, Michigan, USA.	Stored at -20°C and prepared by dissolving 5 mg in 1 ml DMSO.
Sodium fluorescein	Santa Cruz Biotechnology Inc., Texas, USA.	Stored at room temperature (25°C).
Vitamin E – dl- α-tocopherol acetate – 500 mg/ml	Merck, Germany	Stored at 25°C.

5.3.2 Consumables

The consumables used throughout Chapter 5 is detailed in Table 5.2. Any general consumables are detailed in Chapter 2, Section 2.1.2.

Table 5.2 Consumables used throughout Chapter 5.

Consumable	Size	Supplier
Corning cell culture spatulas	N/A	Fisher Scientific UK, Loughborough, UK.
Glass cover slips	22 mm	Menzel Gläser, Gerhard Menzel GmbH, Germany.
Glass slides	76 x 26 mm	Menzel Gläser, Gerhard Menzel GmbH, Germany.

5.3.3 Equipment

The equipment used throughout Chapter 5 is detailed in Table 5.3. Any general equipment is detailed in Chapter 2, Section 2.1.3.

Table 5.3 Equipment used throughout Chapter 5.

Equipment	Supplier
Zeiss Axio Imager M2	Carl Zeiss, UK.

5.3.4 Software

The software used throughout Chapter 5 is detailed below in Table 5.4.

Table 5.4 Software used throughout Chapter 5.

Software	Supplier
Zen lite	Carl Zeiss, UK.

5.4 Methods

5.4.1 Reagents and solutions preparation

5.4.1.1 Antioxidant compounds

5.4.1.1.1 Pentaerythritol tetrakis(3,5-di-tert-butyl-4-hydroxyhydrocinnamate)

Stock solution

A stock solution of Pentaerythritol tetrakis(3,5-di-tert-butyl-4-hydroxyhydrocinnamate) was prepared by adding 10 mg Pentaerythritol tetrakis(3,5-di-tert-butyl-4-hydroxyhydrocinnamate) to 1 ml DMSO. This stock solution was kept at -20°C between uses. This was filter sterilised as described in Chapter 2, Section 2.2.1.5.

5.4.1.2 Inflammatory pathway inhibitors

5.4.1.2.1 Bisindolylmaleimide I

Stock solution

A stock solution of Bisindolylmaleimide I was prepared by adding 1 mg Bisindolylmaleimide I to 1 ml DMSO. This stock solution was kept at -20°C between uses. This was filter sterilised as described in Chapter 2, Section 2.2.1.5.

5.4.1.2.2 Calphostin C

Stock solution

A stock solution of Calphostin C was prepared by adding 100 µg Calphostin C to 1 ml DMSO. This stock solution was kept at -20°C between uses. This was filter sterilised as described in Chapter 2, Section 2.2.1.5.

5.4.1.2.3 Indomethacin

Stock solution

A stock solution of Indomethacin was prepared by adding 10 mg Indomethacin to 1 ml DMSO. This stock solution was kept at -20°C between uses. This was filter sterilised as described in Chapter 2, Section 2.2.1.5.

5.4.1.2.4 MK 886

Stock solution

A stock solution of MK 886 was prepared by adding 1 mg MK 886 to 1 ml DMSO. This stock solution was kept at -20°C between uses. This was filter sterilised as described in Chapter 2, Section 2.2.1.5.

5.4.1.2.5 REV 5901

Stock solution

A stock solution of REV 5901 was prepared by adding 5 mg REV 5901 to 1 ml DMSO. This stock solution was kept at -20°C between uses. This was filter sterilised as described in Chapter 2, Section 2.2.1.5.

5.4.1.3 Fluorescent microscopy stains

5.4.1.3.1 Hoechst® 33342

Stock solution

A stock solution of Hoechst 33342 was prepared by weighing out 10 mg of Hoechst 33342 and adding to 1 ml DPBS. This was covered in foil and kept at -20°C in between uses. This was filter sterilised as described in Chapter 2, Section 2.2.1.5.

Working solution

A working solution of Hoechst 33342 was prepared by adding 1 µl of 10 $mg.ml^{-1}$ stock solution to 1999 µl DPBS to create a 1:2000 working solution.

5.4.1.3.2 Lysotracker red DND-99

Working solution

A working solution of Lysotracker red (75 nM) was created by adding 0.75 µl lysotracker red to 10 ml complete DMEM. This was filter sterilised as described in Chapter 2, Section 2.2.1.5.

5.4.1.3.3 Sodium fluorescein

Stock solution

A stock solution (1 $mg.ml^{-1}$) of sodium fluorescein was prepared by adding 10 mg of sodium fluorescein to 10 ml sterile ultrapure water. This was filter sterilised as described in Chapter 2, Section 2.2.1.5.

5.4.2 Cytokine release in RAW 264.7 murine macrophages in response to UHMWPE wear debris in collagen gel

RAW 264.7 murine macrophages were passaged and counted as described in Chapter 2, Sections 2.2.5.4 and 2.2.8.3. The doses of single and six station generated UHMWPE wear debris (GUR 1020 XL, GUR 1020 XL AOX, GUR 1050 XL and GUR 1050 XL VE) and FluoSphere® particle control were calculated as described in Chapter 2, Sections 2.2.6.2 and 2.2.6.3. RAW cells were seeded at 1 x 10^5 $cells.ml^{-1}$ with 100 $\mu m^3.cell^{-1}$ particles in collagen gels in 48 well tissue culture plates as described in Chapter 2, Section 2.2.7.2. The gels were allowed to set and the plates were incubated at 37°C and 8% (v/v) CO_2 in air. The ATP-lite™ viability assay was carried out at 12 and 24 hours. After 12 and 24 hours, the supernatant was removed

and placed in the corresponding wells of a Nunc F uncoated plate which was frozen at -80°C until use in ELISA. The ATP-lite™ viability assay was then carried out as described in Chapter 2, Section 2.2.8.1. The supernatants were later defrosted and used to carry out TNF-α, IL-1β, IL-6, KC, LTB_4 and PGE_2 ELISA as described in Chapter 2, Section 2.2.8.2.

5.4.3 Cytokine release of LPS-stimulated RAW 264.7 murine macrophages in response to inflammatory pathway inhibitors and antioxidant compounds in collagen gel

Inhibitor growth curve

RAW 264.7 murine macrophages were passaged and counted as described in Chapter 2, Sections 2.2.5.4 and 2.2.8.3. RAW cells were seeded at 5 x 10^4 cells.ml^{-1} in a 96 well tissue culture plate. Each well was filled with 200 µl complete DMEM containing the following concentrations of inflammatory pathway inhibitors (n=3): Bisindolylmaleimide I (0.1, 1, 10 and 100 µmol.L^{-1}), Calphostin C (100 nmol.L^{-1}, 250 nmol.L^{-1}, 500 nmol.L^{-1}, 1 µmol.L^{-1}), Indomethacin (0.1, 1, 10 and 100 µmol.L^{-1}), MK 886 (0.1, 1, 10 and 100 µmol.L^{-1}) and REV 5901 (1, 10, 100 and 1000 µmol.L^{-1}). The plates were incubated at 37°C and 8% (v/v) CO_2 in air and the ATP-lite™ viability assay was carried out at days 0, 1 and 3 as described in Chapter 2, Section 2.2.8.1.

Antioxidant growth curve

RAW 264.7 murine macrophages were passaged and counted as described in Chapter 2, Sections 2.2.5.4 and 2.2.8.3. RAW cells were seeded at 5 x 10^4 cells.ml^{-1} in a 96 well tissue culture plate. Each well was filled with 200 µl complete DMEM containing the following concentrations of antioxidants (n=3): Vitamin E (400 µmol/L, 800 µmol.L^{-1}, 1 mmol.L^{-1}, 2 mmol.L^{-1}, 3 mmol.L^{-1} and 5 mmol.L^{-1}) and Pentaerythritol tetrakis(3,5-di-*tert*-butyl-4-hydroxyhydrocinnamate) (12.5, 25, 50, 100, 300 and 500 µmol.L^{-1}). The plates were incubated at 37°C and 8% (v/v) CO_2 in air and the ATP-lite™ viability assay was carried out at days 0, 1 and 3 as described in Chapter 2, Section 2.2.8.1.

LPS stimulated RAW 264.7 murine macrophages in collagen gel dosed with inflammatory pathway inhibitors and antioxidant compounds

RAW 264.7 murine macrophages were passaged and counted as described in Chapter 2, Sections 2.2.5.4 and 2.2.8.3. RAW cells were seeded at 1 x 10^5 cells.ml^{-1} in collagen gels in 48 well tissue culture plates as described in Chapter 2, Section 2.2.7.2. Each well was then filled with 200 µl complete DMEM containing LPS (200 ng.ml^{-1}). Cells only (no LPS), medium only and cells plus DMSO (200 µl.ml^{-1}) (no LPS) controls were included. Gels were allowed to set and the plates were placed in the incubator at 37°C and 8% (v/v) CO_2 in air for 3 hours. After 3 hours, the plates were

removed from the incubator and the following inflammatory pathway inhibitors and antioxidant compounds were added (n=3): Calphostin C (250 and 500 nmol.L^{-1}), Bisindolylmaleimide I (0.1 and 1 µmol.L^{-1}), Indomethacin (0.1, 1, 10 and 100 µmol.L^{-1}), MK 886 (0.1, 1, 10 and 100 µmol.L^{-1}), REV 5901 (1, 10, 100 and 1000 µmol.L^{-1}), Vitamin E (800 µmol.L^{-1}) and Pentaerythritol tetrakis(3,5-di-tert-butyl-4-hydroxyhydrocinnamate) (25 µmol.L^{-1}). The plates were incubated at 37°C and 8% (v/v) CO_2 in air for 24 hours. After 24 hours, the supernatants were removed from each well and placed in the corresponding wells of a Nunc F uncoated plate which was stored at -80°C until use in ELISA. The ATP-lite™ viability assay was then carried out as described in Chapter 2, Section 2.2.8.1. The supernatants were later defrosted and used to carry out TNF-α, IL-1β, IL-6, LTB_4 and PGE_2 ELISA as described in Chapter 2, Section 2.2.8.2 .

5.4.4 Detection of cellular reactive species in RAW 264.7 murine macrophages in response to UHMWPE wear debris in collagen gel

Table 5.5 Abcam DCFDA cellular ROS detection assay kit components storage and preparation details.

Abcam DCFDA cellular ROS detection assay kit components	Storage and preparation
DCFDA in DMSO (20 mM) – 35 µl	Diluted 20 µl of DCFDA (20 mM) with 3980 µl 1X buffer to create 100 mM DCFDA working solution. Stored at 4°C.
10X buffer - 10 ml	Diluted 10 ml 10X buffer with 90 ml deionised water to created 1X buffer. Stored at 4°C.
TBHP (55 mM) – 50 µl	A working solution (5 mM) of DCFDA was assembled by diluting 13.6 µl TBHP with 136.4 µl 1X buffer. Stored at 4°C.

RAW 264.7 murine macrophages were passaged and counted as described in Chapter 2, Sections 2.2.5.4 and 2.2.8.3. Single and six station multidirectional POP wear simulator generated UHMWPE wear debris particle doses were calculated as described in Chapter 2, Section 2.2.6.2 and 2.2.6.3. RAW cells were seeded at 1 x 10^5 cells.ml^{-1} with 100 μm^3 particles.$cell^{-1}$ in collagen gels in 96 well tissue culture plates with a 50 µl gel plug per well as described in Chapter 2, Section 2.2.7.2. Cells plus FluoSpheres® (100 μm^3.$cell^{-1}$), cells only, cells plus DMSO (200 µl.ml^{-1}), cells plus LPS 200 ng.ml^{-1}) and cells plus TBHP (5 mM) controls were also included. After

20 hours (4 hours prior to measurement), 11 µl of TBHP working solution (5 mM) was added to each well of the cells plus TBHP (250 µM) control. After 23 hours 15 minutes (45 minutes prior to measurement), 50 µl of DCFDA working solution (100 µM) was added to each well (25 µM). After 24 hours, the contents of the well plate were then immediately read at 535 nm using a Multiskan plate reader. The results were analysed relative to the cells only control.

5.4.5 Fluorescent microscopy imaging of RAW 264.7 murine macrophages incubated with UHMWPE wear debris in collagen gel

Six station generated UHMWPE wear debris (GUR 1020 XL, GUR 1020 XL AOX, GUR 1050 XL and GUR 1050 XL VE) was filtered into the size range 0.1 – 1 µm as described in Chapter 2, Section 2.2.6.3. The resultant filter papers were placed into sterile glass vials and the wear particles resuspended in 5 ml complete DMEM. The required volume for 200 µg particles (for each material) was taken and 2 ml of the stock solution of sodium fluorescein was added to each vial in addition to 2 ml of bicarbonate buffered saline solution. The particle suspensions were incubated with the sodium fluorescein solution overnight at 4°C. Each suspension was then passed through a 25 mm diameter 0.015 µm pore sized filter to remove any remaining unbound sodium fluorescein. The filter papers were then dispersed in 1 ml complete DMEM and sonicated prior to cell culture.

RAW 264.7 murine macrophages were passaged and counted as described in Chapter 2, Sections 2.2.5.4 and 2.2.8.3. RAW cells were seeded at 1 x 10^5 cells.ml^{-1} with 100 µm^3 particles.cell^{-1} in collagen gels in 48 well tissue culture plates as described in Chapter 2 Section 2.2.7.2. Cells with FluoSpheres® were also included as a control: the particle dose of FluoSpheres® were calculated as described in Chapter 2, Section 2.2.6.2.

After 48 hours, the plates were removed from the incubator. The supernatant was aspirated and replaced with lysotracker red loading solution (75 nmol). The plate was returned to the incubator at 37°C and 8% (v/v) CO_2 in air for 30 minutes, after which the lysotracker red loading solution was replaced with Hoechst 33342 loading solution (5 ng.ml^{-1}). The plate was returned to the incubator at 37C and 8% (v/v) CO_2 in air for 10 minutes. The supernatant was then removed and each gel plug was removed using a cell spatula and placed onto a glass cover slip. A glass cover slip was allowed to settle on top of each gel prior to imaging. Each gel plug, containing GUR 1020 XL, GUR 1020 XL AOX, GUR 1050 XL, GUR 1050 XL VE or FluoSphere® particles, was imaged as detailed Chapter 2, Section 2.2.2.2.

5.5 Results

The following section reports the pro-inflammatory and osteolytic cytokine release (TNF-α, IL-1β, IL-6, KC, LTB_4 and PGE_2) and cellular reactive oxygen species levels produced by RAW 264.7 murine macrophages in collagen gel developed (in Chapter 3) in response to single and six station wear simulator rig generated GUR 1020 XL, GUR 1020 XL AOX, GUR 1050 XL and GUR 1050 XL VE UHMWPE wear debris. Additionally, the cells were stimulated with LPS followed by treatment with various inflammatory pathway inhibitors (Indomethacin, Calphostin C, Bisindolylmaleimide I, MK 886 and REV 5901) and the antioxidants (Vitamin E and and Pentaerythritol tetrakis(3,5-di-*tert*-butyl-4-hydroxyhydrocinnamate)) to assess the subsequent effect on the production of pro-inflammatory and osteolytic cytokines (TNF-α, IL-1β, IL-6, KC, LTB_4 and PGE_2) in order to elucidate by what mechanism or pathway any potential anti-inflammatory action of antioxidants added to orthopaedic polyethylene might be acting. Finally, the ability of the novel model to uptake the generated UHMWPE wear debris and sequester them in the lysosomes (perinuclear) was assessed by staining the particles, cell nucleus and lysosomes to determine whether the particles and lysosomes are co-localised using fluorescence microscopy.

5.5.1 Cytokine release in response to treatment with highly cross-linked and highly cross-linked, antioxidant doped UHMWPE wear debris

The following section reports the pro-inflammatory and osteolytic cytokine release (TNF-α, IL-1β, IL-6, KC, LTB_4 and PGE_2) produced by RAW 264.7 murine macrophages in collagen gel in response to single and six station wear simulator rig generated GUR 1020 XL, GUR 1020 XL AOX, GUR 1050 XL and GUR 1050 XL VE UHMWPE wear debris. Cells treated with LPS (200 $ng.ml^{-1}$) were included as a positive control. RAW 264.7 murine macrophages, 1 x 10^5 $cells.ml^{-1}$, were treated with particles from each material (100 $\mu m^3.cell^{-1}$) and cytokine release was assessed at 12 and 24 hours post seeding using ELISA. Cell viability was assessed using the ATP-lite viability assay was also assessed at 12 and 24 hours post seeding.

5.5.1.1 Full size range of UHMWPE wear debris

5.5.1.1.1 Cell viability assay of RAW 264.7 murine macrophages in collagen gel stimulated with the full size range of UHMWPE wear debris

All of the treatments had a significant effect on the viability of RAW 264.7 murine macrophages compared to the cells only negative control at 12 and 24 hours post particle exposure (ANOVA; $p<0.05$) except the LPS (200 $ng.ml^{-1}$) positive control. RAW 264.7 murine macrophages incubated with all particle treatments had a significantly higher cell viability than the cells only control (Figure 5.1A). However,

RAW 264.7 murine macrophages cultured with DMSO had a significantly lower cell viability compared to the cells only control (ANOVA; $p<0.05$).

5.5.1.1.2 ELISA of RAW 264.7 murine macrophages in collagen gel stimulated with the full size range of UHMWPE wear debris

TNF-α cytokine release on stimulation with the full size range of UHMWPE wear debris

At 12 and 24 hours post particle exposure, none of the full size range UHMWPE particle treatments stimulated a significantly increased release of TNF-α however the positive control, RAW 264.7 murine macrophages treated with LPS, exhibited significantly elevated TNF-α release when compared to the cells only control (ANOVA; $p<0.05$).

IL-1β cytokine release on stimulation with the full size range of UHMWPE wear debris

At 12 hours post particle exposure, GUR 1050 XL and GUR 1050 XL VE full size range UHMWPE particle treatments stimulated a significant decrease in the release of IL-1β when compared to the cells only control (ANOVA; $p<0.05$). However, at 24 hours particle exposure, none of the particle treatments or controls elicited a significant elevated or reduced release of IL-1β compared to the cells only control (ANOVA: $p>0.05$).

IL-6 cytokine release on stimulation with the full size range of UHMWPE wear debris

At 12 and 24 hours post particle exposure, none of the full size range UHMWPE particle treatments stimulated a significantly increased release of IL-6 however the positive control, RAW 264.7 murine macrophages treated with LPS, exhibited significant IL-6 release when compared to the cells only control (ANOVA; $p<0.05$).

KC chemokine release on stimulation with the full size range of UHMWPE wear debris

At 12 and 24 hours post particle exposure, none of the full size range UHMWPE particle treatments or the positive control, LPS (200 $ng.ml^{-1}$), stimulated a significantly elevated release of KC however the 0.2μm FluoSphere® particle control did exhibit significant KC release when compared to the cells only control (ANOVA; $p<0.05$).

LTB_4 mediator release on stimulation with the full size range of UHMWPE wear debris

At 24 hours post particle exposure, RAW 264.7 murine macrophages incubated with GUR 1020 XL and GUR 1020 XL AOX UHMWPE wear particles exhibited a significant decrease in the release of LTB_4 in comparison to the cells only control (ANOVA; $p<0.05$). RAW 264.7 murine macrophages stimulated with LPS (200 $ng.ml^{-1}$) exhibited significantly increased release of LTB_4 in comparison to the cells only control (ANOVA; $p<0.05$).

PGE_2 mediator release on stimulation with the full size range of UHMWPE wear debris

At 24 hours post particle exposure, RAW 264.7 murine macrophages incubated with GUR 1020 XL and GUR 1020 XL AOX UHMWPE wear particles exhibited a significantly decreased release of PGE_2 in comparison to the cells only control (ANOVA; $p<0.05$). RAW 264.7 murine macrophages stimulated with LPS (200 $ng.ml^{-1}$) exhibited a significantly increased release of PGE_2 in comparison to the cells only control (ANOVA; $p<0.05$).

A)

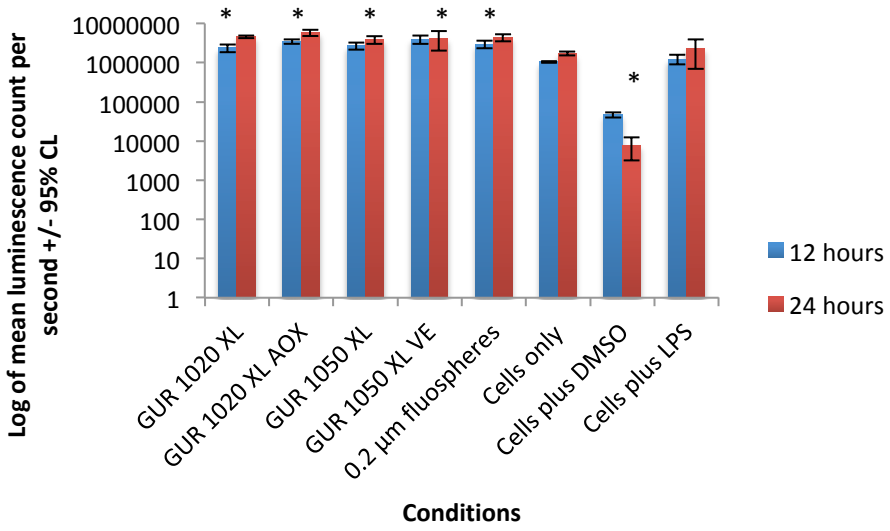

B)

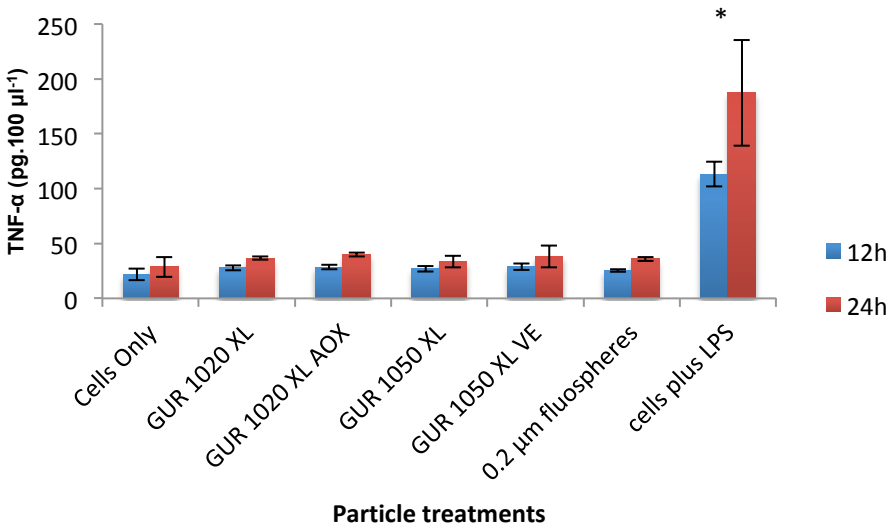
TNF-α (pg.100 µl-1)
250
200
150
100
50
0
*
12h
24h
Cells Only
GUR 1020 XL
GUR 1020 XL AOX
GUR 1050 XL
GUR 1050 XL VE
0.2 µm fluospheres
cells plus LPS
Particle treatments

C)

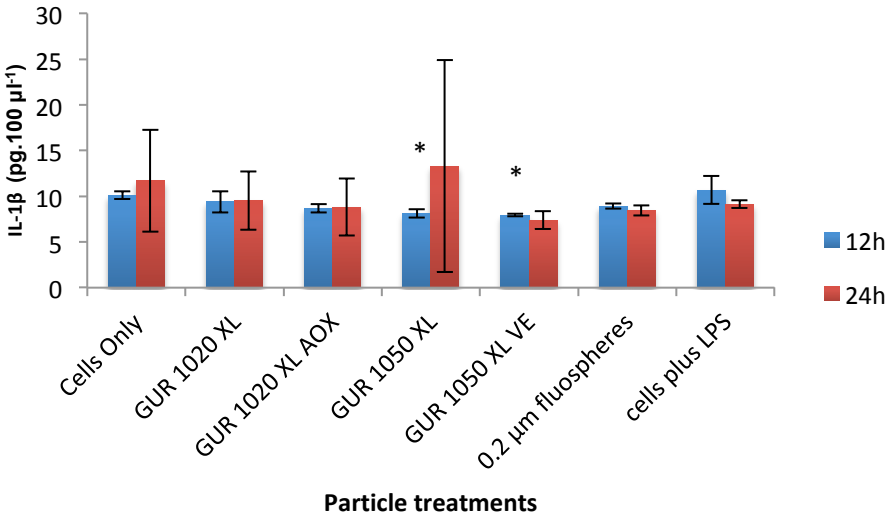
IL-1β (pg.100 µl-1)
30
25
20
15
10
5
0
*
*
12h
24h
Cells Only
GUR 1020 XL
GUR 1020 XL AOX
GUR 1050 XL
GUR 1050 XL VE
0.2 µm fluospheres
cells plus LPS
Particle treatments

D)

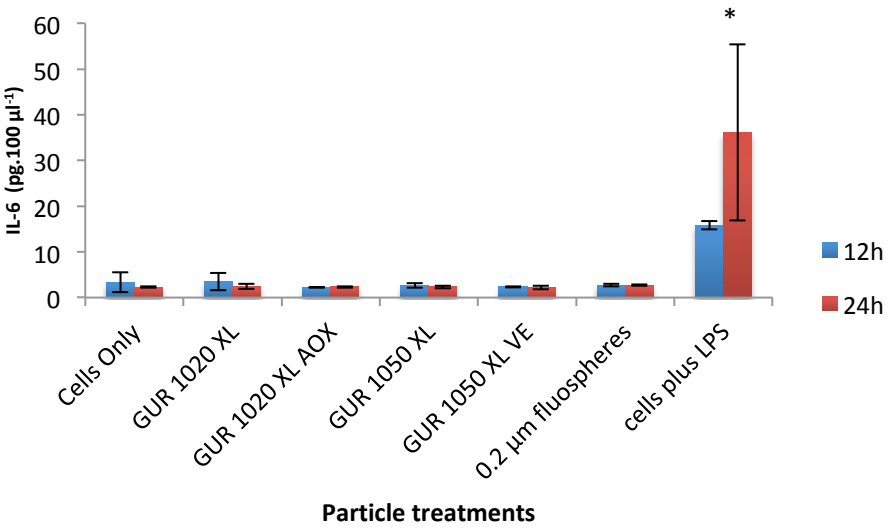
IL-6 (pg.100 µl-1)
60
50
40
30
20
10
0
*
12h
24h
Cells Only
GUR 1020 XL
GUR 1020 XL AOX
GUR 1050 XL
GUR 1050 XL VE
0.2 µm fluospheres
cells plus LPS
Particle treatments

E)

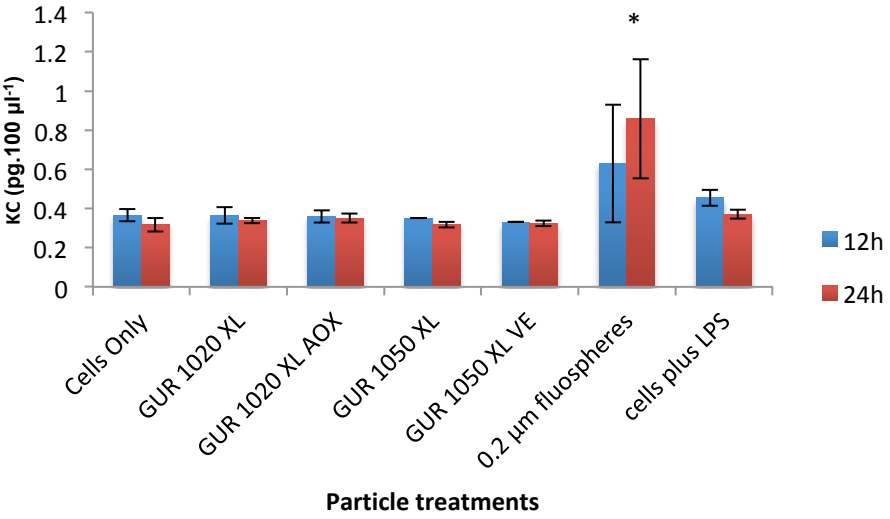
KC (pg.100 µl-1)
1.4
1.2
1
0.8
0.6
0.4
0.2
0
*
12h
24h
Cells Only
GUR 1020 XL
GUR 1020 XL AOX
GUR 1050 XL
GUR 1050 XL VE
0.2 µm fluospheres
cells plus LPS
Particle treatments

F)

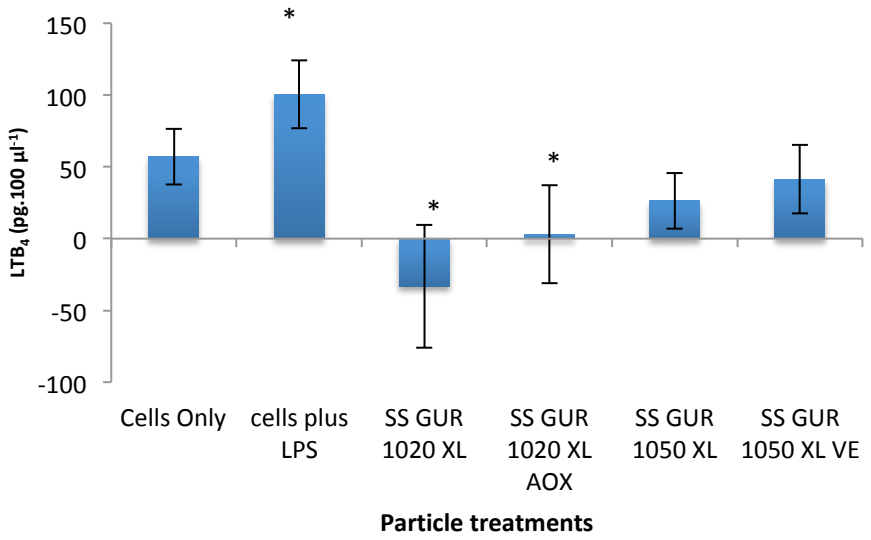

G)

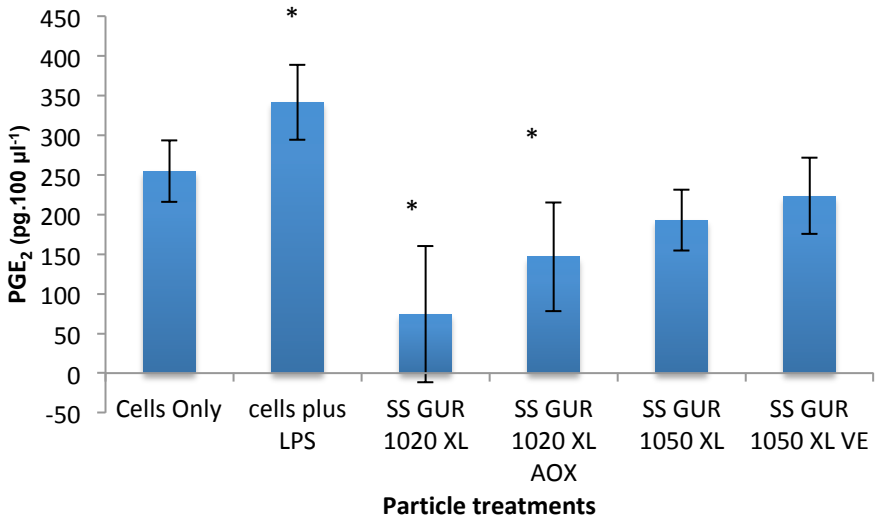

Figure 5.1– A) Cell viability, B) TNF-α release, C) IL-1β release, D) IL-6 release E) KC release, F) LTB_4 release and G) PGE_2 release from RAW 264.7 murine macrophages incubated with full size range UHMWPE particles at a concentration of 100 μm^3 particles per cell in collagen gel at 12 and 24 hours post particle exposure at 37°C in 8% (v/v) CO_2 in air. RAW 264.7 murine macrophages were seeded at a density of 1 x 10^5 cells per well with particle treatments in a 48 well tissue culture plate. RAW 264.7 murine macrophages were exposed to the full size range of particles generated from GUR 1020 XL, GUR 1020 XL AOX, GUR 1050 XL and GUR 1050 XL VE UHMWPE. A cells only negative control and 200 $ng.ml^{-1}$ LPS positive control were included in the conditions. * designates a statistically significant data point (ANOVA, $p<0.05$). Error bars represent 95% confidence intervals, n=4.

5.5.1.2 0.1 - 1 µm UHMWPE wear debris

5.5.1.2.1 Cell viability assay of RAW 264.7 murine macrophages in collagen gel stimulated with 0.1 – 1 µm UHMWPE wear debris

None of the UHMWPE particles treatment had a significant effect on the viability of RAW 264.7 murine macrophages compared to the cells only at 12 hours post particle exposure (ANOVA; $p<0.05$). However, cells cultured with 0.2 µm FluoSpheres® and DMSO (positive control) did exhibit a significant effect on the viability compared to the cells only control 12 hours post particle exposure (ANOVA; $p<0.05$). The cell viability of RAW 264.7 murine macrophages cultured with FluoSpheres® was significantly higher than the cells only control, whereas the cell viability of cells cultured with DMSO was significantly lower than the cells only control (Figure 5.2A). At 24 hours post particle exposure, all conditions except cells treated with LPS elicited a significant effect on cell viability compared to the cells only control. All particle treatments significantly increased cell viability compared to the cells only control, whereas treatment with DMSO significantly decreased the cell viability compared to the cells only control (Figure 5.2A).

5.5.1.2.2 ELISA of RAW 264.7 murine macrophages in collagen gel stimulated with 0.1 - 1 µm UHMWPE wear debris

TNF-α cytokine release on stimulation with 0.1 - 1 µm UHMWPE wear debris

At 12 hour post particle exposure, all of the particle treatments and positive control, except GUR 1020 XL, stimulated a significantly reduced release of TNF-α compared to the cells only control (ANOVA; $p<0.05$) (Figure 5.2B). However the positive control, cells treated with LPS (200 $ng.ml^{-1}$), exhibited significantly increased production of TNF-α compared to the cells only control (ANOVA; $p<0.05$). At 24 hour post particle exposure, all of the particle treatments and positive control, except FluoSpheres®, stimulated a significantly reduced release of TNF-α compared to the cells only control (ANOVA; $p<0.05$). All particle treatments significantly reduced the production of TNF-α compared to the cells only control (Figure 5.2B). However the positive control, cells treated with LPS (200 $ng.ml^{-1}$), significantly increased production of TNF-α compared to the cells only control (ANOVA; $p<0.05$).

IL-1β cytokine release on stimulation with 0.1 - 1 µm UHMWPE wear debris

At 12 hours post particle exposure, GUR 1020 XL 0.1 - 1 µm UHMWPE particle treatments stimulated a significantly increased release of IL-1β when compared to the cells only control (ANOVA; $p<0.05$). However, by 24 hours post particle exposure, the level had decreased so that it was not significantly different compared to the cells only

control. None of the particle treatments or controls elicited a significantly elevated or reduced release of IL-1β when compared to the cells only control (ANOVA: $p>0.05$).

IL-6 cytokine release on stimulation with 0.1 - 1 μm UHMWPE wear debris

At 12 and 24 hours post particle exposure, none of the 0.1 - 1 μm UHMWPE particle treatments stimulated a significantly increased release of IL-6, however the positive control, cells treated with LPS, exhibited significantly elevated levels of IL-6 when compared to the cells only control (ANOVA; $p<0.05$).

KC chemokine release on stimulation with 0.1 - 1 μm UHMWPE wear debris

At 12 and 24 hours post particle exposure, none of the 0.1 - 1 μm UHMWPE particle treatments or the positive control, LPS (200 $ng.ml^{-1}$), stimulated a significant release of KC however the 0.2 μm FluoSphere® particle control did exhibit significant KC release when compared to the cells only control (ANOVA; $p<0.05$).

LTB_4 mediator release on stimulation with 0.1 - 1 μm UHMWPE wear debris

At 24 hours post particle exposure, none of the cells incubated with particle treatments exhibited a significant effect on the release of LTB_4 in comparison to the cells only control (ANOVA; $p<0.05$). Cells stimulated with LPS (200 $ng.ml^{-1}$) exhibited a significantly increased release of LTB_4 in comparison to the cells only control (ANOVA; $p<0.05$).

PGE_2 mediator release on stimulation with 0.1 - 1 μm UHMWPE wear debris

At 24 hours post particle exposure, none of the cells incubated with particle treatments exhibited a significant effect on the release of PGE_2 in comparison to the cells only control (ANOVA; $p<0.05$). Cells stimulated with LPS (200 $ng.ml^{-1}$) exhibited a significantly increased release of PGE_2 in comparison to the cells only control (ANOVA; $p<0.05$).

A)

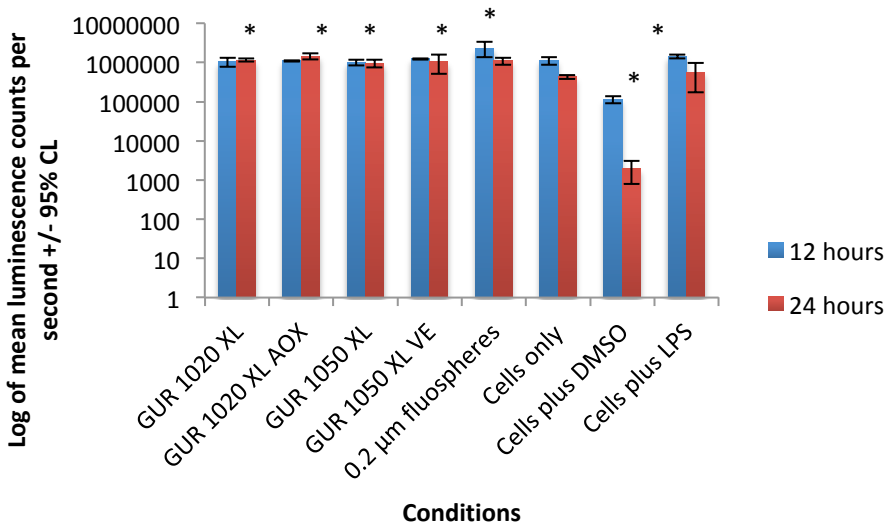
Log of mean luminescence counts per second +/- 95% CL
10000000
1000000
100000
10000
1000
100
10
1
*
GUR 1020 XL
GUR 1020 XL AOX
GUR 1050 XL
GUR 1050 XL VE
0.2 µm fluospheres
Cells only
Cells plus DMSO
Cells plus LPS
Conditions
12 hours
24 hours

B)

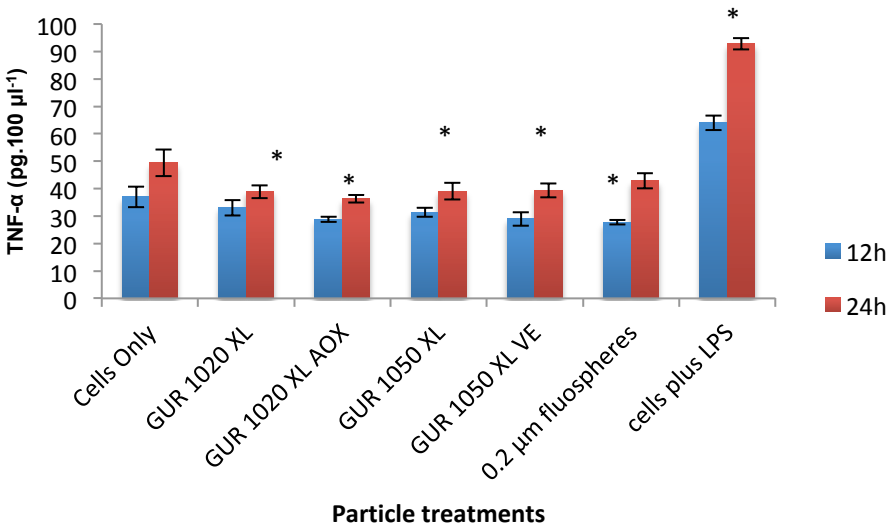
TNF-α (pg.100 µl-1)
100
90
80
70
60
50
40
30
20
10
0
Cells Only
GUR 1020 XL
GUR 1020 XL AOX
GUR 1050 XL
GUR 1050 XL VE
0.2 µm fluospheres
cells plus LPS
Particle treatments
12h
24h

C)

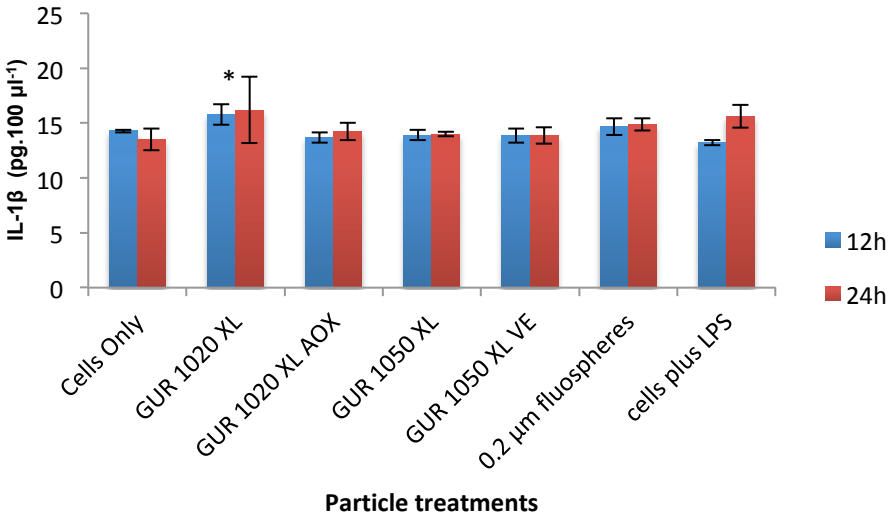
IL-1β (pg.100 µl-1)
25
20
15
10
5
0
Cells Only
GUR 1020 XL
GUR 1020 XL AOX
GUR 1050 XL
GUR 1050 XL VE
0.2 µm fluospheres
cells plus LPS
Particle treatments
12h
24h

D)

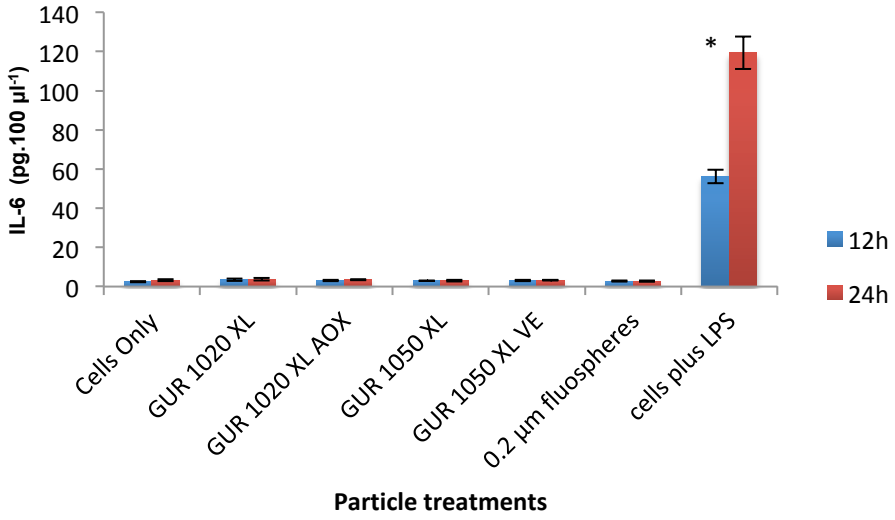
IL-6 (pg.100 µl-1)
140
120
100
80
60
40
20
0
*
12h
24h
Cells Only
GUR 1020 XL
GUR 1020 XL AOX
GUR 1050 XL
GUR 1050 XL VE
0.2 µm fluospheres
cells plus LPS
Particle treatments

E)

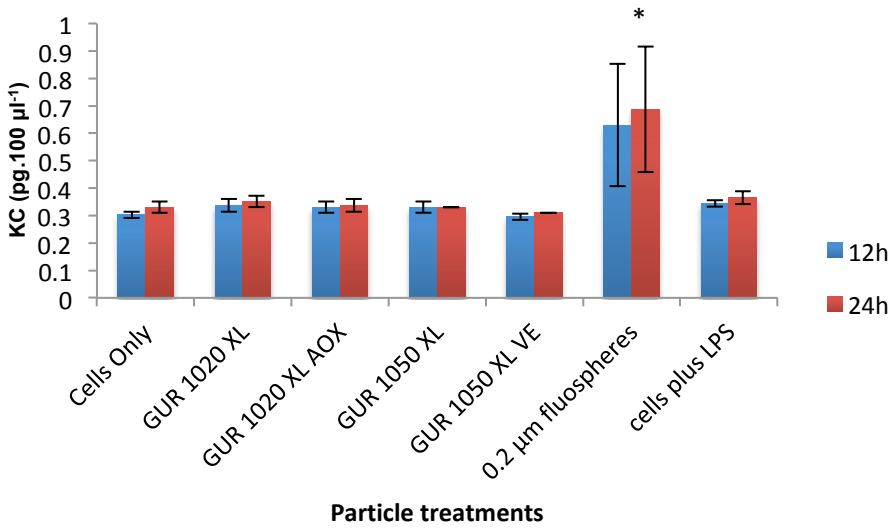
KC (pg.100 µl-1)
1
0.9
0.8
0.7
0.6
0.5
0.4
0.3
0.2
0.1
0
*
12h
24h
Cells Only
GUR 1020 XL
GUR 1020 XL AOX
GUR 1050 XL
GUR 1050 XL VE
0.2 µm fluospheres
cells plus LPS
Particle treatments

F)

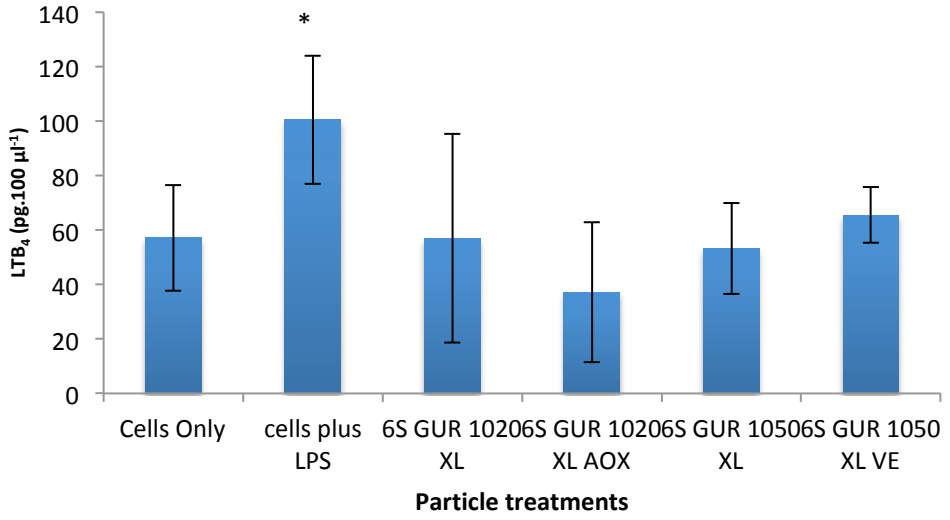

G)

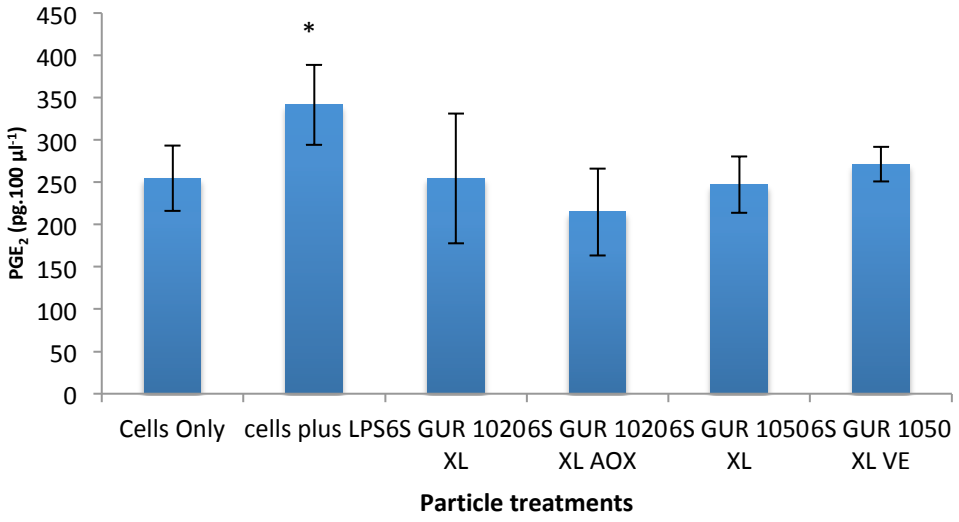

Figure 5.2– A) Cell viability, B) TNF-α release, C) IL-1β release, D) IL-6 release, E) KC release, F) LTB_4 release and G) PGE_2 release from RAW 264.7 murine macrophages incubated with 0.1 - 1 µm UHMWPE wear debris at a concentration of 100 μm^3 particles per cell in collagen gel at 12 (left) and 24 (right) hours post particle exposure at 37°C in 8% (v/v) CO_2 in air. RAW 264.7 murine macrophages were seeded at a density of 1 x 10^5 cells per well with particle treatments in a 48 well tissue culture plate. RAW 264.7 murine macrophages were exposed to 0.1 - 1 µm GUR 1020 XL, GUR 1020 XL AOX, GUR 1050 XL and GUR 1050 XL VE UHMWPE wear debris. A cells only negative control and 200 $ng.ml^{-1}$ LPS positive control were included in the conditions. * designates a statistically significant data point (ANOVA, $p<0.05$). Error bars represent 95% confidence intervals, n=4.

5.5.2 Cytokine release of LPS-stimulated RAW 264.7 murine macrophages in response to treatment with inflammatory pathway inhibitors and antioxidant compounds

The following section reports the pro-inflammatory and osteolytic cytokine release (TNF-α, IL-1β, IL-6, LTB_4 and PGE_2) produced by LPS (200 ng.ml-^{1}) stimulated RAW 264.7 murine macrophages in response to inflammatory pathway inhibitors (CalphostinC, Bisindolylmaleimide I, Indomethacin, MK 886 and REV 5901) and antioxidant compounds (Vitamin E and Pentaerythritol tetrakis(3,5-di-*tert*-butyl-4-hydroxyhydrocinnamate)). Cells treated with LPS only (200 ng.ml^{-1}) and cells only were included as negative controls. RAW 264.7 murine macrophages, 1 x 10^5 cells.ml^{-1}, were treated with inhibitor and antioxidant compounds and cytokine release was assessed at 12 and 24 hours post particle exposure using ELISA (24 hours only for LTB_4 and PGE_2). Cell viability was assessed using the ATP-lite^{TM} luminescence detection assay was also assessed at 12 and 24 hours post seeding. Cell viability assays for RAW 264.7 murine macrophages incubated with four concentrations of each inhibitor and antioxidant compounds were carried out to assess the most appropriate concentrations for use.

5.5.2.1 Cell viability in response to treatment with inflammatory pathway inhibitors and antioxidant compounds

The range of concentrations used in this study were based on those used by Deveraj and Jialal (1999) with higher and lower concentrations included either side of the previous values. The highest concentrations of each inhibitor treatment had a significant effect on the viability of RAW 264.7 murine macrophages compared to the cells only control at days 0, 1 and 3 (ANOVA; $p<0.05$). RAW 264.7 murine macrophages treated with Indomethacin (100 µmol.L^{-1}), REV 5901 (100 µmol.L^{-1} and 1000 µM.L^{-1}), MK 886 (100 µmol.L^{-1}), Bisindolylmaleimide I (10 µmol.L^{-1} and 100 µmol.L^{-1}) and Calphostin C (500 nmol.L^{-1} and 1 µmol.L^{-1}) reduced the viability significantly below that exhibited by the cells only control and to the viability levels demonstrated by the cells plus DMSO (200 µl.ml^{-1}) positive control (Figure 5.3). The remaining concentrations, Calphostin C (100 and 250 nmol.L^{-1}), Bisindolylmaleimide I (0.1 and 1 µmol.L^{-1}), Indomethacin (0.1, 1 and 10 µmol.L^{-1}), MK 886 (0.1, 1 and 10 µmol.L^{-1}) and REV 5901 (1 and 10 µmol.L^{-1}), had no significant adverse effect on the viability of RAW 264.7 murine macrophages over days 0, 1 and 3 (Figure 5.3). The following concentrations of each inhibitor were carried forward: Calphostin C (250 and 500 nmol.L^{-1}), Bisindolylmaleimide I (0.1 and 1 µmol.L^{-1}), Indomethacin (10 µmol.L^{-1}), MK 886 (1 µmol.L^{-1}) and REV 5901 (10 µmol.L^{-1}). These concentrations of inhibitors were used in a previous study by Deveraj and Jialal (1999) and the dose response

study carried out by the candidate showed that these concentrations did not adversely affect cell viability of RAW 264.7 murine macrophages over the 24 hour time period.

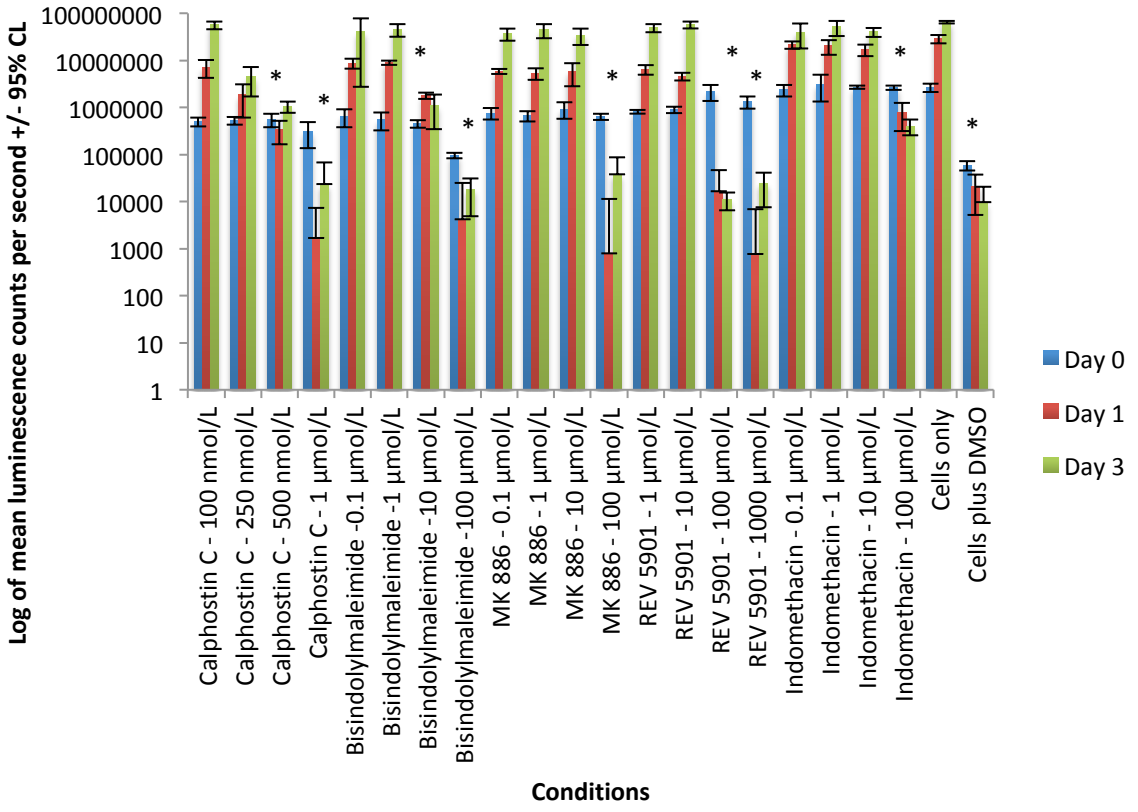

Figure 5.3 Cell viability of RAW 264.7 murine macrophages in collagen gel treated with Bisindolylmaleimide I (0.1, 1, 10 and 100 µmol.L^{-1}), Calphostin C (100 nmol.L^{-1}, 250 nmol.L^{-1}, 500 nmol.L^{-1}, 1 µmol.L^{-1}), Indomethacin (0.1, 1, 10 and 100 µmol.L^{-1}), MK 886 (0.1, 1, 10 and 100 µmol.L^{-1}) and REV 5901 (1, 10, 100 and 1000 µmol.L^{-1}) over three days at 37°C in 8% (v/v) CO_2 in air. Cells were seeded at a density 5 x 10^4 cells.ml^{-1} in a 96 well tissue culture plate. A cells plus DMSO (200 µl.ml^{-1}) positive control was included in the conditions. Cells viability was assessed using the ATP-lite^{TM} luminescence detection assay. * designates a statistically significant data point (ANOVA, $p<0.05$). Error bars represent 95% confidence intervals, n=6.

The highest concentrations of each antioxidant treatment had a significant effect on the viability of RAW 264.7 murine macrophages compared to the cells only control at days 0, 1 and 3 (ANOVA; $p<0.05$). RAW 264.7 murine macrophages treated with Vitamin E (2, 3 and 5 mmol.L^{-1}) and Pentaerythritol tetrakis(3,5-di-*tert*-butyl-4-hydroxyhydrocinnamate) (300 and 500 µmol.L^{-1}) reduced the viability significantly below that exhibited by the cells only control and to the viability levels demonstrated by the cells plus DMSO (200 µl.ml^{-1}) positive control (Figure 5.4) on days 0, 1 and 3. The remaining concentrations of antioxidants, Vitamin E (400 and 800 µmol.L^{-1} and 1 mmol.L^{-1}) and Pentaerythritol tetrakis(3,5-di-*tert*-butyl-4-hydroxyhydrocinnamate) (300 and 500 µmol.L^{-1}) did not have a significant adverse effect on cell viability. The

following concentrations of each antioxidant were carried forward based on a previous study by Bladen *et al.* (2013b): Vitamin E (800 µmol.L^{-1}) and Pentaerythritol tetrakis(3,5-di-*tert*-butyl-4-hydroxyhydrocinnamate) (25 µmol.L^{-1}).

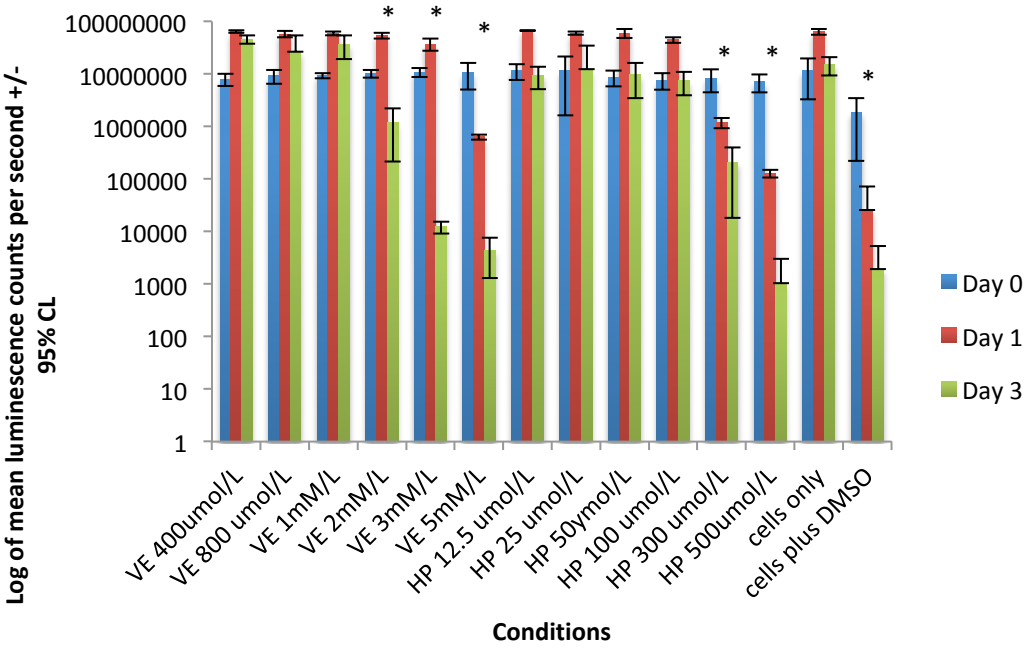

Figure 5.4 Cell viability of RAW 264.7 murine macrophages in collagen gel treated with Vitamin E (400 µmol.L^{-1}, 800 µmol.L^{-1}, 1 mmol.L^{-1}, 2 mmol.L^{-1}, 3 mmol.L^{-1} and 5 mmol.L^{-1}) and Pentaerythritol tetrakis(3,5-di-*tert*-butyl-4-hydroxyhydrocinnamate) (12.5, 25, 50, 100, 300 and 500 µmol.L^{-1}) over three days at 37°C in 8% (v/v) CO_2 in air. Cells were seeded at a density 5 x 10^4 cells.ml^{-1} in a 96 well tissue culture plate. A cells plus DMSO (200 µl.ml^{-1}) positive control was included in the conditions. Cells viability was assessed using the ATP-lite^{TM} luminescence detection assay. * designates a statistically significant data point (ANOVA, $p<0.05$). Error bars represent 95% confidence intervals, n=6.

5.5.2.2 Cell viability of RAW 264.7 murine macrophages in collagen gel stimulated with inflammatory inhibitors and antioxidant compounds

Treatment with Calphostin (250 and 500 µmol.L^{-1}) and DMSO (200 µl.ml-1) (positive control) significantly decreased the viability of LPS stimulated RAW 264.7 murine macrophages compared to the LPS stimulated cells only control at 12 hours post seeding (ANOVA; $p<0.05$). No other treatments exhibited a significantly adverse effect on cell viability at 12 hours post seeding. Treatment with Calphostin (250 and 500 µmol.L^{-1}), Vitamin E (800 µmol.L^{-1}) and DMSO (200 µl.ml^{-1}) (positive control) significantly decreased the viability of LPS stimulated RAW 264.7 murine macrophages (Figure 5.4A) compared to the LPS stimulated cells only control at 24 hours post seeding (ANOVA; $p<0.05$).

5.5.2.3 ELISA of RAW 264.7 murine macrophages in collagen gel stimulated with inflammatory inhibitors and antioxidant compounds

TNF-α cytokine release on stimulation with inflammatory inhibitors and antioxidant compounds

At 12 hours post seeding, LPS stimulated cells treated with Calphostin C (250 and 500 $\mu mol.L^{-1}$), Bisindolylmaleimide I (1 $\mu mol.L^{-1}$), Vitamin E (800 $\mu mol.L^{-1}$) and Pentaerythritol tetrakis(3,5-di-*tert*-butyl-4-hydroxyhydrocinnamate) (25 $\mu mol.L^{-1}$) exhibited significantly decreased levels of TNF-α production (Figure 5.5B) compared to the LPS stimulated cells only control (ANOVA; $p<0.05$). At 24 hours post seeding, LPS stimulated cells treated with Calphostin C (250 $\mu mol.L^{-1}$) and Vitamin E (800 $\mu mol.L^{-1}$) exhibited significantly decreased levels of TNF-α production compared to the LPS stimulated cells only control (ANOVA; $p<0.05$).

IL-1β cytokine release on stimulation with inflammatory inhibitors and antioxidant compounds

At 12 hours post seeding, LPS stimulated cells treated with Calphostin C (250 and 500 $\mu mol.L^{-1}$), Bisindolylmaleimide I (1 $\mu mol.L^{-1}$), Indomethacin (10 $\mu mol.L^{-1}$), MK 886 (1 $\mu mol.L^{-1}$), REV 5901 (10 $\mu mol.L^{-1}$), Vitamin E (800 $\mu mol.L^{-1}$) and Pentaerythritol tetrakis(3,5-di-*tert*-butyl-4-hydroxyhydrocinnamate) (25 $\mu mol.L^{-1}$) exhibited significantly decreased levels of IL-1β production (Figure 5.5C) compared to the LPS stimulated cells only control (ANOVA; $p<0.05$). At 24 hours post seeding, LPS stimulated cells treated with Calphostin C (250 $\mu mol.L^{-1}$), Bisindolylmaleimide I (0.1 $\mu mol.L^{-1}$), Indomethacin (10 $\mu mol.L^{-1}$), REV 5901 (10 $\mu mol.L^{-1}$) and Vitamin E (800 $\mu mol.L^{-1}$) exhibited significantly decreased levels of IL-1β production compared to the LPS stimulated cells only control (ANOVA; $p<0.05$).

IL-6 cytokine release on stimulation with inflammatory inhibitors and antioxidant compounds

At 12 hours post seeding, LPS stimulated cells treated with Calphostin C (250 and 500 $\mu mol.L^{-1}$) and Vitamin E (800 $\mu mol.L^{-1}$) exhibited significantly decreased levels of IL-6 production (Figure 5.5D) compared to the LPS stimulated cells only control (ANOVA; $p<0.05$). At 24 hours post seeding, LPS stimulated cells treated with Calphostin C (250 and 500 $\mu mol.L^{-1}$), Bisindolylmaleimide I (0.1 and 1 $\mu mol.L^{-1}$), Vitamin E (800 $\mu mol.L^{-1}$) and Pentaerythritol tetrakis(3,5-di-*tert*-butyl-4-hydroxyhydrocinnamate) (25 $\mu mol.L^{-1}$) exhibited significantly decreased levels of IL-6 production compared to the LPS stimulated cells only control (ANOVA; $p<0.05$).

LTB_4 cytokine release on stimulation with inflammatory inhibitors and antioxidant compounds

At 24 hours post seeding, LPS stimulated cells treated with Calphostin C (250 nmol.L^{-1}) and Bisindolylmaleimide I (0.1 µmol.L^{-1}) released significantly lower levels of LTB_4 (Figure 5.5.E) in comparison to the LPS stimulated cells only control (ANOVA; $p<0.05$).

PGE_2 cytokine release on stimulation with inflammatory inhibitors and antioxidant compounds

At 24 hours post seeding, LPS stimulated cells treated with Calphostin C (250 nmol.L^{-1}) and Bisindolylmaleimide I (0.1 µmol.L^{-1}) released significantly lower levels of PGE_2 in comparison to the LPS stimulated cells only control (ANOVA; $p<0.05$).

A)

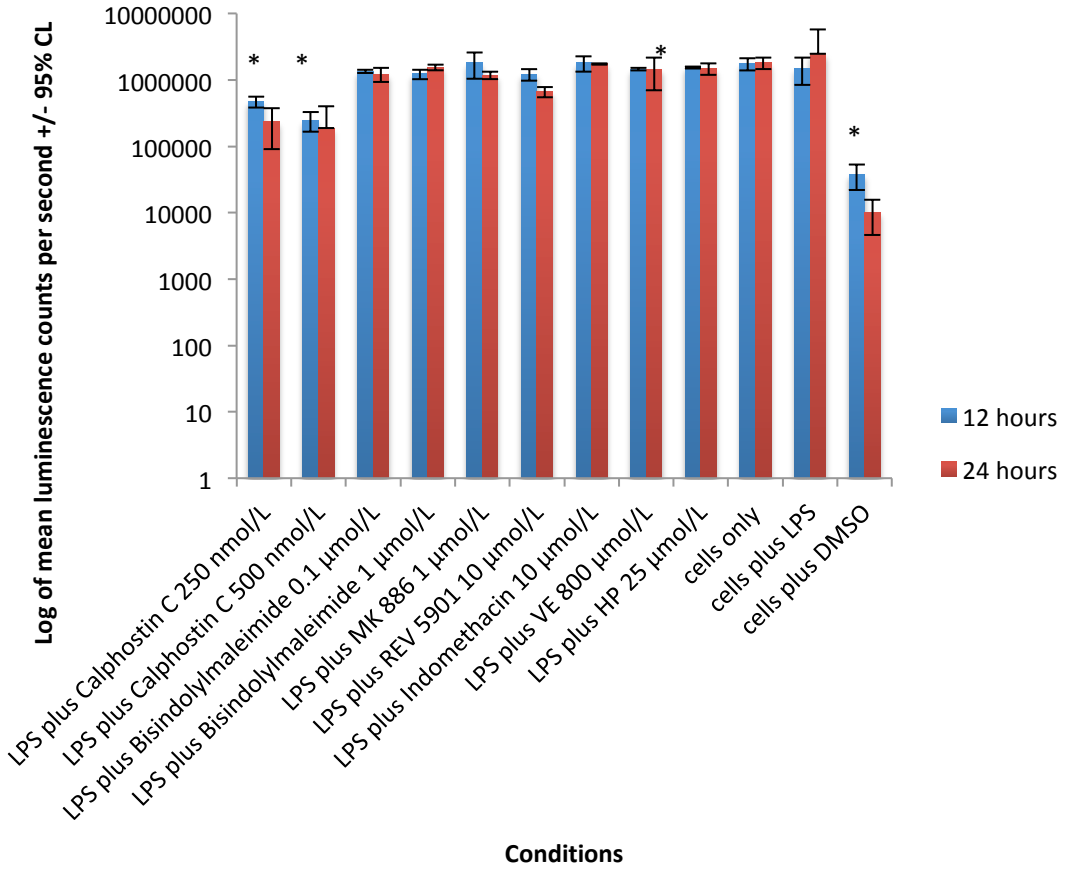

B)

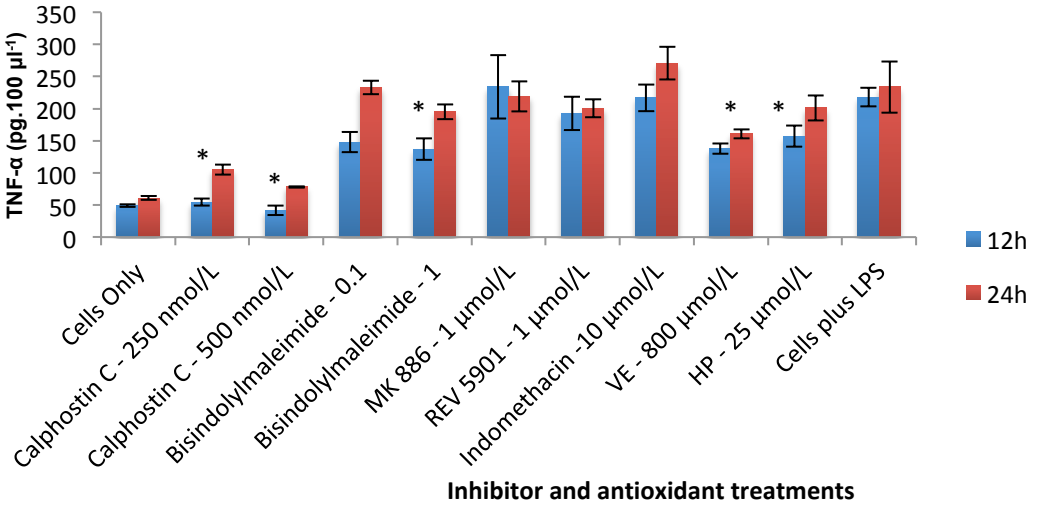
TNF-α (pg.100 µl-1)
350
300
250
200
150
100
50
0
*
*
*
*
Cells Only
Calphostin C - 250 nmol/L
Calphostin C - 500 nmol/L
Bisindolylmaleimide - 0.1
Bisindolylmaleimide - 1
MK 886 - 1 µmol/L
REV 5901 - 1 µmol/L
Indomethacin -10 µmol/L
VE - 800 µmol/L
HP - 25 µmol/L
Cells plus LPS
Inhibitor and antioxidant treatments
12h
24h

C)

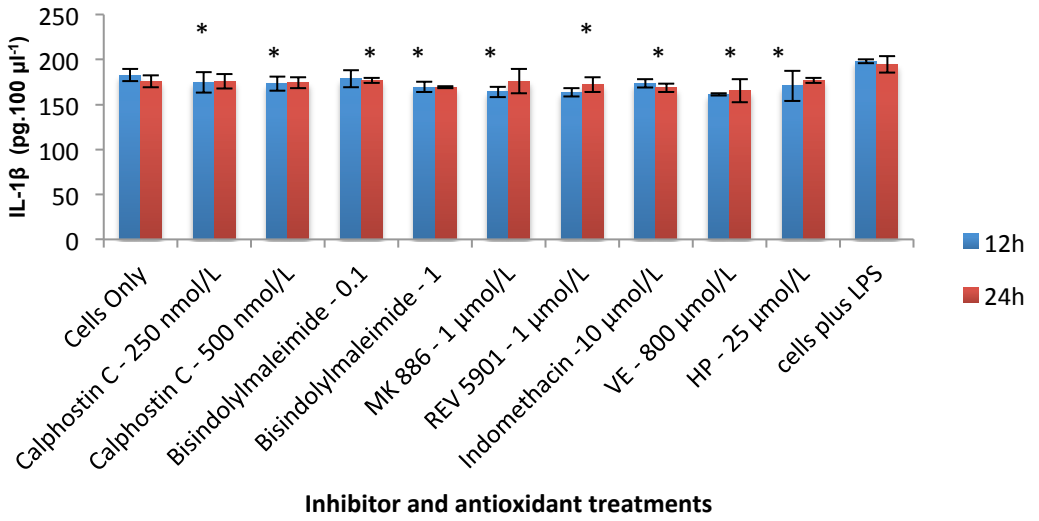
IL-1β (pg.100 µl-1)
250
200
150
100
50
0
*
*
*
*
*
*
*
*
*
Cells Only
Calphostin C - 250 nmol/L
Calphostin C - 500 nmol/L
Bisindolylmaleimide - 0.1
Bisindolylmaleimide - 1
MK 886 - 1 µmol/L
REV 5901 - 1 µmol/L
Indomethacin -10 µmol/L
VE - 800 µmol/L
HP - 25 µmol/L
cells plus LPS
Inhibitor and antioxidant treatments
12h
24h

D)

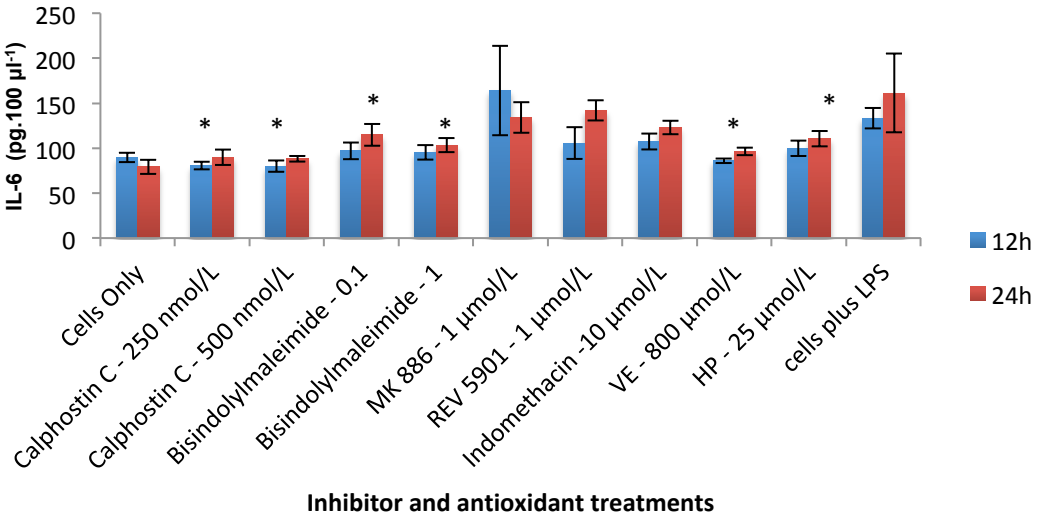
IL-6 (pg.100 µl-1)
250
200
150
100
50
0
*
Cells Only
Calphostin C - 250 nmol/L
Calphostin C - 500 nmol/L
Bisindolylmaleimide - 0.1
Bisindolylmaleimide - 1
MK 886 - 1 µmol/L
REV 5901 - 1 µmol/L
Indomethacin -10 µmol/L
VE - 800 µmol/L
HP - 25 µmol/L
cells plus LPS
12h
24h
Inhibitor and antioxidant treatments

E)

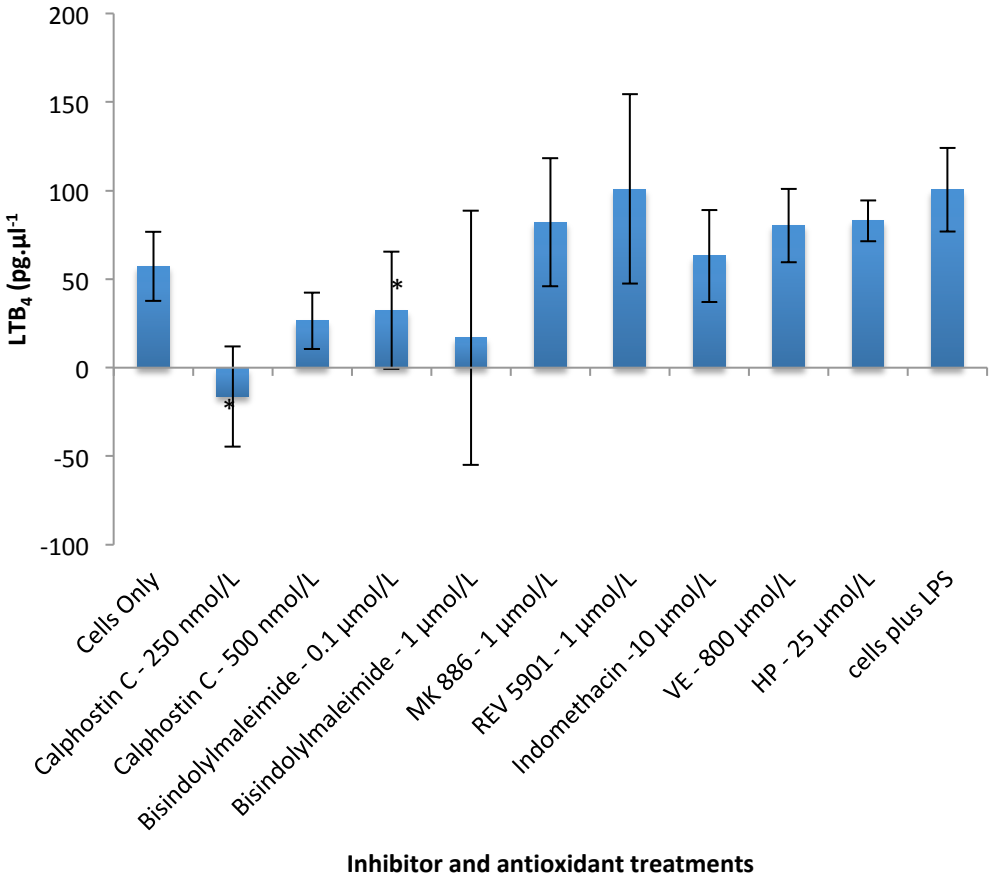
LTB4 (pg.µl-1
200
150
100
50
0
-50
-100
*
Cells Only
Calphostin C - 250 nmol/L
Calphostin C - 500 nmol/L
Bisindolylmaleimide - 0.1 µmol/L
Bisindolylmaleimide - 1 µmol/L
MK 886 - 1 µmol/L
REV 5901 - 1 µmol/L
Indomethacin -10 µmol/L
VE - 800 µmol/L
HP - 25 µmol/L
cells plus LPS
Inhibitor and antioxidant treatments

F)

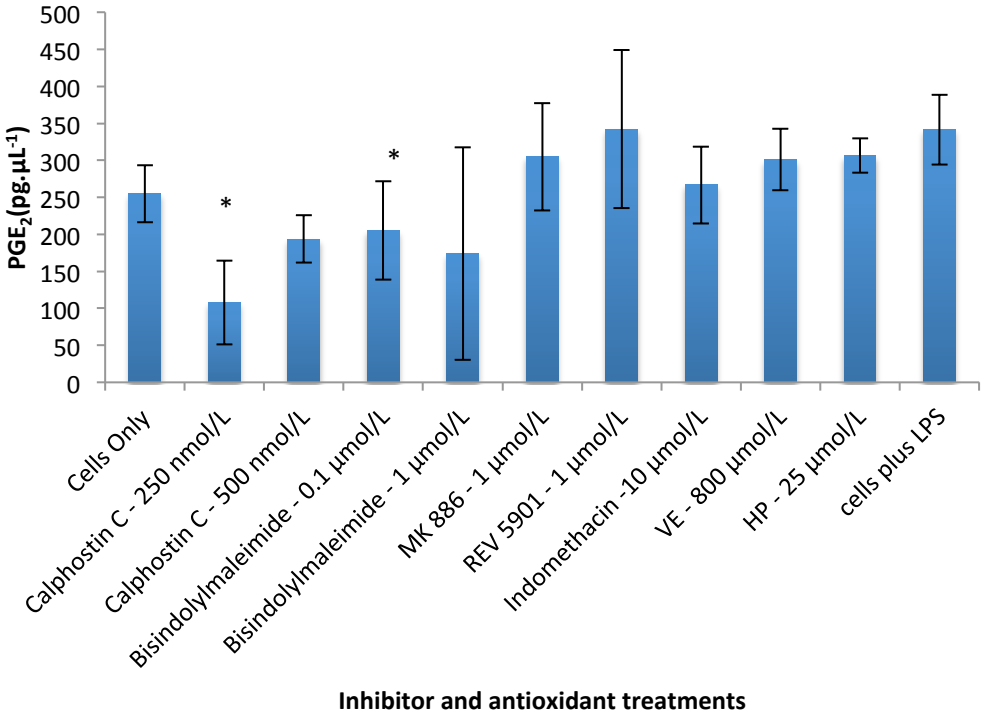

Figure 5.5– A) Cell viability, B) TNF-α release, C) IL-1β release, D) IL-6 release, E) LTB_4 release and F) PGE_2 release from LPS stimulated RAW 264.7 murine macrophages in collagen gel treated with Bisindolylmaleimide I (0.1 and 1 $\mu mol.L^{-1}$), Calphostin C (250 and 500 $nmol.L^{-1}$), Indomethacin (10 $\mu mol.L^{-1}$), MK 886 (1 $\mu mol.L^{-1}$), REV 5901 (10 $\mu mol.L^{-1}$) Vitamin E (800 $\mu mol.L^{-1}$) and Pentaerythritol tetrakis(3,5-di-*tert*-butyl-4-hydroxyhydrocinnamate) (25 $\mu mol.L^{-1}$) after three hours at 12 (left) and 24 (right) hours post seeding at 37°C in 8% (v/v) CO_2 in air. LTB_4 and PGE_2 was only measured after 24 hours. RAW 264.7 murine macrophages were seeded at a density of 1 x 10^5 cells per well in a 48 well tissue culture plate. Cells only and LPS stimulated cells only negative controls were included. A cells plus DMSO (200 $\mu l.ml^{-1}$) positive control was included in the cell viability assay. * designates a statistically significant data point (ANOVA, $p<0.05$). Error bars represent ± the 95% confidence level, n=4.

5.5.3 Reactive oxygen species production for RAW 264.7 murine macrophages in response to full size range and 0.1 – 1 µm GUR 1020 XL, GUR 1020 XL AOX, GUR 1050 XL and GUR 1050 XL VE UHMWPE wear debris

RAW 264.7 murine macrophages were cultured with full size range and 0.1 – 1 µm UHMWPE wear debris (GUR 1020 XL, GUR 1020 XL AOX, GUR 1050 XL and GUR 1050 XL VE) in collagen gel (Section 5.4.4). The particles generated using the six station multidirectional POP wear simulator were filtered in to the size range 0.1 – 1 µm prior to cell culture. The production of reactive oxygen species (ROS) in response to the particulates was assessed using the Abcam cellular reactive oxygen species assay.

At 24 hours post particle exposure, none of the full size range and 0.1 – 1 µm UHMWPE particle treatments resulted in significant production of cellular reactive oxygen species in comparison to the cells only control (ANOVA; $p<0.05$). However, the FluoSphere® particle control (0.2 µm), cells treated with DMSO, cells treated with LPS and cells with TBHP positive control elicited significantly elevated levels of cellular reactive oxygen species (ANOVA: $p>0.05$).

A)

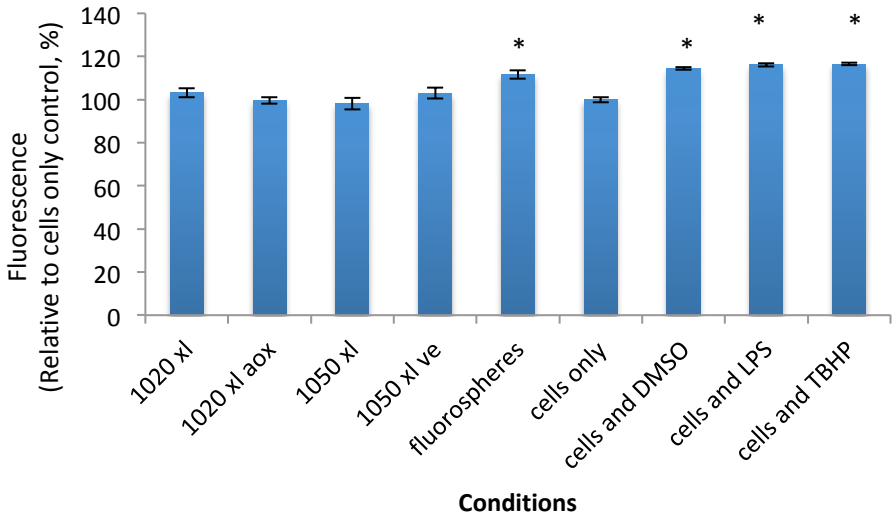

B)

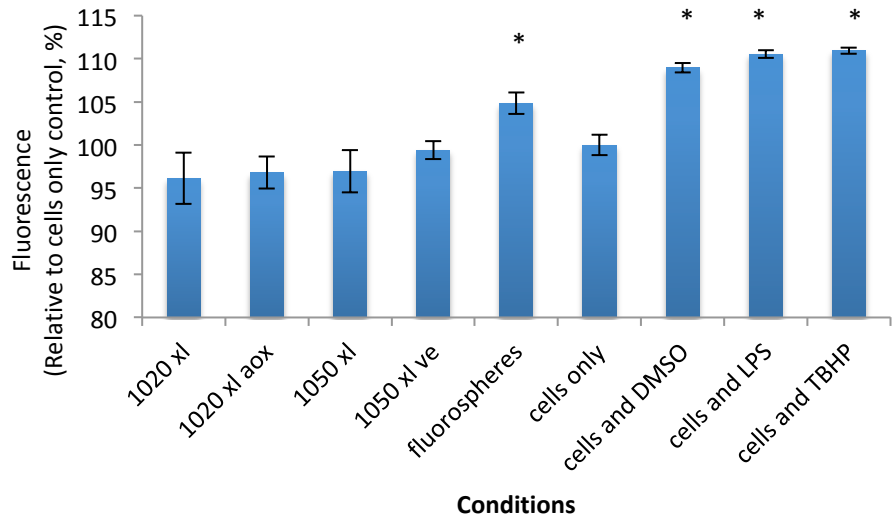

Figure 5.6 Cellular reactive oxygen species concentration (proportional to the level of fluorescence) of RAW 264.7 murine macrophages in response to GUR 1020 XL, GUR 1020 XL AOX, GUR 1050 XL and GUR 1050 XL VE UHMWPE wear debris produced using A) single station and B) six station multidirectional POP wear simulator. A cells only negative control, FluoSpheres® particle control and cells plus LPS (200 $ng.ml^{-1}$), cells plus DMSO (200 $\mu l.ml^{-1}$) and cells plus TBHP (250

μM) positive controls were included. Error bars represent ± the 95% confidence level, n=4.

5.5.4 Visualising internal particle sequestration of 0.1 – 1 μm GUR 1020 XL, GUR 1020 XL AOX, GUR 1050 XL and GUR 1050 XL VE UHMWPE wear debris in RAW 264.7 murine macrophages encapsulated in collagen gels

RAW 264.7 murine macrophages were cultured with 0.1 – 1 μm filtered fluorescein stained UHMWPE wear debris (GUR 1020 XL, GUR 1020 XL AOX, GUR 1050 XL and GUR 1050 XL VE) in collagen gels for 48 hours. The cells were then stained with lysotracker red (locates to the lysosomes) and Hoechst 33342 (stains the nucleus) and the gel plugs were imaged using fluorescent microscopy to observe particle internalisation and localisation of the particles within the cells.

Issues were experienced with the fluorescent labelling of the UHMWPE wear debris and, as such very few particles were visible in Figure 5.7A/B/C/D. However, those few particles that were visible were located around the nucleus. FluoSpheres® were included as a particle control (no fluorescein staining was necessary as the particles are tagged with FITC) and the images taken of cells cultured with FluoSpheres® more clearly show the co-localisation of uptaken particles with the lysosomes around the cell nucleus.

A)

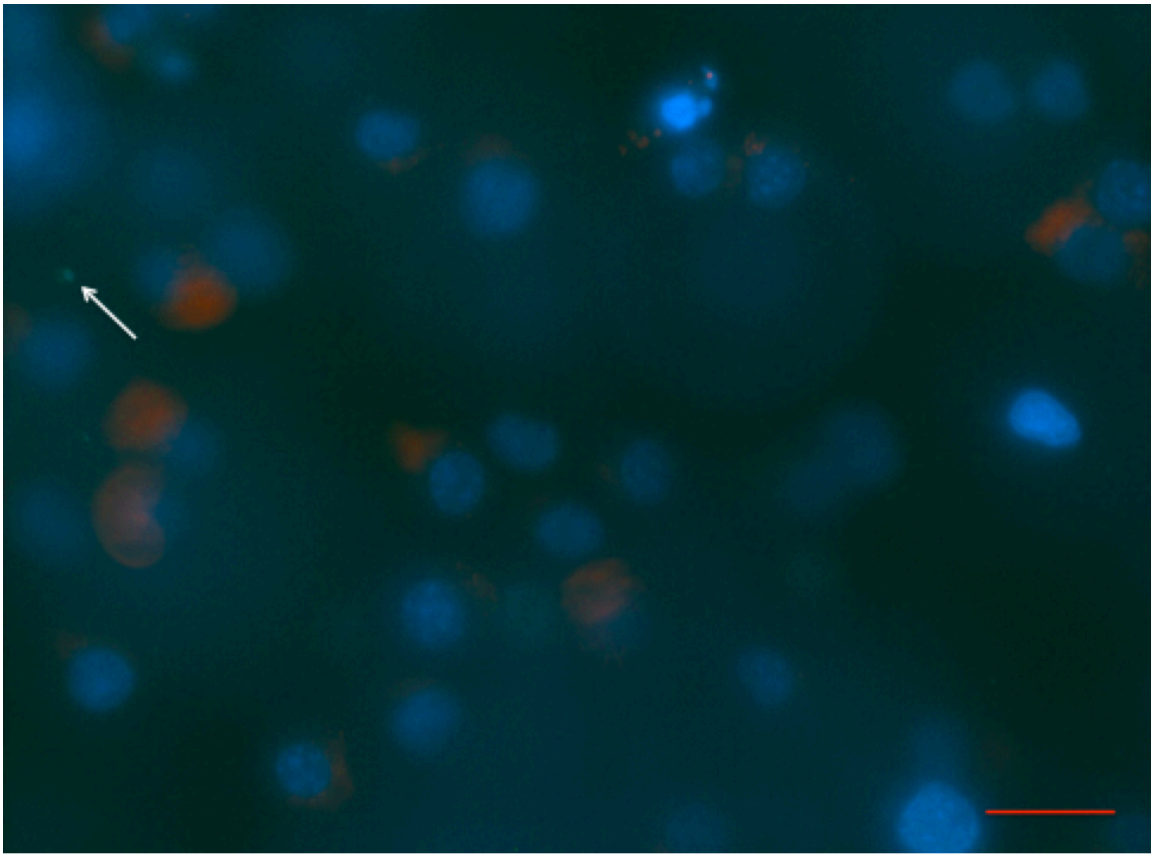

B)

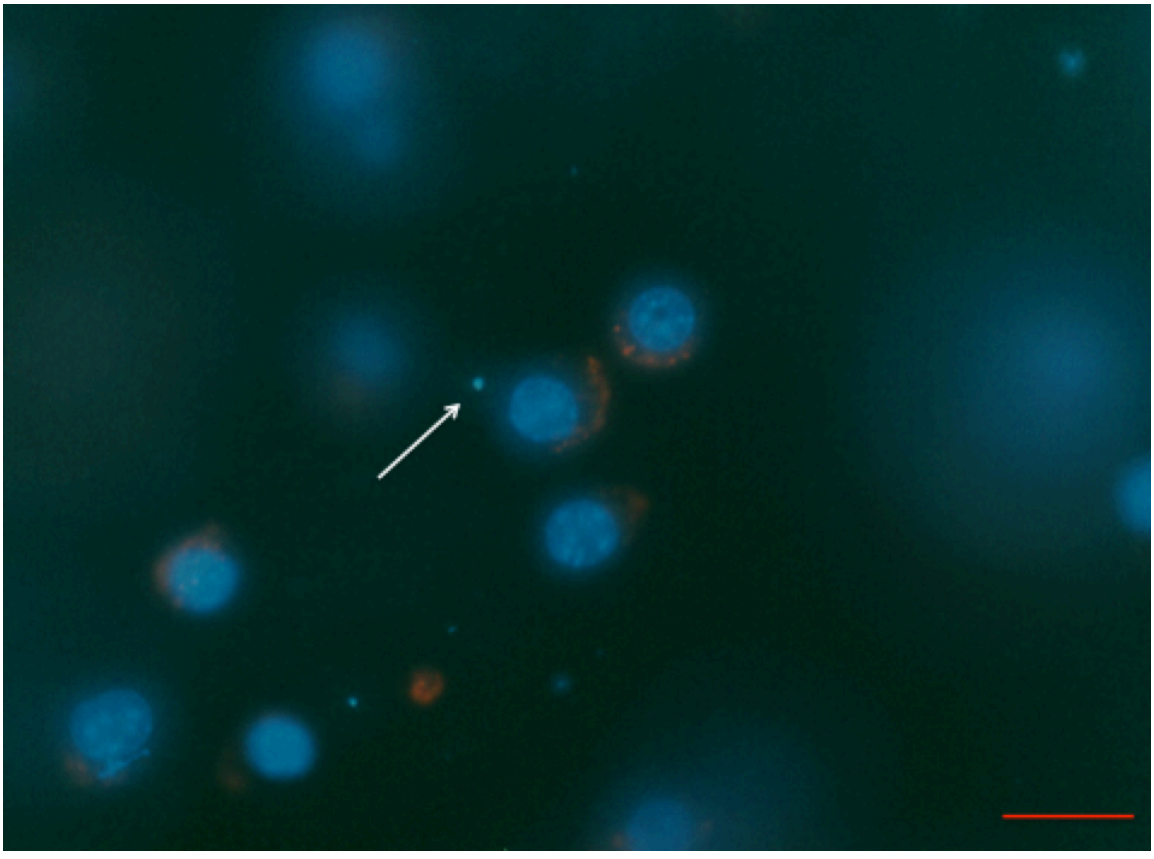

C)

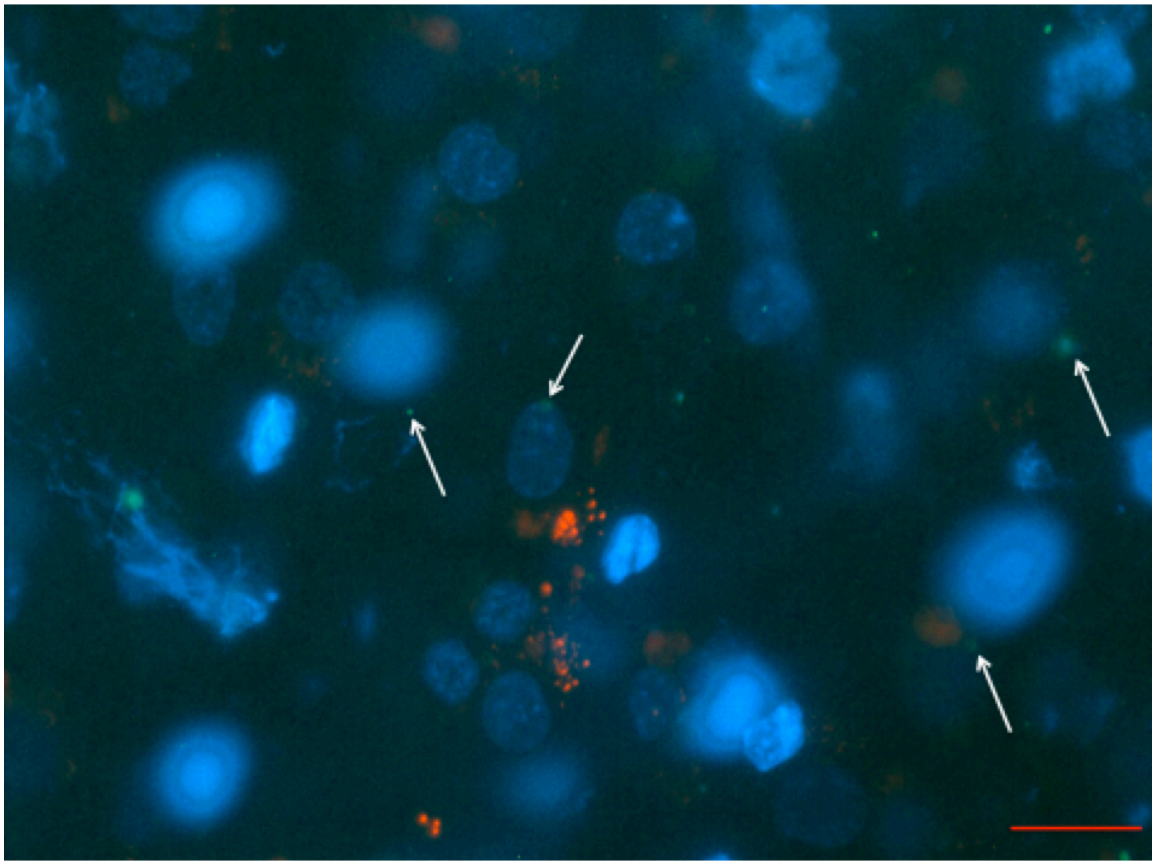

D)

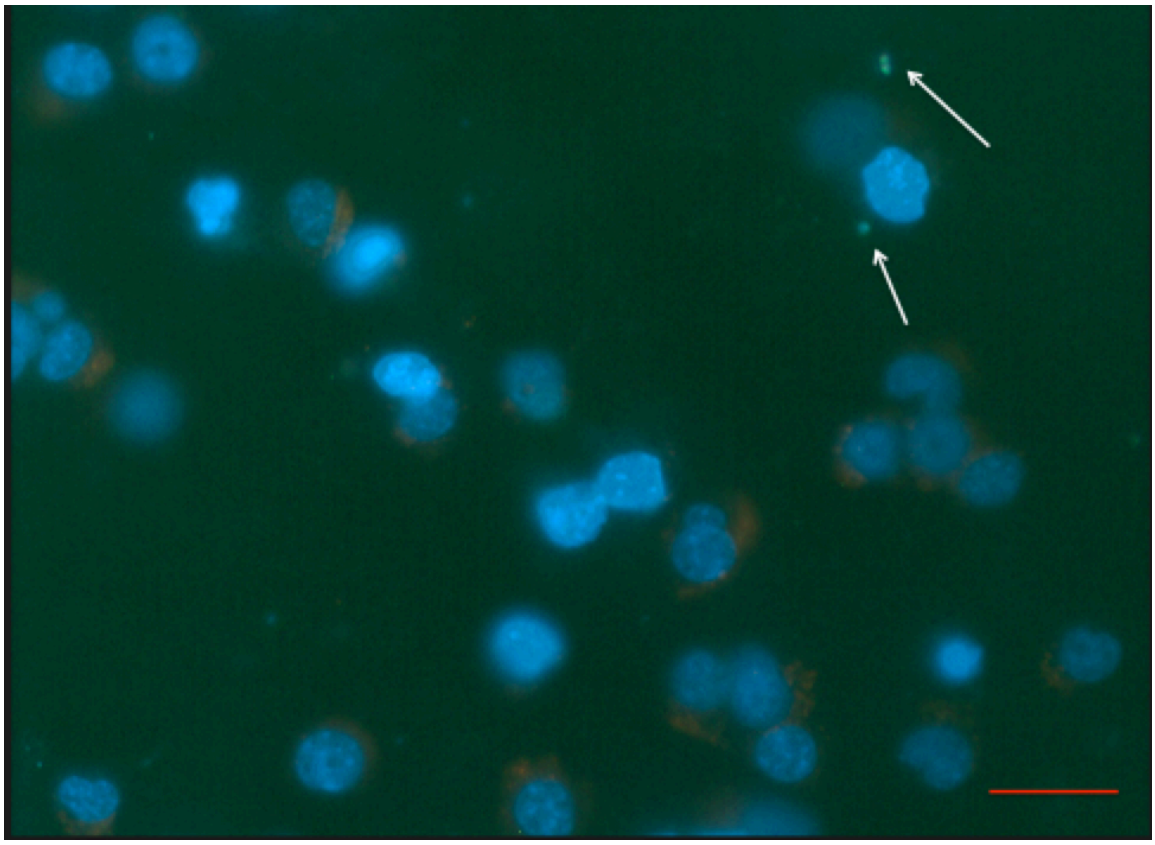

E)

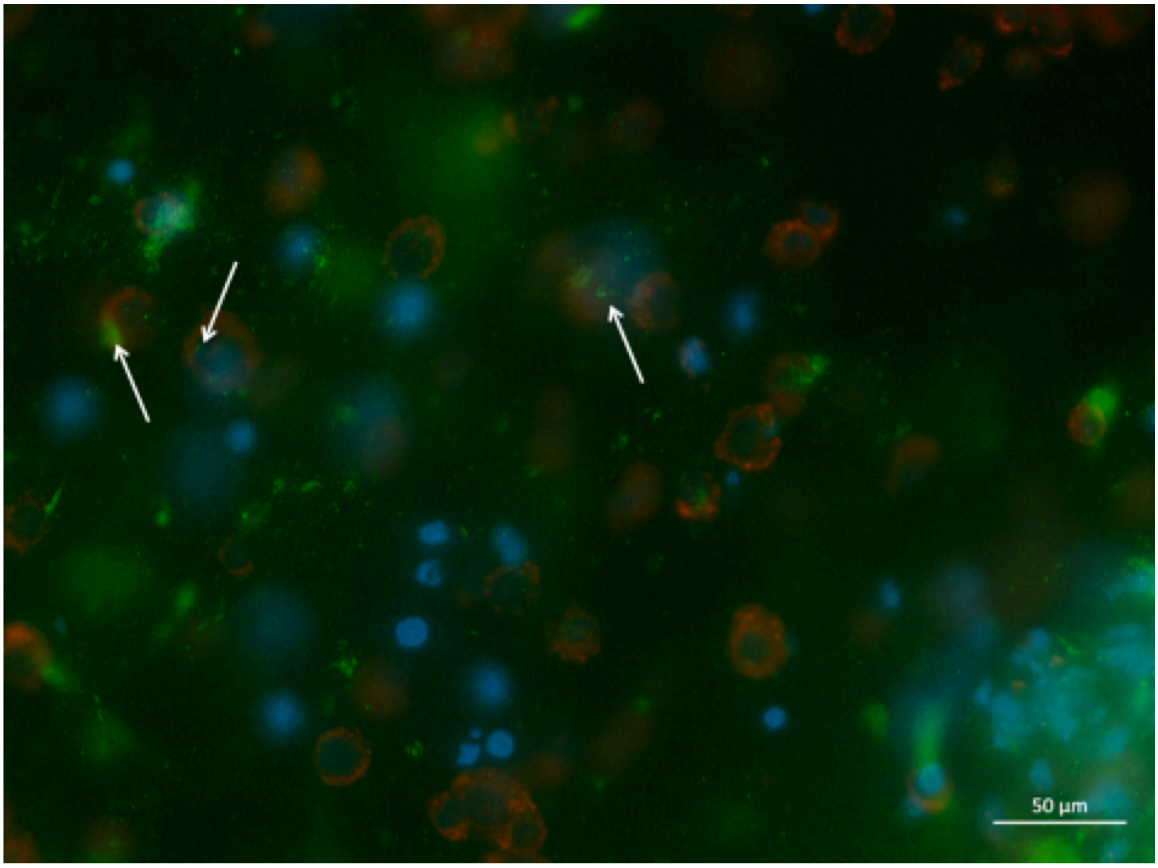

Figure 5.7 Fluorescence microscopy images of RAW 264.7 murine macrophages incubated with fluorescein tagged particles: A) GUR 1020 XL, B) GUR 1020 XL AOX, C) GUR 1050 XL, D) GUR 10150 XL VE and E) FluoSpheres®. The cell nucleus was stained with Hoechst 33342 and the lysosomes were stained with Lysotracker red. Images A to D were taken at 40X magnification (red scale bar represents 10 µm) and Image E was taken at 20X magnification (white scale bar represents 50 µm). White arrows indicate perinuclear particles; in the case of fluorospheres colocalised with lysosomes.

5.6 Discussion

The aim of this part of the study was to compare the novel 3D *in vitro* model developed in Chapter 3 to the outcomes of previous studies; measuring the production of osteolytic cytokines and reactive oxygen species (ROS) in response to treatment with UHMWPE wear debris, comparing particle uptake and sequestration of the novel 3D *in vitro* collagen gel encapsulation model to the previous 2D agarose gel model and treating cells with inflammatory pathway inhibitors and antioxidant compounds and assessing the release of pro-inflammatory, osteolytic mediators in LPS stimulated cells in order to elucidate which inflammatory pathways are affected by the anti-inflammatory activity of antioxidant doped, highly cross-linked UHMWPE. This

comparison was necessary to assess the use of the novel 3D *in vitro* model developed herein for future studies.

Singh and Jialal (2004) showed that treatment of LPS stimulated human mononuclear cells with vitamin E significantly reduced the release of pro-inflammatory cytokines, TNF-α, IL-1β and IL-6. Van Tits *et al.* (2000) also confirmed this and found that treatment of LPS stimulated human mononuclear cells with vitamin E significantly reduced the release of pro-inflammatory chemokine, IL-8. Deveraj and Jialal (1999) also found that treatment of LPS stimulated human mononuclear cells with vitamin E significantly reduced the release of LTB_4 but had no effect on the release of PGE_2. The present study aimed to assess whether these effects were reproducible in the novel 3D in vitro model developed in Chapter 3 in order to elucidate which inflammatory pathways may be affected by the presence of antioxidants, such as vitamin E. The present study found that all of the 0.1 – 1 μm UHMWPE wear debris treatments had no effect on the production of LTB_4 and PGE_2 in RAW 264.7 murine macrophages, whereas treatment with the full size range of GUR 1020 XL and GUR 1020 XL AOX UHMWPE wear debris reduced the levels of LTB_4 and PGE_2 produced by RAW 264.7 murine macrophages. This is not consistent with the findings of Singh and Jialal (2004), Van Tits *et al.* (2000) and Devaraj and Jialal (1999). However, a direct comparison between this study and the highlighted previous studies is not possible as the previous studies were examining the effect of vitamin E treatment on LPS stimulated PBMNC's whereas this study did not treat LPS stimulated cells with UHMWPE wear debris, the cell type used was different (murine cell line rather than human primary) and the antioxidants used were contained within UHMWPE wear debris. Additionally, a negative value for LTB_4 was obtained for cells cultured with the full size range of GUR 1020 XL in the present study – this value is less than the background and should have been repeated. This finding may therefore not be an accurate finding. This study did go onto treat LPS stimulated RAW 264.7 murine macrophages with antioxidant compounds (vitamin E and hindered phenol) alone (alongside inflammatory inhibitors). This study did find that LPS-stimulated RAW 264.7 murine macrophages did exhibit reduced levels of TNF-α, IL-1β and IL-6 upon treatment with vitamin E, which was consistent with Singh and Jialal (2004). Similarly, this study also found that LPS stimulated RAW 264.7 murine macrophages treated with PKC inhibitors, Calphostin C and Bisindolylmaleimide I, also significantly reduced the release of TNF-α, IL-1β, IL-6, LTB_4 and PGE_2. This is also consistent with Singh and Jialal (2004) and suggests that antioxidants, such as vitamin E, may achieve their anti-inflammatory behaviour through the inhibition of PKC phosphorylation in the prostaglandin and leukotriene synthesis reaction pathway. Again, a negative value for LTB_4 was obtained for LPS stimulated cells cultured with Calphostin C – this value is

less than the background and may not be accurate and so should have been repeated.

In the context of orthopaedic UHMWPE wear debris, Bladen *et al.* (2013a) found that PBMNC's incubated with GUR 1050 VE UHMWPE wear debris (3000 and 30,000 ppm) (non-cross-linked) exhibited significantly reduced levels of TNF-α, IL-1β and IL-6 compared to PBMNC's incubated with GUR 1050 virgin UHMWPE wear debris. Bladen *et al.* (2013a) showed that PBMNC's incubated with GUR 1050 VE UHMWPE wear debris (3000 and 30,000 ppm) (non-cross-linked) exhibited no significant reduction in production IL-8 in comparison to PBMNC's incubated with GUR 1050 virgin UHMWPE wear debris. Bladen *et al.* (2013a) also showed that PBMNC's incubated with GUR 1050 VE (1000 ppm) produced significantly lower levels of TNF-α in comparison to PBMNC's incubated with GUR 1050 virgin UHMWPE wear debris. The results of the present study were not consistent with the results presented by Bladen et al (2013). The present study did not find evidence distinguishing between the effects of UHMWPE with and without antioxidant doping on cytokine release. The dosing regime of the particles was the same between studies; 100 μm^3 particles.cell^{-1}. However there were a number of limitations in both studies. Bladen *et al.* (2013a) used only non-cross-linked UHMWPE materials. Antioxidants, such as vitamin E, are typically added to quench the free radicals associated with the cross-linking process. Moreover, cross-linked UHMWPE exhibits a significantly reduced rate of wear in comparison to non-cross-linked, virgin UHMWPE (Galvin *et al.*, 2006) so virgin UHMWPE is used less often in the present day. Additionally, Bladen *et al.* (2013a) used doses of vitamin E that are not clinically relevant (3000 and 30,000 ppm) to show a reduction in the output of TNF-α, IL-1β and IL-6. Bladen *et al.* (2013a) did show that a clinically relevant dosage of 1000 ppm vitamin E in UHMWPE did produce a significant reduction in TNF-α output but failed to do the same for IL-1β and IL-6. The present study did use clinically relevant materials, i.e. highly cross-linked and with clinically relevant doses of antioxidant. The present study also compared the output of antioxidant doped, highly cross-linked to highly cross-linked as opposed to virgin UHMWPE wear debris. However, the present study did experience a number of issues with the storage and treatment of the UHMWPE bar stock used to cut pins from to create UHMWPE wear debris. The suboptimal storage conditions and irradiation treatment could have caused oxidative embrittlement of the polymer which may have affected the overall behaviour of the material *in vitro*. Additionally, the length of time the bar stock was aged on the shelf may have allowed the antioxidant compounds present to degrade over time; meaning at the time of testing a sufficient dose of antioxidant was not present to create a significant anti-inflammatory response *in vitro*. There is no direct evidence in the current literature that vitamin E or hindered phenols degrade over time however the candidate could not find any studies that directly

assess this rather than the overall oxidative stability of the UHMWPE material assessed. However, all studies examined do preserve their samples in vacuum sealed bags and store them frozen in order to reduce unintentional degradation or aging between studies (Berlin *et al.*, 2011) therefore it is acknowledged that UHMWPE and/or antioxidant degradation is possible in suboptimal storage conditions. The present study did however find that the presence of highly cross-linked UHMWPE wear debris, whether antioxidant doped or not, did not affect the levels of KC (a homologue of IL-8 in mice) produced. However, this may not necessarily be a reliable result if the suboptimal storage conditions and irradiation treatment reduced the clinical relevance of the materials tested.

Gowland (2014) treated PBMNC's with aseptic highly cross-linked and highly cross-linked, antioxidant-doped UHMWPE wear debris generated on the single station multidirectional POP wear simulator and assessed the effect on the release of pro-inflammatory and pro-osteolytic cytokine, TNF-α. The particles were not filtered according to size prior to incubation with cells and resembled the wide range of particle sizes that would be found *in vivo*. When PBMNC's seeded at 1 x 10^5 cells.ml^{-1} were dosed with 100 μm^3 particles.cell^{-1}, Gowland (2014) found that there was no significant effect on the release of TNF-α for any of the particle treatments. However, when Gowland (2014) increased the number of cells per well to 2 x 10^5 cells.ml^{-1} and the particle dosage to 500 μm^3 particles.cell^{-1}, PBMNC's treated with GUR 1050 XL VE and GUR 1020 XL AOX UHMWPE wear debris exhibited a significant reduction in the release of TNF-α in comparison to PBMNC's treated with GUR 1050 XL UHMWPE wear debris. The present study found that there was no significant effect on release of TNF-α when RAW 264.7 murine macrophages were treated with any of the full size range UHMWPE wear debris which was consistent with the initial findings of Gowland (2014). The present study did not replicate the findings of Gowland (2014) at a higher dosing regime. There were a number of differences between the two studies and limitations to both. Gowland (2014) increased the particle dose per cell in order to increase the percentage of particles within the critical size range known to activate macrophages however it was not possible to increase the particle dose used in this study. The increased volume of lubricant required would have affected the ratio of components in the collagen gel, reducing the integrity of the gel and resulting in the gel being unable to set. In retrospect, it may have been possible to filter the particles and resuspend them in a smaller volume to achieve a higher dose. However this study did account for this by including UHMWPE wear debris generated using the six station multidirectional POP wear simulator and filtering the debris into the critical size range of 0.1 – 1 μm. RAW 264.7 murine macrophages incubated with 0.1 – 1 μm UHMWPE debris did exhibit a significantly reduced output of TNF-α, however this was the case for all materials tested (highly cross-linked and antioxidant doped, highly cross-linked).

There was no distinct anti-inflammatory effect observed for GUR 1050 XL VE and GUR 1020 XL AOX. Gowland (2014) included GUR 1050 XL as a control to compare the in vitro effects of GUR 1050 XL VE and GUR 1020 XL AOX but was unable to include GUR 1020 XL as a control due to lack of material availability. This study did address this weakness by including GUR 1020 XL as a control material however, as discussed in Chapter 4, significant issues with the storage and irradiation treatment of the UHMWPE materials may have affected accuracy of the *in vitro* outcomes of the study.

Gowland (2014) also compared the intracellular concentration of ROS produced in response to GUR 1050 XL and GUR 1050 XL VE wear debris and found that PBMNC's treated with GUR 1050 XL VE UHMWPE wear debris exhibited significantly decreased levels of ROS in comparison to PBMNC's treated with GUR 1050 XL. The present study did not find any significant effects on the production of ROS in RAW 264.7 murine macrophages in response to any of the particle treatments compared to the cells only control. This was not consistent with the findings of Gowland (2014). Gowland (2014) used the ImageIt LIVE cellular ROS quantitation kit which provided Intracellular ROS levels in addition to fluorescent images showing the sites of oxidation within the cell, whereas this study used the Abcam DCFDA cellular ROS detection assay kit which only provided cellular ROS levels. The previously outlined issues with UHMWPE bar stock (i.e. shelf aging) could have allowed the antioxidants to degrade over time thus a sufficient volume of antioxidants may not have been present in the wear debris to produce a reduction in cellular ROS during this study. Future studies would repeat this assay over 3 or 5 days in order to assess whether a longer time frame is needed to observe the presence of ROS. Additionally, future studies would include cells plus TBHP plus particle treatment conditions in order to assess whether the antioxidants present (or not) in the UHMWPE wear debris quench ROS synthesis and reduce the levels of ROS observed. Additionally, future studies could have viewed the plate using microscopy to provide qualitative images showing intracellular ROS levels.

Finally, Liu (2012) imaged the uptake of GUR 1020 UHMWPE wear debris in PBMNCs and was able to co-localise the particles with the lysosomes around the nucleus. Liu (2012) stained the particles with sodium fluorescein, the cell nucleus with Hoechst 33342 and the lysosomes with CD 63. Gowland (2014) took this further by imaging the uptake of GUR 1050 XL UHMWPE wear debris and FluoSpheres® in PBMNC's. The particles were imaged in the cytoplasm around the nucleus. Gowland (2014) stained the particles with sodium fluorescein and the cell nucleus with Hoechst 33342 however did not include a lysosome specific dye to co-localise the particles in the lysosomes. The present study imaged the uptake and sequestration of both highly

cross-linked and antioxidant doped highly cross-linked UHMWPE: GUR 1020 XL, GUR 1050 XL, GUR 1020 XL AOX and GUR 1050 XL VE (in addition to FluoSpheres® as a control). These materials were chosen in order to assess whether there was any difference in uptake and storage between materials. Unlike Gowland (2014), the present study included lysotracker red to co-localise the particles as Liu (2012) did. The present study was able to ascertain that all particles, irrespective of the material, were located around the nucleus; this was consistent with the findings of Liu (2012) and Gowland (2014). Unfortunately, the UHMWPE wear debris was unable to be clearly co-localised with the lysotracker red dye conclusively as very few fluorescently tagged particles were visible, whereas the FluoSpheres®, already fluorescently tagged, clearly showed co-localisation within the cells lysosomes. It is not clear why so few fluorescein stained UHMWPE particles were visible; it is possible that some particles were lost in the experimental process as there are multiple filtration steps and transfers between vessels.

Overall, the 3D model developed in Chapter 3 was not successful in reproducing the findings of previous studies. There were a number of issues associated with it; notably inadequate development of the model in Chapter 3 and poor quality UHMWPE bar stock used for wear debris development. The overall success of the model will be discussed in more detail in Chapter 6.

There are number of ways in which the present study could be developed further. FluoSpheres® were included as a positive particle control based on the standard practice of previous studies however, in this study, FluoSpheres® did not produce a reliable positive response. During the model development in Chapter 3, >10 μm Ceridust® repeatedly generated a significant release of TNF-α. Although this was unexpected and not consistent with previous studies, this may be a genuine effect in 3D studies and may have provided a more reliable positive particle control than FluoSpheres®. An additional study treating LPS stimulated RAW 264.7 murine macrophages with GUR 1020 XL, GUR 1050 XL, GUR 1020 XL AOX and GUR 1050 XL VE UHMWPE wear debris to assess any reduction in cytokine release could be carried out in order to compare to the reduction in cytokine release by LPS stimulated cells treated with inflammatory pathway inhibitors and antioxidant compounds. Furthermore, other cytokines, MCSF and GM-CSF, which are implicated in osteolysis could have been assessed in response to treatment with UHMWPE wear debris. A potential weakness of the novel *in vitro* model is the use of a mouse cell line which is less representative than human primary cells. The use of U937 human histiocytes in this model could be developed further. Additionally, differentiated osteoclasts could be trialled in the model which could then be used to assess osteolysis directly using relevant assays, such as the TRAP assay.

Table 5.6 Summary table of different UHMWPE materials cultured with the 3D *in vitro* model and the subsequent cytokine (TNF-α, IL-1β, IL-6, KC, LTB_4 and PGE_2) and ROS release. ↑ indicates a significant increase in cytokine release. ↓ indicates a significant decrease in cytokine release and ✖ indicates no significant release of cytokine or ROS in comparison to the cells only negative control.

	TNF-α	IL-1β	IL-6	KC	LTB_4	PGE_2	ROS
SS 1020 XL	X	X	X	X	↓	↓	X
SS 1020 XL AOX	X	X	X	X	↓	↓	X
SS 1050 XL	X	↓	X	X	X	X	X
SS 1050 XL VE	X	↓	X	X	X	X	X
6S 1020 XL	↓	↑	X	X	X	X	X
6S 1020 XL AOX	↓	X	X	X	X	X	X
6S 1050 XL	↓	X	X	X	X	X	X
6S 1050 XL VE	↓	X	X	X	X	X	X

Table 5.7 Summary table of different inhibitors and antioxidants cultured with the 3D *in vitro* model and the subsequent cytokine (TNF-α, IL-1β, IL-6, LTB_4 and PGE_2) release. ↑ indicates a significant increase in cytokine release. ↓ indicates a significant decrease in cytokine release and ✖ indicates no significant release of cytokine or ROS in comparison to the cells only negative control.

	TNF-α	IL-1β	IL-6	LTB_4	PGE_2
Calphostin C 250	↓	↓	↓	↓	↓
Calphostin C 500	↓	↓	↓	X	X
Bisindolylmaleimide I 0.1	X	↓	↓	↓	↓
Bisindolylmaleimide I 1	↓	↓	↓	X	X
MK 886 1	X	↓	X	X	X
REV 5901 10	X	↓	X	X	X
Indomethacin 10	X	↓	X	X	X
Vitamin E	↓	↓	↓	X	X

Hindered phenol	↓	↓	↓	X	X

5.7 Conclusion

- GUR 1050 XL and GUR 1050 XL VE UHMWPE wear debris (full range of particle sizes) significantly reduced the release of IL-1β from RAW 264.7 murine macrophages in collagen gel. GUR 1020 XL and GUR 1020 XL AOX UHMWPE wear debris (full range of particle sizes) significantly reduced the release of LTB_4 and PGE_2 from RAW 264.7 murine macrophages in collagen gel. The full size range of UHMWPE wear debris produced on the single station POP wear simulator rig (GUR 1020 XL, GUR 1020 XL AOX, GUR 1050 XL and GUR 1050 XL VE) had no significant effect on the release of TNF-α, IL-6 and KC from RAW 264.7 murine macrophages in collagen gel. This was not consistent with previous studies and it is difficult to ascertain the potential anti-inflammatory effects (and their mechanism) of vitamin E and hindered phenols in an orthopaedic context from the data generated in this study.
- GUR 1020 XL UHMWPE wear debris (0.1 – 1 μm) significantly elevated the release of IL-1β. GUR 1050 XL, GUR 1050 XL VE and GUR 1020 XL AOX UHMWPE wear debris (0.1 – 1 μm) significantly reduced the release of TNF-α. UHMWPE wear debris filtered into the size range 0.1 – 1 μm (GUR 1020 XL, GUR 1020 XL AOX, GUR 1050 XL and GUR 1050 XL VE) had no significant effect on the release of IL-6, KC, LTB_4 and PGE_2 from RAW 264.7 murine macrophages. This was not consistent with previous studies and it is difficult to ascertain the potential anti-inflammatory effects (and their mechanism) of vitamin E and hindered phenols in an orthopaedic context from the data generated in this study.
- Treatment with Calphostin C and Bisindolylmaleimide I significantly reduced the release of TNF-α, IL-1β, IL-6, LTB_4 and PGE_2 in LPS stimulated RAW 264.7 murine macrophages. Treatment with Vitamin E and Pentaerythritol tetrakis (3,5-di-*tert*-butyl-4-hydroxyhydrocinnamate) significantly reduced the release of TNF-α, IL-1B, and IL-6 in LPS stimulated RAW 264.7 murine macrophages. Treatment with Indomethacin, MK 886 and REV 5901 significantly reduced the release of IL-1B in LPS stimulated RAW 264.7 murine macrophages. It is possible that vitamin E and Pentaerythritol tetrakis (3,5-di-*tert*-butyl-4-hydroxyhydrocinnamate) exhibit anti-inflammatory behaviour by interacting with the PKC pathway in order to reduce the release of TNF-α and IL-6 whereas the antioxidants may act via a more general mechanism to reduce the release of IL-1β.

- GUR 1020 XL, GUR 1020 XL AOX, GUR 1050 XL and GUR 1050 XL VE UHMWPE wear debris created using the full size range and 0.1 – 1 μm did not produce a significant amount of ROS within RAW 264.7 murine macrophages in collagen gel in 24 hours.
- Fluorescent imaging showed that highly cross-linked, antioxidant doped and highly cross-linked UHMWPE wear debris particles are uptaken by RAW 264.7 murine macrophages and are located around the nucleus within the cytoplasm. Further imaging showed the co-localisation of FluoSpheres® within the lysosomes around the cell nucleus. The uptake and co-localisation of UHMWPE wear particles (and FluoSpheres®) is consistent with previous studies, which implies the presence of antioxidant compounds in the polyethylene structure does not affect the uptake and storage mechanism.

Chapter 6
General discussion

6.1 Original project aims

The overall aim of this study was to develop a novel 3D *in vitro* model to assess cellular responses to UHMWPE wear debris that could aid with determining whether the presence of antioxidants, such as vitamin E and hindered phenols, in highly cross-linked UHMWPE can reduce the release of osteolytic cytokines.

Chapter 3 aimed to develop a novel 3D *in vitro* model to assess the cellular response to model polyethylene particles in order to address the problems associated with donor variation and dependence on cell penetration associated with the existing 2D method in order to enhance the reliability and repeatability of the model.

Chapter 4 aimed to aseptically generate both highly cross-linked and antioxidant-doped, highly cross-linked UHMWPE wear debris using both the single and six station wear simulator rigs to culture with the novel 3D *in vitro* model.

Chapter 5 aimed to measure the cellular response to antioxidant doped, highly cross-linked UHMWPE wear debris in the novel 3D *in vitro* model and compare the results to previous studies.

6.2 Overall discussion

Chapter 3 trialled various combinations of three cell types (PBMNCs, U937 human histiocytes and RAW 264.7 murine macrophages) in two different types of gel (agarose and collagen) in terms of the viability of each type of cell in each type of gel and the ability of each cell in each type of gel to release a significantly elevated amount of TNF-α upon stimulation with model polyethylene particles, Ceridust®, and FluoSpheres®; both of which have been shown to induce such a response in PBMNCs, U937 human histiocytes and murine peritoneal macrophages in previous studies by Green *et al.* (1998) and Matthews *et al.* (2000). This study found that none of the cell types experienced a reduction in cell viability upon culture in either agarose or collagen gel over 3 days. This study also found that not all cell and gel combinations tested were able to produce a significantly elevated release of TNF-α. Interestingly, the none of the cell types produced a significantly elevated release of TNF-α in response to model polyethylene particles in the critical size range 0.1 – 10 μm (Green *et al.*, 1998). Only >10 μm Ceridust® particles stimulated a significantly elevated release of TNF-α in PBMNCs in agarose, RAW 264.7 murine macrophages

in both agarose and collagen and non-transformed U937 human histiocytes in collagen. It is not clear why the critical size range of Ceridust® particles failed to stimulated a significant release of TNF-α as previous studies suggested they would. It is possible that the some critical size Ceridust® particles were trapped in the >10 μm fraction however characterisation studies were not carried out on the Ceridust® particles so it is not possible to evidence this either way. The primary objective of this chapter was to develop a novel *in vitro* model in order to address the issues of donor heterogeneity and cell penetration dependence associated with the previous model. To that effect, the use of PBMNCs were discontinued to remove donor heterogeneity. Additionally, the use of agarose gel was discontinued to allow the simultaneous encapsulation of cells and particles and remove the need for cells to penetrate the gel to access the particles. Finally, RAW 264.7 murine macrophages were chosen over U937 human histiocytes as the PMA treatment required to transform U937 human histiocytes into activated U937 human macrophages also inhibits the PKC pathway which was of interest in Chapter 5.

Chapter 4 aseptically generated highly cross-linked and antioxidant doped, highly cross-linked UHMWPE wear debris for use in cell culture studies in Chapter 5. This was carried out using both single and six station multidirectional POP wear simulators. The particles generated were then isolated, imaged using FEGSEM and characterised according to size and volume distribution. Additionally, the particles and wear test lubricants were tested for microbiological and endotoxin contamination. All particles tested were free of microbiological and endotoxin contamination. The particles generated using the single station multidirectional POP wear simulator were used directly in cell culture studies to represent the full size range of particles found *in vivo* which range from several mm to 10 nm (Tipper *et al.*, 2000). Prior to this a pooled sample of particles from each material generated on both types of wear simulator were isolated, imaged and characterised. All particle samples demonstrated the morphologies seen previously by studies such as Tipper *et al.* (2000); such as plate-like particles and particle aggregates. The wear debris volumes and wear factors measured, especially for the materials tested on the six station multidirectional POP wear simulator, were very high; several times higher than demonstrated by Gowland (2014). This was attributed to the lack of optimal storage conditions; allowing the materials to undergo oxidative embrittlement after shelf aging. The size and volume distribution data revealed little similarity between particles of the same material generated using different wear simulator. Particles tended to be larger when generated using the single station rather than the six station multidirectional POP wear simulator. This difference in particle size was attributed to the difference in lubrication regimes between the two wear simulators. The particles generated using

the six station multidirectional POP wear simulator were filtered into the critical size range of 0.1 – 1 μm prior to cell culture.

Chapter 5 assessed the release of inflammatory, osteolytic cytokines, chemokines and mediators in response to the UHMWPE wear debris generated (both the unfiltered, full size range and a filtered, critical size range of 0.1 - 1 μm) and treatment with inflammatory pathway inhibitors and antioxidant compounds from the novel *in vitro* model. Additionally, the release of ROS in response to the UHMWPE wear debris generated (both the unfiltered, full size range and a filtered, critical size range of 0.1 - 1 μm) from the novel *in vitro* model was measured. Finally, the internal sequestration of the UHMWPE wear debris generated (filtered into the critical size range of 0.1 – 1 μm) and FluoSpheres® within RAW 264.7 murine macrophages in collagen gel. Treatment of the novel *in vitro* model with all size ranges of UHMWPE wear debris produced no significant release of inflammatory, osteolytic cytokines, chemokines and mediators. This was not consistent with previous studies by Green *et al.* (1998), Matthews *et al.* (2000a, 2001) and Gowland (2014). Green *et al.* (1998) treated murine peritoneal macrophages with Ceridust® particles therefore the two studies are not necessarily directly comparable as the former used a different cell type and model low density polyethylene particles rather than UHMWPE wear debris. Similarly, both Matthews et al. (2000a, 2001) and Gowland (2014) used different cell types, PBMNCs and U937 human histiocytes, which may not be directly comparable with RAW 264.7 murine macrophages. However all three previous studies are consistent with one another, suggesting that the model and particles used in the present study may be the outlier in terms of the inflammatory response observed. It is possible that the unusual material behaviour of UHMWPE (possibly owing to shelf aging) contributed to the observed release of inflammatory cytokines, chemokines and mediators.

Treatment of LPS stimulated RAW 264.7 murine macrophages in collagen gel with Calphostin C, Bisindolylmaleimide I, Vitamin E and Pentaerythritol tetrakis (3,5-di-*tert*-butyl-4-hydroxyhydrocinnamate) significantly reduced the release of TNF-α, IL-1β, IL-6, LTB_4 and PGE_2 compared to LPS stimulated cells with no treatments; implying that antioxidants may achieve their anti-inflammatory activity through inhibition of the PKC pathway. This was consistent with previous studies by Devaraj and Jialal (1999) and Singh and Jialal (2004).

Treatment of RAW 264.7 murine macrophages in collagen gels with all size ranges of UHMWPE wear debris produced no significant release of ROS. Gowland (2014) was able to show that the amount of intracellular ROS was less for PBMNCs treated with GUR 1050 XL VE in comparison to GUR 1050 XL however the present study was able to make no such distinction as all materials uniformly produced no significantly elevated levels of ROS. The present study carried out a quantitative ROS assay

whereas Gowland (2014) carried out a qualitative imaging study so it is difficult to directly compare the two studies. It is possible that imaging in the present study may have revealed more information. Additionally, a longer study i.e 3 or 5 days, may have been more appropriate to allow for maximum ROS production. It is possible that the suboptimal UHMWPE materials used may have impacted the intracellular ROS levels.

Fluorescent imaging of UHMWPE wear debris internalised by RAW 264.7 murine macrophages in collagen did show that particles are perinuclear which is consistent with the findings of Gowland (2014). The present study was able to take this a step further by co-localising FluoSpheres® with lysosomes in RAW 264.7 murine macrophages.

Overall the novel *in vitro* model developed during this study did not produce data consistent with previous cell-particle studies. This could be due to the potential shelf aging issues associated with the UHMWPE materials used. It is also possible that the model itself is unsuitable for this particular application. The effect of aged UHMWPE material is more likely to account for the inconsistent observations rather than lack of model suitability as the model did generate inflammatory responses consistent with previous studies by Singh and Jialal (2004) when treated with inflammatory inhibitors and antioxidant compounds rather than generated UHMWPE particles. It is possible that non-transformed U937 human histiocytes in collagen gel may have performed better in this context however these cells were not chosen owing to uncertainty regarding the maturity of the cells – non-transformed U937 human histiocytes are not true macrophages as they are at a more immature stage whereas RAW 264.7 murine macrophages are a more mature phenotype.

6.3 Further work

There were numerous areas in which this study could have been developed further with additional time and resources. In particular, the *in vitro* model chosen could have been improved further and the assays and reagents used to assess anti-inflammatory and antioxidant behaviour could have been optimised further.

6.3.1 Development of a novel 3D *in vitro* model for measuring cellular responses to model polyethylene particles

This study did have several limitations. Primarily, there was no data for U937 human histiocytes treated with model particles after 24 hours in either agarose or collagen gel. Unfortunately, this data was lost due to experimental error and the candidate made the decision not to repeat the assay for this time point due to time pressures and that this cell type was not being carried forward to the remaining parts of the

study. Future studies would repeat this time point to give a fuller picture as to how U937 human histiocytes in either agarose or collagen gel functions as a potential novel 3D model to measure cellular response to UHMWPE wear debris. Viability studies of PBMNC's, U937 human histiocytes and RAW 264.7 murine macrophages in agarose and collagen gel could have been supplemented with live/dead staining and fluorescent imaging. This would have added an additional layer of confidence to the overall findings in addition to showing the distribution of cells throughout each type of gel (or lack of in some cases of agarose gel use).

An additional limitation of this study was that no characterisation data, i.e. size and volume distribution, was obtained for the Ceridust® model polyethylene particles used. This was an oversight and would have provided more detail on the true size range of the particle fractions (>10 μm, 1 – 10 μm and 0.1 – 1 μm) used. It may have revealed why cells were producing TNF-α in response to >10 μm Ceridust® rather than those sizes in the critical size range determined by Green *et al.* (1998) which failed to generate a significant TNF-α response in any cell type. Future studies would obtain this characterisation data. It is possible that producing an inflammatory response to >10 μm Ceridust® particles rather than the expected critical size range of 0.1 - 10 μm is a legitimate effect in a 3D model as opposed to 2D. The effect was certainly reproducible with RAW 264.7 murine macrophages in collagen gel however it would be prudent for all experiments showing this effect to be reproduced to assess its validity.

Initial trials of the cell types and gel types used to create a novel *in vitro* model could have been conducted using artificially generated UHMWPE wear debris rather than model polyethylene particles. Moreover, the panel of cytokines tested could have been expanded to include IL-1β and IL-6, which are also common pro-inflammatory, osteolytic cytokines and may further inform which model is a more robust choice for use in this context. Further cell types, such as MG-63 osteoblasts (Vermes *et al.*, 2001) and macrophage cells that have been chemically transformed into osteoclasts, could have been trialled in these models to infer more direct information on the osteolytic pathway.

Future studies could trial the use of non-transformed U937 human histiocytes in collagen gel (as treatment with PMA to transform them into activated macrophages inhibits the actions of PKC which may interfere with anti-inflammatory studies). Non-transformed U937 human histiocytes could be treated with UHMWPE wear debris and compared to transformed U937 human macrophages for the production of a panel of inflammatory cytokines so assess whether they are capable of responding in the same manner to UHMWPE particles. The cell type is human and therefore preferable to a murine cell line for increased clinical accuracy however they remain immature without

treatment with PMA. It is also possible to use this model with PBMNC's that have been magnetically cell sorted (MACS) using CD 14 and CD 68 macrophage markers in order to separate out the relevant phagocytic fraction (usually around 6% (Liu, 2012)).

In hindsight, in order to construct a suitable 3D *in vitro* model, the existing model should have been stripped back and each feature examined and optimised. This was attempted in the present study in terms of trialling new types of gel and new cell types however, upon reflection, this was not detailed enough. The optimal cell seeding density and particle doses in 3D should have been examined in addition to optimising the time points used for ELISA analysis. It is possible that longer culture times were needed for the 3D model to show any effects in terms of inflammatory cytokine and chemokine release. The present study used the cell seeding density established in the existing 2D *in vitro* model however the volume of the gel ought to have been accounted for (rather than simply the 2D area). Since the present study used a cell seeding density of 1 x 10^5 cells in an area of 0.95 cm^2, this ought to have been multiplied by itself and the depth of the well (0.2 cm) in order to estimate a cell seeding density (1.9 x 10^9 cells per well).

6.3.2 Generation, isolation and characterisation of antioxidant doped, highly cross-linked ultra-high molecular weight polyethylene wear debris

There were a number of limitations to this study. Since the primary objective of this chapter was not to determine wear performance data for the materials used, certain measurements were not obtained. The surface roughness of the CoCr plates used were not obtained using Talysurf before and after each test. Future studies would obtain these measurements as they may have provided further insight, such any potential differences between individual plates, as to the unusually high wear debris volumes and wear factors observed during this study. Moreover, EDX analysis of the UHMWPE wear debris was not performed when obtaining FEGSEM images of the particles. Future studies would perform EDX analysis as this may reveal any usual elemental peaks that may relate to the oxidation of the bar stock. The main limitations to this study were the age and storage conditions of the UHMWPE materials used. The shelf aging in oxidative conditions over several years could have decreased the wear resistance of the UHMWPE materials and resulted in the high volume of wear debris and large wear factors observed. Future studies would be improved by obtaining fresh UHMWPE bar stock or pins from industrial collaborators. Additionally, the correct storage of UHMWPE materials in vacuum packaging at -80°C, to prevent oxidation, would remove shelf aging and oxidation as a potential variable in future studies. Similarly, there was a lack of highly cross-linked UHMWPE bar stock so virgin

UHMWPE bar stock was sent for commercial irradiation treatment. The dose (9.39 MRad) was slightly different from the 10 MRad GUR 1050 XL and 8 MRad GUR 1020 XL clinical materials. This slight difference is unlikely to have accounted for the high wear debris volumes and wear factors however irradiating already aged UHMWPE may have increased the deterioration of the materials. In addition, any air trapped in the vacuum packaging may have contributed to this deterioration. As before, future studies would source already cross-linked and sterilised UHMWPE material to ensure these processes had taken place under optimal conditions so as not to influence any future data. Additionally, obtaining industrial materials would provide the necessary information on whether the bar stock had been remelted or annealed following irradiation and also whether the antioxidant was blended or diffused. These processes can also affect the mechanical behaviour of UHMWPE and may have influenced the results obtained in this study.

The size and volume distribution of the particles generated in this study were compared to existing data from previous studies, where possible, in order to validate the particles produced. However, much of the necessary data does not exist as highly cross-linked, antioxidant doped UHMWPE materials are still relatively new. There is data concerning the wear rates of such material but not the specifics regarding the size and volume distribution of the particles. It would have been even more useful to compare the size and volume distribution data of the particles produced in this study to similar data obtained from retrieval studies of identical materials however, as highly cross-linked, antioxidant doped UHMWPE materials are still relatively new and clinical studies often take upwards of 10 years, such data is not yet in existence.

Future studies would trial the generation of sterile UHMWPE wear debris using the six station multidirectional POP wear simulator with lubricant containing FBS in order to maintain a constant lubrication regime between simulators. Moreover, retrieved UHMWPE wear debris is typically coated with adhered proteins which can affect the inflammatory response to the particles therefore the addition of FBS to debris generated using the six station multidirectional POP wear simulator would increase the relevance of the particles tested.

Virgin UHMWPE (GUR 1020 and GUR 1050) could be included in future studies as a further control to distinguish between the biological response to cross-linked and non-cross-linked UHMWPE.

Additionally, it would be useful to assess experimental antioxidant doped UHMWPE materials, such as anthocyanin doped UHMWPE (acquired through collaboration), alongside clinically available vitamin E and hindered phenol UHMWPE.

Finally, future studies would assess the size and volume distribution of the filtered, critical size range (0.1 – 1 μm) in addition to the pre-fractionated particles in all size ranges in order to obtain the true size and volume distribution of the fractionated particles used with which to greater elucidate the *in vitro* response to such particles.

6.3.3 Assessing the anti-inflammatory and antioxidant effects of antioxidant doped, highly cross-linked ultra-high molecular weight polyethylene wear debris using a novel 3D *in vitro* model

Overall, it was not clear whether the model developed in this study was appropriate to take forward in to future work. In order to assess this, further developments could be made to the model. The particle dose could be increased to 500 μm^3 which may result in a significant increase or reduction in the production of inflammatory cytokines. Gowland (2014) demonstrated that PBMNCs treated with 500 μm^3 of UHMWPE wear debris were more likely to release a significant amount of TNF-α than those treated with 100 μm^3 of UHMWPE wear debris. The present study was not able to treat cells with an increased dose of UHMWPE particles as the volume of lubricant required was too large and would have reduced the integrity of the collagen gels used to encapsulate the particles. In hindsight, a higher dose of particles could have been achieved by re-filtering the particles into a smaller volume although this would risk loss of particles when transferring between vessels. Moreover, it is difficult to resuspend UHMWPE in very small volumes as the UHMWPE particles are hydrophobic so all particles may not be incorporated into the cell culture medium. Future work could develop an approach to allow the encapsulation of larger volumes of UHMWPE wear debris without negatively impacting the collagen gel integrity. The test time on the wear simulators could be increased and the volume of lubricant allowed to evaporate towards the end of the test in order to increase the particle concentration whilst reducing the volume of lubricant present. It is possible that the lack of inflammatory response to the critical size range of UHMWPE particles and occasional response to particles greater than 10 μm was a real effect of the 3D model as opposed to the 2D model; in which case, fresh clinical material ought to be sought and the experiments repeated to validate the effect and remove any concern than a lack of response is due to the aging of the material.

An additional study treating LPS stimulated RAW 264.7 murine macrophages with GUR 1020 XL, GUR 1050 XL, GUR 1020 XL AOX and GUR 1050 XL VE UHMWPE wear debris to assess any reduction in cytokine release could be carried out in order to compare to the reduction in cytokine release by LPS stimulated cells treated with inflammatory pathway inhibitors and antioxidant compounds. Furthermore, other

cytokines, such as MCSF and GM-CSF, which are implicated in osteolysis could have been assessed in response to treatment with UHMWPE wear debris.

It is clear that this study would have benefitted from further optimisation of the assays used to assess anti-inflammatory and antioxidant behaviour of UHMWPE wear debris used to treat the *in vitro* model developed herein. Future studies would repeat the ROS assay over 3 and 5 days in order to assess whether a longer time frame is needed to observe the presence of ROS in RAW 264.7 murine macrophages following UHMWPE particle treatment. Additionally, future studies would include cells plus TBHP plus particle treatment conditions in order to assess whether the antioxidants present (or not) in the UHMWPE wear debris quench ROS synthesis and reduce the levels of ROS observed. Moreover, future studies could have viewed the plate using microscopy to provide qualitative images showing intracellular ROS levels. Future studies would assess multiple concentrations of sodium fluorescein used to fluorescently tag the UHMWPE wear debris. The concentration used in this study may not have been sufficient hence the lack of visible UHMWPE wear debris in the microscopy images. Finally, ELISA was used to assess the production of inflammatory cytokines at 12 and 24 hour post particle treatment. Additional time points, such as 36 and 48 hours, could have been introduced in order to assess cytokine production over longer periods of time. Furthermore, LPS was used as a positive control in ELISA studies however, in several instances, RAW 264.7 murine macrophages treated with LPS failed to produce significantly increased release of inflammatory cytokine, chemokine or mediator. Future studies would trial LPS alongside other possible positive control substances, such as Camptothecin, to assess which compound was able to perform most effectively as a positive control.

A potential weakness of the novel *in vitro* model is the use of a mouse cell line which is less representative than human primary cells. This could be addressed by trialling the use of non-transformed U937 human histiocytes as discussed previously. It is also possible to use human PBMNC's differentiated into osteoclasts (although donor heterogeneity would still be problematic) or RAW 264.7 murine macrophages differentiated into murine osteoclasts. The model could then be used to assess osteolysis directly using relevant assays, such as the TRAP assay.

A novel 3D *in vitro* model could also be used to assess the potential anti-inflammatory effect of antioxidant doped UHMWPE at the genetic level using PCR to assess the downstream effect on genetic expression of inflammatory cytokines, such as TNF-α. Moreover, the antioxidant effect could also be assessed at the genetic level by assessing the up or down regulation of common oxidative damage genes; HIF-1α, SOD 1/2/3 and OXR 1/2.

Finally, it would be useful to use the novel 3D *in vitro* model developed during this study for the basis of an *in vitro* model to directly assess osteolysis by culturing osteoclasts (transformed macrophage cells – primary or cell line) onto calcium hydroxyapatite discs and treating with UHMWPE wear debris. The discs could be assessed with micro-CT to account for volumetric changes in the disc which could inform how osteolytic different types of UHMWPE are.

6.4 Conclusion

- This study began to develop a 3D representation of local macrophages in the periprosthetic environment to model the cellular response to UHMWPE wear debris.
- The novel model developed in this study attempted to encapsulate UHMWPE wear debris with RAW 264.7 murine macrophages to create a 3D *in vitro* model composed of ECM material; collagen.
- RAW 264.7 murine macrophages were able to take up and sequester UHMWPE wear debris and FluoSpheres® in the lysosomes as demonstrated in PBMNC's in previous studies by Gowland (2014) and Liu (2012).
- The novel model developed in this study demonstrated the link between proposed anti-inflammatory behaviour of Vitamin E and hindered phenol compounds and the PKC inflammatory pathway.
- However, issues with suboptimal storage and treatment of UHMWPE bar stock prior to wear generation resulted in a skewed distribution of larger particles.
- Cells incubated with generated UHMWPE wear debris failed to produce the patterns of cytokine release observed in a previous study by Gowland (2014).
- The model developed requires significant optimisation; particularly transitioning from 2D into 3D, the cell seeding density, particle dose and culture times require further optimisation.
- Fresh clinical UHMWPE material would also be required for future studies in order to ensure the UHMWPE particles produced were clinically relevant and add confidence to any response or lack thereof being a true and accurate effect of the 3D model.
- Culturing LPS stimulated cells with generated UHMWPE wear debris in this model could further strengthen any potential link between the anti-inflammatory behaviour of antioxidant doped, highly cross-linked UHMWPE and the PKC inflammatory pathway.
- Furthermore, this model could be adapted to include osteoclasts for direct osteolysis studies; for example the TRAP assay.

- 3D *in vitro* collagen gel models, allowing simultaneous cell and particle encapsulation, could provide valuable insight into the chemical and genetic mechanisms of the potential anti-inflammatory and antioxidant behaviour of antioxidant doped, highly cross-linked UHMWPE which may further inform UHMWPE material development with alternative antioxidant compounds.

List of References

Abildtrup, M., Kingsley, G. H. and Scott, D. L. 2015. Calprotectin as a biomarker for rheumatoid arthritis: a systematic review. *The Journal Of Rheumatology*. **42**(5), p. 760–770.

Affatato, S., Spinello, M., Zavalloni, M., Mazzega-Fabbro, C. and Viceconti, M. 2008). Tribology and total hip joint replacement: Current concepts in mechanical simulation. *Medical Engineering And Physics*. **30**(10), p. 1305–1317.

Anderson, D. E. and Johnstone, B. 2017. Dynamic Mechanical Compression of Chondrocytes for Tissue Engineering: A Critical Review. *Frontiers In Bioengineering And Biotechnology*. **5**(December), p. 1–20.

Anderson, J. M., Rodriguez, A. and Chang, D. T. 2008. Foreign body reaction to biomaterials. *Seminars In Immunology*. **20**(2), pp. 86–100.

Arden, N. and Nevitt, M. C. 2006. Osteoarthritis: Epidemiology. *Best Practice And Research: Clinical Rheumatology*. **20**(1), p. 3–25.

Arend, W. P. 1995. Inhibiting the effects of cytokines in human diseases. *Advances In Internal Medicine*. **40**, p. 365 – 394.

De Bandt, M., Grossin, M., Driss, F., Pincemail, J., Bain-Chevaye, C. and Pasquier, C. 2002. Vitamin E uncouples joint destruction and clinical inflammation in a transgenic mouse model of rheumatoid arthritis. *Arthritis And Rheumatism*. **46**(2), p. 522–532.

Barbour, P. S. M. 1999. A hip joint simulator study using simplified loading and motion cycles generating physiological wear paths and rates. *Proceedings Of The Institution Of Mechanical Engineers, Part H: Journal Of Engineering In Medicine*. **213**(6), p. 455–467.

Baxter, R. M. Steinbeck, M. J., Tipper, J. L., Parvizi, J., Marcolongo, M. and Kurtz, S. M. 2009. Comparison of periprosthetic tissue digestion methods for ultra-high molecular weight polyethylene wear debris extraction. *Journal Of Biomedical Materials Research - Part B Applied Biomaterials*. **91**(1), p. 409–418.

Bellare, A., Schnablegger, H., and Cohen, R. E. 1995. A small-angle x-ray scattering study of high-density polyethylene and ultra-high molecular weight polyethylene. *Macromolecules*, **17**, p. 2325–2333.

Bergschmidt, P., Bader, R., and Mittelmeier, W. 2012. Metal hypersensitivity in total knee arthroplasty: Revision surgery using a ceramic femoral component – a case report. *The Knee*. **19**, p. 144 – 147.

Berlin, J. A., Braithwaite, G. J. C., Knight, J., Pletcher, D. and Rufner, A. 2011. *Oxidative Stability of Highly Crosslinked Vitamin E UHMWPE Blends in Extreme and Physiological Accelerated Aging Conditions*. [Poster]. ORS 2011 Annual Meeting, 13 - 16th Jan, California.

Besong , A.A., Hailey, J.L., Ingham, E., Stone, M., Wroblewski, B.M. and Fisher, J. 1997. A study of the combined effects of shelf ageing following irradiation in air and counterface roughness on the wear of UHMWPE. *Biomedical Materials And Engineering.* **7**(1), p. 59–65.

Bichara, D. A., Malchau, E., Sillesen, N. H., Cakmak, S., Nielsen, G. P. and

Muratoglu, O. K. 2014. Vitamin E-diffused highly cross-linked UHMWPE particles induce less osteolysis compared to highly cross-linked virgin UHMWPE particles in vivo. *Journal Of Arthroplasty*. **29**(9 SUPPL.), p. 232–237.

Birnkraut, H. W. 1991. Synthesis of UHMWPE. In Willert, H.G., Buchhorn, G.H., and Eyerer, P. eds. *Ultra-high Molecular Weight Polyethylene As A Biomaterial In Orthopedic Surgery*. Lewiston, New York: Hogrefe & Huber.

Bladen, C. L., Teramura, S., Russell, S. L., Fujiwara, K., FIsher, J., Ingham, E., Tomita, N. and Tipper, J. L. 2013a. Analysis of wear, wear particles, and reduced inflammatory potential of vitamin e ultrahigh-molecular-weight polyethylene for use in total joint replacement. *Journal Of Biomedical Materials Research - Part B Applied Biomaterials*. **101 B**(3), p. 458–466.

Bladen, C. L., Tzu-Yin, L., FIshe, J. and Tipper, J. L. 2013b. In vitro analysis of the cytotoxic and anti-inflammatory effects of antioxidant compounds used as additives in ultra high-molecular weight polyethylene in total joint replacement components. *Journal Of Biomedical Materials Research - Part B Applied Biomaterials*. **101 B**(3), p. 407–413.

Bracco, P., Bellare, A., Bistolfi, A. and Affatato, S. 2017. Ultra-high molecular weight polyethylene: Influence of the chemical, physical and mechanical properties on the wear behavior. A review. *Materials*. **10**(7), p. 791 - 813.

Bracco, P. and Oral, E. 2011. Vitamin E-stabilized UHMWPE for total joint implants: A review. *Clinical Orthopaedics And Related Research*. **469**(8), p. 2286–2293.

Brach Del Prever, E.M., Bistolfi, A., Bracco, P. and Costa, L. 2009. UHMWPE for arthroplasty: past or future?. *Journal Of Orthopaedics And Traumatology : Official Journal Of The Italian Society Of Orthopaedics And Traumatology.* **10**(1), p. 1–8.

Brigelius-Flohé, R. and Traber, M. G. 1999. Vitamin E: function and metabolism. *The FASEB Journal*. **13**(10), p. 1145–1155.

Brooks, R. A., Wimhurst, J. A. and Rushton, N. 2002. Endotoxin contamination of particles produces misleading inflammatory cytokine responses from macrophages in vitro. *The Journal Of Bone And Joint Surgery. British Volume*. **84**(2), p. 295–299.

Brown, C., Fisher, J., and Ingham, E. 2006. Biological effects of clinically relevant wear particles from metal-on-metal hip prostheses. *Proceedings Of The Institution Of Mechanical Engineers, Part H: Journal Of Engineering In Medicine.* 220(2), p. 355 – 369.

Burton, G. W. 1990. Vitamin E: Antioxidant Activity, Biokinetics, And Bioavailability. *Annual Review Of Nutrition.* **10**, p. 357 - 382.

Callaghan, J. J., Templeton, J. E., Liu, S. S., Pedersen, D. R., Goetz, D. D., Sullivan, P. M., and Johnston, R. C. 2004. Results Of Charnley Total Hip Arthroplasty At A Minimum Of Thirty Years. *The Journal Of Bone And Joint Surgery. American Volume*. **86–A**(4), p. 690–695.

Campbell, P., Ma, S., Schmalzreid, T. and Amstutz, H. C. 1996. Tissue digestion for wear debris particle isolation. *Journal Of Biomedical Materials Research*. **29**(10), p. 1393–1397.

Catelas, I., Petit, A., Marchand, R., Zukor, D., Yahia, L., and Huk, O. 1999. Cytotoxicity and macrophage cytokine induced by ceramic and polyethylene particles in vitro. *The Journal Of Bone And Joint Surgery.* **81B**(issue), p. 516 – 521.

Charnley, J. 1961. Arthroplasty of hip – a new operation. *Lancet*, 1(7187), p. 1129–1132.

Chiu, Y. G. and Ritchlin, C. T. 2017. Denosumab: targeting the RANKL pathway to treat rheumatoid arthritis. *Expert Opinion On Biological Therapy*. **17**(1), p. 119–128.

Cho, D. R., Shanbhag, A. S., Hong, C. Y., Baran, G. R. and Goldring, S. R. 2002. The role of adsorbed endotoxin in particle-induced stimulation of cytokine release. *Journal Of Orthopaedic Research*. 20(4), p. 704–713.

Chumakov, M. 2009. *Nitroxides as free radical scavengers in UHMWPE.* [Poster]. 55th Annual Meeting of the Orthopaedic Research Society, 22-25th Feb, Las Vegas.

Collier, J.P., Sperling, D.K., Currier, J.H., Sutula, L.C., Saum, K.A. and Mayor, M. B. 1996. Impact of gamma sterilization on clinical performance of polyethylene in the knee. The *Journal Of Arthroplasty. 11*(4), p. 377–389.

Conner, E.M. and Grisham, M. B. 1996. Inflammation, free radicals, and antioxidants. *Nutrition*. **12**(4), p. 247–277.

Cooper, J. R., Dowson, D. and Fisher, J. 1993. Macroscopic and microscopic wear mechanisms molecular weight polyethylene in ultra-high. *Wear*. **162-164** (A), p. 378–384.

Costa, A.G., Cusano, N.E., Silva, B.C., Cremers, S. and Bilezikian, J. P. 2011. Cathepsin K: its skeletal actions and role as a therapeutic target in osteoporosis. *Nature Reviews Rheumatology*. **7**(8), p. 447–456.

Costa, L. and Bracco, P. 2009. Mechanisms of Crosslinking, Oxidative Degradation and Stabilization of UHMWPE. In Kurtz, S. M. ed. *UHMWPE Biomaterials Handbook*. San Diego: Elsevier Academic Press Inc, pp. 309–323.

Craig, R. Vlycou, M., McCArthy, C. L., Gibbons, C. L. M. H. and Athanasou, N. A. 2017. Metal wear-induced pseudotumour following an endoprosthetic knee replacement for Ewing sarcoma. *Skeletal Radiology*. **46**(7), p. 967–974.

Cummings, S. R., Kelsey, J.L., Nevitt, M. and O'Dowd, K. J. 1985. Epidemiology of osteoporosis and osteoporotic fractures. *Australian Prescriber*. **20**(SUPPL. 3), p. 13–17.

Devaraj, S. and Jialal, I. 1999. Alpha-Tocopherol Decreases Interleukin-1β Release From Activated Human Monocytes by Inhibition of 5-Lipoxygenase'. *Arteriosclerosis, Thrombosis And Vascular Biology*. **19(**4), p. 1125 - 1133.

Devaraj, S., Li, D. and Jialal, I. 1996. The effects of alpha tocopherol supplementation on monocyte function: Decreased lipid oxidation, interleukin 1β secretion, and monocyte adhesion to endothelium. *Journal Of Clinical Investigation*. **98**(3), p. 756–763.

Devine, T.M. and Wulff, J. 1975. Cast vs. wrought cobalt-chromium surgical implant alloys. *Journal Of Biomedical Materials Research.* **9**(2), p. 151–67.

Dolezel, B. and Adamirova, L. 1982. *Method of hygienically safe stabilization of polyolefines against thermoxidative and photoxidative degradation*. Czechislovakian Socialist Republic Patent, 221:403.

Dorlot, J-M., Christel, P. and Meunier, A. 1989. Wear analysis of retrieved alumina heads and sockets of hip prostheses. *Journal Of Biomedical Materials Research.* **23**(A3 suppl), p. 299–310.

Duff, G. W. 1993. Cytokines and anti-cytokines. *British Journal Of Rheumatology*. **32**(1), p. 15–20.

Dumbleton, J. H., Manley, M. T. and Edidin, A. A. 2002. A literature review of the association between wear rate andosteolysis in total hip arthroplasty. *Journal Of Arthroplasty.* **17**(5), p. 649 - 661.

Edidin, A.A. and Kurtz, S. M. 2000. The influence of mechanical behavior on the wear of four clinically relevant polymeric biomaterials in a hip simulator. *Journal Of Arthroplasty*. **15**(3), p. 321–331.

Endo, M. M., Barbour, P. S., Barton, D. C., Fisher, J., Tipper, J. L., Ingham, E. and Stone, M. H. 2001. Comparative wear and wear debris under three different counterface conditions of crosslinked and non-crosslinked ultra high molecular weight polyethylene. *Biomedical Materials And Engineering*. **11**(1), p. 23–35.

Endo, M., TIpper, J. L., Barton, D. C., Stone, M. H., Ingham, E. and Fisher, J. 2002. Comparison of wear, wear debris, and functional biological activity of moderately crosslinked and non-crosslinked polyethylenes in hip prostheses. *Proceedings Of The Institution Of Mechanical Engineers, Part H: Journal Of Engineering In Medicine.* **216** (2), p. 111 - 122.

Feldman, L.A. and Hui, H. K. 1997. Compatibility of medical devices and materials with low-temperature hydrogen peroxide gas plasma. *Medical Device And Diagnostic Industry.* **19**(12), p. 57–62.

Franzen, H., Carlsson, Å., Johnsson, R., Rydholm, A., Önnerfält, R. 1994. Bony atrophy after mega total hip replacement for bone tumors: 11 cases followed for 3-15 years. *Acta Orthopaedica*. **65**(5), p. 513–516.

Fröhlich, S. M., Dorrer, V., Archodoulaki, V-M., Allmaier, G. and Marchetti-Deschmann, M. 2014. Synovial fluid protein adsorption on polymer-based artificial hip joint material investigated by MALDI-TOF mass spectrometry imaging. *EuPA Open Proteomics*. **4**(2014), pp. 70–80.

Fu, J., Shen, J., Gao, G., Xu, Y., Hou, R., Cong, Y. and Cheng, Y. 2013. Natural polyphenol-stabilised highly crosslinked UHMWPE with high mechanical properties and low wear for joint implants. *Journal Of Materials Chemistry B*. **1**(37), p. 4727–4735.

Gallardo, L. A., Knowlton, C. B., Kunze, J., Jacobs, J. J., Wimmer, M. A. and Laurent, M. P. 2011a. Effect of europium(II) stearate on the mechanical properties and the oxidation resistance of UHMWPE. *Journal Of The Mechanical Behavior Of Biomedical Materials*. **4**(5), p. 821–826.

Gallardo, L. A., Carpentieri, I., Laurent, M. P., Costa, L. and Wimmer, M. A. 2011b. Europium stearate additives delay oxidation of UHMWPE for orthopaedic applications: A pilot study. *Clinical Orthopaedics And Related Research*. **469**(8), p. 2294–2301.

Galvin, A., Kang, L., Tipper, J., Stone, M., Ingham, E., Jin, Z. and Fisher, J. 2006. Wear of crosslinked polyethylene under different tribological conditions. *Journal of Materials Science: Materials In Medicine*. **17**(3), p. 235–243.

Germain, M., Hatton, A., Williams, S., Matthews, J. B., Stone, M. H., Fisher, J. and Ingham, E. 2003. Comparison of the cytotoxicity of clinically relevant cobalt-chromium and alumina ceramic wear particles in vitro. *Biomaterials*. **24**(3), p. 469 – 479.

Gijsman, P., Smelt, H.J. and Schumann, D. 2010. Hindered amine light stabilizers: An

alternative for radiation cross-linked UHMWPE implants. *Biomaterials*. **31**(26), p. 6685–6691.

Goldring, M. B. and Goldring, S. R. 2007. Osteoarthritis. *Journal Of Cellular Physiology*. **213**(3), p. 626–634.

Goode, A. E., Perkins, J. M., Sandison, A., Karunakaran, C., Cheng, H., Wall, D., Skinner, J. A., Hart, A. J., Porter, A. E., McComb, D. W. and Ryan, M. P. 2012. Chemical speciation of nanoparticles surrounding metal-on-metal hips. *Chemical Communications*. **48**(67), p. 8335–8337.

Goodman, S. M. 2013. Rheumatoid Arthritis Preoperative Evaluation for Total Hip and Total Knee Replacement Surgery. *Journal Of Clinical Rheumatology*. **19**(4), p. 187–92.

Gowland, N. 2014. *The Wear and Biological Activity of Antioxidant UHMWPE for use in Total Hip Replacements*. Ph.D. thesis, University of Leeds.

Granchi, D., Cenni, E., Giunti, A., and Baldini, N. 2012. Metal hypersensitivity testing in patients undergoing joint replacement: a systematic review. *The Journal Of Bone And Joint Surgery.* **94B**(8), p. 1126–1134.

Granchi, D., Cennis, E., Trisolino, G., Giunti, A., and Baldini, N. 2006. Sensitivity to implant materials in patients undergoing total hip replacement. *Journal Of Biomedical Material Research B: Applied Biomaterials.* 77(2), p. 257 – 264.

Gray, H. 2019a. *Gray's Anatomy: Hip anatomy.* [online]. [Accessed: 22 April 2019]. Available from: https://upload.wikimedia.org/wikipedia/commons/f/f1/Gray339.png

Gray, H. 2019b. Gray's Anatomy: Hip anatomy. [online]. [Accessed: 22 April 2019]. Available from: https://upload.wikimedia.org/wikipedia/commons/3/33/Gray340.png

Gray, H. 2014a. *Gray's Anatomy. Pelvis anatomy.* [online]. [Accessed: 31 August 2014]. Available from: http://upload.wikimedia.org/wikipedia/commons/9/98/Gray241.png

Gray, H. 2014b. *Grays Anatomy. Femoral head anatomy.*, online]. [Accessed: 31 August 2014]. Available from: http://upload.wikimedia.org/wikipedia/commons/9/97/Gray243.png

Green, J.M., Hallab, N.J., Senyurt, A., Liao, P., O'Keefe, R.J., Schwarz, E.M. and Xie, C. 2012. Effects of anti-oxidation treatments during the manufacturing of ultra high molecular weight polyethylene prosthetic components on their osteolytic and osteogenic properties as wear debris particles in a murine calvaria model. *Current Rheumatology Reports*. **26**(1951), p. 61307.

Green, T. R., Fisher, J., Stone, M. H., Wroblewski, B. M and Ingham, E. 1998. Polyethylene particles of a "critical size" are necessary for the induction of cytokines by macrophages in vitro. *Biomaterials*. **19**(24), p. 2297–2302.

Green, T. R., Fisher, J., Matthews, J. B., Stone, M. H. and Ingham, E. 2000. Effect of size and dose on bone resorption activity of macrophages by in vitro clinically relevant ultra high molecular weight polyethylene particles. *Journal Of Biomedical Materials Research*. **53**(5), p. 490–497.

Han, K.H., Ryu, J.W., Lim, K.E., Lee, S.H., Kim, Y., Hwang, C.S., Choi, J. Y. and Han, K. O. 2014. Vascular expression of the chemokine CX3CL1 promotes osteoclast recruitment and exacerbates bone resorption in an irradiated murine model. *Bone*. **61**, p. 91–101.

Hannouche, D., Hamadouche, M., Nizard, W., Bizot, P., Meunier, A. and Sedel, L. 2005. Ceramics in total hip replacement. *Clinical Orthopaedics And Related Research.* **Jan**(430), p. 62–71.

He, S., Le, K-P., Blitz, J.W., Yau, S-S., Korduba, L.A. and Wang, A. 2009. *Anthocyanin doped UHMWPE : oxidation, wear and mechanical properties.* [Poster]. 55th Annual Meeting of the Orthopaedic Research Society, 22-25th Feb, Las Vegas.

He, S., Yau, S-S., Wang, A. and Lawrynowicz, D. E. 2012. *Polyethylene Cross-linked With An Anthocyanin*. Patent. US8133436B2.

Holliday, L.S., Bubb, M.R., Jiang, J., Hurst, I.R. and Zuo, J. 2005. Interactions between vacuolar H+-ATPases and microfilaments in osteoclasts. *Journal Of Bioenergetics And Biomembranes.* **37**(6), p. 419–423.

Howling, G. I., Barnett, P. I., Tipper, J. L., Stone, M. H., Fisher, J. and Ingham, E. 2001. Quantitative characterization of polyethylene debris isolated from periprosthetic tissue in early failure knee implants and early and late failure Charnley hip implants. *Journal Of Biomedical Materials Research*. **58**(4), p. 415–420.

Inada, M., Wang, Y., Byrne, M.H., Miyaura, C. and Krane, S. M. 2003. The collagenase, matrix metalloproteinase-13 (MMP-13), is required for osteoclast formation and function. *Journal Of Bone And Mineral Research.* **18**, p. 195.

Ingham, E. and Fisher, J. 2000. Biological Reaction to Wear Debris in Total Joint Replacement. *Proceedings Of The Institution Of Mechanical Engineers. Part H*. **73**(2), p. 21–37.

Ingham, E. and Fisher, J. 2005. The role of macrophages in osteolysis of total joint replacement. *Biomaterials*. **26**(11), p. 1271–1286.

Ingram, J. H., Stone, M. H., Fisher, J. and Ingham, E. 2004. The influence of molecular weight, crosslinking and counterface roughness on TNF-alpha production by macrophages in response to ultra high molecular weight polyethylene particles. *Biomaterials*. **25**(17), p. 3511–3522.

Isaac, G. H., Dowson, D. and Wroblewski, B. M. 1996. An investigation into the origins of time-dependent variation in penetration rates with Charnley acetabular cups-wear, creep or degradation ? *Proceedings Of The Institution Of Mechanical Engineers, Part H: Journal Of Engineering In Medicine*. **210**(3), p. 209–216.

Jacobsen, S., Rømer, L., and Søballe, R. 2006. The other hip in unilateral hip dysplasia. *Clinical Orthopaedics And Related Research*. **446**, p. 239 – 246.

Jahan, M.S., Wang, C., Schwartz, G. and Davidson, J. A. 1991. Combined chemical and mechanical effects on free radicals in UHMWPE joints during implantation. *Journal Of Biomedical Materials Research*. **25**(8), p. 1005–1017.

James, S.P., Oldinski, R., Zhang, M. and Schwartz, H. 2016. UHMWPE-hyaluronan microcomposite biomaterials. In: Kurtz, S. *Ultrahigh Molecular Weight Polyethylene In Total Joint Replacements And Medical Devices*. San Diego: Elsevier academic press, p. 352 – 368.

Janeway, C. A., Travers, P., Walport, M. and Schlomchik, M. J. 2001. *Immunobiology*. 5th Edition. New York: Garland Science.

Jarrett, B. T., Cofske, J., Rosenberg, A. E., Oral, E., Muratoglu, O., and Malchau, H. 2010. In Vivo Biological Response to Vitamin E and Vitamin-E-Doped Polyethylene. *The Journal Of Bone And Joint Surgery American Volume*. **92A**(16), p. 2672–2681.

Jazrawi, L. M., Bogner, E., Della Valle, C. J., Chen, F. S., Pak, K. I., Stuchin, S. A., Frankel, V. H., and Di Cesare, P. E. 1999. Wear rates of ceramic-on-ceramic bearing surfaces in total hip implants. A 12-year follow-up study. *The Journal Of Arthroplasty*. 12(7), p. 781 - 787.

Kannu, P. and Howard, A. 2014. Perthes' disease. *British Medical Journal*. **349**, p.5584.

Khan, H., Riva, F., Presacco, M., Meswania, J., Panagiotidou, A., Coathup, M., and Blunn, G. W. 2018. Development of the Lima ceramic hip resurfacing system: revision of hip resurfacing using a dual taper ceramic head and taper adaptor in an in vitro model. *Orthopaedic Proceedings*. **99B**(4), p.61

Kim, M.S., Day, C.J. and Morrison, N. A. 2005. MCP-1 is induced by receptor activator of nuclear factor-kappa B ligand, promotes human osteoclast fusion, and rescues granulocyte macrophage colony-stimulating factor suppression of osteoclast formation. *Journal Of Biological Chemistry*. **280**(16), p. 16163–16169.

Kim, K., Lee, S-H., Kim, J. H., Choi, Y. and Kim, N. 2006. NFATc1 induces osteoclast fusion via up-regulation of osteoclast fusion and increased bone formation. *Nature Medicine.* **12**, p. 1403–1409.

Kim, Y., Sato, K., Asagiri, M., Morita, I., Soma, K. and Takayanagi, H. 2005. Contribution of nuclear factor of activated T cells c1 to the transcriptional control of immunoreceptor osteoclast-associated receptor but not triggering receptor expressed by myeloid cells-2 during osteoclastogenesis. *Journal Of Biological Chemistry*. **280**(38), p. 32905–32913.

King, R; Arscott, E and Narayan, V. 2010. *Biocompatibility Study of Gamma-irradiated UHMWPE Stabilized with a Hindered-Phenol Antioxidant.* [Poster]. 56th Annual Meeting of the Orthopaedic Research Society, 6th-9th Mar, New Orleans, Louisiana.

Klaue, K., Durnin, C.W. and Ganz, R. 1991. The acetabular rim syndrome - a clinical presentation of dysplasia of the hip. *Journal Of Bone And Joint Surgery - British Volume.* **73**(3), p. 423–429.

Koureas, G., Wicart, P., and Serine, R. 2007. Etiology of developmental hip dysplasia or dislocation: review article. *HIP International.* **17**(5), p. 1–7.

Kurtz, S.M., Muratoglu, O.K., Evans, M. and Edidin, A. A. 1999. Advances in the processing, sterilization, and crosslinking of ultra-high molecular weight polyethylene for total joint arthroplasty. *Biomaterials*. **20**(issue), p. 1659–1688.

Kurtz, S. 2004a. Chapter 1: A primer on UHMWPE. Kurtz, S. Ed. *The UHMWPE Handbook*. San Diego: Elsevier academic press, p. 1 - 12.

Kurtz, S. 2004b. Chapter 2: From ethylene gas to UHMWPE component: the process of producing orthopedic implants. Kurtz, S. Ed. *The UHMWPE Handbook*. San Diego: Elsevier academic press, p. 13 - 36.

Kurtz, S. 2004c. Chapter 3: Packaging and sterilzation of UHMWPE. Kurtz, S. Ed. *The UHMWPE Handbook*. San Diego: Elsevier academic press, p. 37 - 51.

Kyomoto, M., Moro, T. and Ishihara, K. 2016. Phospholipid polymer grafted highly cross-linked UHMWPE. In: Kurtz, S. ed. *Ultrahigh molecular weight polyethylene in total joint replacements and medical device*. 3rd Edition. San Diego: Elsevier academic Press, p. 352 – 368.

Lancaster, J. G., Dowson, D., Isaac, G. H. and Fisher, J. 1997. The wear of ultra-high

molecular weight polyethylene sliding on metallic and ceramic counterfaces representative of current femoral surfaces in joint replacement. *Proceedings Of The Institution Of Mechanical Engineers, Part H: Journal Of Engineering In Medicine*. **211**(1), p. 17–24.

Laslo P, Spooner CJ, Warmflash A, Lancki DW, Lee HJ, Sciammas R, Gantner, B. N., Dinner, A. R. and Singh, H. 2006. Multilineage transcriptional priming and determination of alternate hematopoietic cell fates. *Cell*. **126**(4), p. 755–766.

Lee, D. M. and Weinblatt, M. E. 2001. Rheumatoid arthritis. *Lancet*. **358**(9285), p. 903–911.

Lee, H. 2016. *Spinal Cord Cellular Response To Wear Debris From Metal-on-Metal Total Disc Replacements*. Ph.D. thesis, University of Leeds.

Liu, A. 2012. *Determination of the biological response and cellular uptake mechanisms of nanometre-sized UHMWPE wear particles from total hip replacements*. Ph.D. thesis, University of Leeds.

Liu, A., Richards, L., Bladen, C. L., Ingham, E., Fisher, J. and Tipper, J. L. 2015. The biological response to nanometre-sized polymer particles. *Acta Biomaterialia*. 23, p. 38 - 51.

Malik, J., Hrivik, A. and Tomova, E. 1992. Diffusion of hindered amine light stabilizers in low-density polyethylene and isotactic polypropylene. *Polymer Degradation And Stability*. **35**(1), p. 61–66.

Man, G. S. and Mologhianu, G. 2014. Osteoarthritis pathogenesis - a complex process that involves the entire joint. *Journal Of Medicine And Life*. **7**(1), p. 37–41.

Margevicius, K. J., Bauer, T. W., McMahon, J. T., Brown, S. A. and Merritt, K. 1994. Isolation and characterization of debris in membranes around total joint prostheses. *Journal Of Bone And Joint Surgery - Series A*. **76**(11), p. 1664–1675.

Martell, J., Berkson, E. and Jacobs, J. J. 2000. The performance of 2D vs. 3D computerized wear analysis in the Harris Galante acetabular component. *Orthopaedic Transactions*. **25**(564), p. 88.

Matsumoto, M., Kogawa, M., Wada, S., Takayanagi, H., Tsujimoto, M., Katayama, S., Hisatake, K. and Nogi, Y. 2004. Essential role of p38 mitogen-activated protein kinase in cathepsin K gene expression during osteoclastogenesis through association of NFATc1 and PU.1. *Journal Of Biological Chemistry*. **279**(44), p. 45969–45979.

Matsusaki, T., Kawanabe, K., Ise, K., Nakayama, T., Toguchida, J., and Nakamura, T. Gene Expression Profile of Macrophage-Like U937 Cells in Response to Polyethylene Particles. A Novel Cell-Particle Culture System. *Journal Of Arthroplasty*. **22**(7), p. 960–965.

Matthews, J. B., Green, T. R., Stone, M. H., Wroblewski, B. M., Fisher, J. and Ingham, E. 2000a. Comparison of the response of primary human peripheral blood mononuclear phagocytes from different donors to challenge with model polyethylene particles of known size and dose. *Biomaterials*. **21**(20), p. 2033–2044.

Matthews, J. B., Green, T. R., Stone, M. H.,Wroblewski, B. M., Fisher, J. and Ingham, E. 2000c. Comparison of the response of primary murine peritoneal macrophages and the U937 human histiocytic cell line to challenge with in vitro generated clinically relevant UHMWPE particles. *Biomedical Materials And Engineering*. **10**(3–4), p. 229–240.

Matthews, J. B., Besong, A. A., Green, T. R., Stone, M. H., Wroblewski, B. M., Fisher, J. and Ingham, E. 2000b. Evaluation of the response of primary human peripheral blood mononuclear phagocytes to challenge with in vitro generated clinically relevant UHMWPE particles of known size and dose. *Journal Of Biomedical Materials Research*. **52**(2), p. 296–307.

Matthews, J. B., Green, T. R., Stone, M. H., Wroblewski, B. M., FIsher, J .and Ingham, E. 2001. Comparison of the response of three human monocytic cell lines to challenge with polyethylene particles of known size and dose. *Journal Of Materials Science: Materials n Medicine*. **12**(3), p. 249–258.

McGill, I. 2005. *Rare Earth Elements*. Weinheim: Wiley-VCH.

McKellop, H., Shen, F., Lu, B., Campbell, P. and Salovey, R. 1999. Development of an extremely wear-resistant ultra high molecular weight polythylene for total hip replacements. *Journal Of Orthopaedic Research*. **17**(2), p. 157–167.

Medley , J.B., Chan, F.W., Krygier, J.J. and Bobyn, J. D. 1996. Comparison of alloys and designs in a hip simulator study of metal on metal implants. *Clinical Orthopaedics And Related Research.* Aug(329 Suppl), p. 148-159.

Menaa, C., Kurihara, N., and Roodman, G. D. 2000. CFU-GM-derived cells form osteoclasts at a very high efficiency. *Biochemical And Biophysical Research Communications.* **267**(3), p. 943–946.

Mercier, C. and Chabardes, P. 1994. Organometallic chemistry in industrial vitamin-a and vitamin-e synthesis. *Pure And Applied Chemistry.* **66**(7), p. 1509–1518.

Milosev, I., Kovac, S., Topolovec, M., Pisot, V. and Trebse, R. 2009. Total hip replacements with metal-on-metal bearings. *Zdravniski Vestnik.* 78(Supp. II), p. 34–40.

Minkara, A.A., Westermann, R.W., Rosneck, J. and Lynch, T. S. 2018. Systematic review and meta-analysis of outcomes after hip arthroscopy in femoralacetabular impingement. *American Journal Of Sports Medicine. Jan(1), p.036354651774947.*

Miyamoto , T., Ohneda, O., Arai, F., Iwamoto, K., Okada, S., Takagi, K., Anderson, D. M. and Suda, T. 2001. Bifurcation of osteoclasts and dendritic cells from common progenitors. *Blood*. **98**(8), p. 2544–2554.

Molini, L., Precerutti, M., Gervasio, A., Draghi, F. and Bianchi, S. 2011. Hip: Anatomy and US technique. *Journal Of Ultrasound*. **14**(2), p. 99–108.

Mont, M.A. and Hungerford, D. S. 1995. Nontraumatic avascular necrosis of the femoral-head. *Journal Of Bone And Joint Surgery: American Volume*.. **77A**(3), p. 459–474.

Mont, M., Ragland, P. S., Etienne, G., Seyler, T. M. and Schmalzried, T. P. 2006. Hip resurfacing arthroplasty. *The Journal of the American Academy of Orthopaedic Surgeons*. **14**(8), p. 454–463.

Moretti, B., Pesce, V., Maccagnano, G., Vicenti, G., Lovreglio, P., Soleo, L. and Apostoli, P. 2012. Peripheral neuropathy after hip replacement failure: is vanadium the culprit? *Lancet*. **379**(9826). p. 1676.

Morsi, E., Habib, M. E., Elseedy, A. and Eid, T. 2016. Revision of failed hip hemiarthroplasty: Classification, management, and follow-up. *Journal Of Orthopaedics*. **13**(2), p. 63–68.

Musib, M. and Saha, S. 2010. Effect of wear-debris particles on RAW 264.7 cells.

Proceedings Of The 2010 IEEE 36th Annual Northeast Bioengineering Conference, 26-28 March 2010, New York, USA. New York: IEEE, p. 32 - 33.

Narayan, V. S., Ernsberger, C. and King, R. 2009. *Pin-on-Disk wear studies of antioxidant-stabilized UHMWPE materials.* [Poster]. 55th Annual Meeting of the Orthopaedic Research Society, 22-25th Feb, Las Vegas.

National Joint Registry. 2016. *NJR reports 2016*. [online]. [Accessed: 31 August 2014]. Available from: http://www.njrreports.org.uk/hips-primary-procedures-patient-characteristics/H05v1NJR?reportid=351A3B2E-F983-4D53-BC1E-D9A90DC93AAA&defaults=DC__Reporting_Period__Date_Range=%22MAX%22,J__Filter__Calendar_Year=%22MAX%22,H__Filter__Joint=%22Hip%22.

National Joint Registry. 2017. *2017 14th Annual Report - National Joint Registry For England, Wales, Northern Ireland And The Isle Of Man*. [online]. [Accessed: 31 August 2014]. Available from: http://www.njrreports.org.uk/Portals/0/PDFdownloads/NJR 14th Annual Report 2017.pdf.

Navarro-Zarza, J. E., Villaseñor-Oviesb, P., Vargas, A., Canoso, J. J., Chiapas-Gasca, K., Hernández-Díaz, C., Saavedra, M. A. and Kalish, R. A. 2012. Clinical Anatomy of the Pelvis and Hip. *Reumatologia Clinica*. **8**(SUPPL.2), p. 33–38.

Nich, C., Goodman, S. B. and Hospital, T. 2014 The role of macrophages in the biological reaction to wear debris from joint replacements. *Journal Of Long Term Effects Of Medical Implants*. **24**(4), p. 259–265.

Niche, C., Sariali, el-H., Hannouche, D., Nizard, R., Witvoet, J., Sedel, L. and Bizot, P. 2003. Long-term results of alumina-on-alumina hip arthroplasty for osteonecrosis. *Clinical Orthopaedics And Related Research.* **417**, p. 102–111.

Nizard, R., Sedel, L., Christel, P. Meunier, A., Soudry, M. and Witviet, J. 1992. Ten-year survivorship of cemented ceramic-ceramic total hip prosthesis. *Clinical Orthopaedics.* **Sept**(282), p. 53 – 63.

Noordin, S., Umer, M., Hafeez, K. and Nawaz, H. 2010. Developmental dysplasia of the hip. *Orthopedic Reviews*. **2**(2), p. 19.

Oral, E., Greenbaum. E. S., Malhi, A. S., Harris, W. H. and Muratoglu, O. K. 2005. Characterization of irradiated blends of α-tocopherol and UHMWPE. *Biomaterials*. **26**(33), p. 6657–6663.

Oral, E., Christensen, S. D., Malhi, A. S., Wannomae, K. K. and Muratoglu, O. K. 2006. Wear Resistance and Mechanical Properties of Highly Cross-linked, Ultrahigh-Molecular Weight Polyethylene Doped With Vitamin E. *Journal Of Arthroplasty*. **21**(4), p. 580–591.

Oral, E., Wannomae, K. K., Rowell, S. L. and Muratoglu, O. K**.** 2007. Diffusion of vitamin E in ultra-high molecular weight polyethylene. *Biomaterials*. **28**(35), p. 5225–5237.

Oral, E., Malhi, A. S., Wannomae, K. K. and Muratoglu, O. K. 2008. Highly Crosslinked UHMWPE with Improved Fatigue Resistance for Total Joint Arthroplasty. *Journal Of Arthroplasty*. **23**(7), p. 1037–1044.

Oral, E., Malhi, A. S. and Muratoglu, O. K. 2006. Mechanisms of decrease in fatigue crack propagation resistance in irradiated and melted UHMWPE. *Biomaterials*. **27**(6), p. 917–925.

Oral, E and Muratoglu, O. 2009. Chapter 18: Highly cross-linked UHMWPE doped with vitamin E. Kurtz, S. Ed. *UHMWPE Biomaterials Handbook*. 2nd Edition. San Diego: Elsevier academic press, p. 307 - 325.

Pandit, H., Glyn-Jones, S., McLardy-Smith, P., Gundle, R., Whitwell, D., Gibbons, C.L.M., Ostlere, S., Athanasou, N, Gill, H.S. and Murray, D. W. 2008. Pseudotumours associated with metal-on-metal hip resurfacings. *Journal Of Bone And Joint Surgery: British Volume*. **90**(7), p. 920–3.

Pandit, H., Vlychou, M., Whitwell, D., Crook, D., Luqmani, R., Ostlere, S., Murray, D. W. and Athanasou, N. A. 2008. Necrotic granulomatous pseudotumours in bilateral resurfacing hip arthroplasties: evidence for a type IV immune response. *Virchows Archiv.* **453**(5), p. 529 – 534.

Peng, Z.B., Hu, B., Su, Q.D. and Qu, J. Z. 2003. Study on mechanism of rare earth PVC stabilizer. *Journal Of Rare Earths.* **21**(3), p. 328–330.

Pennekamp, P. H., Caicedo, M., Catelas, I., Kunze, J., Laurent, M. P., Hallab, N. J., and WImmer, M. A. 2009. *Lanthanides induce Diverse Cell Responses in Murine Macrophages*. [Poster]. 55th Annual Meeting of the Orthopaedic Research Society, 22-25th Feb, Las Vegas

Peterson, E. D., Nemanich, J. P., Altenburg, A. and Cabenela, M. E. 2009. Hip arthroplasty after previous arthrodesis. *Clinical Orthopaedics And Related Research*, **467**(11), p. 2880–2885.

Petis, S., Howard, J. L., Lanting, B. L. and Vasarhelyi, E. M. 2015. Surgical approach in primary total hip arthroplasty: Anatomy, technique and clinical outcomes. *Canadian Journal Of Surgery*. **58**(2), p. 128–139.

Popoola, O.O., Yao, J.A.Q., Johnson, T.S. and Blanchard, C. R. 2010. Wear, Delamination, and Fatigue Resistance of Melt-Annealed Highly Cross linked UHMWPE Cruciate-Retaining Knee Inserts under Activities of Daily Living. *Journal Of Orthopaedic Research.* **28**(9), p. 1120–1126.

Premnath, V., Harris, W.H., Jasty, M. and Merrill, E. W. 1996. Gamma sterilization of UHMWPE articular implants: An analysis of the oxidation problem. *Biomaterials*. **17**(18), p. 1741–1753.

Proff, P. and Römer, P. 2009. The molecular mechanism behind bone remodelling: A review. *Clinical Oral Investigations*. **13**(4), p. 355–362.

Puertolas, J.A. and Kurtz, S. M. 2016. UHMWPE matrix composites. In: Kurtz, S. ed. *Ultrahigh Molecular Weight Polyethylene In Total Joint Replacements And Medical Devicse*. London: Elsevier, p. 369–397.

Rader, C. P., Sterner, T., Jakob, F., Schütze, N and Eulert, J. 1999. Cytokine response of human macrophage-like cells after contact with polyethylene and pure titanium particles. *Journal Of Arthroplasty*. **14(**7), p. 840–848.

Raisz, L. G. 1988. Local and systematic factors in the pathogenesis of osteoporosis. *The New England Journal Of Medicine*. **298**(6), p. 337–339.

Raisz, L. G. 2005. Pathogenesis of osteoporosis : concepts , conflicts , and prospects. *Journal Of Clinical Investigation.* **115**(12), p. 3318–3325.

Richards, L., Brown, C., Stone, M. H., Fisher, J., Ingham, E. and Tipper, J. L. 2008. Identification of nanometre-sized ultra-high molecular weight polyethylene wear particles in samples retrieved *in vivo*. *Journal Of Bone And Joint Surgery: British*

Volume. **90**(issue), p. 1106–1113.

Richards, L. (2008) *The biological activity of nanometre sized polymer particles*. Ph.D. thesis, University of Leeds.

Roodman, G. D. 2012. Vitamin E: Good for the heart, bad for the bones? *Nature Medicine*. **18**(4), p. 491–492.

Scholes, S. C. and Unsworth, A. 2006. The effects of proteins on the friction and lubrication of artificial joints. *Proceedings Of The Institution Of Mechanical Engineers, Part H: Journal Of Engineering In Medicine*. **220**(6), p. 687–693.

Schubert, D., Dargusch, R., Raitano, J. and Chan, S. W. 2006. Cerium and yttrium oxide nanoparticles are neuroprotective. *Biochemical And Biophysical Research Communications.* 342(1), p. 86–91.

Shishido, T., Clarke, I. C., Weber, F., Shoji, H. and Imakiire, A. 2002. *Analysis of retrieved THR cups of highly cross-linked UHMWPE from South Africa.* [Poster]. 48th Annual Meeting of the Orthopaedic Research Society, Feb, Dallas, Texas.

Silverman, E. J., Ashley, B. and Sheth, N. P. 2016. Metal-on-metal total hip arthroplasty: is there still a role in 2016? *Current Reviews In Musculoskeletal Medicine*. **9**(1), p. 93–96.

Singh, U., Devaraj, S. and Jialal, I. 2005. Vitamin E, oxidative stress, and inflammation. *Annual Review Of Nutrition*. p. 151–174.

Siskey, R., Smelt, H., Boon-Ceelan, K. and Persson, M. 2016. UHMWPE homocomposites and fibers. *Ultrahigh Molecular Weight Polyethylene In Total Joint Replacements And Medical Device*. 225(1), p. 398 – 411.

Smith, J. T. (2016) *A 3d culture model to investigate cellular responses to mechanical loading in spinal cord injury*. Ph.D. thesis, University of Leeds.

Smolen, J., Aletaha, D. and McInnes, I. B. 2016. Rheumatoid arthritis. *Lancet*. **388**(10055), p. 2023–2038.

Sokol, R. J. 1993. Vitamin E deficiency and neurological disorders. In: Packer, L. and Fuchs, J. eds. *Oxidants, Antioxidants And Free Radicals.* New York: Marcel Dekker.

Suñer, S., Gowland, N., Craven, R., Joffe, R., Emami, N. and Tipper, J. L. 2018. Ultrahigh molecular weight polyethylene/graphene oxide nanocomposites: Wear characterization and biological response to wear particles. *Journal Of Biomedical Materials Research - Part B Applied Biomaterials*. **106**(1), p. 183–190.

Sutula, L.C., Collier, J.P., Saum, K.A., Currier, B.H., Currier, J.H., Sanford, W.M., Mayor, M. B., Wooding, R. E., Sperling, D. K. and Williams, I. R. 1995. Impact of gamma-sterilization on clinical-performance of polyethylene in the hip. *Clinical Orthopaedics And Related Research.* **319**(issue), p. 28–40.

Teitelbaum, S. L. 2006. Osteoclasts and integrins. in Zaidi, M. (ed.) *Skeletal Development And Remodeling In Health, Disease, And Aging*. Oxford: Blackwell Publishing, pp. 95–99.

Teng, G. G., Curtis, J. R. and Saag, K. G. 2008. Mortality and osteoporotic fractures: Is the link causal, and is it modifiable?. *Clinical And Experimental Rheumatology*. **26**(5 SUPPL. 51), p. 125 - 137.

Teramura, S., Sakoda, H., Terao, T., Endo, M. M., Fujiwara, K. and Tomita, N. 2009. Reduction of wear volume from accelerated aged UHMWPE knee components by the

addition of vitamin E. *Journal Of Biomechanical Science And Engineering*. **4**(4), p. 589–596.

Tipper, J., Ingham, E., Jin, Z., and Fisher, J. 2005. The science of metal-on-metal articulation. *Current Orthopaedics*. **19**(4), p. 280 – 287.

Tipper, J.L., Galvin, A.L., Williams, S., McEwen, H.M.J., Stone, M.H., Ingham, E., and Fisher, J. 2006. Isolation and characterization of UHMWPE wear particles down to ten nanometers in size from in vitro hip and knee joint simulators. *Journal Of Biomedical Materials Research Part A*. **78**(3), p. 473–480.

Tipper, J. L., Firkins, P. J., Ingham, E., Fisher, J., Stone, M. H. and Farrar, R. 2000. Quantitative analysis of polyethylene wear debris, wear rate and head damage in retrieved Charnley hip prostheses. *Journal Of Materials Science: Materials In Medicine*. **11**(2), p. 117–124.

Tonino, A. J., Thèrin, M. and Doyle, C. 1999. Hydroxyapatite-coated femoral stems. Histology and histomorphometry around five components retrieved at post mortem. *The Journal Of Bone And Joint Surgery: British volume*. **81**(1), p. 148–54.

Traina, F., De Fine, M., and Affatato, S. 2012. Anatomy of the hip and suitable prostheses. *Wear Of Orthopaedic Implants And Artificial Joints*. 2013, p.93-114.

Traina, F. De Fine, M., Di Martino, A. and Faldini, C. 2013. Fracture of ceramic bearing surfaces following total hip replacement: A systematic review. *BioMed Research International*. 2013, p. 157247.

Tubby, A. H. 1908. A clinical lecture on coxa valga. *British Medical Journal.* 2(2482), p. 185.

Vaidya, C., Alvarez, E., Vinciguerra, J., Bruce, D. A. and Desjardins, J. D. 2011. Reduction of total knee replacement wear with vitamin e blended highly cross-linked ultra-high molecular weight polyethylene. *Proceedings Of The Institution Of Mechanical Engineers, Part H: Journal Of Engineering In Medicine*. **225**(1), p. 1–7.

Vermes, C., Chandrasekaran, R., Jacobs, J. J., Galante, J. O., Roebuck, K. A., and Glant, T. T. 2001. The effects of particulate wear debris, cytokines, and growthfactors on the functions of MG-63 osteoblasts. *The Journal Of Bone And Joint Surgery: American Volume*. **83A**(2), p. 201–211.

Vignery, A. 2005. Macrophage fusion: are somatic and cancer cells possible partners? *Medicine Science.* **21**(12), p. 1070–1075.

Wang, A., Zeng, H., Yau, S.S., Essner, A., Manely, M. and Dumbleton, J. 2006. Wear, oxidation and mechanical properties of a sequentially irradiated and annealed UHMWPE in total joint replacement. *Journal Of Physics D-Applied Physics.* **39**(15), p. 3213–3219.

Wannomae, K. K., Christensen, S. D., Freiberg, A. A., Bhattacharyya, S., Harris, W. H. and Muratoglu, O. K. 2006. The effect of real-time aging on the oxidation and wear of highly cross-linked UHMWPE acetabular liners. *Biomaterials*. **27**(9), p. 1980–1987.

Wei, S., Kitaura, H., Zhou, P., Ross, F.P. and Teitelbaum, S. L. 2005. IL-1 mediates TNF-induced osteoclastogenesis. *Journal Of Clinical Investigation.* **115**(2), p. 282–290.

Weir, E.C., Lowik, C., Paliwal, I. and Insogna, K. L. 1996. Colony stimulating factor-1 plays a role in osteoclast formation and function in bone resorption induced by parathyroid hormone and parathyroid hormone-related protein. *Journal Of Bone And*

Mineral Research. **11**(10), p. 1474–1481.

Williams, D. F. 1999. *The Williams Dictionary Of Biomaterials*. Liverpool, UK.: Liverpool University Press.

Willmann, G. 1998. Ceramics for total hip replacement--what a surgeon should know. *Orthopedics*. **21**(2), p. 173–177.

Wolf, C., Lederer, K. and Muller, U. 2002. Tests of biocompatibility of alpha-tocopherol with respect to the use as a stabilizer in ultrahigh molecular weight polyethylene for articulating surfces in joint endoprostheses. *Journal Of Materials Science: Materials In Medicine*. **13**(7), p. 701–705.

Wolf, C., Lederer, K., Pfragner, R., Schauenstein, K., Ingolic, E. and Siegl, V. 2007. Biocompatibility of ultra-high molecular weight polyethylene (UHMW-PE) stabilized with α-tocopherol used for joint endoprostheses assessed in vitro. *Journal Of Materials Science: Materials In Medicine*. **18**(6), p. 1247–1252.

Wolfarth, D. L., Han, D. L., Bushar, G. and Parks, N. L. 1997. Separation and characterization of polyethylene wear debris from synovial fluid and tissue samples of revised knee replacements. *Journal Of Biomedical Materials Research*. **34**(1), p. 57–61.

Wu, J., Peng, Z. and Tipper, J. 2013. Mechanical properties and three-dimensional topological characterisation of micron, submicron and nanoparticles from artificial joints. *Tribology Letters*. **52**(3), p. 449–460.

Yavropoulou, M. P. and Yovos, J. G. 2008. Osteoclastogenesis--current knowledge and future perspectives. *Journal Of Musculoskeletal & Neuronal Interactions*. **8**(June), p. 204–16.

Zhang, W., Ouyang, H., Dass, C. R. and Xu, J. 2016. Current research on pharmacologic and regenerative therapies for osteoarthritis. *Bone Research*. **4**(October), p. 15040 - 15054.

Zheng, Y.Y., Cai, W.L., Fu, M.L., Wang, C.Y. and Zhang, X. 2005. Rare earth stearates as thermal stabilizers for rigid poly(vinyl chloride). *Journal Of Rare Earths.* **23**(2), p. 172–177.